CONVERSION OF BIO-OIL AND REPRESENTATIVE MODEL COMPOUNDS TO SYNTHESIS GAS FOR DISTRIBUTED HYDROGEN PRODUCTION

by
Jonathan R. Marda

A thesis submitted to the Faculty and the Board of Trustees of the Colorado School of Mines in partial fulfillment of the requirements for the degree of Doctor of Philosophy (Chemical Engineering).

Golden, Colorado
Date _____

Signed: _____
Jonathan R. Marda

Approved: _____
Dr. Anthony M. Dean
Thesis Advisor

Golden, Colorado
Date _____

Signed: _____
Dr. James F. Ely
Professor and Head
Department of Chemical Engineering

ABSTRACT

The world's rapidly increasing energy demands, coupled with the need to reduce CO_2 emissions, make it prudent to look to biomass as a fuel source. This research focuses on the conversion of bio-oil, the product of fast pyrolysis of biomass, to synthesis gas in the context of distributed hydrogen production. It has been shown that it is possible to convert up to 80% of the carbon in bio-oil to CO without the need for a catalyst. This was accomplished by first mixing the bio-oil with methanol to reduce its viscosity. This mixture was then volatilized using an ultrasonic nozzle and mixed with controlled amounts of oxygen at high temperatures (625-850ºC) for short residence times (~0.3 s). The oxygen concentration was varied to give equivalence ratio (λ) of up to 0.42 with the optimum range for synthesis gas production being between 0.31 and 0.35. Under these conditions, the H_2 yields were as high as 30% while the CO_2 yields were only ~10%. The effect of methanol dilution was explored by performing experiments using both a 50:50 and 70:30 (wt.%) bio-oil:methanol mixtures. Based on these encouraging results, process simulations have been performed to determine the thermal efficiency and to provide the basis for an economic analysis. The thermal efficiency was estimated to be 57% and the cost of H_2 production and distribution via this process was estimated at \$4.24/kg H_2.

To further characterize this system, experiments were performed using several different reactor configurations with the bio-oil:methanol mixture. Similar results were obtained. Experiments using model compounds containing the oxygen functionalities found in bio-oil confirmed that the high CO yields observed with bio-oil could be understood in terms of the structure of the bio-oil components. Detailed kinetic modeling of methanol pyrolysis and partial oxidation experiments confirmed that the observed conversion and product distribution were consistent with a free radical gas-phase reaction mechanism. Experiments with a catalyst added downstream of the reaction zone showed that

it was possible to convert the products to an equilibrium composition that was rich in hydrogen.

TABLE OF CONTENTS

ABSTRACT ..... **iii**
LIST OF FIGURES ..... **ix**
LIST OF TABLES ..... **xvi**
LIST OF SYMBOLS AND ABREVIATIONS ..... **xviii**
ACKNOWLEDGEMENTS ..... **xix**
DEDICATION ..... **xx**
CHAPTER 1 INTRODUCTION **1**
1.1 Past Research 3
1.2 Present Research 4
CHAPTER 2 EXPERIMENTAL DETAILS **7**
2.1 System at the National Renewable Energy Laboratory 7
2.2 NREL System Modifications 11
2.2.1 Changes to Outer Tube 11
2.2.2 Changes to the Entrance Region 12
2.2.3 Nozzle Upgrade 12
2.2.4 Other Reactor Configurations 13
2.3 Molecular Beam Mass Spectrometer Analysis 14
2.4 System at the Colorado Fuel Cell Center 15
2.5 CFCC System Modifications 17
2.5.1 Bypass 19
2.5.2 Column Changes 19
2.5.3 Upgrade of Mass Flow Controllers 19
2.6 GC Analysis 19
2.7 Feedstocks 20
2.7.1 Bio-oil 20
2.7.2 Model compounds 21
2.8 Bio-oil Rheology 22
2.9 Larger NREL Reactor 22

CHAPTER 3 PRELIMINARY NON-CATALYTIC BIO-OIL REFORMING 25
3.1 Definitions 27
3.1.1 Effective Oxygen to Carbon and Equivalence Ratios 27
3.1.2 Overall Product Yields 28
3.1.3 Bio-oil Product Yields 28
3.1.4 Carbon to Gas Conversion 31
3.1.5 Carbon Accounting 31
3.2 Carbon Deposition 31
3.3 Preliminary NPOX at 650ºC 34
3.4 Effect of Temperature 36
3.5 Reduction of Methanol Content 38
3.6 Staged Oxygen Addition 42
3.7 Reduction of Residence Time 44
3.8 Summary 46
CHAPTER 4 NON-CATALYTIC REFORMING OF 50:50 BIO-OIL METHANOL MIXTURE 49
4.1 Methanol Conversion 50
4.2 Hydrogen 51
4.3 Carbon Monoxide 52
4.4 Carbon Dioxide 53
4.5 Methane 55
4.6 Gas Production 56
4.7 Benzene 57
4.8 Higher Aromatics 58
4.9 Residual Carbon 60
4.10 Carbon Accounting 61
4.11 Summary 61
CHAPTER 5 COMPARISON 70:30 BIO-OIL:METHANOL NPOX 50:50 RESULTS 65
5.1 Methanol 65
5.2 Hydrogen 66

5.3 Carbon Monoxide 67
5.4 Carbon Dioxide 67
5.5 Methane 69
5.6 Gas Production 71
5.7 Benzene 71
5.8 Residual Carbon 73
5.9 Carbon Accounting 74
5.10 Summary 74
CHAPTER 6 NPOX OF BIO-OIL:METHANOL MIXTURES USING THE LARGER NREL REACTOR 77
6.1 50:50 Bio-oil:Methanol 77
6.2 70:30 Bio-oil:Methanol 79
6.3 90:10 Bio-oil:Methanol 81
6.4 Summary 83
CHAPTER 7 CATALYTIC BIO-OIL REFORMING 85
7.1 Catalyst Survey 85
7.2 Importance of NPOX Residence Time 87
7.3 Staged Oxygen Addition 93
7.4 Summary 95
CHAPTER 8 PROCESS SIMULATION AND ECONOMIC ANALYSIS 97
8.1 Surrogate Development 98
8.2 Assumptions for First Generation Process Simulation 100
8.3 First Generation Process Simulation 101
8.4 Additional Assumptions for Second Generation Process Simulation 105
8.5 Second Generation Process Simulation 105
8.6 H2A Results 106
8.6.1 Centralized Cases 106
8.6.2 Distributed Cases 108
8.6.3 Results of H2A for Present Study 109
8.7 Summary 109
CHAPTER 9 METHANOL EXPERIMENTS AND MODELING 111
9.1 Modeling of NREL Experimental Data 112

9.1.1 Methanol 114
9.1.2 Formaldehyde 115
9.1.3 Carbon Monoxide 116
9.1.4 Carbon Dioxide 117
9.1.5 Hydrogen 118
9.1.6 Water 119
9.1.7 Carbon, Hydrogen and Oxygen Balances 119
9.1.8 Summary 121
9.2 Modeling of CFCC Experimental Data 121
9.2.1 Modeling of Pyrolysis Data 124
9.2.2 Modeling of Partial Oxidation Data 127
9.2.3 Summary 128
9.3 Large NREL Reactor Methanol Experiments 129
9.4 Summary 131
CHAPTER 10 OTHER MODEL COMPOUNDS 133
10.1 Pure Components 134
10.2 Model Compound Mixtures 140
10.3 Summary 145
CHAPTER 11 CONCLUSIONS AND FUTURE WORK 147
10.1 Conclusions 147
10.2 Future Work 148
REFERENCES CITED 151
APPENDIX A METHODS FOR ESTIMATING SOURCE OF CO AND CO_2 157
APPENDIX B CONTENTS OF DVD 161
DVD ..... Pocket

LIST OF FIGURES

2.1 Schematic of the initial set-up of experimental apparatus at NREL 9

2.2 Picture of 120 kHz ultrasonic nozzle creating a fine mist 10

2.3 Schematic of initial set-up of experimental apparatus at CFCC..... 16

2.4 Valve configurations for gas sampling system 18

2.5 Initial column configuration 18

3.1 MBMS spectrum at 650ºC and residence time of 0.3 s for pyrolysis (effective O:C ratio = 0.7; λ = 0) of 50:50 (wt. %) bio-oil:methanol mixture 26

3.2 MBMS spectrum at 650ºC and residence time of 0.3 s for NPOX (effective O:C of 1.6; λ = 0.35) of 50:50 (wt. %) bio-oil:methanol mixture..... 26

3.3 Comparison of methanol conversion during neat methanol experiments and 50:50 bio-oil:methanol mixture (wt. %) experiments 30

3.4 Ternary C-H-O diagram showing the region where carbon deposits (graphite) are predicted by equilibrium..... 33

3.5 Temperature profile measured along the reactor at 650ºC with a helium flow 34

3.6 Preliminary overall CO and CO_2 yield as a function of effective O:C (650ºC and ~0.3 s)..... 35

3.7 Estimates of bio-oil CO and CO_2 yield in the preliminary experiments as a function of effective O:C (650ºC and ~0.3 s) 36

3.8 Preliminary yields of H_2 and H_2O as a function of effective O:C (650ºC and ~0.3 s)..... 37

3.9 CO yields during preliminary temperature survey for temperatures between 625 and 700ºC as a function of effective O:C (from 0.7 to ~1.6) at a residence time of ~0.3 s 37

3.10 H_2 yields during preliminary temperature survey for temperatures between 625 and 700ºC as a function of effective O:C (from 0.7 to ~1.6) at a residence time of ~0.3 s..... 38

3.11 Viscosity of bio-oil as a function of methanol concentration (0 to 50 wt. %) and temperature (10 to 40ºC) 39

3.12 Overall CO yield as a function of λ (0 to 0.5) for 50:50, 70:30, and 90:10 bio-oil:methanol mixtures (650ºC; ~0.3 s) 40

3.13 Bio-oil CO yield as a function of λ (0 to 0.5) for 50:50, 70:30, and 90:10 bio-oil:methanol mixtures (650ºC; ~0.3 s) 40

3.14 Overall CO_2 yield as a function of λ (0 to 0.5) for 50:50, 70:30, and 90:10 bio-oil:methanol mixtures (650ºC; ~0.3 s) 41

3.15 Bio-oil CO_2 yield as a function of λ (0 to 0.5) for 50:50, 70:30, and 90:10 bio-oil:methanol mixtures (650ºC; ~0.3 s) 41

3.16 Overall H_2 yield as a function of λ (0 to 0.5) for 50:50, 70:30, and 90:10 bio-oil:methanol mixtures (650ºC; ~0.3 s) 42

3.17 Overall H_2O yield as a function of λ (0 to 0.5) for 50:50, 70:30, and 90:10 bio-oil:methanol mixtures (650ºC; ~0.3 s) 43

3.18 Comparison of estimated bio-oil CO and CO_2 yield for shorter reactor to longer reactor using 50:50 bio-oil methanol mixture at 650 ºC 45

3.19 Comparison of H_2 and H_2O yield for shorter reactor to longer reactor using 50:50 bio-oil methanol mixture at 650 ºC 46

3.20 Comparison of maximum bio-oil CH_4 yield for shorter reactor to longer reactor using 50:50 bio-oil methanol mixture at 650 ºC 47

3.21 Comparison of maximum bio-oil benzene yield for shorter reactor to longer reactor using 50:50 bio-oil methanol mixture at 650 ºC 48

3.22 Comparison of maximum bio-oil residual carbon yield for shorter reactor to longer reactor using 50:50 bio-oil methanol mixture at 650 ºC 48

4.1 Methanol conversion as a function of effective O:C ratio (oxygen in water removed) for λ = 0 to 0.35 observed during 50:50 bio-oil methanol experiments at temperatures between 625 and 850˚C 50

4.2 Overall H_2 yield as a function of effective O:C ratio (oxygen in water removed) for λ = 0 to 0.35 observed during 50:50 bio-oil methanol experiments at temperatures between 625 and 850˚C 51

4.3 Overall CO yield as a function of effective O:C ratio (oxygen in water removed) for λ = 0 to 0.35 and temperature for 50:50 bio-oil methanol experiments 52

4.4 Estimated CO yield from bio-oil as a function of effective O:C ratio (oxygen in water removed) for λ = 0 to 0.35 and temperature for 50:50 bio-oil methanol experiments 53

4.5 Overall CO_2 yield as a function of effective O:C ratio (oxygen in water removed) for λ = 0 to 0.35 and temperature for 50:50 bio-oil methanol experiments temperatures between 625 and 850˚C 54

4.6 Estimated CO_2 yield from bio-oil as a function of effective O:C ratio (oxygen in water removed) for λ = 0 to 0.35 and temperature for 50:50 bio-oil methanol experiments temperatures between 625 and 850˚C 54

4.7 Maximum methane yield from bio-oil as a function of effective O:C ratio (oxygen in water removed) for λ = 0 to 0.35 and temperature for 50:50 bio-oil methanol experiments 55

4.8 Overall carbon to gas conversion as a function of effective O:C ratio (oxygen in water removed) for λ = 0 to 0.35 and temperature for 50:50 bio-oil methanol experiments 56

4.9 Estimated bio-oil carbon to gas conversion as a function of effective O:C ratio (oxygen in water removed) for λ = 0 to 0.35 and temperature for 50:50 bio-oil methanol experiments 57

4.10 Maximum benzene yield from bio-oil as a function of effective O:C ratio (oxygen in water removed) for λ = 0 to 0.35 and temperature for 50:50 bio-oil methanol experiments 58

4.11 Impact of added oxygen for λ = 0 to 0.35 and temperature on the sum of all species with m/z greater than 78 as a percentage of the total signal .. 59

4.12 Impact of added oxygen for λ = 0 to 0.35 and temperature on sum of all species with m/z greater than 128 (given as a percentage of the total signal) 59

4.13 Impact of added oxygen for λ = 0 to 0.35 and temperature on sum of all species with m/z greater than 178 (given as a percentage of the total signal) 60

4.14 Maximum residual carbon yield from bio-oil as a function of effective O:C ratio (oxygen in water removed) for λ = 0 to 0.35 and temperature for 50:50 bio-oil methanol experiments 61

4.15 Overall carbon accounting as a function of effective O:C ratio (oxygen water removed) for λ = 0 to 0.35 and temperature for 50:50 bio-oil methanol experiments 62

4.16 Estimated bio-oil carbon accounting as a function of effective O:C ratio (oxygen in water removed) for λ = 0 to 0.35 and temperature for 50:50 bio-oil methanol experiments 63

5.1 Comparison of methanol conversion for 70:30 bio-oil:methanol mixture to the 50:50 mixture results as a function of λ (0 to 0.42) at temperatures between 650 and 750ºC 66

5.2 Comparison of overall hydrogen yield for 70:30 bio-oil:methanol mixture to the 50:50 mixture results as a function of λ (0 to 0.42) at temperatures between 650 and 750ºC 67

5.3 Comparison of overall CO yield for 70:30 bio-oil:methanol mixture to the 50:50 mixture results as a function of λ (0 to 0.42) at temperatures between 650 and 750ºC 68

5.4 Comparison of estimated CO yield from bio-oil (Method 2) for 70:30 bio-oil:methanol mixture to the 50:50 mixture results as a function of λ (0 to 0.42) at temperatures between 650 and 750ºC 68

5.5 Comparison of overall CO_2 yield for 70:30 bio-oil:methanol mixture to the 50:50 mixture results as a function of λ (0 to 0.42) at temperatures between 650 and 750ºC 69

5.6 Comparison of estimated CO_2 yield from bio-oil (Method 2) for 70:30 bio-oil:methanol mixture to the 50:50 mixture results as a function of λ (0 to 0.42) at temperatures between 650 and 750ºC 70

5.7 Comparison of maximum methane yield from bio-oil for 70:30 bio-oil:methanol mixture to the 50:50 mixture results as a function of λ (0 to 0.42) at temperatures between 650 and 750ºC 70

5.8 Comparison of overall carbon to gas conversion for 70:30 bio-oil:methanol mixture to the 50:50 mixture results as a function of λ (0 to 0.42) at temperatures between 650 and 750ºC 71

5.9 Comparison of estimated bio-oil carbon to gas conversion for 70:30 bio-oil:methanol mixture to the 50:50 mixture results as a function of λ (0 to 0.42) at temperatures between 650 and 750ºC 72

5.10 Comparison of maximum benzene yield from bio-oil for 70:30 bio-oil:methanol mixture to the 50:50 mixture results as a function of λ (0 to 0.42) at temperatures between 650 and 750ºC 72

5.11 Comparison of maximum residual carbon yield from bio-oil for 70:30 bio-oil:methanol mixture to the 50:50 mixture results as a function of λ (0 to 0.42) at temperatures between 650 and 750ºC 73

5.12 Comparison of overall carbon accounting for 70:30 bio-oil:methanol mixture to the 50:50 mixture results as a function of λ (0 to 0.42) at temperatures between 650 and 750ºC 75

5.13 Comparison of estimated carbon accounting from bio-oil for 70:30 bio-oil:methanol mixture to the 50:50 mixture results as a function of λ (0 to 0.42) at temperatures between 650 and 750ºC 75

7.1 Comparison of major product yields (wt. %) with equilibrium calculations (performed using Chemkin 4.1) for three runs using the longer reactor (T = 650ºC; O:C = 1.7; S:C ~ 0.7; t ~0.3 s) with a bed of University of Minnesota catalyst (1 % Rhodium, 1 % Ceria on alumina support) 88

7.2 Comparison of major product yields (wt. %) with equilibrium calculations (performed using Chemkin 4.1) for three runs using the shorter reactor (T = 650 ºC; O:C = 1.7; S:C ~ 0.7; t~0.2 s) with a bed of University of Minnesota catalyst (1 % Rhodium, 1 % Ceria on alumina support) 89

7.3 Benzene profile for Run 1 (long reactor)..... 89

7.4 Profile of all other species for Run 1 (long reactor)..... 90

7.5 Comparison of minor product yields (wt. %) with equilibrium calculations (performed using Chemkin 4.1) for three runs using the longer reactor (T = 650 ºC; O:C = 1.7; S:C ~ 0.7: t~0.3 s) with a bed of University of Minnesota catalyst (1 % Rhodium, 1 % Ceria on alumina support) 91

7.6 Comparison of minor product yields (wt. %) with equilibrium calculations (performed using Chemkin 4.1) for three runs using the shorter reactor (T = 650 ºC; O:C = 1.7; S:C ~ 0.7; t~0.2 s) with a bed of University of Minnesota catalyst (1 % Rhodium, 1 % Ceria on alumina support) 91

7.7 Carbon balances and methanol conversion (wt. %) for gas phase and the first run of catalytic (University of Minnesota catalyst) experiments (T = 650 ºC; O:C = 1.7)..... 92

7.8 Major product yields (wt. %) for gas phase as well as catalytic experiments (University of Minnesota catalyst) using both the longer and shorter reactor (T = 650 ºC; O:C = 1.7)..... 93

7.9 Minor product yields (wt. %) for gas phase as well as catalytic experiments (University of Minnesota catalyst) using both the longer and shorter reactor (T = 650 ºC; O:C = 1.7)..... 94

8.1 Schematic of typical biomass pyrolysis process..... 97

8.2 Process outline used for ASPEN model 101

8.3 Details of feed conditioning..... 102

8.4 Details of reforming and heat recuperation..... 103

9.1 Temperature profiles under reactive conditions at varied molar O:C ratios for NREL methanol experiments (650ºC; ~0.45 s) 113

9.2 Temperature profiles in the zone where they deviate from each other under reactive conditions at varied molar O:C ratios for NREL methanol experiments (650ºC; ~0.45 s) 113

9.3 Methanol mole fraction compared to three kinetic mechanisms available in the literature as well as the CSM models as a function of O:C ratio at 650ºC and a residence time of ~0.45 s..... 114

9.4 CH_2O mole fraction compared to kinetic mechanisms as a function of O:C ratio at 650ºC and a residence time of ~0.45 s..... 115

9.5 CH_2O mole fraction compared to kinetic mechanisms with as a function of O:C ratio at 650ºC and a residence time of ~0.45 s. (CSM model +2 added.)..... 116

9.6 CO mole fraction compared to kinetic mechanisms as a function of O:C ratio at 650ºC and a residence time of ~0.45 s..... 117

9.7 CO_2 mole fraction compared to kinetic mechanisms as a function of O:C ratio at 650ºC and a residence time of ~0.45 s..... 118

9.8 H_2 mole fraction compared to kinetic mechanisms as a function of O:C ratio at 650ºC and a residence time of ~0.45 s..... 119

9.9 H_2O mole fraction compared to kinetic mechanisms as a function of O:C ratio at 650ºC and a residence time of ~0.45 s..... 120

9.10 Carbon balances for methanol experiments using NREL system at 650ºC and a residence time of ~0.45 s..... 120

9.11 Hydrogen balances for methanol experiments using NREL system at 650ºC and a residence time of ~0.45 s..... 121

9.12 Oxygen balances for methanol experiments using NREL system at 650ºC and a residence time of ~0.45 s..... 122

9.13 Temperature profiles for CFCC methanol experiments. These profiles were taken under N_2 flow such that the residence time was ~1 s..... 126

9.14 Mole fractions of CH_3OH, H_2, CO, CH_4 (x10) and CO_2 (x10) for pyrolysis experiments at the CFCC (900ºC; ~0.5 s) compared to kinetic models. 127

9.15 Model predictions of CH_2O yield for pyrolysis experiment at the CFCC (900ºC; ~0.5 s) 128

9.16 Mole fractions of CH_3OH, H_2, CO, and CH_4 (x100) for partial oxidation experiment at the CFCC (650ºC; ~0.4 s; λ = 0.04) compared to kinetic models 129

9.17 Model predictions of CH_2O yield for pyrolysis experiment at the CFCC (650ºC; ~0.4 s; λ = 0.04) 130

10.1 Outlet flow of CO and CO_2 during acetic acid and acetaldehyde experiments at 650ºC 135

10.2 Outlet flow of CO and CO_2 from glyoxal and ethanol experiments at 650ºC 136

10.3 Outlet flow of CO and CO_2 from hydroxyacetaldehyde (HAA) and formaldehyde (CH_2O) experiments at 650ºC 137

10.4 Outlet flow of CO and CO_2 from methanol (MeOH) and acetone experiments at 650ºC 138

10.5 Outlet flow of CO and CO_2 from anisole and phenol experiments at 650ºC 138

10.6 Outlet flow of CO and CO_2 from eugenol and dimethoxybenzene (DMB) experiments at 650ºC 139

10.7 Outlet flow of CO and CO_2 from furfural and guaiacol experiments at 650ºC 140

10.8 Outlet flow of CO and CO_2 from experiments using mixtures of phenol with either methanol or HAA at 650ºC 141

10.9 Conversion of phenol during experiments where it was mixed with HAA or methanol at 650ºC 142

10.10 Outlet flow of CO and CO_2 from experiments using mixtures of anisole with either methanol or HAA at 650ºC 143

10.11 Outlet flow of CO and CO_2 from experiments using mixtures of guaiacol with either methanol or HAA at 650ºC 143

10.12 Outlet flow of CO and CO_2 from experiments using mixtures of furfural with either methanol or HAA at 650ºC 144

10.13 Outlet flow of CO and CO_2 from experiments using mixtures of eugenol with either methanol or HAA at 650ºC 145

LIST OF TABLES

2.1 Typical Composition of Biomass 21

3.1 Value of λ compared to effective O:C for pure methanol, 50:50, 70:30, and 90:10 (wt. %) bio-oil:methanol mixtures as well as pure bio-oil 28

3.2 Results of staged oxygen addition 44

6.1 Results of 50:50 bio-oil:methanol mixture experiments using the larger reactor system at NREL 78

6.2 Results of 70:30 bio-oil:methanol mixture experiments using the larger reactor system at NREL 80

6.3 Results of 90:10 bio-oil:methanol mixture experiments using the larger reactor system at NREL 81

7.1 Equilibrium predictions and NPOX results compared to the results obtained in catalytic experiments (O:C = 1.3) 86

7.2 Equilibrium predictions compared to results of the gas phase and catalytic experiments (O:C = 1.7) 86

7.3 Results of catalytic staged oxygen addition experiments at 650ºC 95

8.1 Typical composition of biomass 99

8.2 Composition of surrogate 99

8.3 Elemental mass closures (from Aspen simulations) RYIELD reactor 103

8.4 Results of 6 cases of first generation aspen modeling 104

8.5 H2A results for centralized cases 107

8.6 H2A results for distributed cases 108

9.1 Methanol experimental results using the CFCC system that illustrate the difficulty of obtaining mass closure 123

9.2 Methanol experimental results using CFCC system illustrating the difficulty associated with reproducibility 125

9.3 Methanol experiments performed using large NREL reactor 131

10.1 Composition of surrogate developed in Chapter 8..... 134

LIST OF SYMBOLS AND ABREVIATIONS

$C.A._{bio\text{-}oil}$ – Bio-oil carbon accounting (%)
$C.A._{overall}$ – Overall carbon accounting (%)
$C.G._{bio\text{-}oil}$ – Bio-oil carbon to gas conversion (%)
$C.G._{overall}$ – Overall carbon to gas conversion (%)
CFCC – Colorado Fuel Cell Center
DMB – Dimethoxybenzene
EtOH – Ethanol
GC – Gas choromatograph
HAA – Hydroxyacetaldehyde
MeOH – Methanol
MBMS – Molecular beam mass spectrometer
NREL – National Renewable Energy Laboratory
NPOX – Non-catalytic partial oxidation
O:C – Oxygen to carbon ratio (molar)
Effective O:C – Oxygen to carbon ratio with water removed (molar)
PAH – Poly-aromatic hydrocarbon
PSA – Pressure swing adsorption
$R_{CO\text{-}CO2}$ – Ratio of CO to CO2 in neat methanol experiments
R.T. – Residence time (s)
S:C – Steam to carbon ratio (molar
SCCM – Standard cubic centimeters per minute (25ºC, 1 atm)
SLPM – Standard liters per minute (25ºC, 1 atm)
T_{SR} – Steam reformer temperature (ºC)
$Y_{i,bio\text{-}oil}$ – Yield for species i from bio-oil (%)
$Y_{i,overall}$ – Overall yield of species i (%)
λ – Equivalence ratio (ratio of oxygen added to that needed for complete combustion)

ACKNOWLEDGEMENTS

I would like to express my deepest gratitude to Dr. Anthony M. Dean for his patience, guidance and support. I cannot imagine a better mentor for me than he was. I would also like to thank Dr. Robert J. Evans who served as co-advisor for much of my research. His knowledge and experience was a great asset to me during my research. Dr. Richard French and Dr. Stefan Czernik were available for guidance as I learned about the process and how to properly conduct the experiments at the National Renewable Energy Laboratory (NREL). Their support was truly appreciated. Dr. Matt Ratcliff also added ideas early on, which proved very helpful. Joelle DiBenedetto and Shannon McKibben assisted with many of the experiments at NREL. I was lucky to have two such capable people helping out. Mike Penev from NREL did much of the Aspen modeling. His efforts are greatly appreciated and made the modeling much easier than it would have otherwise been.

Dr. Hans-Heinrich Carstensen was always available to give invaluable advice and encouragement, especially during experiments performed at the Colorado Fuel Cell Center (CFCC). I thank him for that. I want to thank Dr. Stephanie Villano and Jessica Hoffman for their collaborations during experiments at CFCC. I would also like to thank Matthew Hurliman who, under the direction of Dr. Matt Liberatore, performed the rheology experiments at the Colorado School of Mines. I thank my thesis committee for their service and patience.

I would also like to thank the U.S. Department of Energy: Office of Energy Efficiency and Renewable Energy's support under the Hydrogen, Fuel Cells & Infrastructure Technologies Program. This support was provided via NREL.

I dedicate my thesis to my family, particularly my wife.
Without her love and support,
I would not have accomplished this work.

CHAPTER 1
INTRODUCTION

With the world's energy demands rapidly increasing, it is necessary to look to sources other than fossil fuels, preferably those that minimize greenhouse gas emissions. One such renewable source of energy is biomass that has the added advantage of being a near-term source for producing hydrogen as the US transitions to a hydrogen economy. A Billion-Ton Vision study[1] identified a potential 1.3 billion ton renewable supply of biomass in the United States that could be used as a resource to produce transportation fuels. This represents the potential for the annual production of 100–130 million tons of hydrogen, which is sufficient to fuel 300 million fuel cell vehicles[2] and displace more than 30% of the current petroleum usage.

Although there are a variety of potential biomass feedstocks that could be used for producing hydrogen, their use presents several challenges. These include handling and drying as well as regional and seasonal availability and variability. An additional challenge is the impact of impurities such as sulfur, nitrogen or chlorine on catalytic conversion and on product purification steps. Processes based on biomass must be feedstock flexible and must minimize costs for feedstock collection, transport, and processing to become commercially viable.

While there are several potential routes for the thermal conversion of biomass to produce hydrogen, given the near-term technical barriers to hydrogen storage and delivery, distributed technologies at or near the point of use are especially attractive. One such route combines the fast pyrolysis of biomass with non-catalytic partial oxidation. The fast pyrolysis is performed close to the source of the biomass to create a higher energy-density product, bio-oil, which is then transported to the location where it is converted to hydrogen and carbon dioxide. This route is especially well suited for smaller-scale reforming plants located at

hydrogen distribution sites such as service stations. There is also the potential for automated operation of the conversion system[3,4].

Fast pyrolysis is a thermal decomposition process that converts biomass to liquids with yields as high as 70–80% (including water) based on the starting biomass weight[5]. This technology has been under development since the 1980s, mostly for producing alternative liquid fuels and chemicals. Typical lower heating values (LHV) of bio-oil are in the range of 15-19 MJ/kg. The first commercial plant producing bio-oil (100 tons/day) for energy applications was constructed by DynaMotive in West Lorne, Canada in 2005. Bio-oil is also a feedstock for several processes for producing fuels, chemicals, and materials[6].

Bio-oils are multi-component mixtures comprised of different size molecules derived primarily from depolymerization and fragmentation reactions of the three key biomass building blocks: cellulose, hemicellulose, and lignin. As a result the elemental composition of bio-oil has a much higher oxygen content than is found in petroleum, leading to properties that are significantly different from those for standard fuels. In fact, using the same distillation processes as for petroleum would lead to a 50% residue in the case of bio-oil. The residue is due both to the non-volatile components that are initially present in bio-oil as well as the high reactivity of bio-oil which leads to the formation of additional non-volatile species during heating. Typical elemental analysis of bio-oil indicate 54-58 wt.% carbon, 5.5-7 wt.% hydrogen, 35-40 wt.% oxygen, ~0.2 wt.% nitrogen, and ~0.2 wt.% ash (dry basis). The typical water content is between 15 and 30 wt.%. Other physical and chemical properties of bio-oil have been reported by Oaasma and Czernik[7]. Based on the elemental composition given above, the maximum hydrogen yield is between 20.4 and 22.1 kg hydrogen per 100 kg bio-oil (dry basis), with much of the hydrogen coming from steam used in the reforming process. Assuming a 60% yield of water-free bio-oil, 12-13 kg hydrogen can be potentially produced from 100 kg of wood using such an approach.

1.1 Past Research

Past research at NREL focused on catalytic steam reforming of bio-oil[4,8-12]. Other researchers have studied this approach with[13-25] or without[26-30] steam addition (i.e. only steam generated from the moisture content of the oil is available). Such processes are typically conducted at temperatures greater than 800ºC in the presence of different catalysts. A group at the University of Twente in the Netherlands have looked at a non-catalytic partial oxidative (NPOX) approach, but only reported results at temperatures similar to those used in catalytic steam reforming[31]. In their NPOX run, they use a fluidized bed of sand and found that oxygen addition led to higher carbon to gas conversions than pyrolysis. This was true during both non-catalytic and catalytic experiments. They also observed enhanced gasification with increased temperature under pyrolysis conditions (fluidized bed), which were much improved with the presence of a catalyst.

From pyrolysis of pine derived bio-oil at 790ºC, the group at the University of Twente observed a CO to CO_2 ratio of 8 with carbon to gas conversion of 65%. From NPOX of beech derived bio-oil (equivalence ratio = 0.23) at 835ºC, the observed ratio of CO to CO_2 was 1.8 with carbon to gas conversion of 87%. The substantial decrease in the ratio of CO to CO_2 in the NPOX experiment was due primarily to increased CO_2. It is not clear how much of the CO_2 increase was due to differences in temperature and feedstock rather than the addition of oxygen. A more consistent data set is required using the same bio-oil in order to truly determine how oxygen addition affects bio-oil conversion and product selectivity. Additionally, the group from the University of Twente looked at decoupling evaporation, primary conversion of bio-oil, and gas conditioning. They found that this would be beneficial. A similar approach is proposed in the present research, but without the presence of a fluidized bed.

Researchers at the Institute for Technical Chemistry at Karlruhe used a high-pressure oxygen-blown entrained flow reactor that operated at 1200ºC to gasify a bio-oil/char slurry[32]. A group at the University of Minnesota has begun investigations into the catalytic partial oxidation/autothermal reforming of model

compounds of bio-oil, but again at temperatures similar to catalytic steam reforming[33]. Previous research at NREL demonstrated that the formation of thermally stable aromatics and polycyclic-aromatic hydrocarbons (PAHs) increases significantly at temperatures higher than 700°C under pyrolysis conditions of biomass model compounds[34-36]. Similar observations have been reported elsewhere[37,38].

1.2 Present Research

The objective of this research is to address the challenge of distributed hydrogen production from bio-oil with the target of producing hydrogen at $2.00 to 3.00/kg by 2012[39]. The focus is the non-catalytic partial oxidation (NPOX) of bio-oil over a wide temperature range starting at temperatures well below those used for catalytic steam reforming (625ºC) and ending at temperatures similar to catalytic steam reforming (850ºC). A much wider range of added oxygen is explored than is used by the group from the University of Twente[31]. Rather than use a fluidized bed as is the case in their study, a simple tubular reactor configuration is utilized. The current research seeks to determine how the extent of conversion is affected by temperature and oxygen addition, with particular emphasis on identifying those regimes where CO and H_2 production are maximized with minimal production of aromatics and carbon deposits. This research is funded by the Department of Energy's Hydrogen Fuel Cell and Infrastructure Technology Program through the National Renewable Energy Laboratory (NREL).

A system has been developed for volatilizing bio-oil with manageable carbon deposits using ultrasonic atomization and by modifying bio-oil properties, such as viscosity, by blending/reacting bio-oil with methanol. Non-catalytic partial oxidation of bio-oil is then used to achieve significant conversion to CO with minimal aromatic hydrocarbon formation. The non-catalytic reactions occur primarily in the gas phase. However, some nonvolatile components of bio-oil present as aerosols may react heterogeneously. The product gas can then be

passed over a packed bed of catalyst where further reforming as well as water gas shift reactions would complete the conversion to hydrogen[40].

The approach described above should require significantly less energy and lower catalyst loadings than conventional catalytic steam reforming due to the significant conversion in the non-catalytic step. The goal of the catalytic step is to complete the reforming and selective oxidation of the bio-oil as well as to catalyze the water gas shift reaction without catalyzing methanation or oxidation of CO and H_2, thus attaining equilibrium levels of H_2, CO, H_2O, and CO_2 at the exit of the catalyst bed. The focus of this research is on the NPOX step. However, limited catalytic results are presented in order to demonstrate the potential for the overall process.

The experimental set-up used for the NPOX experiments described above will be discussed in Chapter 2. The initial set-up was inherited from previous work at NREL. However, modifications were required to make the apparatus more suitable for the present work. Also discussed in Chapter 2 is an additional experimental apparatus located at the Colorado Fuel Cell Center on the Colorado School of Mines Campus. Again, the initial set-up was inherited from previous researchers, but was modified. This apparatus was used for kinetic modeling experiments discussed below. A discussion of the feedstocks and some rheology experimental details will conclude the chapter.

Following the discussion of the experimental systems is a discussion of the experimental results of both the NPOX (Chapters 3 through 6) and limited catalytic (Chapter 7) bio-oil reforming experiments. As discussed above, the effects of both temperature and added oxygen were explored during NPOX experiments. Because methanol was added to the bio-oil, the effects of this methanol addition on the NPOX chemistry were also explored by varying the amount of methanol added. Rheological experiments were also performed to determine the extent of viscosity reduction by methanol addition (see Chapter 3). The NPOX experiments demonstrated the potential for surprisingly high conversion of the carbon in bio-oil to CO, suggesting this might be a viable approach to produce distributed H_2.

Given the encouraging results, these results were used as the basis for developing an ASPEN model of the process (Chapter 8). A preliminary simulation focused primarily on mass and energy balances. A more detailed simulation was used to get more realistic results and was the basis for a hydrogen analysis (H2A), which is the method used by the DOE to evaluate the cost effectiveness of the various potential routes to Hydrogen.

In addition to experiments performed using the bio-oil itself, representative model compounds were selected for experiments to gain further insight into the chemistry involved in the complex bio-oil system. Since methanol was added to the bio-oil, experimental efforts began with it. The results of these experiments as well as kinetic modeling are presented in Chapter 9. Further model compound experiments, including mixtures of model compounds, were also performed (Chapter 10).

Following the discussion of the results is a summary and conclusion section (Chapter 11), which also includes recommendations for future experiments.

CHAPTER 2
EXPERIMENTAL DETAILS

Two principal experimental systems were used during the course of this research. One was located at the National Renewable Energy Laboratory (NREL). This system was ideal for experiments performed using bio-oil since it included a nozzle suitable for feeding bio-oil/methanol mixtures as well as a triple-quadrupole molecular beam mass spectrometer (MBMS), which served as a universal detector. In addition, the mass spectrometer was capable of handling particulate matter that might result from the bio-oil reactions. The NREL data acquisition system allowed rapid data collection. However, the temperature-distance profiles along the reactor were not as well defined with this system, making it less suitable for detailed kinetic measurements that could be compared to model predictions. The other system, located in the Colorado Fuel Cell Center (CFCC) on the Colorado School of Mines campus was used for kinetic experiments with model compounds. Conversions and product distributions were determined by quantitative gas chromatography. Methanol experiments were done on both systems, allowing a convenient check on the consistency of the data.

In this chapter, the two experimental systems as well as modifications to each and the methods used to analyze data for each will be discussed. Next, the composition of the bio-oil feedstock will be discussed. This is followed by a discussion of the rationale for the choice of model compounds. The procedure used to measure the viscosity of bio-oil with varied amounts of methanol added will be then described. A discussion of a scaled up version of the NREL reactor will conclude the chapter.

2.1 System at the National Renewable Energy Laboratory

The initial set-up of the experimental apparatus located at the NREL is shown in Figure 2.1. Several changes to this apparatus, which were made to

make the apparatus more suitable for the non-catalytic partial oxidation (NPOX) as well as the catalytic experiments, will be discussed in section 2.2. These modifications included changes to the outer tube, changes to the entrance region of the reactor, an upgraded nozzle, and other reactor configurations.

As shown in Figure 2.1, the bio-oil (mixed with varied amounts of methanol) as well as all the liquids used either for calibrations or for model compound experiments were fed into the top of the vertical quartz reactor using a syringe pump followed by a 120 kHz ultrasonic nozzle (Sono-Tek) to ensure steady flow at low flow rates. Figure 2.2 is a picture of the ultrasonic nozzle producing a fine mist while flowing water. (A similar mist was observed when using bio-oil.) The fine mist allowed for optimal conditions of heat transfer, mixing, and contact between the components of the bio-oil:methanol mixture (or other liquid) and oxygen. These conditions were especially important with respect to non-volatile components (oligomers) of the pyrolytic lignin fraction of bio-oil as they allowed for the possibility of reaction of those components.

The nozzle was fitted with a shroud (not shown) through which a carrier gas (helium with 10 sccm argon as an internal standard) and oxygen can be admitted. This shroud directed the flow of the carrier gas/oxygen mixture through a 0.23 mm gap around the tip of the nozzle in order to ensure that the stream of mist traveled mainly down the center of the reactor rather than getting on the walls. When too much bio-oil accumulated on the wall, a char residue plug was formed from the nonvolatile components due to slower heat transfer. This char residue was analogous to the residue left behind when distilling bio-oil.

The quartz reactor was 32 cm long with an inside diameter (ID) of 1.1 cm and an outside diameter (OD) of 1.3 cm. A Tygon tube and tube clamps were used to connect and create a seal between the reactor and the nozzle. The reactor was inserted into a 2 piece quartz tube (ID = 4 cm) inside an electric furnace with 5 different heating zones, each with its own thermocouple and controller. The first 22 cm of the reactor were used to heat the feed to the reaction temperature. In order to prevent overheating, a 6 cm long 1 cm thick chamber full of insulating material was installed around the reactor starting 6 cm

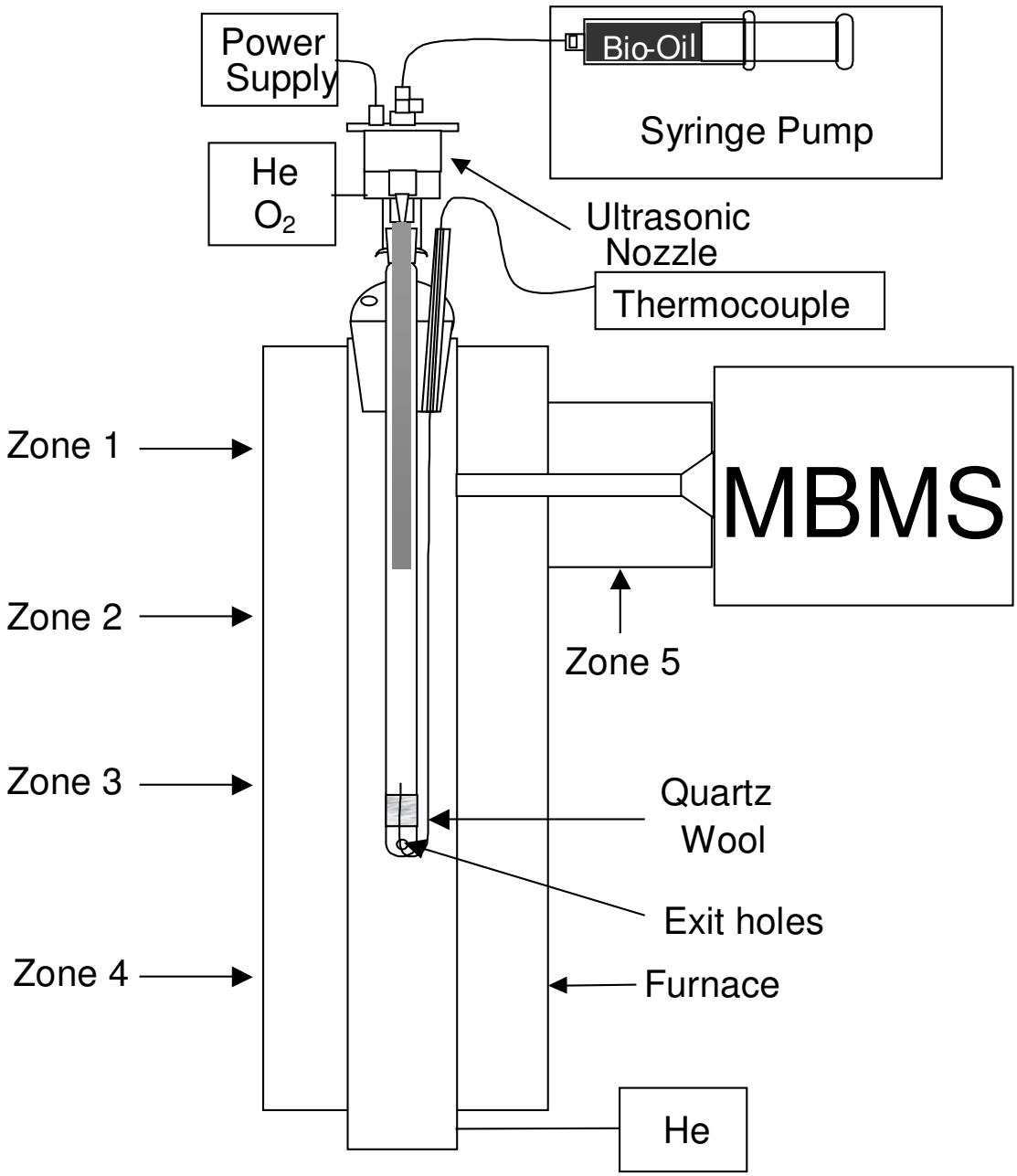

Figure 2.1. Schematic drawing of the initial set-up of experimental apparatus at NREL. The bio-oil/methanol mixture is fed through the syringe pump and dispersed by the ultrasonic nozzle at the top of the vertical reactor (1.1 cm I.D. and 32 cm long). A shroud surrounding the nozzle directs the oxygen/helium (400-550 sccm combined) flow around the tip of the nozzle to help direct the bio-oil/methanol down the center of the reactor. The reactant stream is quenched by passing into the outer tube, where a large helium flow (10 SLPM) dilutes and carries these species to the molecular-beam-mass-spectrometer for analysis. A small (1 cm) layer of quartz wool is located at the bottom of the reactor to catch any particulate matter.

from the top, which was approximately the same point that the reactor enters the furnace.

The actual reaction zone (defined as the region where the temperature was within 15 K of the set point temperature) was typically 10 cm long. However, it should be noted that more reactive species probably started reacting before reaching the “reaction zone”. It should also be noted that the effective length of this zone was longer during experiments with more added oxygen due to the exothermicity of the partial oxidation reaction. The estimated residence time in the hot zone was maintained at ~0.3 s, which takes into account the inlet and outlet flow rates as well as the temperature profile. The temperature profile was measured by moving a thermocouple along the length of the reactor while flowing a representative amount of helium through the reactor and taking readings every centimeter. In all experiments, a small amount of quartz wool (~ 1 cm high) was placed at the bottom of the reactor to catch any particulates.

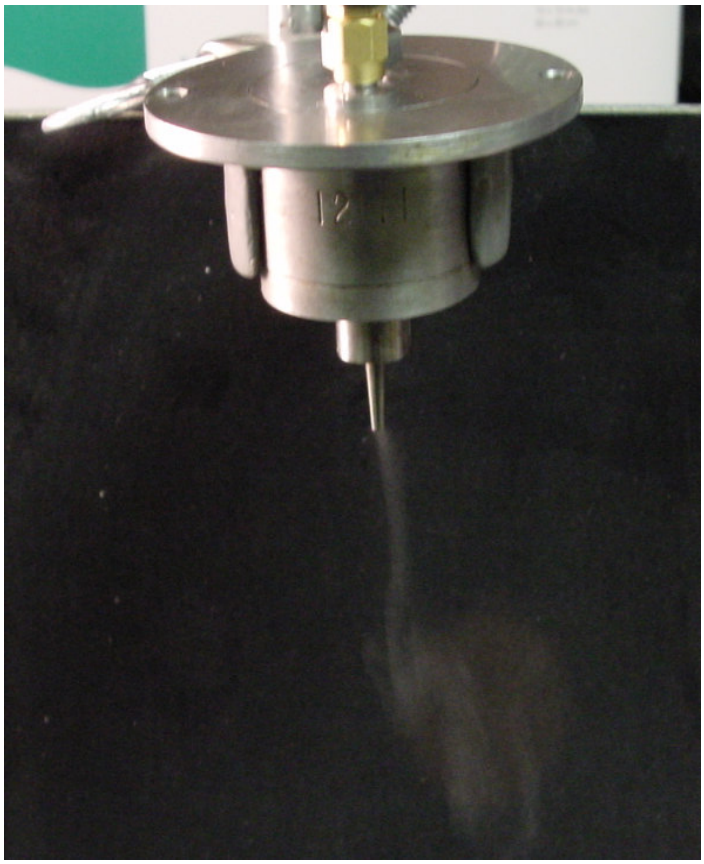

Figure 2.2. Picture of 120 kHz ultrasonic nozzle creating a fine mist. This nozzle was used during preliminary and other experiments to introduce bio oil:methanol mixtures into the reactor and ensure steady flow down the center of the reactor.

For the limited experiments where a catalyst bed was used, the fixed bed of spheres was 0.8 to 3 cm high (1 – 2 g) and was located just above the quartz wool shown in Figure 2.1. The catalysts used for these experiments included 0.5

wt. % rhodium, ruthenium, platinum, and palladium (all supported on alumina and supplied by Englehard). Experiments were performed using pure alumina as well. Additional catalytic experiments were performed using a 1 wt % rhodium and 1 wt % ceria (based on initial weight of support), both on a spherical alumina support (1.3 mm diameter), that was obtained from Prof. Lanny Schmidt's group at the University of Minnesota. The catalyst was similar to that used in several of their studies[33,44] except that spheres were used rather than foam monoliths.

The reactor effluent passed through four pinholes (3mm) near the bottom of the reaction tube and entered the larger outer tube where it was diluted by approximately a factor of 20 by a high flow of helium (10 SLPM) entering through the bottom of the larger tube. This helium stream served several purposes:

(1) The dilution resulting from this high flow served to effectively quench the reaction and rapidly carry the products to the triple-quadrupole MBMS for analysis. The estimated residence time in this larger tube was ~0.4 s.

(2) The dilution allowed for higher concentrations inside the reactor than would have otherwise been possible without saturating the mass spec. detector.

(3) The high flow rate resulted in a combined stream that was typically 98-99% helium, thus minimizing matrix effects (i.e., response factors being dependent on composition). A small amount of argon (10 sccm) added to the gas feed to the reactor also assisted in minimizing these matrix effects as the signal of each species was normalized to the argon signal during analysis.

2.2 NREL system modifications

The modifications made to the NREL system were made as issues with the system were identified. The issues as well as the solutions are discussed in this section.

2.2.1 Changes to Outer Tube

The residence time (~0.4 s) of the reactor effluent in the outer tube was deemed unacceptable as this was longer than the ~0.3 s residence time in the hot zone of the reactor. Accordingly, the ID of the upper piece of outer tubing was reduced from 4.0 cm to 1.7 cm. This reduction led to a decrease in the

residence time to approximately ~0.04 seconds in the outer tube region, which was deemed much more acceptable. The original two-piece construction was replaced with a single piece to maintain a better seal.

2.2.2 Changes to the Entrance Region

As discussed previously, bio-oil accumulation on the upper wall of the reactor was undesirable and led to the formation of a carbonaceous plug about 10 cm from the top of the reaction. In the original design, ~5% of the bio-oil reached the wall and formed the plug. To correct this problem, this entrance region was expanded to an ID of 2.0 cm and tapered back down to the original 1.1 cm just before reaching the higher temperature the reaction zone. Coupled with an upgrade to a 25 kHz nozzle (described below), this change led to a decrease in the amount of bio-oil accumulation on the walls to a much more manageable 1-2%, which did not cause any problems with reactor operation.

A second issue with the feeding of the bio-oil was the melting of the Tygon tubing initially used as a connection and seal between the ultrasonic nozzle and quartz reactor. This tubing was replaced with a quartz plate attached to the top of the reactor. The nozzle was then placed on top of this plate and an o-ring and c-type clamps were used to create a more effective and consistent seal. An additional benefit was the plate kept the nozzle more level and pointed directly down the center of the reactor. A fan was also employed for cooling of the nozzle and the entrance region external to the furnace such that bio-oil:methanol mixture or other liquid was introduced at close to room temperature.

2.2.3 Nozzle Upgrade

Due to the high viscosity of the feed, the addition of methanol was necessary to reduce the viscosity sufficiently such that it could be fed using the original 120 kHz ultrasonic nozzle. Methanol was used since it is the most cost effective solvent of the polar solvents that could be used. This nozzle was rated for a power setting of up to 5 Watts. A 50:50 bio-oil:methanol (wt. %) mixture required a power setting of ~2.7 Watts for optimal atomization. The optimal

settings for a 70:30 and 90:10 bio-oil methanol mixtures using this nozzle were 6.3 W and 9.8 W, respectively. Running at higher powers than the nozzle rating for any extended period was not advisable since it could burn out the nozzle.

Since the 120 kHz nozzle was not suitable for feeding bio-oil without mixing with at least 50 % methanol, some of the bio-oil was sent to Sono-Tek to evaluate whether any nozzle would be capable of feeding this viscous fluid. Tests performed by Sono-Tek demonstrated that bio-oil without methanol addition could be fed using a 25 kHz nozzle. The nozzle and corresponding power supply were purchased. This nozzle was rated for power settings up to 15 watts. Although not necessarily reflected in the required power settings (2.9-3.4 W for 50:50, 5.0-5.5 W for 70:30, 8.2-8.3 W for 90:10, and 12.9-15.0 W for bio-oil with no methanol addition), this nozzle provided significantly more efficient atomization than the 120 kHz (even for the 50:50 mixture). The more efficient atomization was reflected by a more steady signal in the data. It was not completely clear why this was the case. It may have been due to the larger atomizing surface or simply because the nozzle was newer.

2.2.4 Other Reactor Configurations

Initial attempts to obtain temperature profiles of the reactor under reactive conditions showed changes in the chemistry due to the presence of the thermocouple (i.e., it was acting as a catalyst). A new reactor was constructed with a quartz thermocouple well down the center such that a thermocouple could be introduced through the bottom of the reactor without coming into contact with the reactive mixture. Although the presence of the thermocouple well could also impact both the extent of reaction and the temperature reading, it allowed for a more accurate determination of the temperature profile under reactive conditions than would have been possible otherwise. During temperature profiling experiments, the temperature was measured every 1 cm along the reactor axis.

Another reactor was designed to explore the effects of staged oxygen addition. This reactor had a small tube running down the side of the reactor. At the end of the tube was a ring surrounding the reactor. In order to assist with

mixing, four opposite holes on each side of the reactor were made. Because the outer tube did not allow this reactor to be inserted into the 1.7 cm ID outer tube, a new outer tube with an ID of ~1.9 cm was made.

In order to look at the importance of the NPOX step with respect to the process as a whole, the residence time before the catalyst was varied. Rather than risk altering transport effects and to assure that any changes in the results were due to the changes in the residence time, the reactor length was shortened without changing the flow rates of the liquid (bio-oil/methanol and water) or gaseous feeds (helium, oxygen, and argon).

2.3 Molecular Beam Mass Spectrometer Analysis

The MBMS served as a universal detector and allowed for real time data collection. The analysis of pyrolysis products by MBMS has been described by Evans and Milne[43]. The electron ionization energy used in this study was 25 eV. The dilution of the reactor effluent (described above) reduced the potential problems caused by matrix effects associated with the MBMS analysis. Argon was introduced at a constant flow rate (10 sccm) as an internal standard for the quantitative analysis of all the major products. The peaks used to quantify each product species were as follows: CO – m/z = 28, CO_2 – m/z = 44, CH_4 – m/z = 15, H_2 – m/z = 2, H_2O – m/z = 18, and benzene – m/z = 78. Any residual carbon formed during the reaction was determined by subsequent oxidation of carbon (monitored as mainly CO_2 with small amounts of CO as well) after shutting off the feed and maintaining the oxygen/helium flow. All signals were normalized to the signal of argon during analysis to further correct for any potential variations in the instrument response. Any unreacted methanol was also quantified using m/z = 31 rather than 32 due to the oxygen potentially present in the system. Wherever possible and deemed necessary, fragment ions attributed to higher molecular weight species were subtracted from a particular m/z using the measured ratio of that m/z to the m/z of the parent species in the calibration experiments.

Calibrations were performed daily by flowing each measured species individually (with the exception of benzene and methanol which were introduced

as a 1:99 benzene:methanol mixture on a weight basis) at a minimum of 3 flow rates to establish a 3 point calibration curve. A response factor for each species was derived from the slope of the linear least-squares fit of the calibration data. Flow rates for these calibrations were typically chosen such that the highest value was higher than the highest flow observed for that species and the lowest was lower than the lowest flow observed for that species. Gases were introduced using mass flow controllers. Flows were verified and corrected (if necessary) using a digital bubble flowmeter. Liquids were introduced using the syringe pump and ultrasonic nozzle. A calibration curve for the syringe pump was created by measuring the time it took to inject a given volume at different flow rates.

Typical R^2 values from the linear least squares fit for all species other than H_2 and H_2O were greater than 0.998. The R^2 value for H_2O was typically greater than 0.97. However, H_2O had a tendency to stick to the walls inside the instrument creating a great deal of uncertainty in its signal. H_2 also typically had R^2 values greater than 0.97. However, there was a larger uncertainty with H_2 stemming from the fact that its response factor was approximately an order of magnitude lower than for other species. The uncertainties in calibration are accounted for during the propagation of error analysis discussed in Chapter 3.

2.4 System at the Colorado Fuel Cell Center

The initial set-up of the experimental apparatus at the Colorado Fuel Cell Center (CFCC) is shown in Figure 2.3. This set-up was nearly identical to that used by Al Shoaibi[41] and was set up to allow flowing up to 2 liquid and 3 gas feeds to the reactor. Several changes were made to improve the versatility of this system; these will be discussed in Section 2.5.

Liquid feeds were pumped using milliGAT™ pumps (Global FIA), which were capable of pumping between 0.0001 and 167 µL/s at a steady flow rate. Calibrations revealed that the flow was typically good to within 3%. The liquids are pumped into a vaporizer (to dampen any pulsations and allow for better mixing of reactants) where a type K thermocouple was used to measure the temperature, which is controlled by a Eurotherm 2216e PID. Gas feeds were

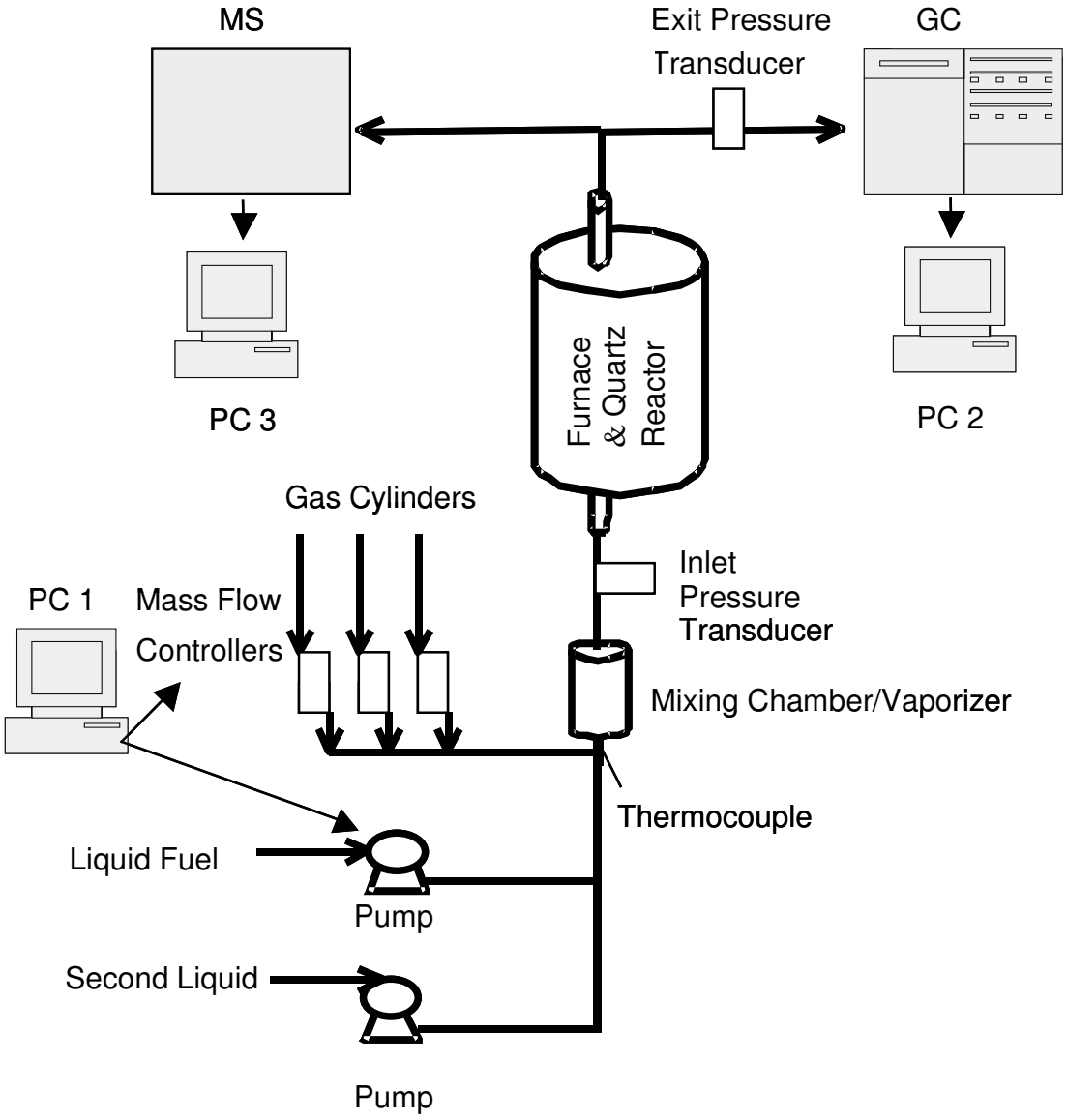

Figure 2.3. Schematic of initial set-up of experimental apparatus at CFCC.

adjusted using mass flow controllers (MFCs) from MKS (model 1479A). LabView software by National Instruments was used to control the mass flow controllers as well as the pumps. The lines between the vaporizer and the reactor were heated to above 120°C using OMEGALUX heating tape to keep the fuel and water from condensing in the plumbing.

The reactor itself was made of quartz and was 32 cm long with an inside diameter of 6 mm. Quartz was used as it is generally inert and allowed for investigation of gas phase chemistry. The reactor was placed inside a furnace with three separate heating zones, each with its own thermocouple and temperature controller (Eurotherm 2216e PID). The lines from the reactor to the analytical equipment were also heated to temperatures above 120°C with OMEGALUX heating tape.

Two separate instruments were used for data acquisition and analysis. An MKS Cirrus mass spectrometer was used to monitor species exiting the reactor and to determine when steady-state had been achieved. An HP5890 GC was used to detect and quantify hydrocarbons/oxygenates, H_2, CH_4, CO, and CO_2 as well as nitrogen, which served both as a diluent and a reference gas. This GC is affixed with a TCD detector as well as a flame ionization detector (FID). Two ten port gas sampling valves affixed with sample loops (see Figure 2.4 for configuration) are used to introduce the reactor effluent into the GC for analysis. Preceding the TCD are 60/80 mesh Hayesep R (1/8" x 20 ft; Supelco) and 80/100 mesh Carboxen 1000 (1/8" x 20 ft) columns (see Figure 2.5). The Hayesep R serves to separate the permanent gases (H_2, CH_4, CO, CO_2, N_2) from higher molecular weight species which would ruin the Carboxen column. At a prescribed time (typically 10 minutes) the valve is switched back to the closed position such that these species are vented. An SPB-1 column separates the higher molecular weight species prior to the FID (see Figure 2.5).

2.5 CFCC System Modifications

Changes were made to the CFCC system in order to make the system more versatile. These changes are discussed in this section.

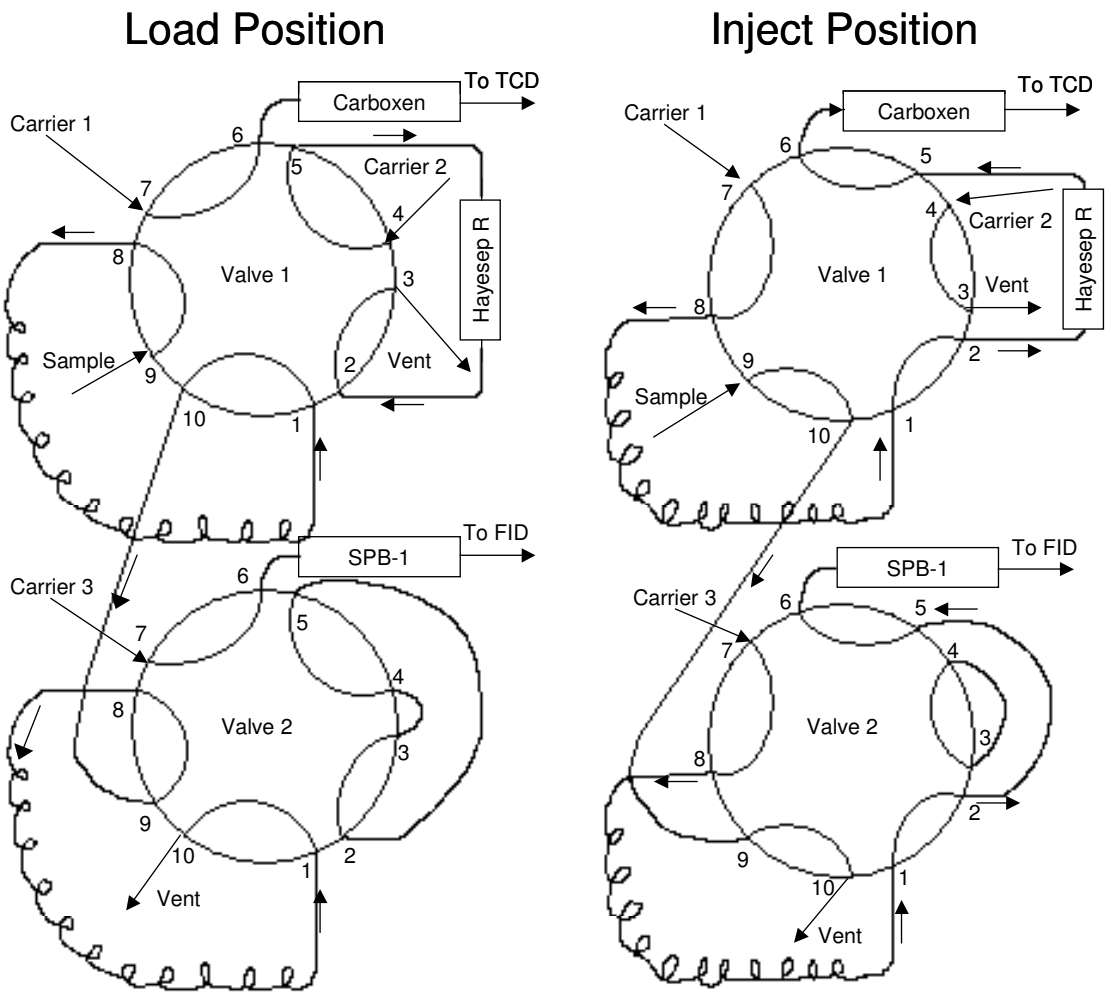

Figure 2.4. Valve configurations for gas sampling system. In the load position, sample is loaded into the sample loop. In the inject position, the sample is pushed into the GC column by the carrier gas.

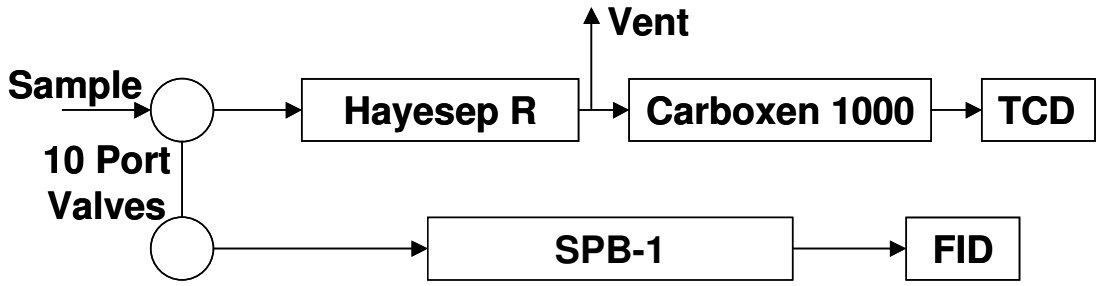

Figure 2.5. Initial column configuration. The two circles represent the two ten port valves shown in Figure 2.4. The vent in between the Hayesep R and Carboxen 1000 columns is the same as the vent coming off Port 3 of Valve 1.

2.5.1 Bypass

Since the concentration in the mixing chamber could take 10-20 minutes to reach steady-state, it was desirable to bypass the chamber during burn-off to avoiding having to wait for the return to steady-state. The original configuration did not allow for such a bypass. A two way valve and a three way valve were inserted into the system to provide the necessary bypass. The two way valve serves to open the bypass. The three way valve connected either the bypass or the mixing chamber to the reactor.

2.5.2 Column Changes

Through inspections of chromatograms provided by Supelco, it was determined that the analysis time could be reduced without losing any analysis capabilities (or risking damage to the Carboxen column) by decreasing the length of the Hayesep R Column. Accordingly, a 6 ft x 1/8 inch 60/80 mesh Porapak R (same packing as Hayesep R) column was acquired (Supelco). This column reduced the time for CO_2 (the longest eluting species on the TCD side) elution from ~20 to ~15 minutes. About ten minutes of that time was spent on the Carboxen column.

2.5.3 Upgrade of Mass Flow Controllers

During calibration of the MKS mass flow controllers (MFCs), internal leaks were discovered. Repairs to these MFCs proved to be almost as costly as buying new ones. Accordingly, new MFCs were acquired (Alicat 16 series). Calibrations using a DryCal were performed. The agreement was within 3%.

2.6 GC Analysis

Calibration curves with a minimum of three concentrations (mole basis) were created for each species (CO, CO_2, CH_4, N_2, H_2, and CH_3OH) in order to obtain response factors to be used to determine the concentration of experimental data. Typical purities of gases (General Air) used for these calibrations were greater than 99%. Two to three gases with varied

concentrations were introduced using MFCs to create the calibration curve. The typical R^2 values from a linear least square fit were greater than 0.99 for all species. By running a calibration standard (General Air) of known concentrations of CO, CO_2, CH_4 and H_2), it was determined that the error in these calibrations was ± 0.02 mole fractions. This error can lead to large uncertainties in the case of small mole fractions. Due to tailing of the methanol peak, its absolute error is estimated to be 6%. The large error for methanol combined with the uncertainty of dilute species leads to a great deal of uncertainty in the mass balances.

2.7 Feedstocks

This section describes the composition of the bio-oil used and the choice of model compounds selected to gain further insight into the chemistry in the complex bio-oil mixture.

2.7.1 Bio-oil

The bio-oil used in this work was produced by fast pyrolysis of poplar wood in 1997. The details of the conditions under which the bio-oil (M2-10) was produced as well as its characterization have been reported by Scahill et al.[42]. Due to the long storage time at ~4ºC, the oil had aged such that variations in the feedstock from one experiment to the next were not of concern during the present study, which was confirmed by the consistency of the data even when extended periods of time passed between experiments. The elemental composition of the M2-10 bio-oil (wt. %) prior to the methanol addition was 48.2% carbon, 7.2% hydrogen, and 44.6% oxygen including the 17% water by weight. The maximum stoichiometric H_2 yield (from steam reforming) for this oil would be 17.9 kg H_2 per 100 kg bio-oil on a wet basis (Eqn. 2.1).

$$CH_{1.32}O_{0.46}\cdot 0.23H_2O + 1.31H_2O \rightarrow CO_2 + 2.19H_2 \qquad (2.1)$$

Using the partial oxidation process that this study employs would reduce the maximum stoichiometric H_2 yield to 13.4 kg H_2 per 100 kg bio-oil (Eqn. 2.2).

$$CH_{1.32}O_{0.46}\cdot 0.23H_2O + 0.27O_2 + 0.77H_2O \rightarrow CO_2 + 1.66H_2 \qquad (2.2)$$

The bio-oil was mixed with methanol (50 wt. %) to reduce the viscosity to allow for optimal flow through the ultrasonic nozzle as well as to homogenize the bio-oil.

2.7.2 Model Compounds

Bio-oil can have different compositions based on the source of the original feedstock. The model compounds used during experiments were selected based on the typical composition of bio-oil as given in "Fast Pyrolysis of Biomass: A Handbook" edited by Bridgewater et al.[45] (see Table 2.1). The molecules chosen, with typical wt. % found in bio-oil in parenthesis, were: methanol (up to 2.4%), acetic acid (up to 12%), formaldehyde (up to 3.3%), acetaldehyde (up to 8.6%), glyoxal (up to 4.6%), hydroxyacetaldehyde (up to 13%), acetone (2.8%), phenol (up to 3.8%), guaiacol (up to 1.1%), eugenol (up to 2.3%), furfural (up to 1.1%), anisole (not in bio-oil), and dimethoxybenzene (not in bio-oil). Although anisole and dimethoxybenzene are not components of bio-oil, they were selected since they have methoxy groups on the benzene ring and can represent the more complex aromatic ethers found in bio-oil. It should be noted that many of the species used for experiments were also included in the surrogate developed for process simulations (see Chapter 8).

Table 2.1 Typical composition of biomass.

Species	Typical percentage
organic acids	5 to 10
aldehydes	5 to 20
ketones	0 to 10
phenolics	20 to 30
Furans	0 to 8.6
water	15 to 30

Aqueous solutions were required in the case of the following compounds with their wt. % in parenthesis: formaldehyde (37%), glyoxal (40%), hydroxyacetaldehde (10%), and phenol (5%). The rest of the compounds (see above) were at least 98% pure. Each compound was introduced into the NREL reactor with varied amounts of oxygen added. Mixtures of phenol (in solution), guaiacol, eugenol, and anisole with either hydroxyacetaldehyde (in solution) or methanol were also introduced into the NREL reactor with varied amounts of oxygen added. All model compound experiments were performed with the

furnace set to 650ºC in the reaction zone (described below). In addition to the model compound experiments performed at NREL, kinetic experiments were performed using methanol at CFCC in order to validate a detailed kinetic model.

2.8 Bio-oil Rheology

In order to determine the extent of viscosity reduction by methanol addition, rheological measurements using a TA Instruments AR-G2 stress controlled rheometer were performed on bio-oil with varied amounts of methanol added (0 to 50 % by weight). These measurements utilized a stainless steel cone (40 mm diameter, 2 degree) and plate geometry in steady or oscillatory shear. Evaporation of the sample was minimized by using a solvent trap in conjunction with the geometry. Temperature was controlled to within ± 0.1 ºC using a Peltier plate (cone and plate). Calibration with viscosity standard oils showed agreement with an error of less than 3%. Of note, the bio-oil begins to show non-Newtonian characteristics (i.e., shear thinning) at 10 ºC. Representative viscosities are reported at a single shear rate (100 s^{-1}) although 20 data points across the shear rate range of 0.1 to 500 s^{-1} were measured.

2.9 Larger NREL Reactor

Because of the favorable results obtained using the system described above, Dr. Richard French designed and constructed a system with a 50 cm long 3.6 cm inside diameter quartz reactor with 1 mm thick walls. Approximately 7.5 cm of the length of the reactor extended above the furnace. The hot zone itself was ~35.5 cm. Because of the larger size, mixing was more of a concern than with the smaller system. Specially designed inserts to reduce the inside diameter of the reactor near the nozzle have been utilized to assist with this. However, issues with mixing persisted.

A pulse diaphragm pump was used to feed a nominal flow of 1 g/min (either bio-oil:methanol mixtures or methanol) through the 25 kHz (upgraded) nozzle and into the top of the vertical reactor. In order to ensure accuracy, the liquid was placed on a scale to measure the change in weight as it was fed to the

reactor. A new shroud was designed for this system that includes a cooling jacket of copper tubes where a flow of chilled water was used to keep the nozzle from overheating. The combined flow of air (used as the oxidant) and N_2 was between 4 and 6 SLPM. The estimated residence time varied from ~0.9 to 1.4 s, which was much longer than that used for the experiments with the smaller reactor. During experiments where a catalyst was used, 4.5 g of catalyst from Dr. Lanny Schmidt's group at the University of Minnesota was mixed with 39 g of alumina and inserted at the bottom of the hot zone. Both the catalyst and alumina were ~12 to 18 mesh.

Upon exiting the reactor, the effluent entered a series of two condensers where water was removed prior to the analytical equipment. A non-dispersive infrared (NDIR) spectrometer was used for continuous monitoring of the experiment, while a micro GC was used for quantitative analysis.

CHAPTER 3
PRELIMINARY NON-CATALYTIC BIO-OIL REFORMING

The focus of the present work was to characterize the non-catalytic partial oxidation (NPOX) of bio-oil. Earlier research at NREL had shown that PAH formation from biomass model compounds increases with temperature under pyrolysis conditions and is especially prevalent at temperatures greater than 700ºC[34-36]. Accordingly, the present work initially focused on NPOX at 650ºC to assure that the exothermic reactions did not lead to temperatures greater than 700ºC. However, because NPOX reactions are significantly different than pyrolysis reactions, other temperatures have also been explored. Figures 3.1 and 3.2 are representative mass spectra under pyrolysis and partial oxidative conditions, respectively. These figures illustrate the significant impact that oxygen addition has on the conversion of bio-oil. Note the dramatic decrease in the signal of higher molecular weight species as well as methanol when oxygen is added to the system. Adding oxygen to the system led to significant conversion of both bio-oil and methanol.

This chapter begins by defining key variables. A discussion of carbon deposition as predicted by equilibrium will follow. Preliminary NPOX results using the 120 kHz nozzle will then be discussed. This discussion will include initial experiments at 650ºC as well as a temperature survey from 625 to 700ºC. The majority of experiments were performed using a 50:50 (wt. %) bio-oil:methanol mixture. However, limited experiments were performed using 30 and 10 wt. % methanol. The effect of varying the methanol concentration on the viscosity of the mixture is also described. As part of the preliminary experiments, the effect of residence time on NPOX results was explored as was the effect of staged oxygen addition.

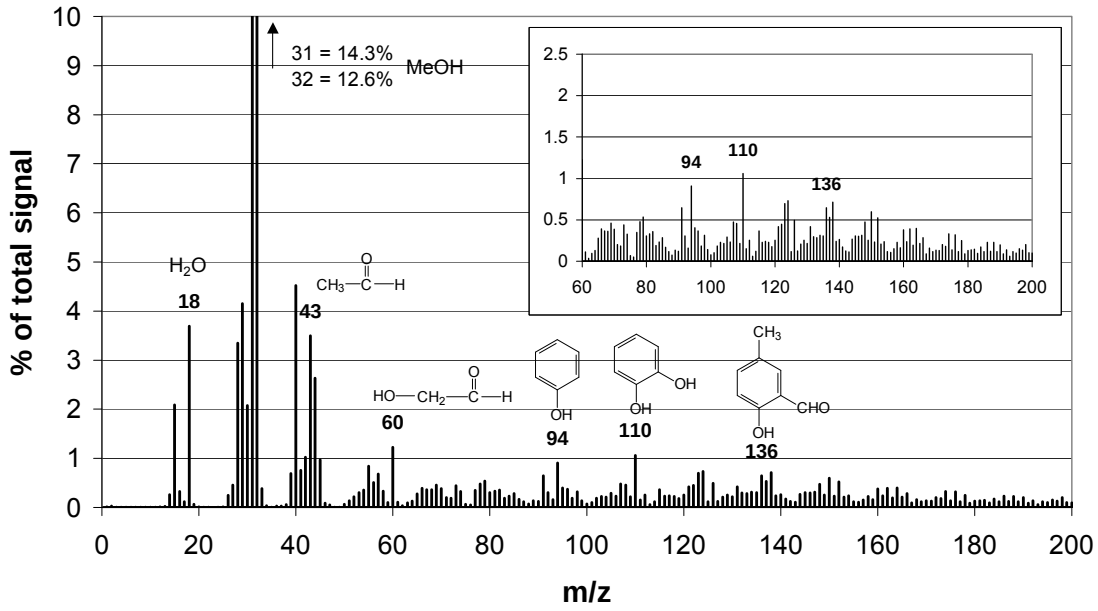

Figure 3.1 MBMS spectrum at 650ºC and residence time of 0.3 s for pyrolysis (effective O:C ratio = 0.7; λ = 0) of 50:50 (wt. %) bio-oil:methanol mixture. The smaller, imbedded spectrum is a blow-up of m/z > 60.

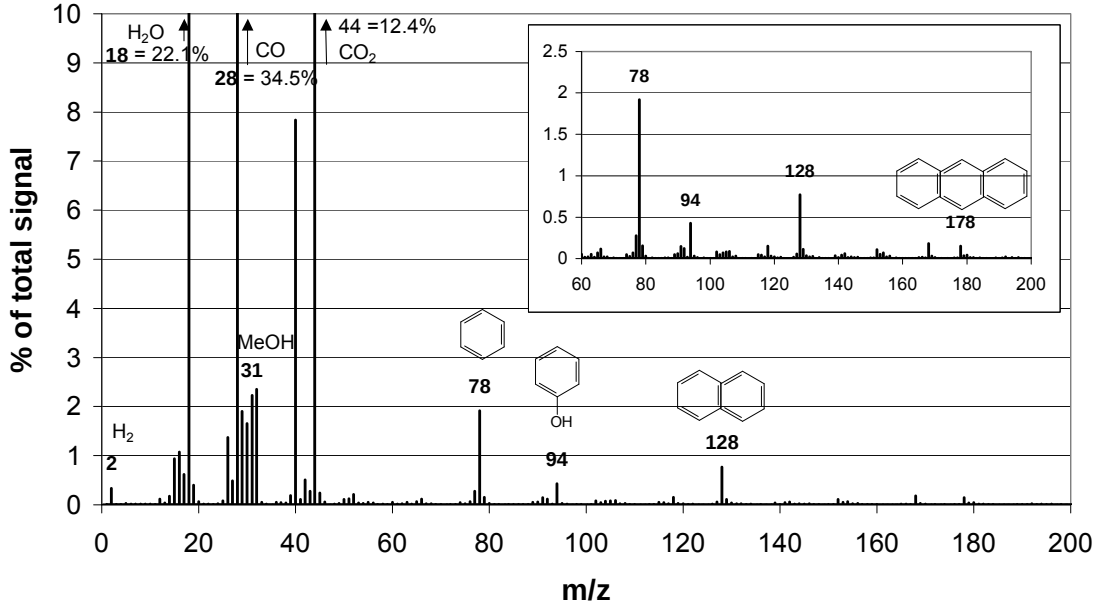

Figure 3.2 MBMS spectrum at 650ºC and residence time of 0.3 s for NPOX (effective O:C of 1.6; λ = 0.35) of 50:50 (wt. %) bio-oil:methanol mixture. The smaller, imbedded spectrum is a blow-up of m/z > 60.

3.1 Definitions

Prior to commencing a discussion of the experimental data, key variables will be defined.

3.1.1 Effective Oxygen to Carbon and Equivalence Ratios

The overall oxygen to carbon (O:C) molar ratio includes oxygen present in organic molecules of bio-oil and methanol as well as the oxygen in the water entering with bio-oil and that introduced as O_2. However, under the conditions used in this study, water is inert in the absence of a catalyst. Accordingly, the oxygen in water is subtracted from the O:C ratio to give an effective O:C ratio which is 0.13, 0.17, and 0.22 less than the overall O:C ratio for the 50:50, 70:30, and 90:10 bio-oil:methanol mixtures, respectively. The results of NPOX experiments will be plotted as a function of the effective O:C ratio, whereas the overall O:C ratio is more appropriate for the catalytic experiments.

The effective O:C ratio is related to the equivalence ratio (λ), a parameter commonly used in combustion and gasification processes, by the following equations (applicable mixture in parenthesis):

$$effective\ O:C\,(50:50) = 2.55 * \lambda + 0.7 \qquad (3.1)$$

$$effective\ O:C\,(70:30) = 2.40 * \lambda + 0.6 \qquad (3.2)$$

$$effective\ O:C\,(90:10) = 2.28 * \lambda + 0.5 \qquad (3.3)$$

Here, the equivalence ratio is the ratio of actual O_2 added to that required for complete combustion (again assuming that the oxygen in water is unreactive). The equivalence ratio is useful for comparing the different mixtures since bio-oil requires less oxygen for complete combustion than does methanol due its higher initial oxygen content. In cases where the data from different mixtures are compared, data will be plotted against λ rather than effective O:C ratio. Table 3.1 compares effective O:C to λ.

Table 3.1 Value of λ compared to effective O:C for pure methanol, 50:50, 70:30, and 90:10 (wt. %) bio-oil:methanol mixtures as well as pure bio-oil. Note that the effective O:C for methanol is the same as the overall O:C.

effective O:C	Pure Methanol	50:50 Mix	70:30 Mix	90:10 Mix	Pure Bio-oil
0.46	N/A	N/A	N/A	N/A	0.00
0.5	N/A	N/A	N/A	0.00	0.02
0.6	N/A	N/A	0.00	0.04	0.06
0.7	N/A	0.00	0.04	0.09	0.11
1.0	0.00	0.12	0.17	0.22	0.25
1.2	0.07	0.20	0.25	0.31	0.34
1.4	0.13	0.27	0.33	0.39	0.43
1.5	0.17	0.31	0.38	0.44	0.47
1.6	0.20	0.35	0.42	0.48	0.52
1.7	0.23	0.39	0.46	0.53	0.57
2.0	0.33	0.51	0.58	0.66	0.70

3.1.2 Overall Product Yields

The overall yield for all species is defined as follows (weight basis):

$$Y_{i,overall} = \frac{carbon\ or\ hydrogen\ in\ species\ i\ (measured)}{total\ carbon\ or\ hydrogen\ entering} * 100 \qquad (3.4)$$

The yield based on hydrogen will only be used for species that do not contain carbon (i.e., H_2 and H_2O).

3.1.3 Bio-oil Product Yields

It is important to assess which products are derived from bio-oil vs. methanol. Two methods were used to obtain an estimate of the CO and CO_2 yields from bio-oil. Method 1 assumed that all of the methanol that reacted produced CO as the only carbon-containing product. Since the data obtained from neat methanol experiments suggested that some CO_2 was formed as well, this approach likely overestimated the CO production from methanol and thus underestimated that produced from bio-oil. The CO yield for Method 1 can be expressed as follows (weight basis):

$$Y_{CO,bio-oil,\min} = \frac{total\ carbon\ in\ CO\ (measured) - carbon\ in\ converted\ CH_3OH}{carbon\ entering\ \ from\ bio-oil} * 100 \qquad (3.5)$$

Conversely, Method 1 likely overestimated the CO_2 yield from bio-oil. The CO_2 yield can be expressed as follows (weight basis):

$$Y_{CO2,bio-oil,\max} = \frac{total\ carbon\ in\ CO_2\ (measured)}{carbon\ entering\ \ from\ bio-oil} * 100 \qquad (3.6)$$

An alternative method (Method 2) assumed that the measured selectivity for CO production in the neat methanol experiments (discussed in Chapter 9) was unchanged when bio-oil was added. Using the measured methanol conversion in the mixture experiments, this selectivity factor was used to calculate the amount of CO produced from the methanol, thereby allowing that produced from the bio-oil to be determined by difference. This approach thus corrects for the expected CO_2 production from methanol, thereby increasing the estimated CO yield from the bio-oil. Further details of this method can be found in Appendix A. The estimated yield of CO and CO_2 from bio-oil using Method 2 can be expressed as follows (weight basis):

$$Y_{i,bio-oil,estimated} = \frac{estimated\ carbon\ in\ species\ i\ \ from\ bio-oil}{carbon\ entering\ \ from\ bio-oil} * 100 \qquad (3.7)$$

This alternative method assumed that there were no interactions between the methanol and bio-oil. Obviously such interactions might exist. In fact, the observed methanol conversion might be slightly higher during bio-oil:methanol mixture experiments than during neat methanol experiments at the same λ (see Figure 3.3). A possible explanation for this phenomenon is that there were species in the bio-oil that were more reactive than methanol. These species could generate a larger free radical pool at a given temperature, thus increasing methanol conversion. It is possible that the increased free radical pool might affect the relative rates of production of CO and CO_2 from methanol. However, such an increased free radical pool might also produce additional CO_2 from methanol by oxidizing the CO, which would lead to even higher CO production from bio-oil than obtained with Eqn. 3.7. In summary, the use of Eqn. 3.7 to

obtain the CO and CO_2 yield from bio-oil is probably more accurate. However, Eqns. 3.5 and 3.6 provide a firm lower limit to the bio-oil CO yield and a firm upper limit to the bio-oil CO_2 yield, respectively.

Since CO and CO_2 were the dominant products during neat methanol experiments, it was assumed all other carbon containing compounds were produced only from bio-oil. Therefore, their yields can be easily calculated using the following equation:

$$Y_{i,bio-oil,\max} = \frac{total\ carbon\ entering}{carbon\ entering\ \ from\ bio-oil} * Y_{i,overall} = 1.78 * Y_{i,overall} \qquad (3.8)$$

where 1.78 is the ratio of the total carbon entering to the carbon entering from bio-oil.

In principle, H_2 and H_2O coming from bio-oil could be estimated using methods similar to those described above. However, the low signal to noise observed in the hydrogen data as well as the uncertainty caused by water sticking to the walls of the MBMS was such that this approach was not feasible.

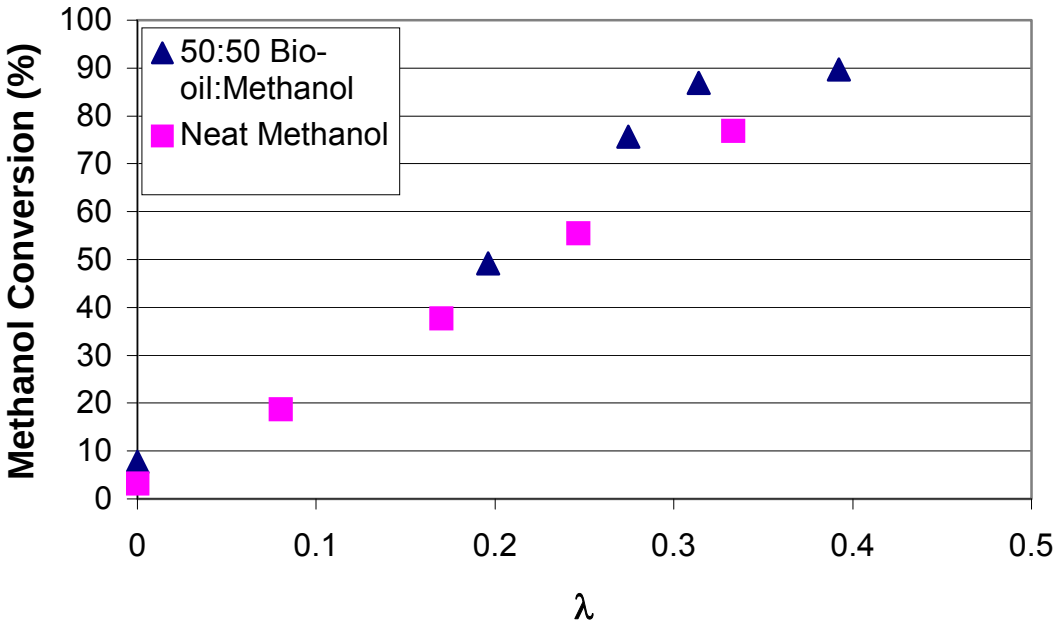

Figure 3.3. Comparison of methanol conversion as a function of λ during neat methanol experiments and 50:50 bio-oil:methanol mixture (wt. %) experiments. (Note: Data shown in this figure was generated using a 120 kHz nozzle)

3.1.4 Carbon to Gas Conversion

Because CO, CO_2, and CH_4 were the only carbon containing permanent gases with significant yields, their sum gave a good estimate of the carbon to gas conversion. This carbon to gas conversion is an important parameter for determining the efficiency of gasification of non-volatile bio-oil components. The conversion from bio-oil does not depend on which assumption is used to determine the CO contribution from methanol.

3.1.5 Carbon Accounting

The term carbon accounting rather than carbon balance was used since not all species were quantified. This parameter quantifies the amount of carbon that was measured in the experiments. The overall carbon accounting is defined as follows (weight basis):

$$C.A._{overall} = \frac{carbon\,exiting\ (measured)}{total\ carbon\,entering} * 100 \qquad (3.9)$$

The Carbon accounting from bio-oil is given by the following (wt. basis):

$$C.A._{bio-oil} = \frac{carbon\,exiting\,(measured) - carbon\,entering\ from\ CH_3OH}{carbon\,entering\ from\ bio-oil} * 100 \qquad (3.10)$$

The measured carbon exiting the reactor in the above equations includes all carbon containing species (CO, CO_2, CH_4, methanol, benzene, and residual carbon) that were quantitatively analyzed with the MBMS system (e.g., it did not include any species with molecular weights higher than benzene). The total carbon entering the system in the above comes from both the bio-oil and the methanol in the feed. In order to determine the carbon accounting from bio-oil, it was necessary to assume that all of the carbon entering as methanol was accounted for in the measured carbon containing species (a reasonable assumption based on neat methanol experiments).

3.2 Carbon Deposition

When working with carbon containing species, the formation of carbon deposits is possible. Several researchers have used thermodynamics and a

ternary C-H-O diagram to predict regions where carbon deposition will occur[46,47]. Using the same idea, a ternary diagram has been constructed as a guideline for the present research (Figure 3.4). This diagram shows two isotherms (650ºC and 850ºC) representing the compositions where equilibrium predicts 1 ppm carbon deposits (in the form of graphite). The carbon deposition that occurs during partial oxidation would be amorphous carbon[48], which is less stable than graphitic carbon. Using graphite as the criteria for deposition is therefore a more conservative approach. The units for this figure are mole fractions. The carbon rich region above each isotherm in Figure 3.4 represents conditions where deposition as graphite is predicted to occur. The opposite is true of regions below each isotherm.

While thermodynamic predictions are a useful guideline for where deposit formation might occur, kinetics often govern where deposit formation actually do occur. Hence, carbon deposits can be observed in the region that is expected to be deposit free if the kinetics that lead to deposit formation are faster than those removing deposits. For example, Strohm et al.[48] report deposits from JP-8 reforming at S/C = 3 and 512ºC, even though this is not in the region where deposits are anticipated by equilibrium[49]. Conversely, one might not observe deposits for a composition within the carbon deposit region if the deposit-forming kinetics are slow.

In Figure 3.4, points for the compositions of bio-oil, methanol and water are labeled. The points labeled 1, 2, and 3 represent the compositions of 90:10, 70:30, 50:50 (wt. %) bio-oil methanol mixtures, respectively. The points on the dotted lines extending from Points 1, 2, and 3 towards oxygen correspond to effective O:C ratios of 1.2 and 1.6 for each of the mixtures. The addition of pure oxygen leads to the overall composition of the mixture to move in a straight line from the composition of the mixture to the composition of oxygen. Similarly, if steam were added the overall composition would shift in a straight line towards the composition of water. In both cases, sufficient oxygen or steam addition leads to the overall composition moving from a region where deposits are predicted to one where they are not.

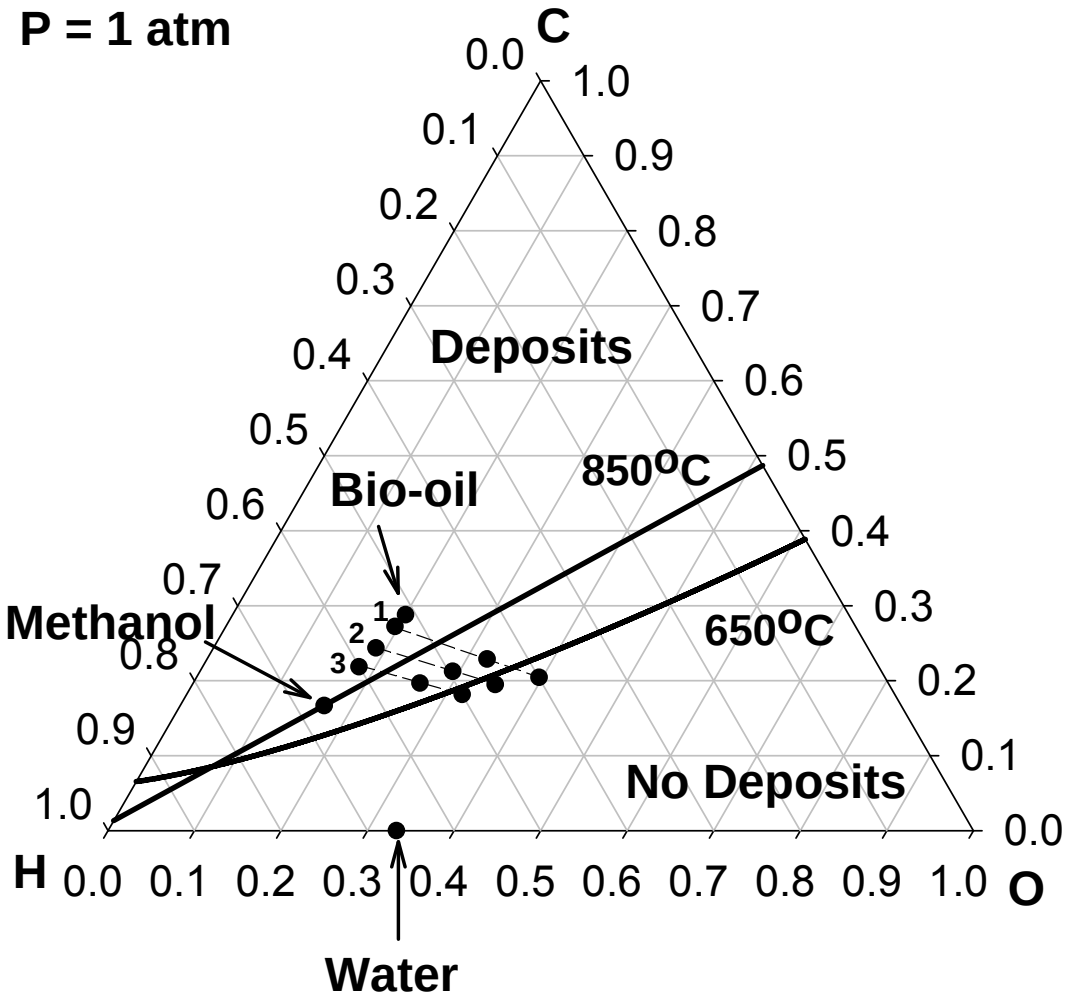

Figure 3.4. Ternary C-H-O diagram showing the region where carbon deposits (graphite) are predicted by equilibrium. The axes are in units of mole fraction. Two isotherms representing 1 ppm graphitic carbon at 850 ^{o}C and 650 ^{o}C are shown. The carbon rich region above the isotherm represents the region where carbon deposition is predicted to occur.

During non-catalytic experiments, it was expected and observed that kinetics where controlling the system. Equilibrium was not attained and the carbon deposition was only moderately affected by changes in either temperature or effective O:C. Where these calculations become important is during the catalytic step where equilibrium is expected.

3.3 Preliminary NPOX at 650ºC

Preliminary NPOX experiments were performed using the 120 kHz nozzle and a 50:50 bio-oil:methanol mixture with a nominal residence time of ~0.3 s at 650ºC. The flow rates of helium and oxygen to achieve the nominal residence (~0.3 s) time were 490-554 and 0-64 sccm (0ºC and 1 atm), respectively, with the total flow maintained at 554 sccm. The argon flow (used as an internal standard) was 10 sccm. The 50:50 bio-oil:methanol mixture flow rate was 0.16 g/min. Figure 3.5 shows the measured temperature profile obtained by flowing just helium and was used to calculate the estimated residence time. The oxygen flows used correspond to effective oxygen to carbon (O:C) molar ratios of 0.7

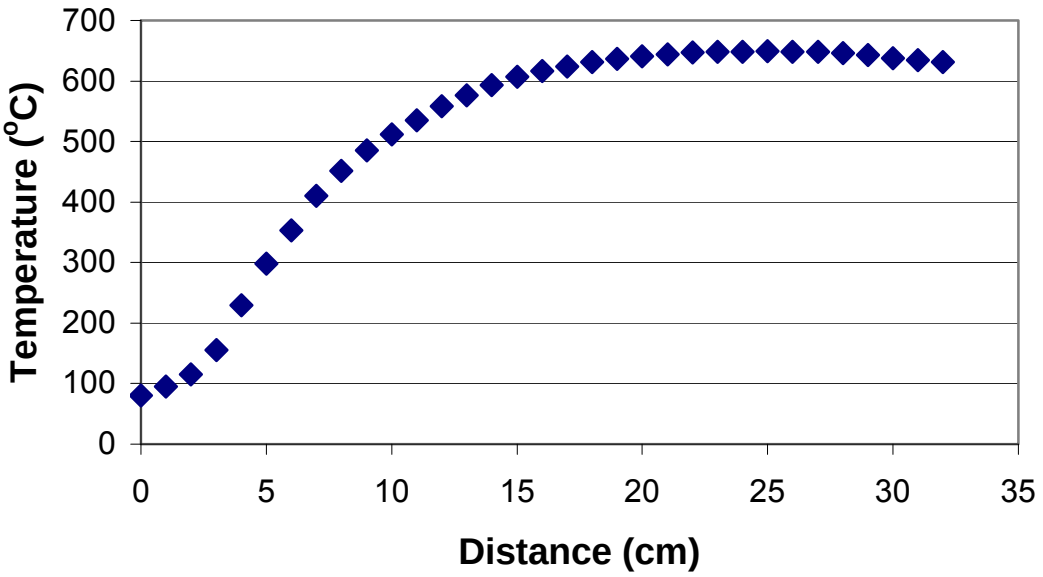

Figure 3.5. Temperature profile measured along the reactor at 650ºC with a helium flow. Zero corresponds to the entrance of the reactor while 32 cm corresponds to the exit.

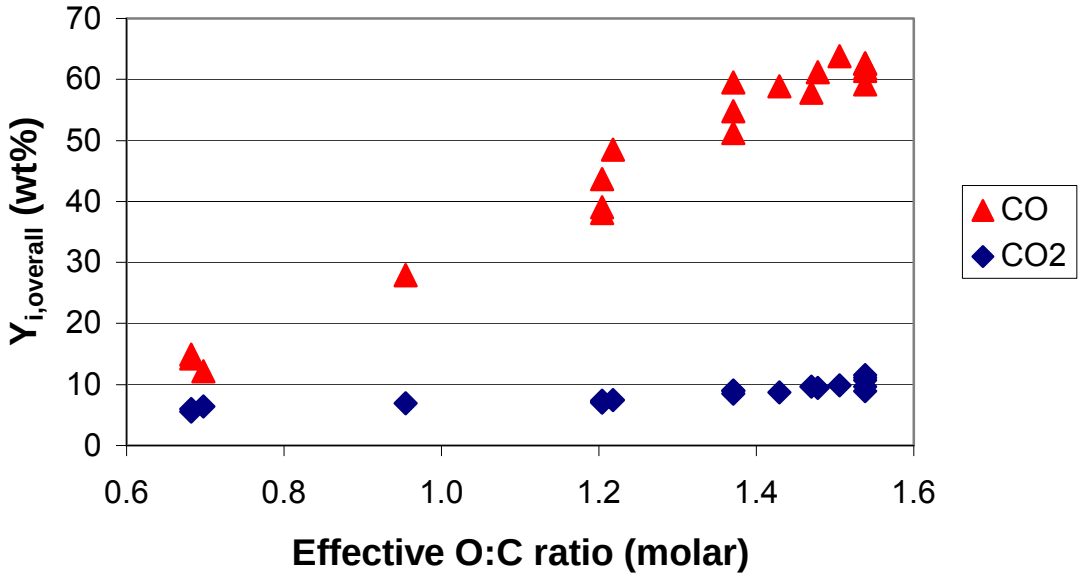

Figure 3.6. Preliminary overall CO and CO_2 yield as a function of effective O:C (650ºC and ~0.3 s).

(pyrolysis) to ~1.55. The temperature was expected to increase with increasing O:C due to the exothermic partial oxidation reactions. However, it will be shown that temperature has a much smaller impact on the final products than does increasing the effective O:C. As discussed above, the effective O:C ratio does not include oxygen in water as it was not reactive under these conditions.

Figure 3.6 shows the overall of CO and CO_2 yields (defined as discussed in Section 3.1). It was remarkable and somewhat surprising to see such a large increase in the CO yield without seeing a significant increase in CO_2 yield as the effective O:C was increased. The maximum overall CO yield was ~60 % while the maximum overall CO_2 yield was only ~10 % for the same effective O:C. Increasing the oxygen above an effective O:C of ~1.55 led to undesirable combustion conditions.

Bio-oil yields of CO and CO_2 as estimated by both methods (discussed in Section 3.1 and Appendix A) are shown in Figure 3.7. Based on these estimates, the large increase in CO yield without a significant increase in the CO_2 yield is not just due to the methanol. In theory, Method 1 should always give a lower estimate for the CO yield than Method 2. The fact that this is not always the case

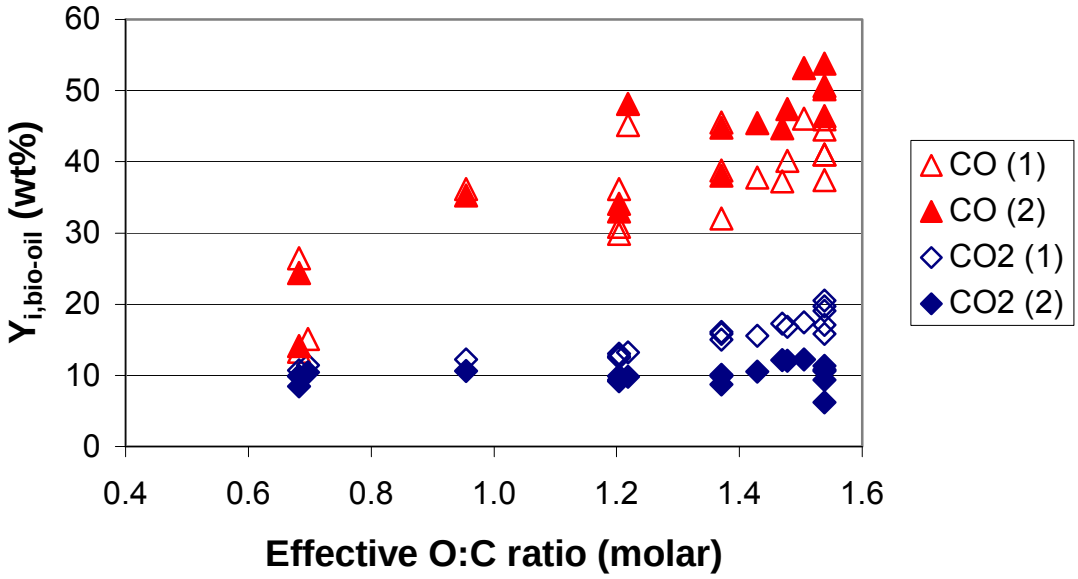

Figure 3.7. Estimates of bio-oil CO and CO_2 yield in the preliminary experiments as a function of effective O:C (650ºC and ~0.3 s). The number in parenthesis in the legend corresponds to the method used for the estimate (see text).

reflects the uncertainty in the data. The maximum estimated bio-oil CO yield from Method 1 is ~40-50% while that from Method 2 is ~45-55%. The maximum estimates for CO_2 are ~15-20% from Method 1 and 8-12% from Method 2. Figure 3.8 shows the overall yield for both H_2 and H_2O (as defined in Section 3.1) as a function of effective O:C. As with CO, the maximum H_2 yield (~20-25%) occurs at effective O:C between ~1.4 and ~1.55. The maximum H_2O yield (~45-40%) occurs over this range as well. The water yield is significant since it can be utilized over a catalyst for steam reforming of unreacted species as well as for water gas shift reaction.

3.4 Effect of Temperature

A preliminary temperature survey was performed at temperatures between 625 and 700ºC (~0.3 s; effective O:C between 0.7 and ~1.6). Little reaction occurred at temperatures of 600ºC or lower. The flow rates were adjusted to account for the change in temperature. The results showed that temperature had little effect on the CO yield over this temperature range (see Figure 3.9). The

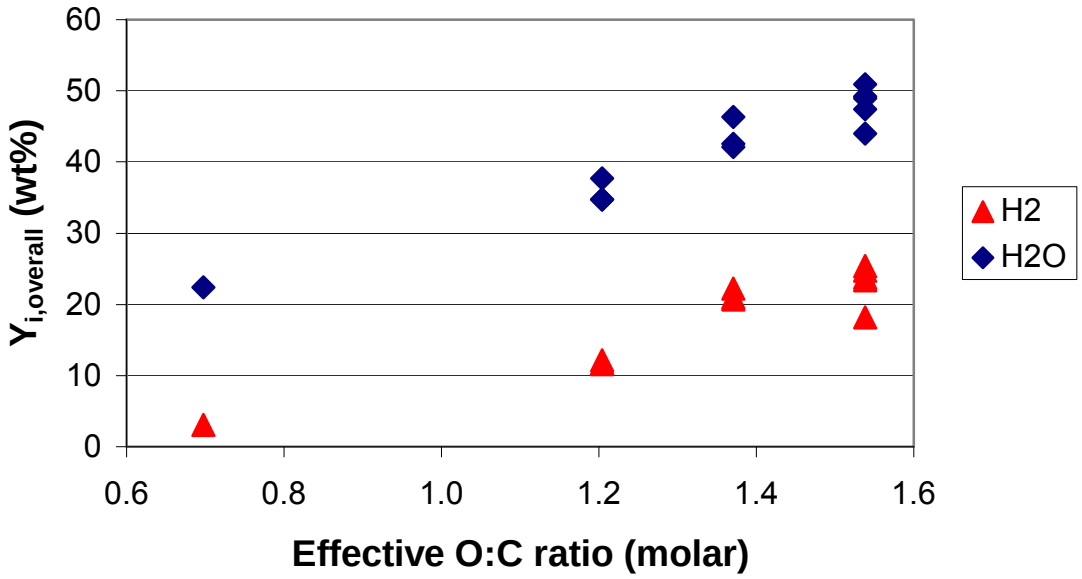

Figure 3.8. Preliminary yields of H_2 and H_2O as a function fo effective O:C (650ºC and ~0.3 s).

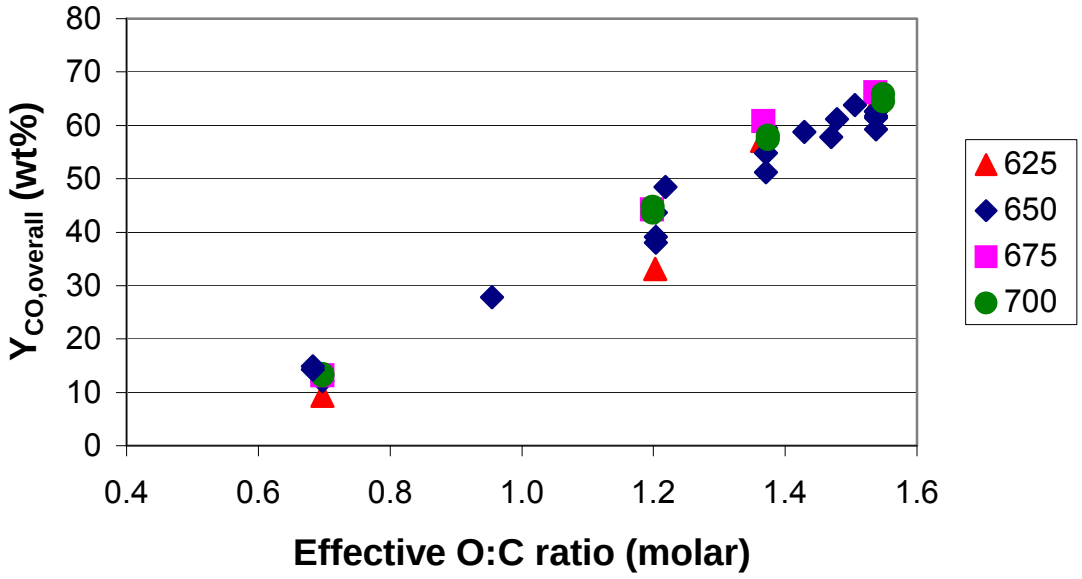

Figure 3.9. CO yields during preliminary temperature survey for temperatures between 625 and 700ºC as a function of effective O:C (from 0.7 to ~1.6) at a residence time of ~0.3 s.

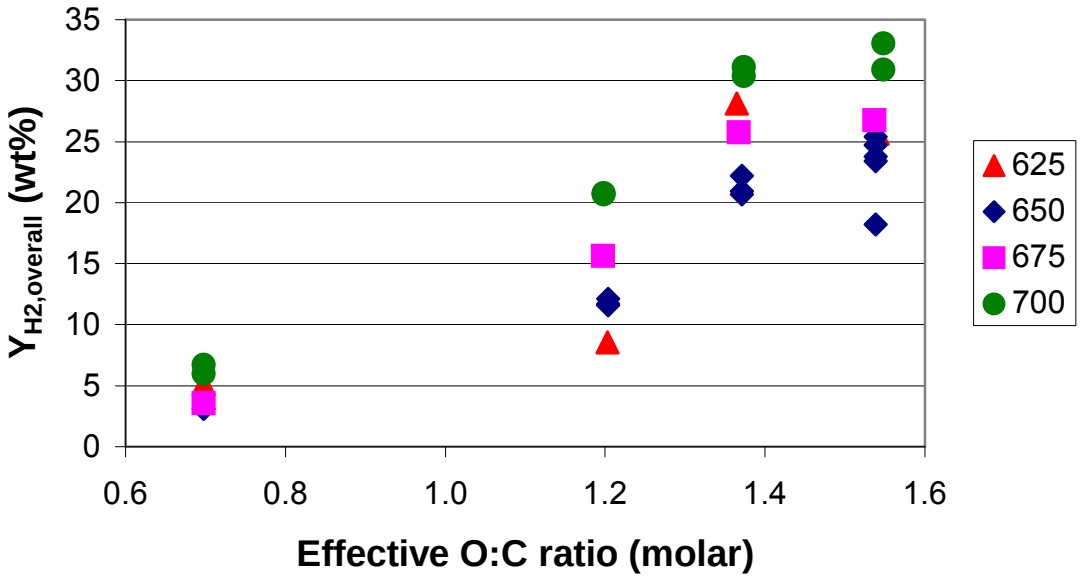

Figure 3.10. H_2 yields during preliminary temperature survey for temperatures between 625 and 700ºC as a function of effective O:C (from 0.7 to ~1.6) at a residence time of ~0.3 s.

effect of temperature on the H_2 yield is uncertain (Figure 3.10). There appears to be an increase in H_2 yield (as high as ~30%) at 700ºC.

3.5 Reduction of Methanol Content

Although the 120 kHz nozzle was not rated for power settings as high as those required to feed bio-oil:methanol mixtures with less than 50 wt. % methanol (see Section 2.2), a limited number of experiments were performed with both a 70:30 and 90:10 (wt. %) bio-oil:methanol mixture. The effect of methanol addition (0 to 50 wt. %) on the viscosity was explored through rheological measurements at temperatures from 10 to 40°C (see Figure 3.11). At all temperatures, the viscosity decreases significantly with increasing methanol content with the most dramatic decrease in the viscosity typically occurring between 10 and 30% methanol. Greater than a 90% decrease in the viscosity at 25°C is observed between the bio-oil with no methanol added and oil with 30% methanol added. Further addition of methanol results in very little change in the viscosity.

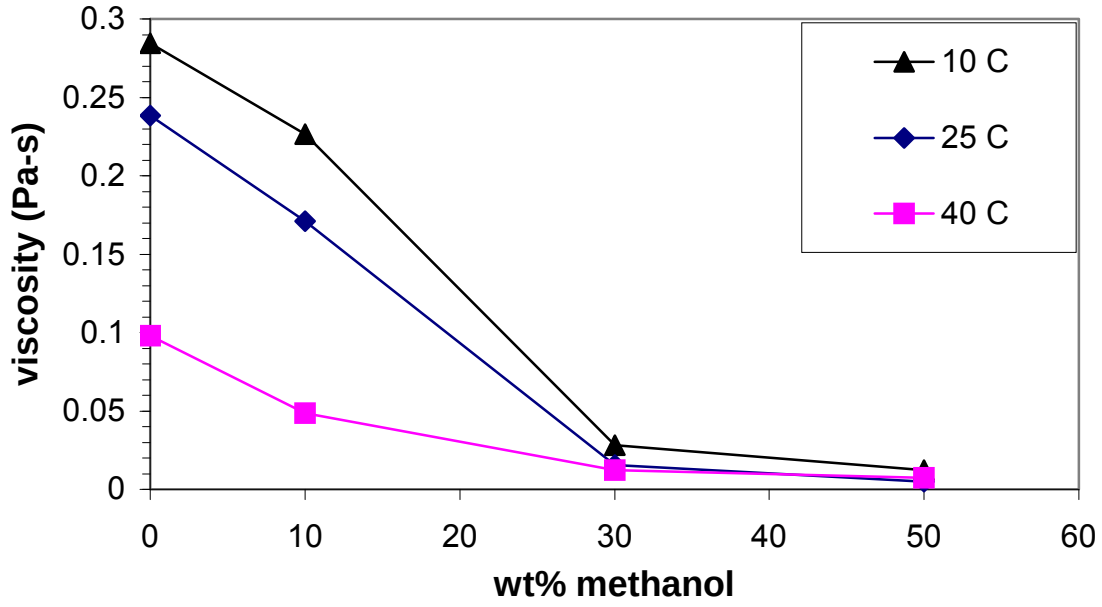

Figure 3.11. Viscosity of bio-oil as a function of methanol concentration (0 to 50 wt. %) and temperature (10 to 40ºC). All measurements shown were taken at a shear rate of 100 s^{-1}.

The overall and bio-oil CO (Method 2) yields are shown as a function of λ in Figures 3.12 and 3.13, respectively. The overall yield was quite similar at a given λ for the 50:50 and 70:30 mixtures. The 90:10 mixture gave lower CO yields (~50% maximum rather than the 60% for the other two.). There was also a significant increase in the scatter of the data with the 90:10 mixture, which was due to inconsistent atomization. This increased scatter illustrated that the 120 kHz nozzle was not suited for these experiments. Because all the mixtures have similar bio-oil CO yields (see Figure 3.13), the lower overall CO yield can be attributed to the lower methanol content. Since the estimated CO yields are so similar in Figure 3.13, one can conclude that Method 2 does a good job of accounting for the CO yield from methanol. The agreement between the three mixtures is even better for the both the overall and bio-oil (Method 2) CO_2 yields (see Figures 3.14 and 3.15). The dramatic decrease in CO (and corresponding increase in CO_2) for λ greater than 0.4 in the case of the 70:30 and 90:10 mixtures was attributed to entrance into a region where combustion occurred.

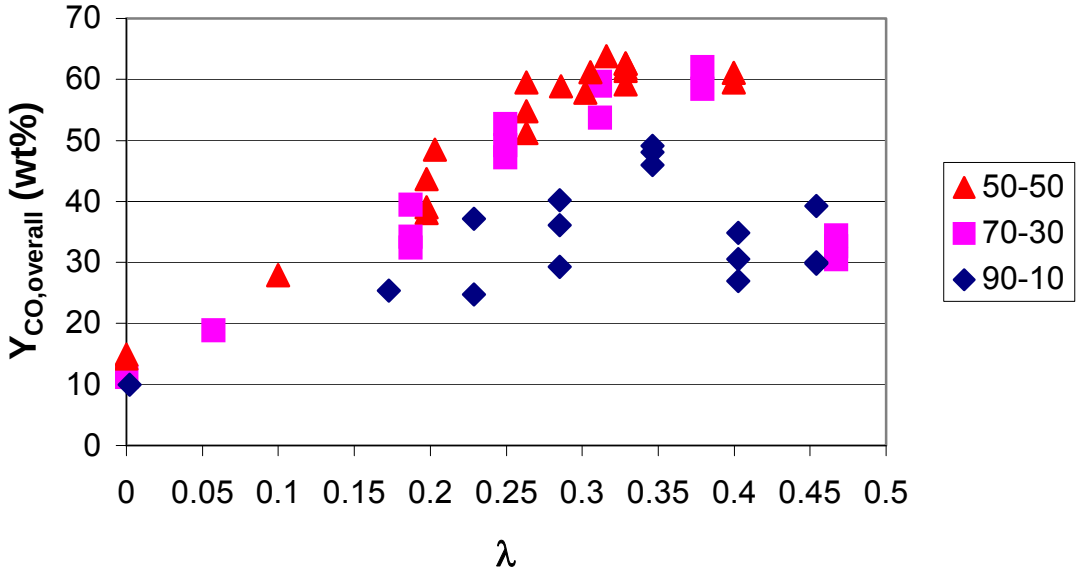

Figure 3.12. Overall CO yield as a function of λ (0 to 0.5) for 50:50, 70:30, and 90:10 bio-oil:methanol mixtures (650ºC; ~0.3 s).

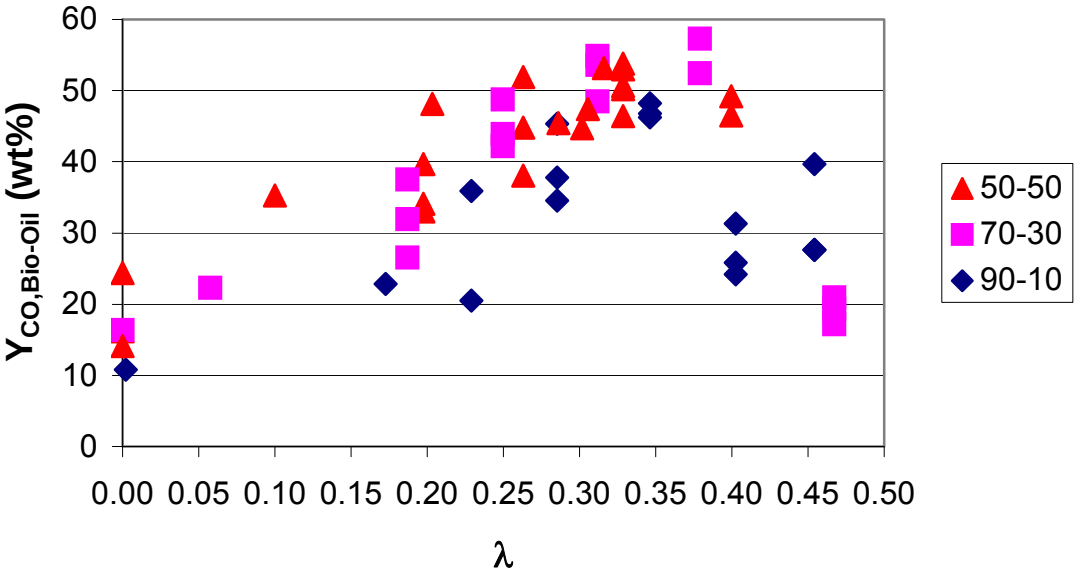

Figure 3.13. Bio-oil CO yield as a function of λ (0 to 0.5) for 50:50, 70:30, and 90:10 bio-oil:methanol mixtures (650ºC; ~0.3 s).

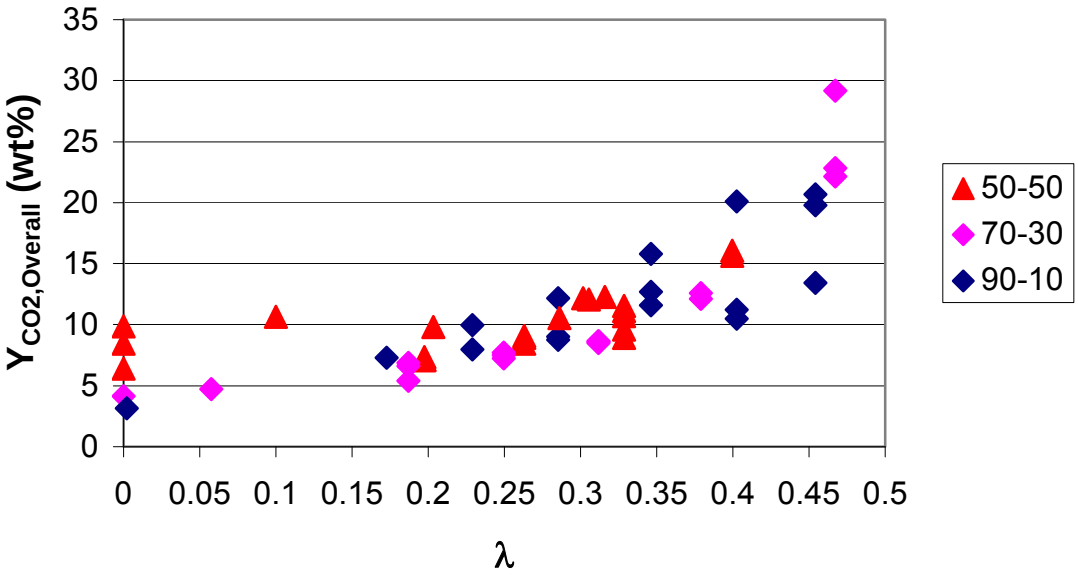

Figure 3.14. Overall CO_2 yield as a function of λ (0 to 0.5) for 50:50, 70:30, and 90:10 bio-oil:methanol mixtures (650ºC; ~0.3 s).

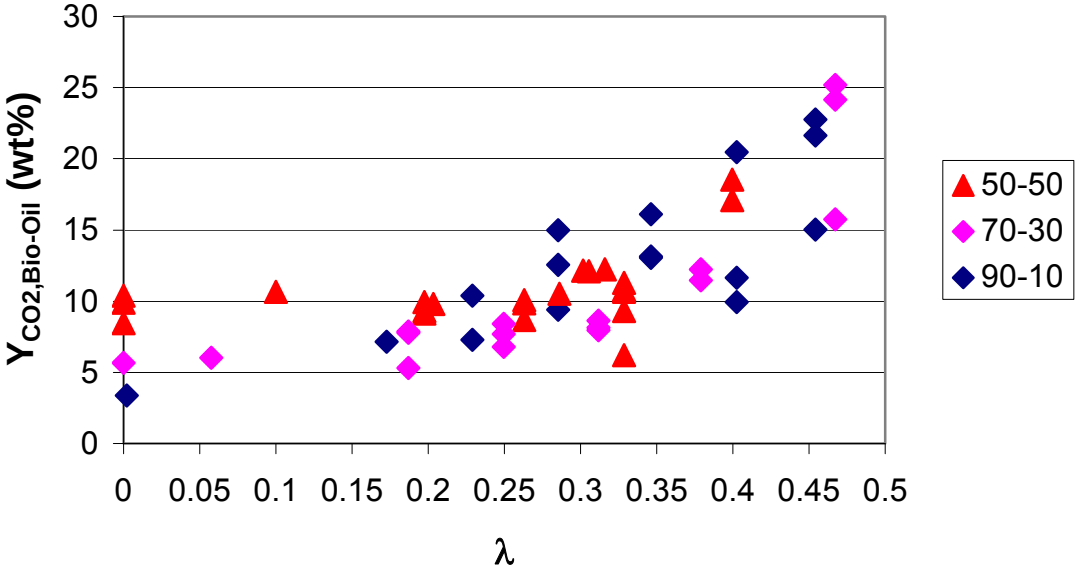

Figure 3.15. Bio-oil CO_2 yield as a function of λ (0 to 0.5) for 50:50, 70:30, and 90:10 bio-oil:methanol mixtures (650ºC; ~0.3 s).

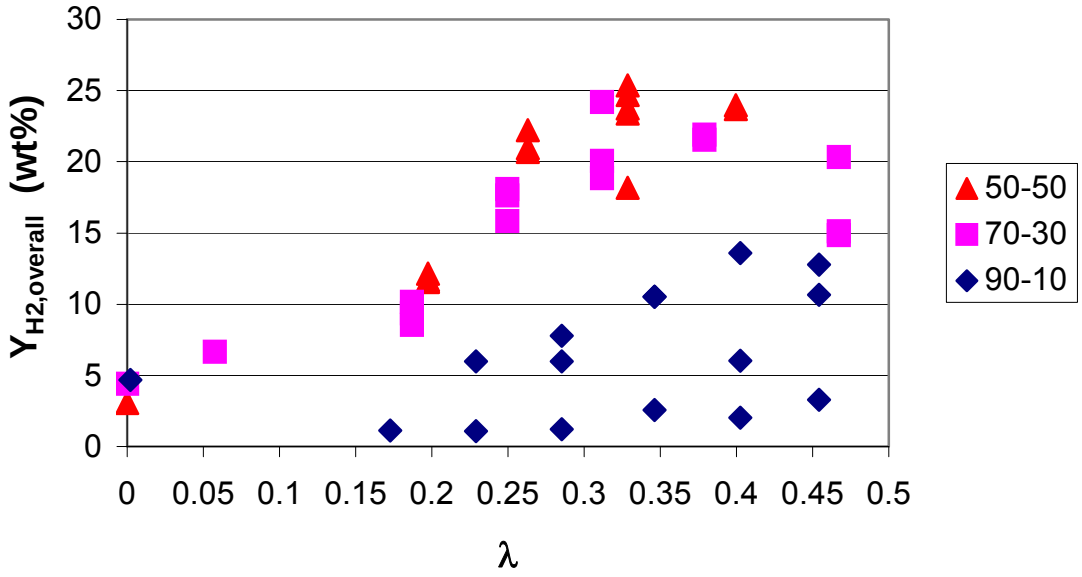

Figure 3.16. Overall H_2 yield as a function of λ (0 to 0.5) for 50:50, 70:30, and 90:10 bio-oil:methanol mixtures (650ºC; ~0.3 s).

Figure 3.16 shows that the overall H_2 yield is in good agreement for the 50:50 and 70:30 mixtures. The H_2 yields for the 90:10 mixture were lower. This could be due to the difficulty of feeding the higher viscosity liquid. It could also mean that much of the H_2 is due to the presence of methanol. Although this might at first seem to defeat the purpose of the present research, the significantly high yields of CO can react with H_2O over a water gas shift catalyst to give more H_2. The H_2O yields are shown in Figure 3.17. Unlike H_2, all mixtures show good agreement.

3.6 Staged Oxygen Addition

The experiments discussed above have been limited by the entrance into a combustion regime, which may have been due in part to the high concentration of O_2 being fed. However, it appeared from the data that adding more oxygen might lead to even better results. In order to assess whether adding more oxygen would be beneficial while avoiding combustion due to high O_2 concentrations, staged oxygen addition experiments were performed under conditions similar to

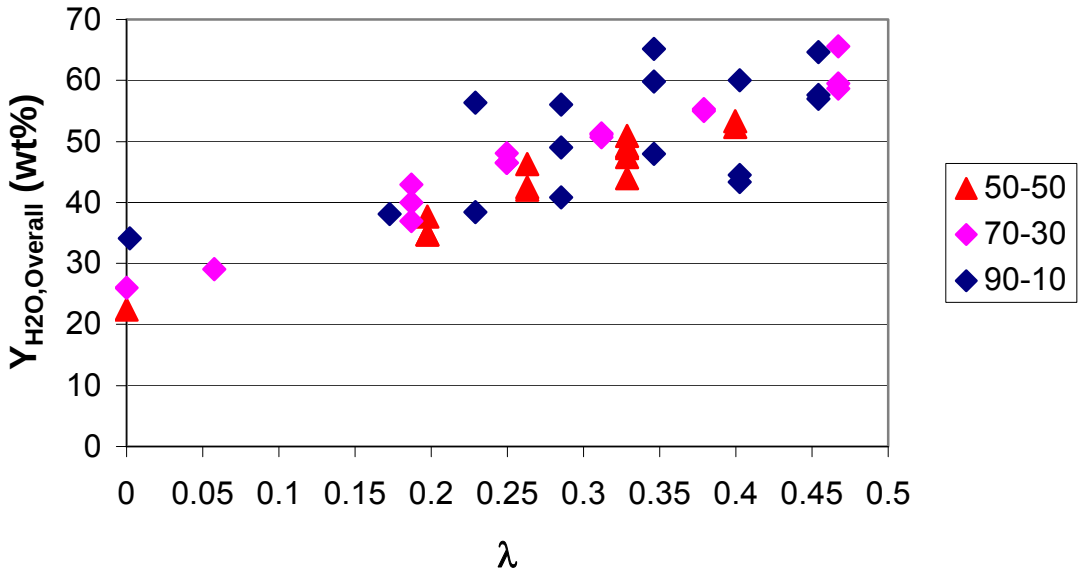

Figure 3.17. Overall H_2O yield as a function of λ (0 to 0.5) for 50:50, 70:30, and 90:10 bio-oil:methanol mixtures (650ºC; ~0.3 s).

those described earlier in this chapter using the 50:50 mixture and the 120 kHz nozzle. A specially designed reactor was used, which allowed for O_2 addition at the top as well as further down in the reactor (~8 cm from the bottom). The conditions and results of these experiments are presented in Table 3.2.

By comparing Run 1 to Run 4 and Run 2 to Run 5, several undesirable trends were observed. When some of the oxygen was introduced downstream (i.e., staging), lower H_2 and CO yields were observed. Methanol conversion was slightly lower. An increase in CO_2 yield was especially noticeable when comparing Run 2 to Run 5. Both the carbon to gas conversion and the carbon accountings decreased as more of the oxygen was shifted to the lower entry point. The results of Run 2 were similar to data presented earlier in this chapter. In short, there did not appear to be any clear advantage to staged oxygen addition. The results of staged addition during catalytic runs will be discussed in Chapter 7.

Table 3.2. Results of staged oxygen addition. Helium flow was 512 to 522 sccm. The 50:50 bio-oil:methanol mixture flow was 0.16 g/min.

Run	1	2	3	4	5
Upper O_2 flow (sccm)	36	36	27	27	27
Lower O_2 flow (sccm)	0	18	0	10	28
effective O:C	1.3	1.6	1.1	1.3	1.6
Methanol Conversion (%)	90.7	94.6	81.2	87.8	92.7
$Y_{H2,Overall}$ (wt. %)	22.5	21.9	13.8	17.5	14.6
$Y_{H2O,Overall}$ (wt. %)	42.3	48.2	34.1	40.6	52.3
$Y_{CO,Overall}$ (wt. %)	57.8	62.4	43.0	52.8	48.1
$Y_{CO2,Overall}$ (wt. %)	7.9	10.4	6.0	8.3	22.7
$C.G._{Overall}$ (wt. %)	69.2	76.5	52.1	64.7	73.7
$C.A._{Overall}$ (wt. %)	75.1	80.1	62.3	71.7	79.0
$Y_{CO,Bio-oil}$ (wt. %)	43.8	51.7	21.3	31.5	23.8
$Y_{CO2,Bio-oil}$ (wt. %)	4.0	5.9	3.5	5.3	28.5
$Y_{CH4,Bio-oil,max}$ (wt. %)	6.4	6.7	5.4	6.4	5.2
$Y_{Benzene,Bio-oil,max}$ (wt. %)	1.5	1.4	0.9	1.1	1.1
$Y_{Residual\ carbon,Bio-oil,max}$ (wt. %)	1.7	0.6	2.6	1.6	2.4
$C.G._{Bio-oil}$ (wt. %)	54.3	64.3	30.2	43.2	57.5
$C.A._{Bio-oil}$ (wt. %)	55.8	64.7	33.0	49.6	62.6

3.7 Reduction of Residence Time

While an increase of the flow rates could have accomplished a reduction in the residence time (from ~0.3 s to ~0.2 s), the length of the reactor was decreased by 3.5 cm instead in preparation for the catalytic runs where changes in the flow rate could also lead to changes in the mass transfer properties. Keeping the mass transfer properties the same ensures that differences are due to kinetics. During the experiments presented in this section, the flow rates were the same as earlier experiments and the temperature was 650ºC. The reactor

used for the previous experiments is designated the long reactor. The 50:50 bio-oil:methanol mixture was fed using the 120 kHz nozzle.

The shorter residence time did not have a large impact on the major product yields. Figure 3.18 shows the estimated bio-oil CO and CO_2 yields (Method 2) for both the long and the short reactor. With the exception of the estimated bio-oil CO yield under pyrolysis conditions (effective O:C = 0.7), the CO yield for the shorter residence time was similar to that for the longer residence time at all effective O:C. Just as with the CO yield, the shorter reactor has little effect on the CO_2 yield except that it was lower under pyrolysis conditions. Similar trends were observed with the overall CO and CO_2 yields. The overall H_2 and H_2O yields are shown on Figure 3.19. The H_2 yields were unaffected by the shorter reactor, while the H_2O yields were affected only at affected under pyrolysis conditions. Under such conditions, slightly lower yields were observed in the case of the shorter reactor.

The decrease in the residence time had a much more apparent impact on the minor products than was the case with the major products. The methane

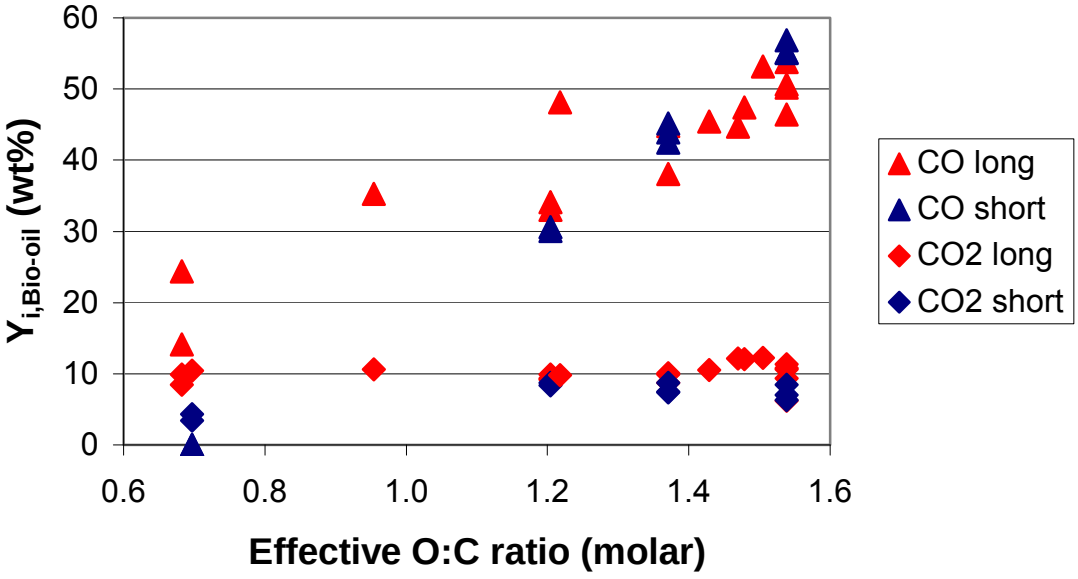

Figure 3.18. Comparison of estimated bio-oil CO and CO_2 yield for shorter reactor to longer reactor using 50:50 bio-oil methanol mixture at 650 ºC. The residence time for the shorter reactor was ~0.2 s rather than ~0.3 s.

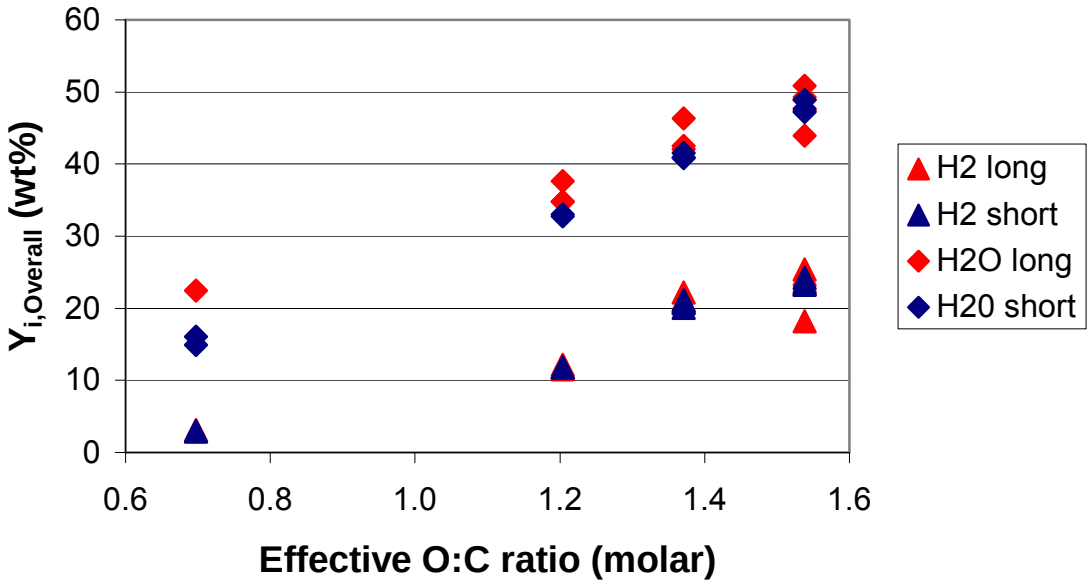

Figure 3.19. Comparison of H_2 and H_2O yield for shorter reactor to longer reactor using 50:50 bio-oil methanol mixture at 650 ºC. The residence time for the shorter reactor was ~0.2 s rather than ~0.3 s.

yield was lower in the case of the shorter residence time (see Figure 3.20). The same was true for the benzene yield (Figure 3.21). The residual carbon yield was similar for both reactors (Figure 3.22). The scatter in the residual carbon data can be attributed to two effects. First, there were times when drops would fall from the nozzle resulting in more CO and CO_2. Second, there was some uncertainty in determining the start time for the integration. (i.e., Where did the reaction stop and the burn-off begin?)

3.8 Summary

The preliminary data above suggested the following about the NPOX chemistry:

1. Surprisingly high CO yields were obtained from non-catalytic chemistry. Siginificant increases in CO yield were observed with increasing O_2 without a similar increase in CO_2 yield.
2. The optimal effective O:C for synthesis gas yields was between ~1.4 and ~1.6 (λ between ~0.27 and ~0.35).
3. With oxygen added, there appeared to be little temperature dependence. However, temperatures greater than 600ºC were required.
4. Method 2 for estimating bio-oil CO and CO_2 yields appears to do a good job since varying the amount of methanol added did not lead to significant differences.
5. Other than possibly increasing the overall H_2 yield, methanol addition did not appear to have a significant impact.
6. There were no apparent advantages to staged addition of O_2.
7. Decreasing the NPOX residence does not have a significant impact on major product yields. However, the change leads to lower yields in the case of methane and benzene.

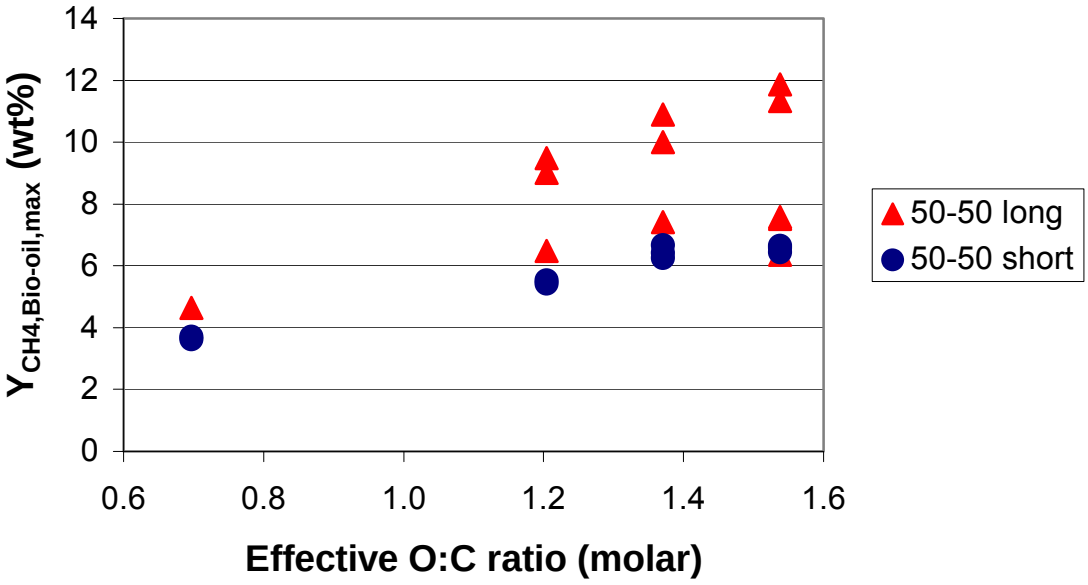

Figure 3.20. Comparison of maximum bio-oil CH_4 yield for shorter reactor to longer reactor using 50:50 bio-oil methanol mixture at 650 ºC. The residence time for the shorter reactor was ~0.2 s rather than ~0.3 s.

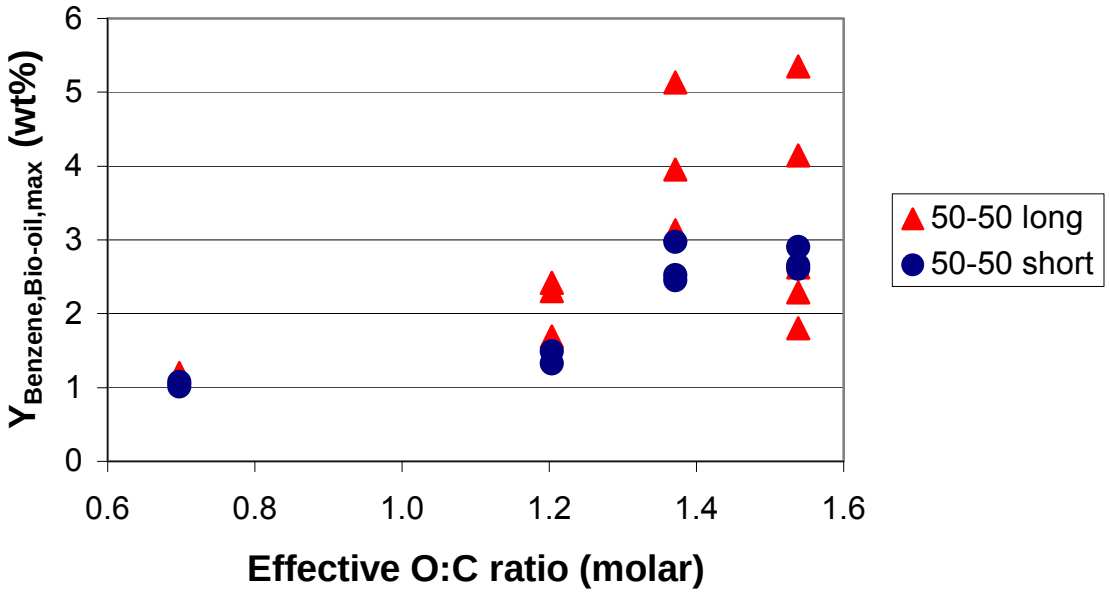

Figure 3.21. Comparison of maximum bio-oil benzene yield for shorter reactor to longer reactor using 50:50 bio-oil methanol mixture at 650 ºC. The residence time for the shorter reactor was ~0.2 s rather than ~0.3 s.

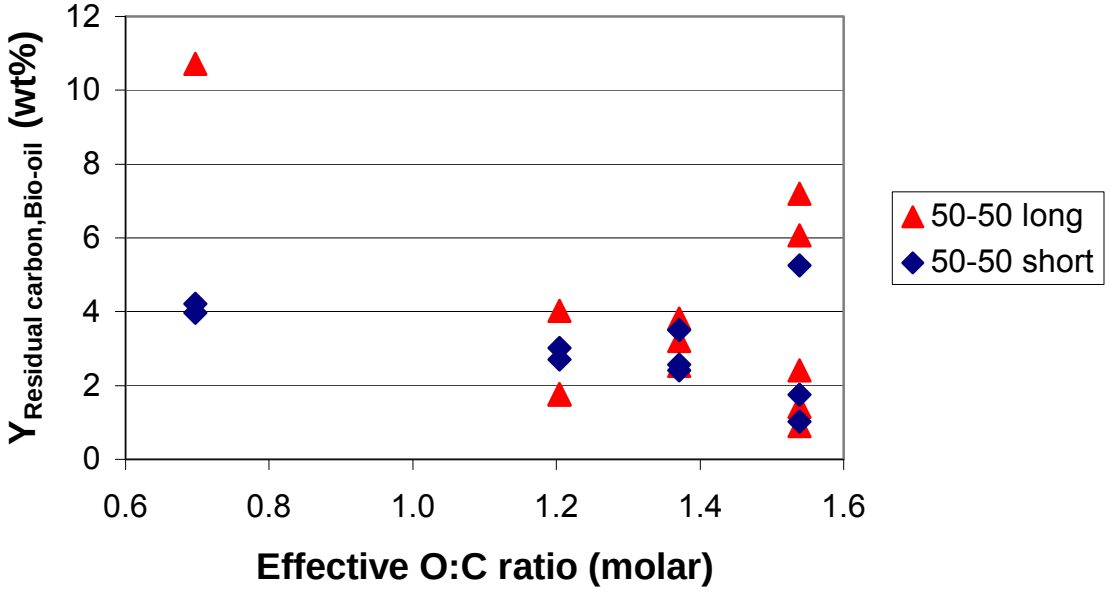

Figure 3.22. Comparison of maximum bio-oil residual carbon yield for shorter reactor to longer reactor using 50:50 bio-oil methanol mixture at 650 ºC. The residence time for the shorter reactor was ~0.2 s rather than ~0.3 s.

CHAPTER 4
NON-CATALYTIC REFORMING OF 50:50 BIO-OIL METHANOL MIXTURE

Both the effects of temperature and added oxygen have been explored using the 25 kHz nozzle and a 50:50 (wt. %) bio-oil:methanol mixture. As will be seen, the results using this nozzle are even better than those observed using the 120 kHz nozzle. Presumably this was due to more efficient atomization. Temperatures were varied between 625 and 850ºC at a constant residence time (~0.3 s). The effective O:C ratio was varied from pyrolysis conditions (0.7 for the 50:50 mixture; $\lambda = 0$) to a maximum of ~1.6 ($\lambda = \sim 0.35$). The effect of these process parameters will be discussed in this chapter. As is discussed in Section 3.1, the effective O:C ratio does not include oxygen in water as it was not reactive under these conditions. It should be noted that the effective O:C ratio is 0.13 lower than the actual O:C ratio. At 800 and 850ºC, the maximum effective O:C ratio was only 1.5 due to observable flames in the entrance region. Likewise, in the case of the other temperatures, effective O:C ratios higher than 1.6 yielded observable flames in the entrance region.

A propagation of error analysis was performed. For this analysis, three types of errors were considered. The largest contribution came from noise in the mass spectrometer signal. The other two types of error were due to errors in the calibrations of the MBMS and the feed (i.e., syringe pump), but their total contribution was never more than 25% of the total error. The error bars shown in all figures are a result of this propagation of error analysis. It should also be noted that the data presented are typically the average of at least two runs (with the exception of the higher aromatics data where only one run for each condition was performed). In spite of the error discussed above, the results of the different runs with the same conditions were typically in good agreement. (Note: The definitions explained in Section 3.1 will be used in this chapter as well.)

4.1 Methanol Conversion

The effect of temperature as well as added oxygen on the extent of methanol conversion in the 50:50 (wt. %) bio-oil:methanol mixture experiments was explored. The conversion of methanol from these experiments is shown in Figure 4.1. It is notable that the conversion of methanol in mixtures with bio-oil might be higher than that for pure methanol (see Figure 3.3). It also showed a dramatic temperature dependence at lower effective O:C ratios (0.7 to 1.2; λ = 0 to 0.2). However, even at the highest temperature, the methanol conversion was only around 45% under pyrolysis conditions. The increase in methanol conversion was more significant (to a maximum conversion of greater than 90%) when oxygen was added to the system. At lower effective O:C ratios pyrolysis reactions, which typically are more temperature dependent, controlled the kinetics. As the effective O:C increased, partial oxidative reactions become more important and the temperature dependence is much weaker.

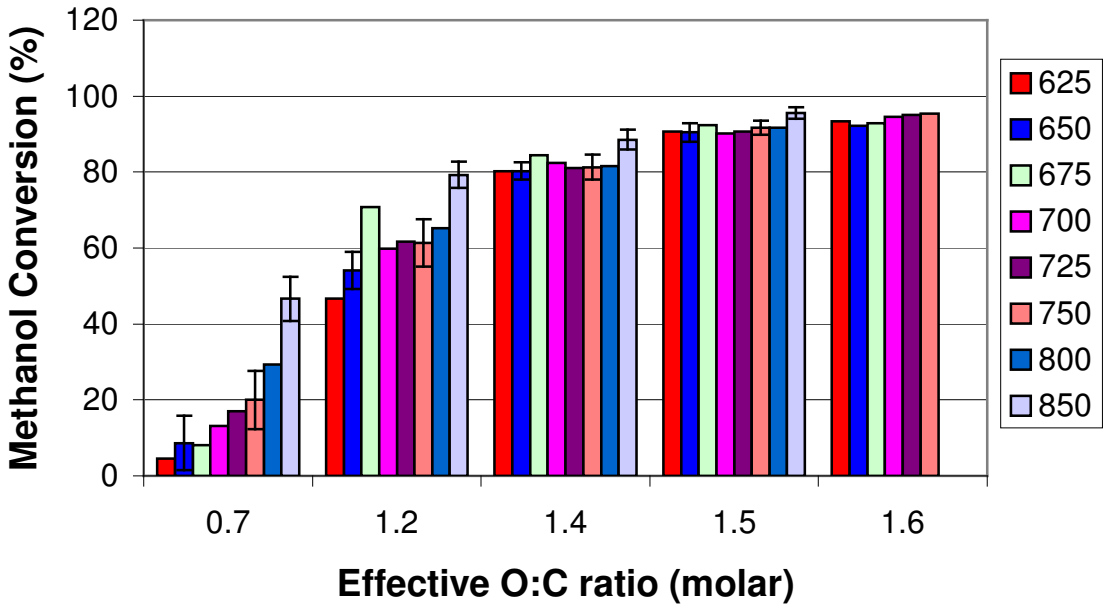

Figure 4.1. Methanol conversion as a function of effective O:C ratio (oxygen in water removed) for λ = 0 to 0.35 observed during 50:50 bio-oil methanol experiments at temperatures between 625 and 850˚C.

4.2 Hydrogen

Figure 4.2 shows the overall hydrogen yield (Eqn. 3.4) as a function of effective O:C ratio for the entire temperature range. At lower effective O:C ratios, the hydrogen yield increased with increasing temperature (pyrolysis reactions controlled the kinetics). In general, the maximum hydrogen yield (~25%) occurred at effective O:C ratios between 1.4 and 1.6 (λ = 0.27 to 0.35) independent of temperature (partial oxidation reactions controlled kinetics). Although this yield was low, a significant amount of H_2O (~50-60 % yield under these conditions with similar trends at other conditions) and CO (discussed below) were observed. These can be reacted over a water gas shift catalyst to increase the hydrogen yield. The water can also assist with steam reforming of hydrocarbons over the catalyst, decreasing the amount of water that must be added to prevent carbon deposition. Equilibrium yields of hydrogen (~80% at 650ºC) have been observed during preliminary catalytic experiments over a rhodium based catalyst without water addition (see Chapter 7).

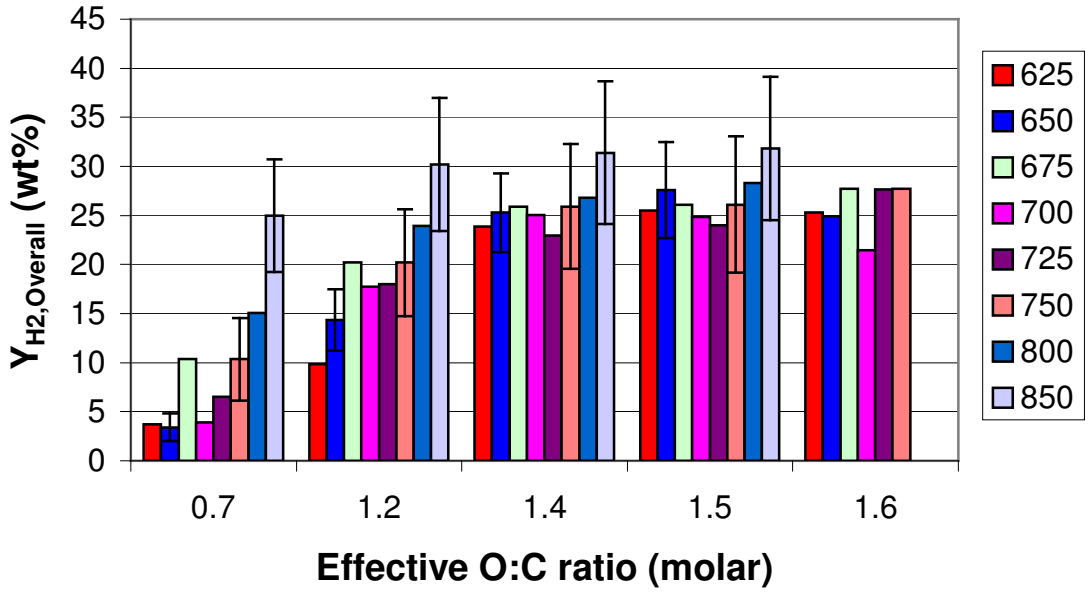

Figure 4.2. Overall hydrogen yield as a function of effective O:C ratio (oxygen in water removed) for λ = 0 to 0.35 observed during 50:50 bio-oil methanol experiments at temperatures between 625 and 850˚C.

4.3 Carbon Monoxide

As shown in Figures 4.3 and 4.4, the maximum of both the overall CO yield and the estimated CO yield from bio-oil (with both estimation values shown) occurred over nearly the same range of effective O:C ratios (1.5 to 1.6; λ = 0.31 to 0.35) as the maximum H_2 yield. It is remarkable that a bio-oil CO yield of ~70-80% (assuming Eqn. 3.7) was observed from this non-catalytic chemistry. Even employing the conservative assumption that all of the methanol was converted to CO (Eqn. 3.5), the CO yield from bio-oil is still surprisingly high (~50-65%). The higher yields were attributed to more efficient atomization. As was the case with hydrogen, the temperature had a large effect on CO yield at low effective O:C ratios and nearly no effect on CO yield at higher effective O:C ratios. Even at the highest temperatures, the CO yield at low effective O:C ratios did not approach that at higher O:C ratios produced at lower temperatures. Clearly, the amount of oxygen added was more important to the CO yield than was the temperature confirming the results of the preliminary data.

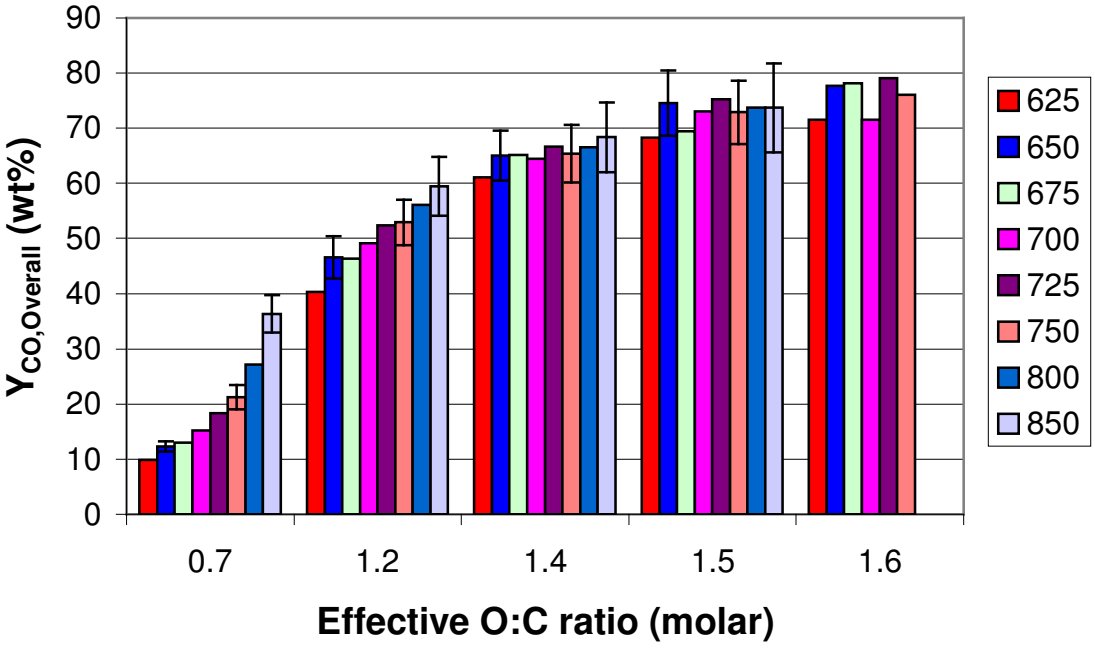

Figure 4.3. Overall CO yield as a function of effective O:C ratio (oxygen in water removed) for λ = 0 to 0.35 and temperature for 50:50 bio-oil methanol experiments.

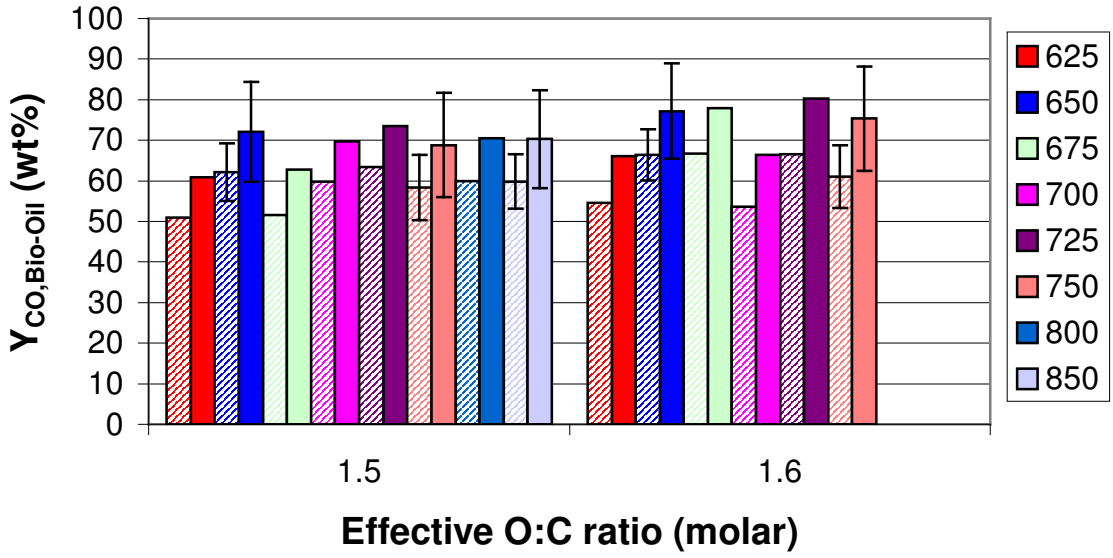

Figure 4.4. Estimated CO yield from bio-oil as a function of effective O:C ratio (oxygen in water removed) for λ = 0 to 0.35 and temperature for 50:50 bio-oil methanol experiments. Includes both the minimum CO from bio-oil (lighter shading on left) that assumes all methanol was converted to CO, and the value (darker shading on right) estimated assuming the selectivity for CO production from methanol was the same in the mixture as in the neat methanol experiments.

4.4 Carbon Dioxide

Fortunately, the increased oxygen that led to increased CO yields led to only a gradual increase in the overall CO_2 yield (Figure 4.5). The temperature effect on the bio-oil component of CO_2 production was even less (Figure 4.6). This indicated that the CO_2 was likely derived primarily from components of bio-oil (e.g., from organic acids such as acetic acid) rather than from oxidation of CO. As with CO, we obtained two estimates of the CO_2 yield from bio-oil. The larger yield results from the assumption that methanol conversion produces only CO (Eqn. 3.6), meaning that all the observed CO_2 came from bio-oil. Thus, this estimate represents an upper bound to the CO_2 yield from bio-oil. The lower yield assumed that the CO_2 selectivity from methanol was the same as in the neat methanol experiments and was defined by Eqn. 3.7. Both values are shown in

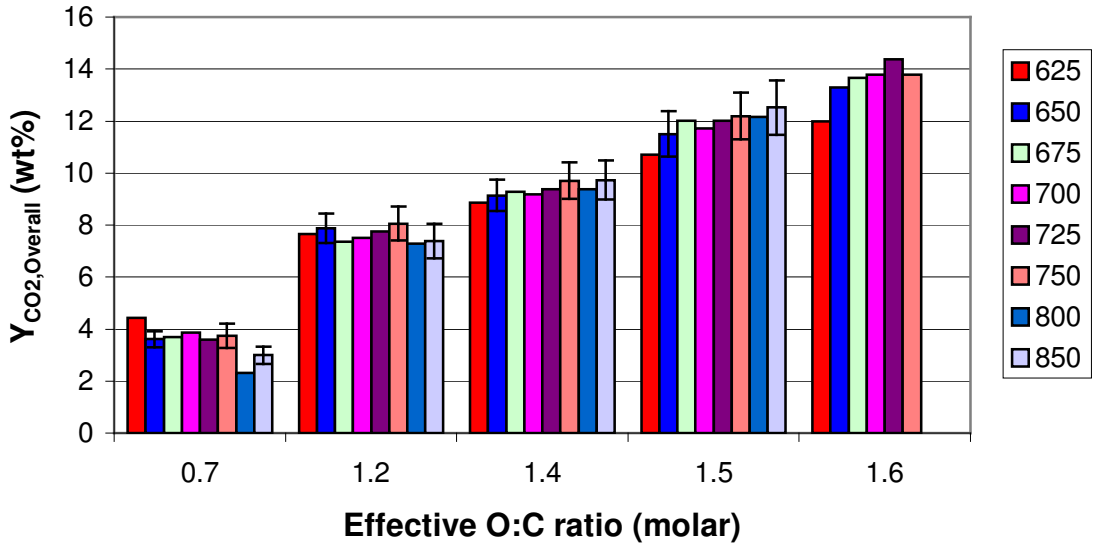

Figure 4.5. Overall CO_2 yield as a function of effective O:C ratio (oxygen in water removed) for λ = 0 to 0.35 and temperature for 50:50 bio-oil methanol experiments temperatures between 625 and 850˚C.

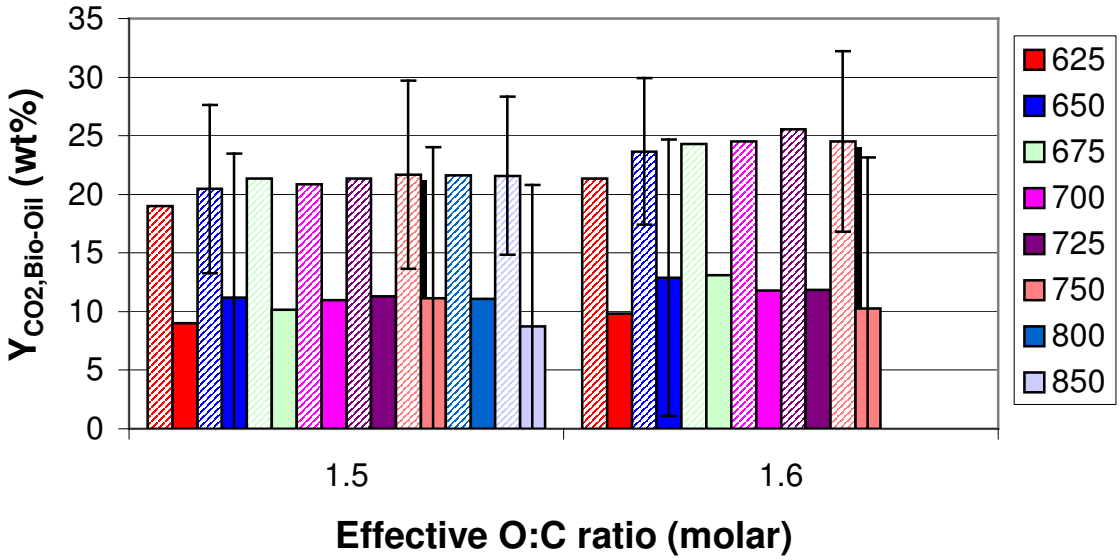

Figure 4.6. Estimated CO_2 yield from bio-oil as a function of effective O:C ratio (oxygen in water removed) for λ = 0 to 0.35 and temperature for 50:50 bio-oil methanol experiments temperatures between 625 and 850˚C. Includes the maximum CO_2 yield from bio-oil (lighter shading on left) that assumes all CO_2 is derived from bio-oil and the value (darker shading on right) estimated assuming the selectivity for CO_2 production from methanol was the same in the mixture as in the neat methanol experiments.

Figure 4.6. The overall CO_2 yield peaked at 14% (Figure 4.5). The maximum CO_2 yield from bio-oil (Method 1 represented as diagonal fill in Figure 4.6) is only shown for the optimal conditions (i.e., where CO and H_2 were maximized) and typically had a value between 20 and 25%. Likewise, the lower estimated CO_2 yield (Method 2; solid value shown in Figure 4.6) from bio-oil is only shown for the optimal conditions and was typically between 9 and 13%. This value attempted to account for CO_2 production from methanol.

4.5 Methane

The fact that conversion to methane (Figure 4.7) was significant during bio-oil:methanol experiments while only very small amounts of methane were observed in the neat methanol experiments suggests that there was a much larger pool of methyl radicals present in the mixture experiments. At low effective O:C ratios, the methane yield (from Eqn. 3.8) increased with increasing temperature. This phenomenon is consistent with pyrolysis control as described above. Increased O:C ratio led to lower methane yields suggesting that either

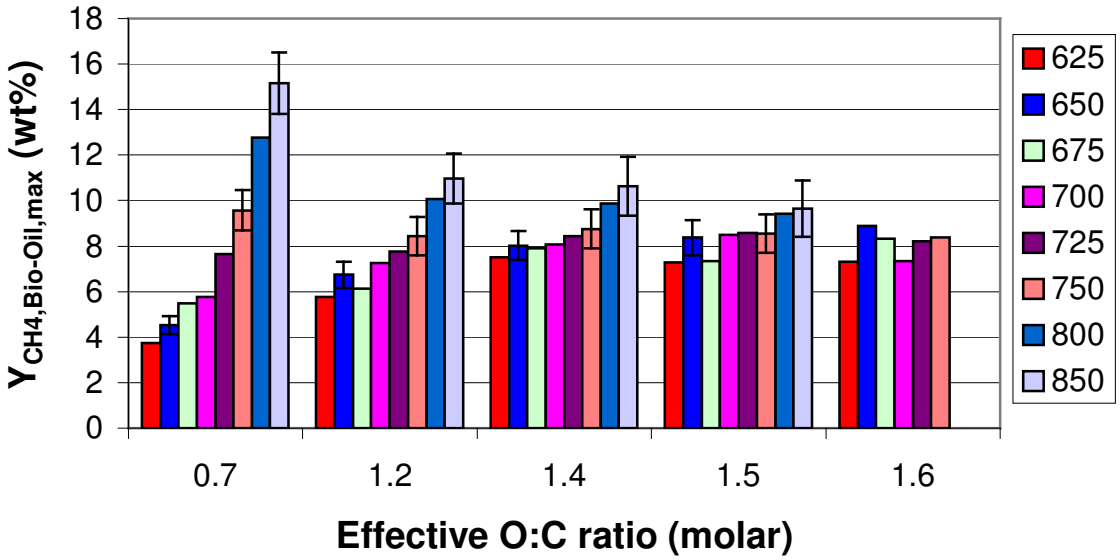

Figure 4.7. Maximum methane yield from bio-oil as a function of effective O:C ratio (oxygen in water removed) for λ = 0 to 0.35 and temperature for 50:50 bio-oil methanol experiments.

methane was consumed by reaction with oxygen or that the presence of oxygen facilitated pathways to other species thus avoiding methane production. Under optimal conditions (effective O:C of 1.5 to 1.6; λ = 0.31 to 0.35), the maximum methane yield from bio-oil was typically ~8%.

4.6 Gas Production

Figures 4.8 and 4.9 show the overall carbon to gas conversion and the estimated carbon to gas conversion from bio-oil. This represents the amount of carbon converted to CO, CO_2, and CH_4. Under optimal conditions (effective O:C of ~1.5 to 1.6; λ of ~0.31 to 0.35), the carbon to gas conversion (both overall and estimated from bio-oil) was 85 to 95%, showing excellent gasification efficiencies. This result can be compared to what was reported by van Rossum et al.[31] They reported 87 % carbon to gas (similar to carbon to gas conversion given in this work) from a bio-oil derived from beech wood under NPOX conditions at 835ºC and equivalence ratio of 0.23. However, their result under pyrolysis conditions for bio-oil derived from pine wood at 790ºC (65 % carbon to gas) was significantly higher than the present study. Even at 850ºC, the carbon to gas conversion

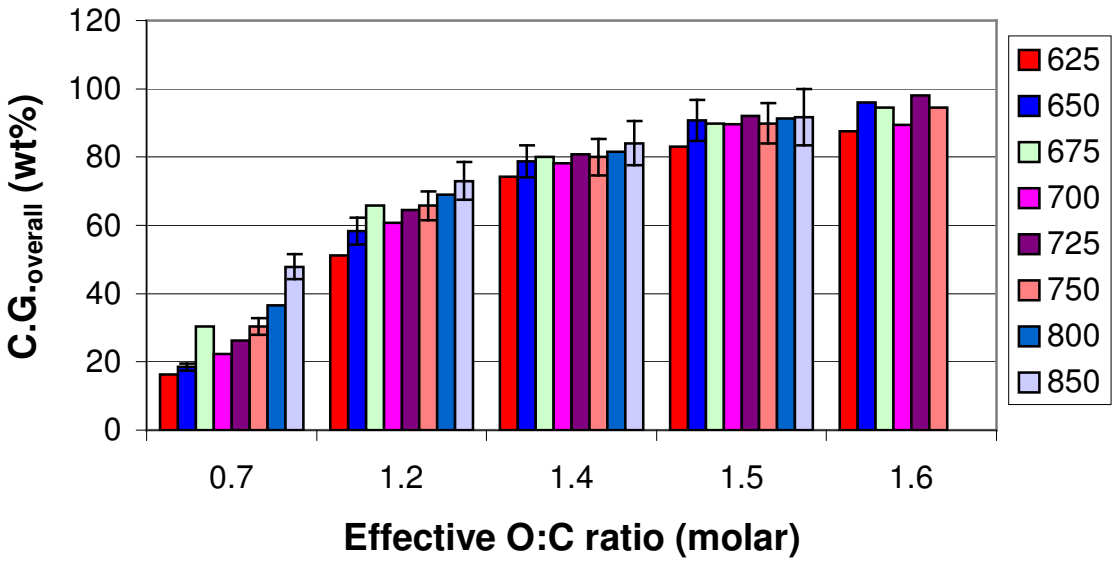

Figure 4.8. Overall carbon to gas conversion as a function of effective O:C ratio (oxygen in water removed) for λ = 0 to 0.35 and temperature for 50:50 bio-oil methanol experiments.

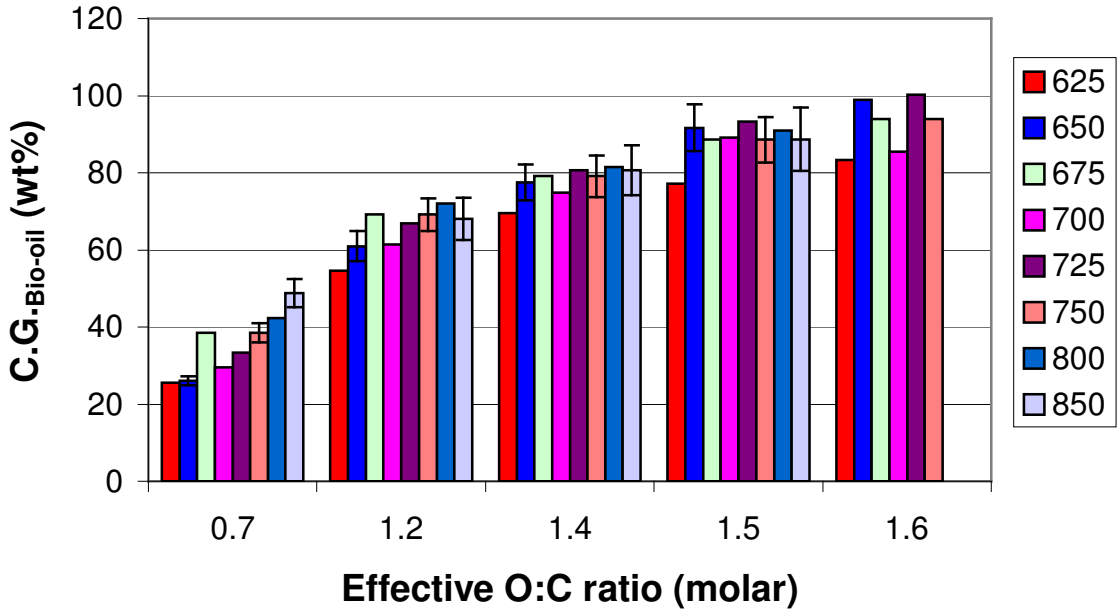

Figure 4.9. Estimated bio-oil carbon to gas conversion as a function of effective O:C ratio (oxygen in water removed) for λ = 0 to 0.35 and temperature for 50:50 bio-oil methanol experiments.

(both overall and bio-oil) was only ~50 % under pyrolysis conditions (effective O:C = 0.7; λ = 0). The difference between the results reported by van Rossum et al. and the present results is likely due to the difference in bio-oil composition. Beech pyrolysis oil used in their studies had much less carbon and more water than our bio-oil suggesting that a part of oligomeric lignin fraction phase separated from beech bio-oil used in their tests.

4.7 Benzene

The maximum benzene yield from bio-oil (Eqn. 3.8) is presented in Figure 4.10. The benzene yield increased with increasing temperature at low effective O:C (0.7 and 1.2; λ = 0 and 0.20). At higher effective O:C ratios, temperature effects were not quite clear. The benzene yield tended to decrease with increasing effective O:C ratio. However, under all conditions, the benzene yield was below 4.5 %, which is comparable to that observed for oak gasification experiments performed at NREL[50].

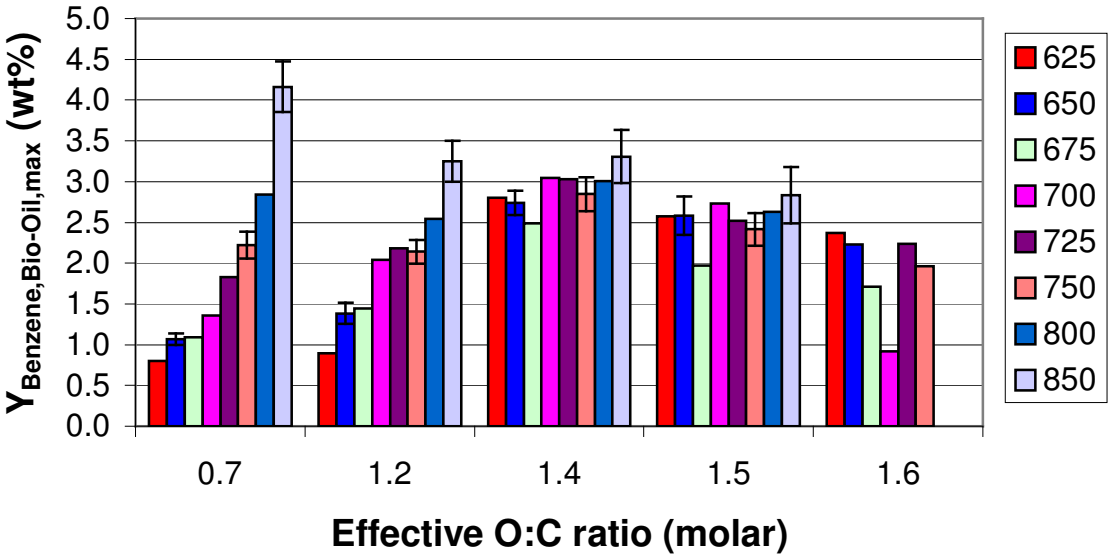

Figure 4.10. Maximum benzene yield from bio-oil as a function of effective O:C ratio (oxygen in water removed) for λ = 0 to 0.35 and temperature for 50:50 bio-oil methanol experiments.

4.8 Higher Aromatics

Figures 4.11 to 4.13 illustrate the impact of added oxygen on the amount of aromatics formed. These figures show the sum of all species with m/z greater than 78, 128, and 178, respectively, as a percentage of the total signal. At the higher O:C ratios, temperature had less impact on the extent of cracking of these higher molecular weight species than observed at lower O:C values. The addition of oxygen led to a significant decrease in these higher molecular weight species. Since these significant decreases did not lead to corresponding increases in benzene and naphthalene, one can conclude that the cracking of the higher molecular weight species was not limited to the loss of side groups on aromatic rings. These data suggest that oxygen addition converts larger aromatic species to smaller molecules.

The fact that aromatic formation was relatively insensitive to temperature for the O:C ratios that produce the high yields of CO suggests that the aromatics yield is not a major factor in terms of identifying an optimal temperature for bio-oil conversion. The lack of any significant temperature dependence suggests that

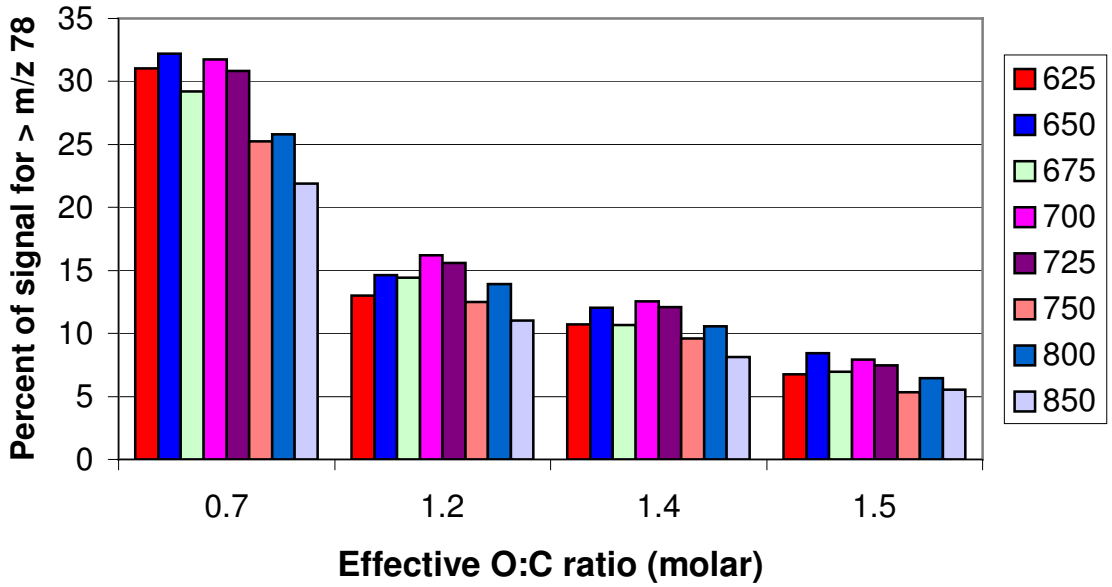

Figure 4.11. Impact of added oxygen for λ = 0 to 0.35 and temperature on the sum of all species with m/z greater than 78 as a percentage of the total signal.

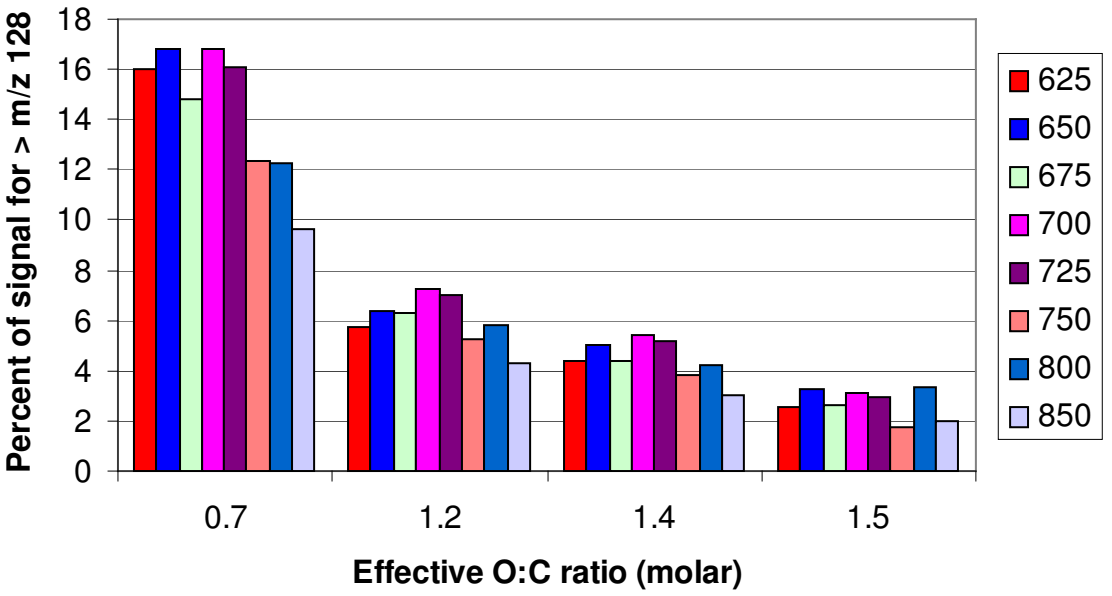

Figure 4.12. Impact of added oxygen for λ = 0 to 0.35 and temperature on sum of all species with m/z greater than 128 (given as a percentage of the total signal).

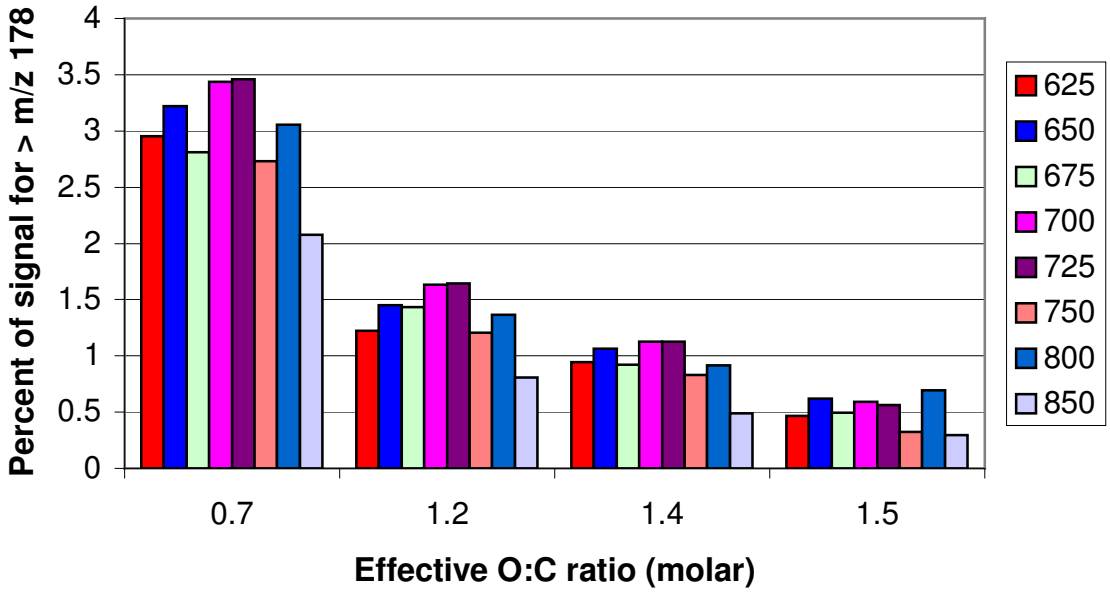

Figure 4.13. Impact of added oxygen for λ = 0 to 0.35 and temperature on sum of all species with m/z greater than 178 (given as a percentage of the total signal).

the expected increase in aromatics formation with increasing temperature is offset by the addition of oxygen. Additionally, there actually appeared to be a decrease in the higher molecular weight species with increasing temperature under pyrolysis conditions rather than the increase that was expected[34-38]. It should be noted that the earlier experiments were performed using model compounds rather than much more complex bio-oil system.

4.9 Residual Carbon

The overall residual carbon yield observed and the maximum residual carbon yield from bio-oil (Figure 4.14) are again related by Eqn. 3.8. Due to the high degree of uncertainty of the residual carbon data (calculated from CO_2 signal observed during the burn-off of the carbon deposits after partial oxidation), it was difficult to quantitatively determine any clear trends. Drips from the nozzle often occurred during burn-off and there was some uncertainty in the determination of when the reaction ended and burn-off began. However, in

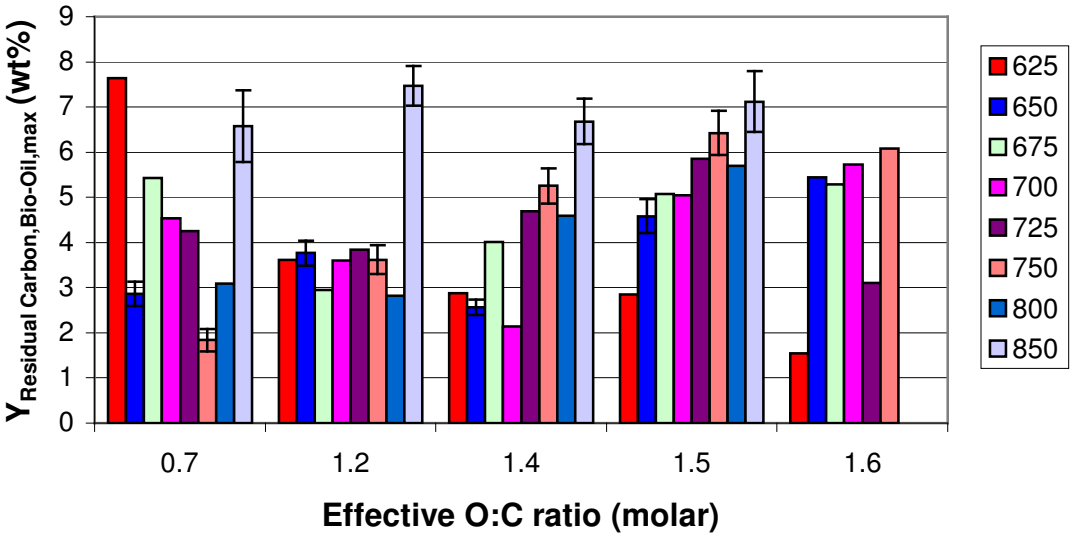

Figure 4.14. Maximum residual carbon yield from bio-oil as a function of effective O:C ratio (oxygen in water removed) for λ = 0 to 0.35 and temperature for 50:50 bio-oil methanol experiments.

general, the overall residual carbon yield was less than 4% while the maximum bio-oil residual carbon yield was less than 8%.

4.10 Carbon Accounting

Figures 4.15 and 4.16 show that higher effective O:C ratios and higher temperatures lead to carbon accountings (both overall – Eqn. 3.9 – and bio-oil – Eqn. 3.10) closer to 100%. Presumably, this was due to higher conversions (particularly of higher molecular weight species) to measured species. Added oxygen was a more important parameter than temperature as it had a greater impact on increasing the conversion to measured species**.**

4.11 Summary

The following conclusions were drawn from the 50:50 bio-oil methanol experiments using the 25 kHz nozzle:

1. The surprisingly high CO yield from non-catalytic chemistry was even higher than seen in preliminary experiments. The significant increase in

CO yield with increasing oxygen without a similar increase in CO_2 yield was confirmed.

2. The optimal effective O:C for synthesis gas yields was narrowed to between ~1.5 and ~1.6 (λ between ~0.31 and ~0.35).

3. Just as in preliminary experiments, very little temperature dependence was observed during NPOX. With the exception of a possible increase in the hydrogen yield at 850 ºC, there were no clear advantages to temperatures higher than 700ºC. In fact, there might be a disadvantage to going above 700 ºC since there was some evidence that this leads an increase in undesirable products (i.e., residual carbon and perhaps benzene).

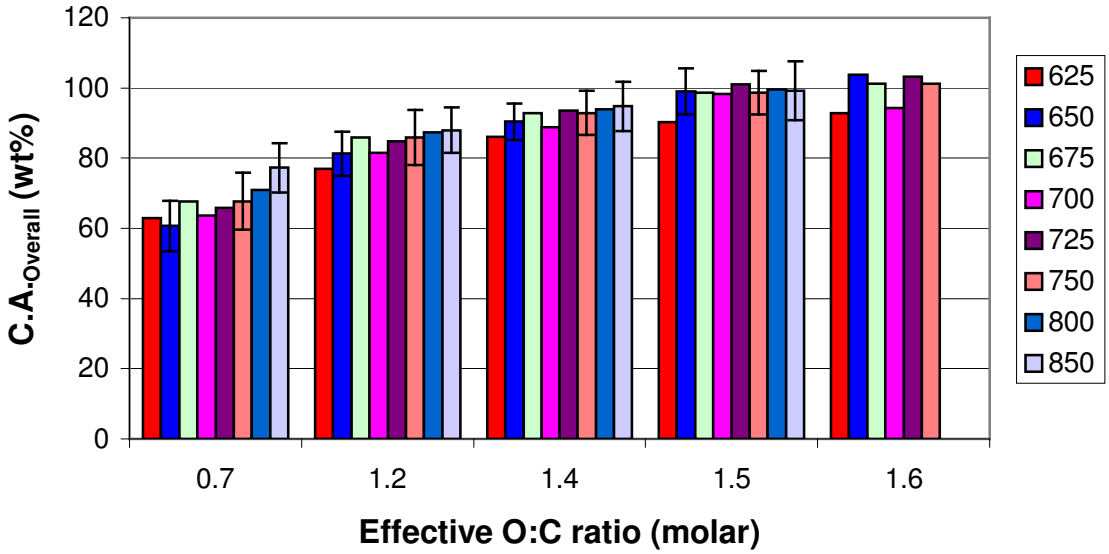

Figure 4.15. Overall carbon accounting as a function of effective O:C ratio (oxygen in water removed) for λ = 0 to 0.35 and temperature for 50:50 bio-oil methanol experiments.

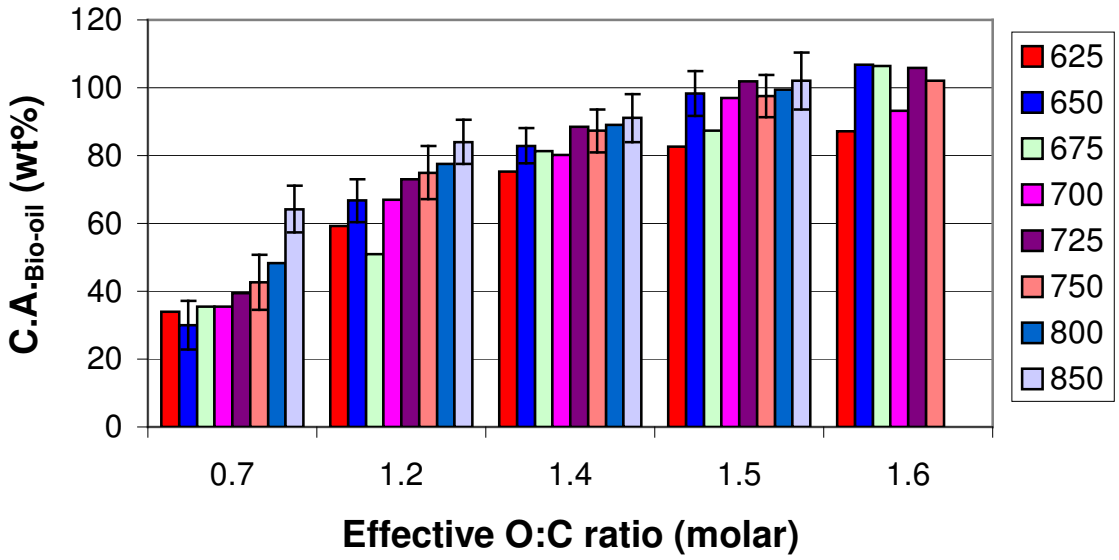

Figure 4.16. Estimated bio-oil carbon accounting as a function of effective O:C ratio (oxygen in water removed) for λ = 0 to 0.35 and temperature for 50:50 bio-oil methanol experiments. Assumes that all carbon entering as methanol is accounted for.

CHAPTER 5
COMPARISON OF 70:30 BIO-OIL:METHANOL NPOX TO 50:50 RESULTS

Further insight into the NPOX reforming of bio-oil was gained by comparing the results of the 50:50 bio-oil:methanol mixture experiments to the NPOX of a 70:30 (wt. %) bio-oil:methanol mixture. Experiments using a 70:30 (wt. %) bio-oil:methanol mixture were designed to ensure that the carbon concentration was the same as during the 50:50 mixture experiments described in Chapter 4 while still maintaining the same residence time of ~0.3 s. Because bio-oil has a higher carbon content than methanol, the bio-oil:methanol flow rate from the 70:30 mixture experiments was lower than that of the 50:50 mixture experiments. The bio-oil:methanol mixture was fed using the 25 kHZ (upgraded) nozzle to allow explicit comparison to the 50:50 mixture.

The temperature was varied from 650 to 750ºC. The oxygen that was added to the system was increased until flaming conditions were observed either visually or through observed pressure pulsations. At 650 and 675ºC, the equivalence ratio (λ) was varied from 0 to 0.42. At the higher temperatures, the highest equivalence ratio was 0.39. The equivalence ratio is a better parameter for comparing the different mixtures than the effective O:C ratio since the compositions are different. Bio-oil requires less added oxygen for full oxidation than methanol due to its higher degree of oxidation.

5.1 Methanol

Over the temperature range (650 to 750ºC) used in the 70:30 bio-oil methanol mixture experiments, the methanol conversion from the 70:30 mixture was similar to that observed during 50:50 mixture experiments (see Figure 5.1). Conversions increased with increasing λ. As was the case with the 50:50 mixture, the temperature had a greater effect on the methanol conversion at lower λ (up to 0.25 for the 70:30 mixture). The effect of temperature seemed to

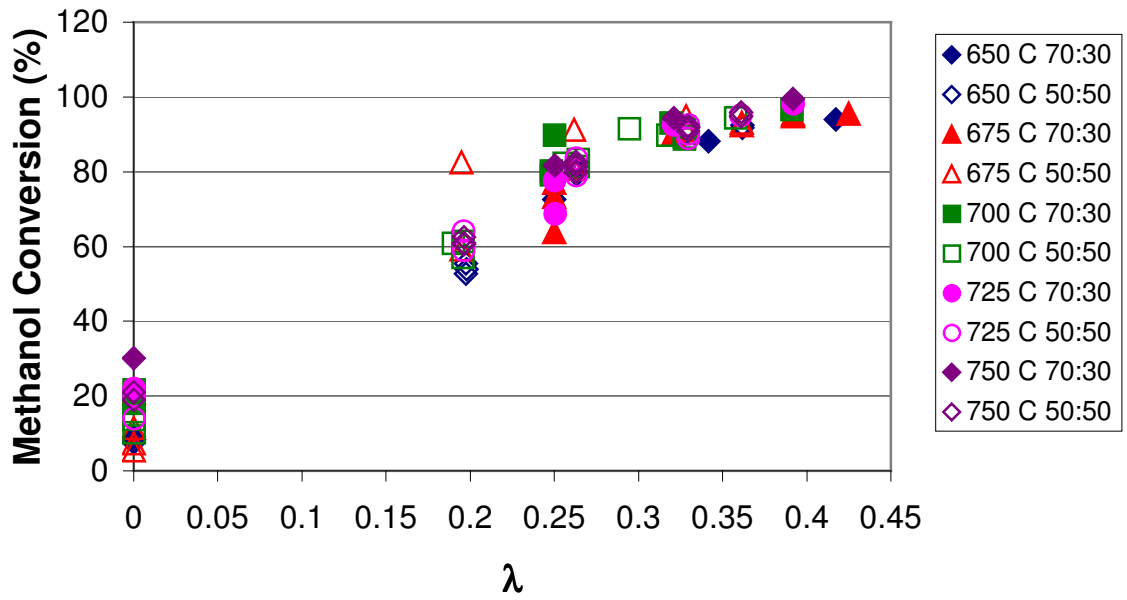

Figure 5.1. Comparison of methanol conversion for 70:30 bio-oil:methanol mixture to the 50:50 mixture results as a function of λ (0 to 0.42) at temperatures between 650 and 750ºC.

be less in the case of the 50:50 mixture since its temperature dependence was only observed to be significant up to λ = 0.2.

5.2 Hydrogen

Figure 5.2 compares the overall H_2 yield (obtained using Eqn. 3.4) from the 70:30 mixture experiments to the 50:50 experiments as a function of λ and temperature. The H_2 yield was lower during 70:30 experiments. Presumably, this was due to the decrease in the methanol content of the feed and suggested that much of the H_2 yield was derived from methanol. If the same yields of H_2 were assumed from methanol in the mixture experiments as were observed during neat methanol experiments, the reduction in methanol content would lead to a 6 to 8% drop in the overall yield. The expected decrease in H_2 yield was similar to that observed. Due to the scatter in the data, the effect of temperature is uncertain for either mixture. The maximum H_2 yield occurred over nearly the same range of λ for both mixtures.

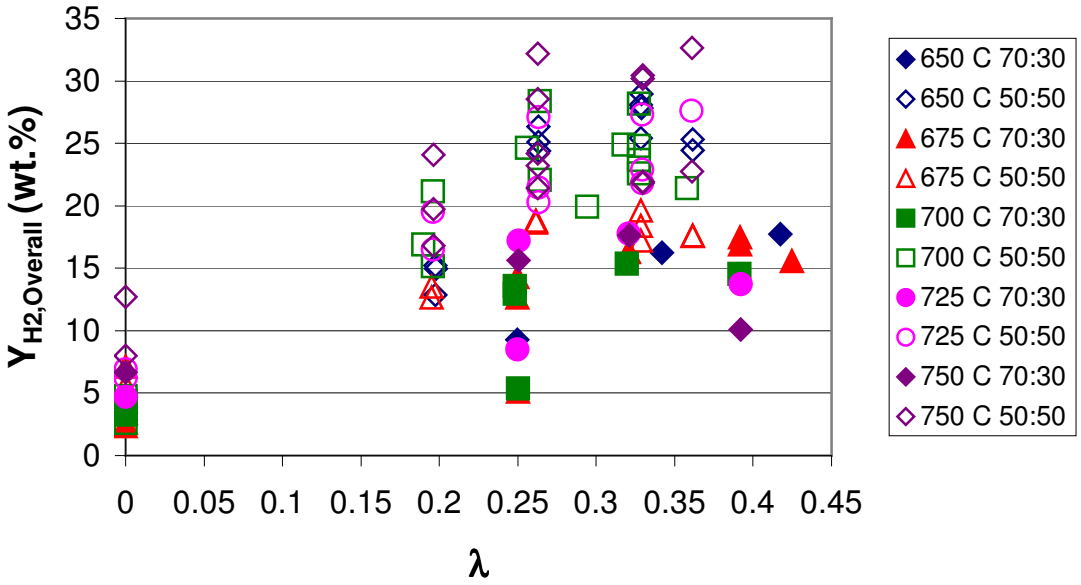

Figure 5.2. Comparison of overall hydrogen yield for 70:30 bio-oil:methanol mixture to the 50:50 mixture results as a function of λ (0 to 0.42) at temperatures between 650 and 750ºC.

5.3 Carbon Monoxide

Although there was significantly more scatter in the 70:30 mixture experiments (see Figures 5.3 and 5.4), both the overall CO yield and the estimated bio-oil CO yield (obtained using Eqn 3.7) were similar for both mixtures under all conditions. The increased scatter illustrated how even a slightly more viscous liquid was more difficult to feed through the nozzle at the low flow rates used in these experiments. The maximum of both the overall CO yield and the estimated CO yield from bio-oil occurred over nearly the same range of λ (0.30 to 0.35) for both mixtures, which was also the same range as the maximum H_2 yield. Again, the amount of oxygen added was more important to the CO yield than was the temperature.

5.4 Carbon Dioxide

As was the case with the 50:50 bio-oil:methanol mixture, the CO_2 yield increased with increasing λ during 70:30 mixture experiments (see Figures 5.5

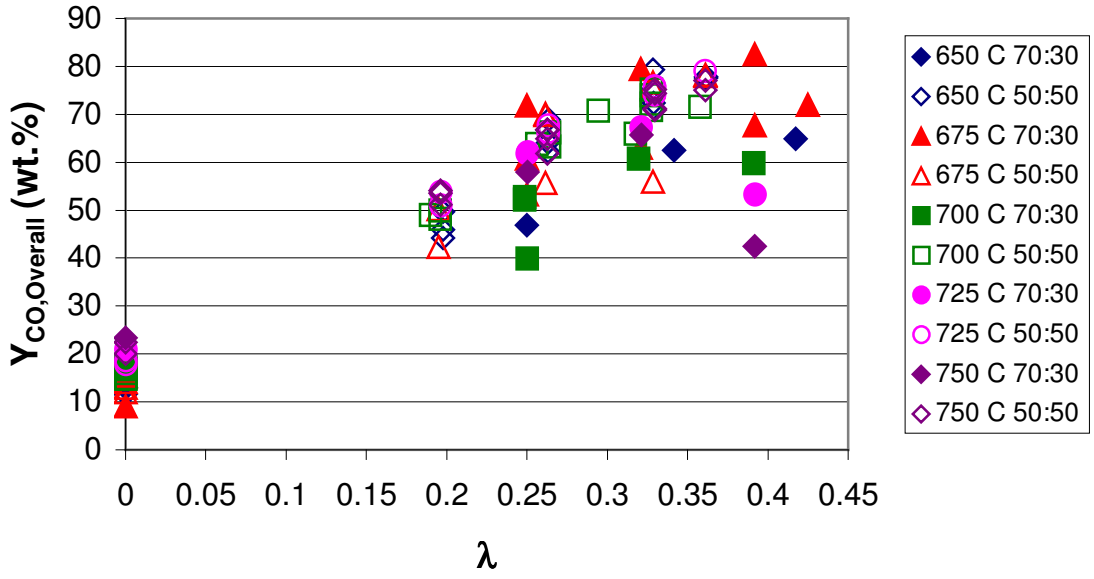

Figure 5.3. Comparison of overall CO yield for 70:30 bio-oil:methanol mixture to the 50:50 mixture results as a function of λ (0 to 0.42) at temperatures between 650 and 750ºC.

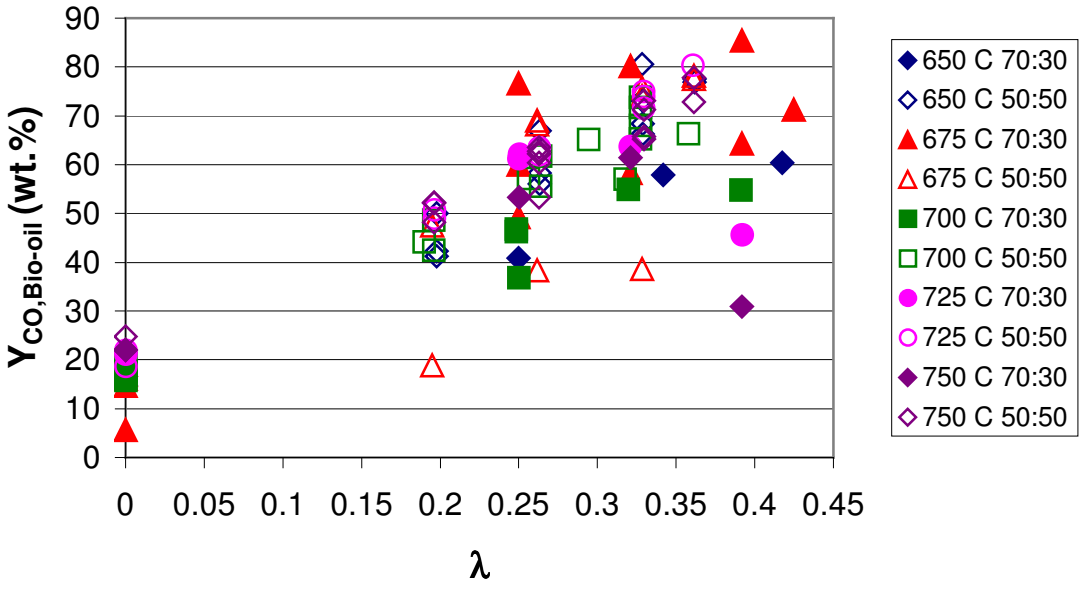

Figure 5.4. Comparison of estimated CO yield from bio-oil (Method 2) for 70:30 bio-oil:methanol mixture to the 50:50 mixture results as a function of λ (0 to 0.42) at temperatures between 650 and 750ºC.

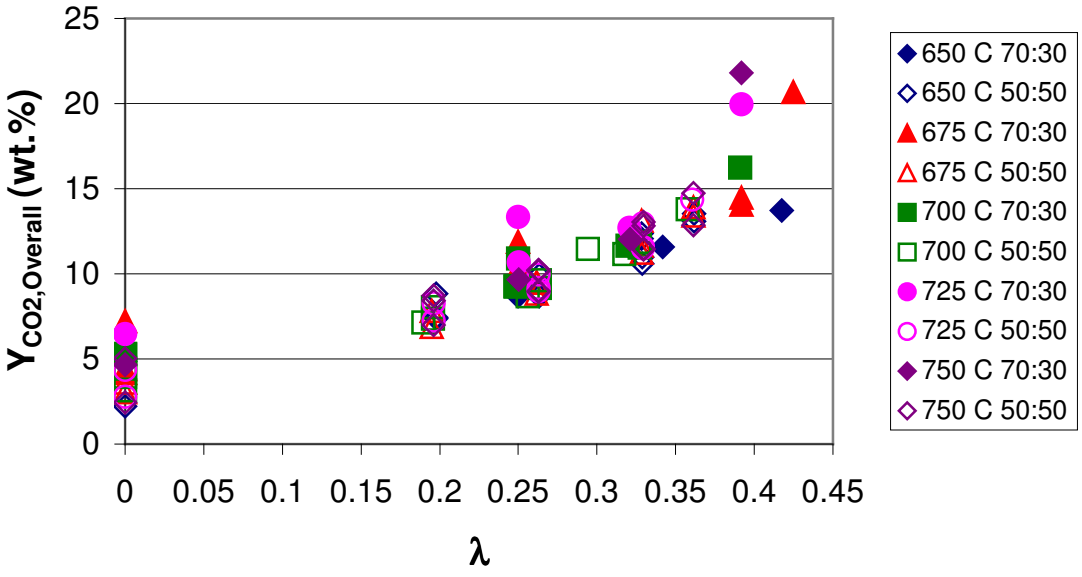

Figure 5.5. Comparison of overall CO_2 yield for 70:30 bio-oil:methanol mixture to the 50:50 mixture results as a function of λ (0 to 0.42) at temperatures between 650 and 750ºC.

and 5.6). However, the increase was not to the same degree as was the case with the CO yield. In general, both the overall and estimated bio-oil (obtained using Eqn. 3.7) CO_2 were nearly the same for both mixtures. Both the higher CO_2 yield and the increased scatter at λ = 0.4 in the case of the 70:30 mixture were likely due to entrance into a higher combustion regime.

5.5 Methane

The bio-oil methane yields (obtained using Eqn. 3.8) from the 70:30 mixture were generally slightly lower than those observed during the 50:50 experiments. Figure 5.7 compares the methane yields from the two mixtures for λ = 0 to 0.42 and temperatures between 650 and 750ºC. At the highest λ (~0.4), the methane yields from the 70:30 mixture appeared to be lower than at other λ. This observation could be due to oxidation of methane. Alternatively, it could be due to the oxygen facilitating reaction pathways to other species.

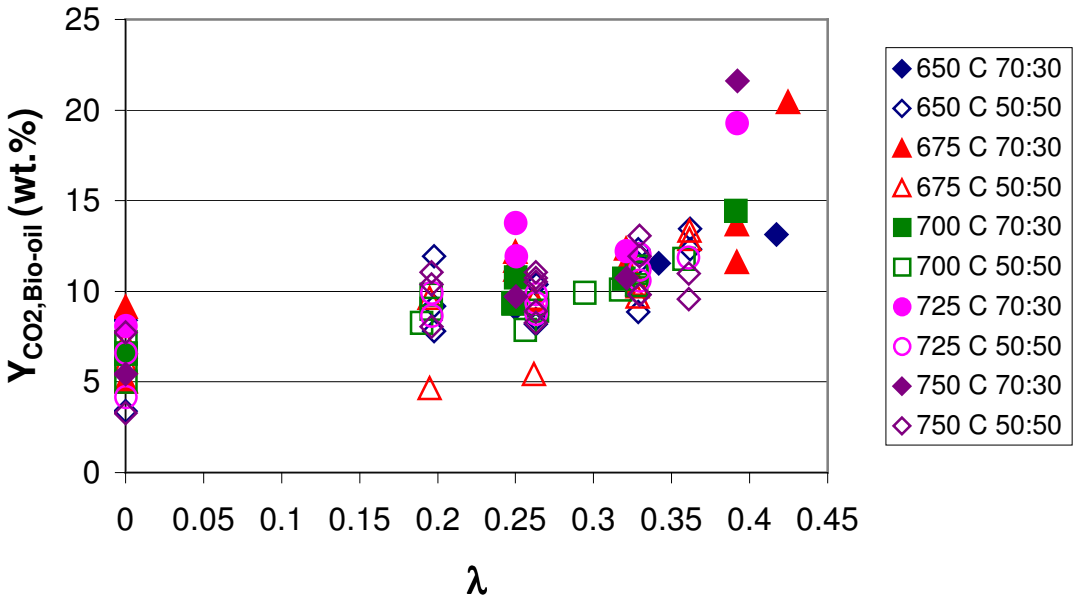

Figure 5.6. Comparison of estimated CO_2 yield from bio-oil (Method 2) for 70:30 bio-oil:methanol mixture to the 50:50 mixture results as a function of λ (0 to 0.42) at temperatures between 650 and 750ºC.

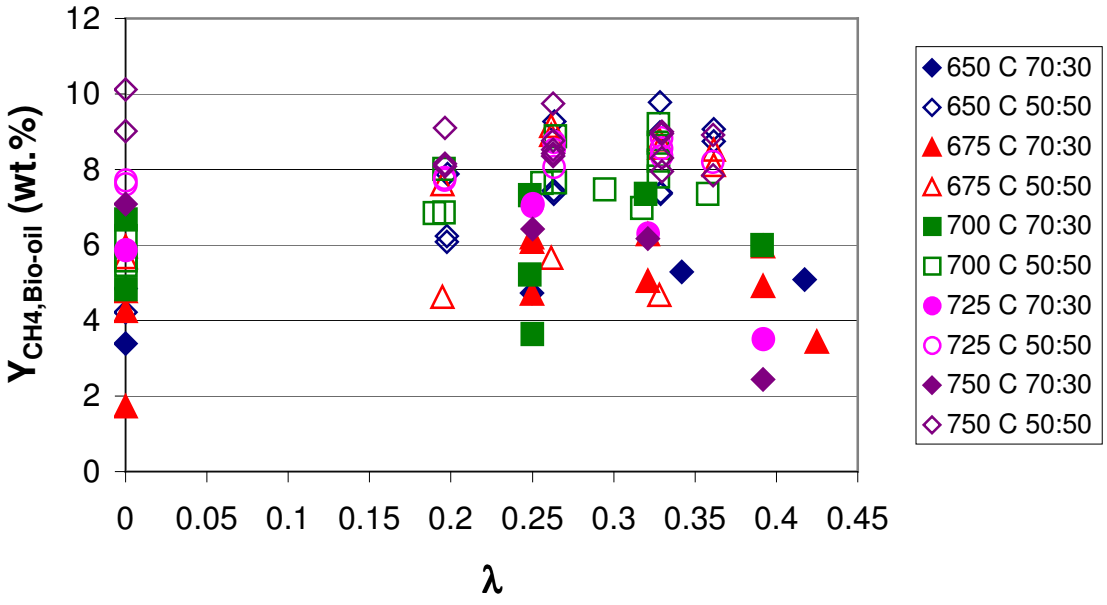

Figure 5.7. Comparison of maximum methane yield from bio-oil for 70:30 bio-oil:methanol mixture to the 50:50 mixture results as a function of λ (0 to 0.42) at temperatures between 650 and 750ºC.

5.6 Gas Production

The overall and estimated bio-oil carbon to gas conversions from the 70:30 bio-oil:methanol mixture experiments are compared to those from the 50:50 experiments in Figures 5.8 and 5.9. This represents the amount of carbon converted to CO, CO_2, and CH_4. The 70:30 mixture results had more scatter than did the 50:50 mixture results. However, the results were generally quite similar between the two mixtures. The 70:30 may have had slightly lower carbon to gas conversions, but it was hard to be sure due to the scatter. Under optimal conditions (λ of ~0.31 to 0.35), the carbon to gas conversion (both overall and estimated from bio-oil) was 80 to 95% for both mixtures, showing excellent gasification efficiencies.

5.7 Benzene

The maximum benzene yield from bio-oil (Eqn. 3.8) for the 70:30 mixture were lower than for the 50:50 mixture (see Figure 5.10). The yields for the 70:30 mixture did decrease with increasing λ except at λ = ~0.4 (combustion

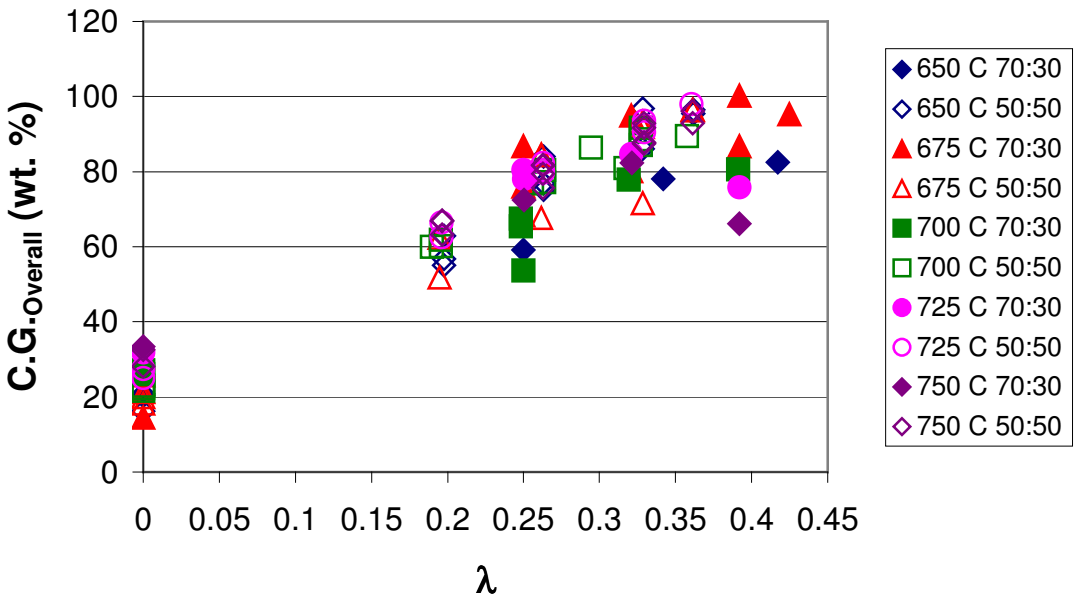

Figure 5.8. Comparison of overall carbon to gas conversion for 70:30 bio-oil:methanol mixture to the 50:50 mixture results as a function of λ (0 to 0.42) at temperatures between 650 and 750ºC.

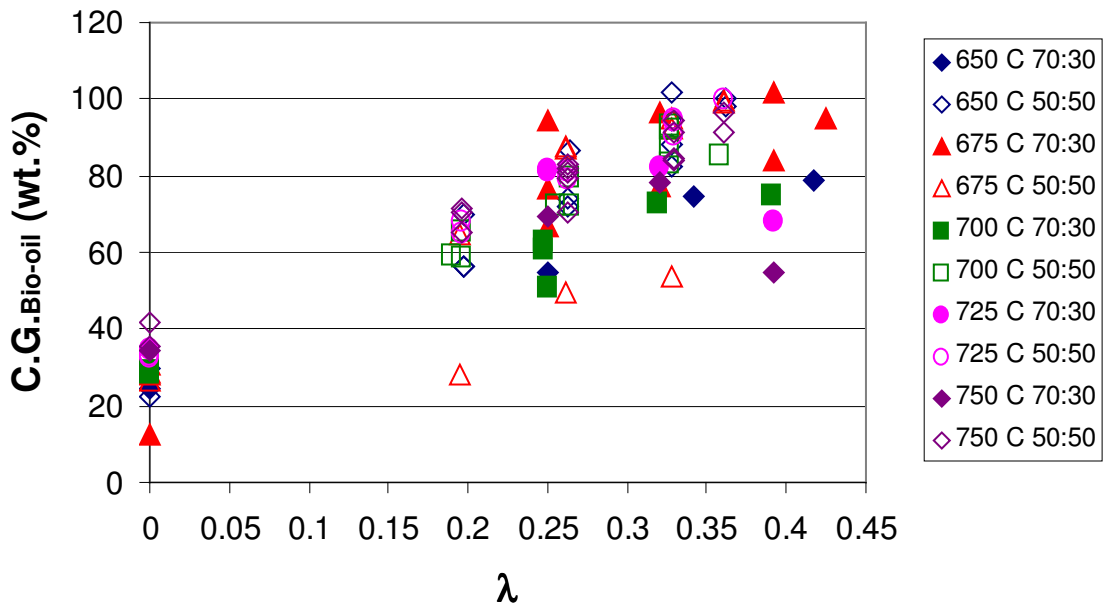

Figure 5.9. Comparison of estimated bio-oil carbon to gas conversion for 70:30 bio-oil:methanol mixture to the 50:50 mixture results as a function of λ (0 to 0.42) at temperatures between 650 and 750ºC.

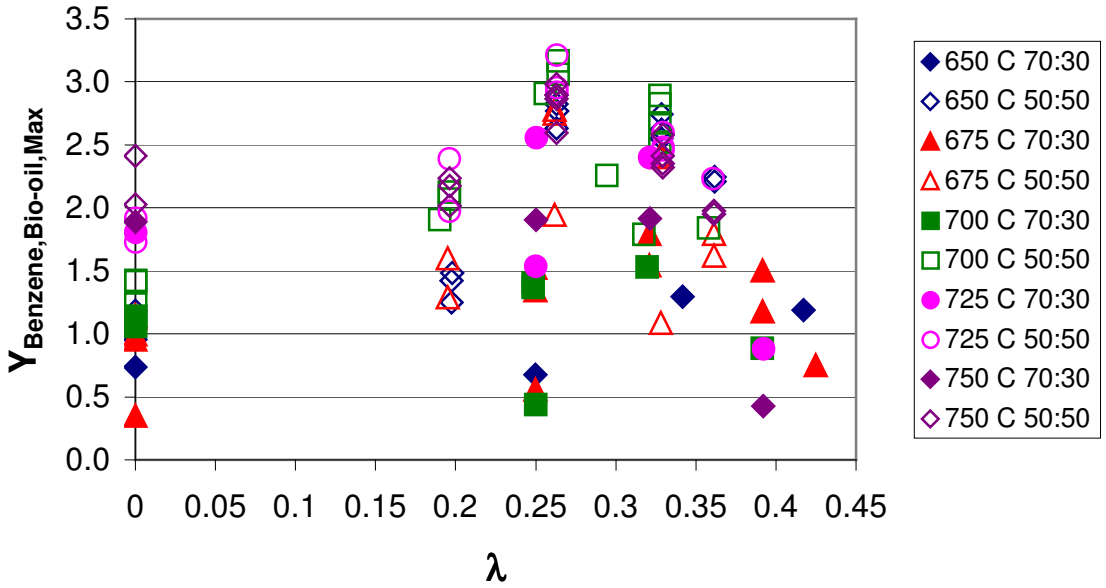

Figure 5.10. Comparison of maximum benzene yield from bio-oil for 70:30 bio-oil:methanol mixture to the 50:50 mixture results as a function of λ (0 to 0.42) at temperatures between 650 and 750ºC.

conditions). Under optimal conditions (λ between 0.3 and 0.35), the benzene yield was typically below 4.5 %, which is comparable to that observed for oak gasification experiments performed at NREL[50].

5.8 Residual Carbon

The overall residual carbon yield observed and the maximum residual carbon yield from bio-oil (Figure 5.11) are related by Eqn. 3.8. Figure 5.11 shows that the residual carbon yields from the 70:30 mixture were generally comparable to those from the 50:50 mixture. Due to the high degree of uncertainty of the residual carbon data (calculated from CO_2 signal observed during the burnoff of the carbon deposits after partial oxidation), it was difficult to quantitatively determine any clear trends. However, in general, the maximum bio-oil residual carbon yield was less than 10% for both mixtures.

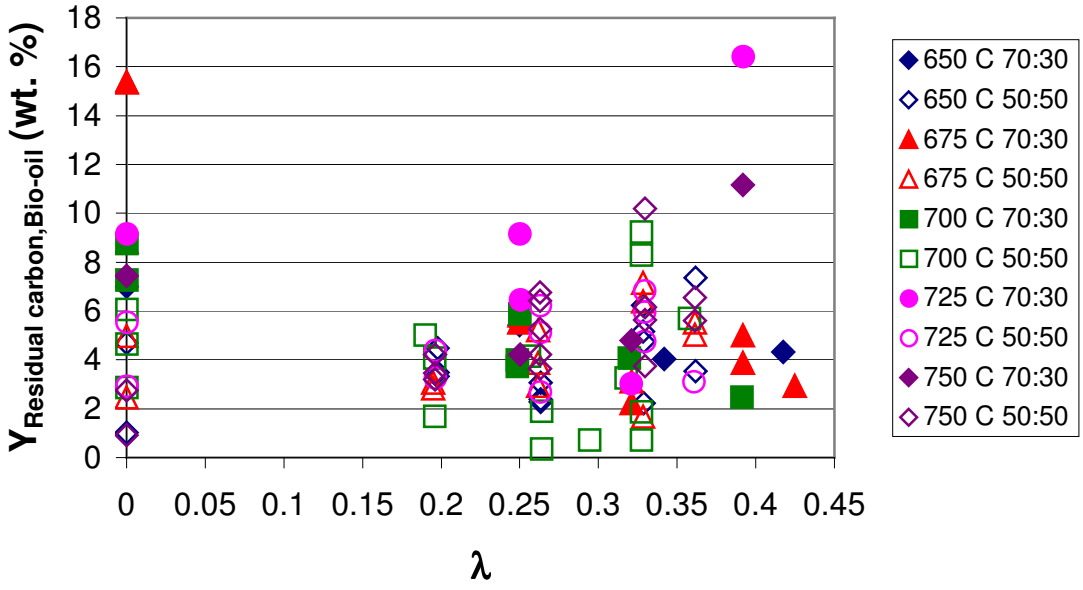

Figure 5.11. Comparison of maximum residual carbon yield from bio-oil for 70:30 bio-oil:methanol mixture to the 50:50 mixture results as a function of λ (0 to 0.42) at temperatures between 650 and 750ºC.

5.9 Carbon Accounting

Figures 5.12 and 5.13 show that higher λ leads to carbon accountings (both overall – Eqn. 3.9 – and bio-oil – Eqn. 3.10) closer to 100% for both mixures. Presumably, this was due to higher conversions (particularly of higher molecular weight species) to measured species. Added oxygen was a more important parameter than temperature as it had a greater impact on increasing the conversion to measured species**.**

5.10 Summary

The following conclusions were drawn from the comparison of the 70:30 bio-oil methanol mixture experiments to the 50:50 bio-oil methanol experiments using the 25 kHz nozzle:

1. Overall H_2 yields were lower for the 70:30 mixture than were observed during the 50:50 experiments. This was presumed to be due to the decreased methanol content and suggested that a large portion of the produced H_2 was due to methanol. Observed methanol yields during neat methanol experiments were as high as 40%.

2. The surprisingly high CO yield from bio-oil was unaffected by reduction of methanol concentration. Of particular interest is the observation that added oxygen increases the CO concentration much faster than it does CO_2. The fact that these observations persist even with only 30% methanol added is of particular interest since it is hoped to be able to decrease the methanol content to 5 to 10% in the final process.

3. The optimal λ (between ~0.31 and ~0.35) was consistent for both mixtures.

4. Very little temperature dependence was observed during NPOX for either mixture.

5. Benzene yields were generally higher for the 70:30 mixture than for the 50:50 mixture.

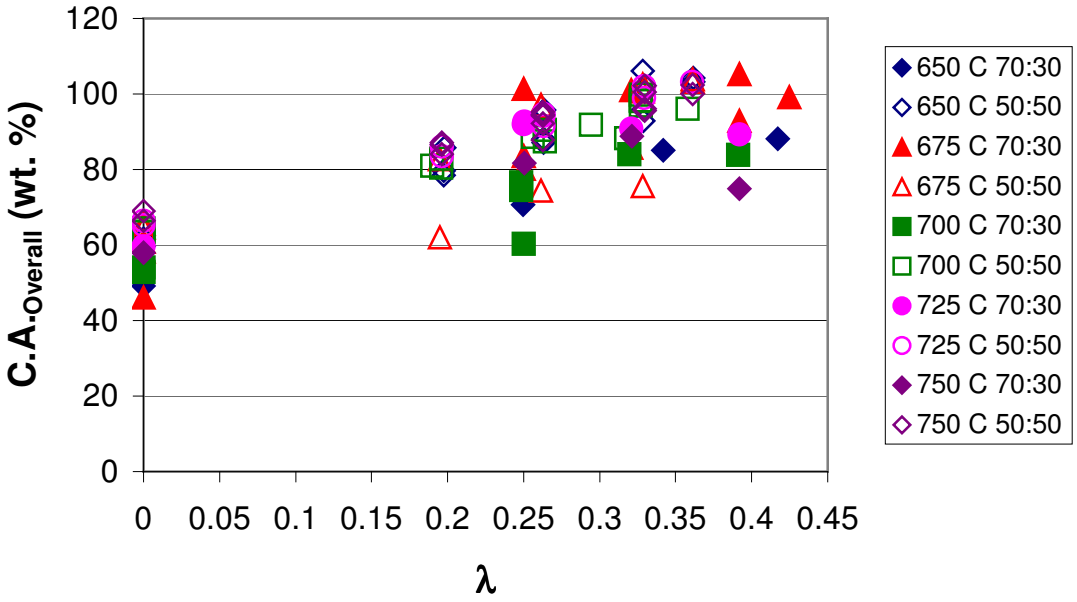

Figure 5.12. Comparison of overall carbon accounting for 70:30 bio-oil:methanol mixture to the 50:50 mixture results as a function of λ (0 to 0.42) at temperatures between 650 and 750ºC.

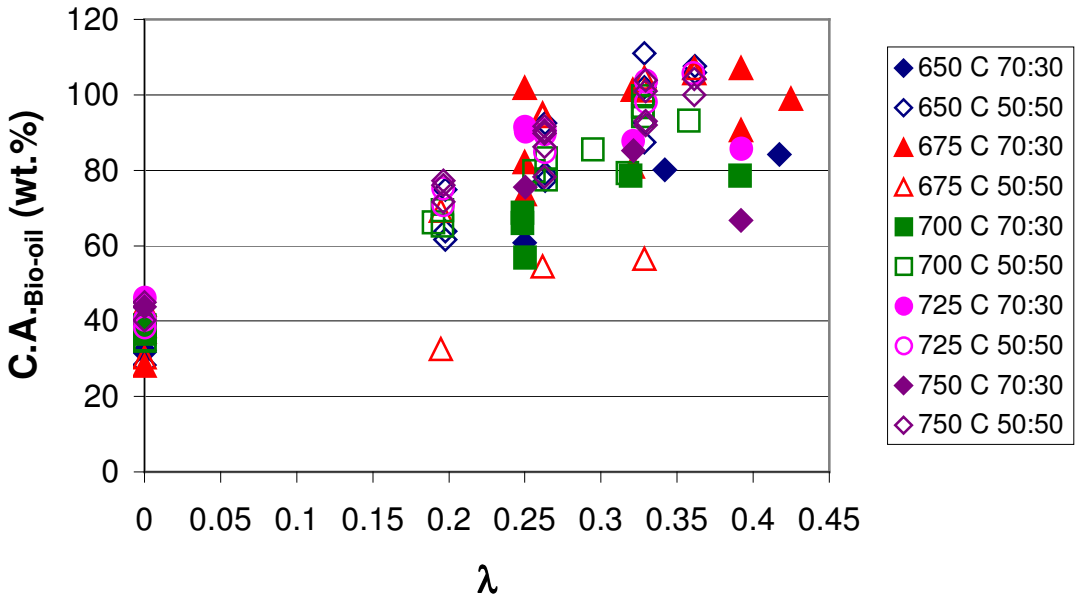

Figure 5.13. Comparison of estimated carbon accounting from bio-oil for 70:30 bio-oil:methanol mixture to the 50:50 mixture results as a function of λ (0 to 0.42) at temperatures between 650 and 750ºC.

CHAPTER 6
NPOX OF BIO-OIL:METHANOL MIXTURES USING THE LARGER NREL REACTOR

In order to begin to assess the scalability of the NPOX process, experiments have been performed by Dr. Richard French and Dr. Stefan Czernik using a larger reactor at NREL. The effect of varying both temperature and equivalence ratio was explored. The residence time during these experiments were much longer than those from the smaller system (~0.9 to 1.4 s vs. 0.3 s). The results of experiments performed using each of the three bio-oil:methanol mixtures (50:50, 70:30, and 90:10) will be discussed in this chapter. Because the methanol condensed with the water before entering the analytical instruments, it was not possible to estimate the contribution of CO and CO_2 from bio-oil since these estimations stem from the methanol conversion. Consequently, all yields discussed in this chapter are overall yields. Additionally, benzene was likely condensed as well, but was observed in small quantities in a few experiments. However, the observed benzene was likely less than the actual benzene yields. One advantage that the smaller reactor system had over the larger system was that the MBMS could handle large quantities of water whereas the GC could not.

6.1 50:50 Bio-oil:Methanol

The results of the larger reactor experiments using the 50:50 (wt. %) bio-oil:methanol mixture (1 g/min) are given in Table 6.1. The upper heater set point varied between 730 and 840ºC, while the lower heater set point was between 680 and 800ºC. However, even when the furnace set points were the same, the measured gas temperature was not always the same. In these experiments, the gas temperature varied between 700 and 820ºC. The combined N_2 and O_2 flow was always 4.3 SLPM. The resulting estimated residence time (Est. R.T.) based on the gas temperature for these experiments was ~1.2 to 1.3 seconds. During

Table 6.1. Results of 50:50 bio-oil:methanol mixture experiments using the larger reactor system at NREL.

Run	Temperature (°C)			Est. R.T. (s)	λ	C.G. (%)	Yields (%)				
	Upper heater	Lower heater	Gas				CO	H_2	CO_2	CH_4	C_2H_4
1	730	680	700	1.3	0.28	67.6	50.5	22.1	10.2	3.1	3.1
2	750	700	730	1.3	0.26	64.9	48.1	20.4	10.6	2.8	2.8
3	750	700	730	1.3	0.27	67.7	50.4	21.8	10.6	2.9	3.0
4	750	700	740	1.3	0.37	80.5	55.9	24.0	18.3	3.0	3.0
5	800	750	780	1.2	0.27	71.7	53.2	25.3	10.8	3.5	3.6
6	840	800	800	1.2	0.27	74.6	54.5	27.6	11.6	3.7	3.9
7	840	800	810	1.2	0.38	82.7	57.2	28.1	18.4	3.5	3.1
8	840	800	820	1.2	0.42	85.7	55.5	26.0	24.5	3.0	2.3

Note: The carbon to gas percent (C.G.) and the yields are on a weight basis and defined as in Chapter 3 except that the C.G. includes ethylene as well as ethane and ethyne.

these experiments, the equivalence ratio (λ) was varied between 0.26 and 0.42. Benzene was not observed during any of these experiments.

As noted below Table 6.1, small amounts of ethane and ethyne were observed and were included in C.G. as was ethylene. The ethylene yield was typical between 2 and 4%, which was similar to the overall methane yields. During experiments using the smaller reactor, the overall methane yields were typically 4 to 5% over the same λ range. Ethylene was not observed during experiments using the smaller reactor.

The C.G. was between 64.9 and 85.7 % and generally increased with increasing λ. During experiments on the smaller system using the 50:50 mixture, G.G. was typically 80 to 85% over the same range of λ (see Figure 5.8). The C.G. on the larger reactor approached this only at λ close to 0.4. However, much of the increase was due to an increase in the CO_2 yield, which jumped from 10-11.6% to 18.3-24.5% when λ was increased from 0.26-0.28 to 0.37-0.42. The higher λ is in the region where higher levels of combustion were expected based on the experiments using the smaller reactor.

The CO yield increased only slightly (from ~50% to ~56%) when λ and was increased from 0.26 to 0.42. The temperature was also increased, but experiments performed using the smaller reactor demonstrated that the amount of O_2 was more important than temperature. The range of λ used in the larger reactor experiments was similar to the optimal range (0.31 to 0.35) established during 50:50 experiments using the smaller reactor where 70 to 80% CO yields were observed (see Figure 5.3).

The H_2 yield increased from 20 to 28% as both λ and temperature were increased. However, there may have been a slight dip to 26% at the highest λ. This difference was within the experimental error. The H_2 yield was similar (20 to 30% from Figure 5.2) during 50:50 experiments using the smaller reactor over the same λ and temperature range. However, the temperature effects were less apparent.

6.2 70:30 Bio-oil:Methanol

Table 6.2 shows the results of the larger reactor experiments using the 70:30 (wt. %) bio-oil:methanol mixture (1.5 g/min). During these experiments, the upper heater set point was 680 to 850ºC, while the lower heater set point was 650 to 800ºC. The measured gas temperatures were between 670 and 840ºC. The combined N_2 and O_2 flow was always 4.3 SLPM resulting in estimated residence times between 1.1 and 1.4 (the variation was due to the temperature). For these experiments, the flow rate of oxygen was constant, which should have led to a constant λ of 0.38. However, slight variations in the flow led to a measured λ of 0.37 for Run 3. Benzene was observed (0.7 to 1.3% yield) during a few of these experiments.

The C.G. increased with increasing temperature from 73.6 to 83.8% for experiments using the 70:30 mixture and the larger reactor. However, this increase was due primarily to increases in the less desirable products (CO_2, CH_4, and C_2H_4) rather than CO. The observed C.G. from the 70:30 experiments using the smaller reactor at this λ was typically ~80% (see Figure 5.8).

Table 6.2. Results of 70:30 bio-oil:methanol mixture experiments using the larger reactor system at NREL.

Run	Temperature (°C)			Est. R.T. (s)	λ	C.G. (%)	Yields (%)				
	Upper heater	Lower heater	Gas				CO	H_2	CO_2	CH_4	C_2H_4
1	680	650	670	1.4	0.38	73.6	47.4	20.7	17.2	4.1	3.3
2	750	700	700	1.3	0.38	77.0	47.8	20.8	18.7	4.1	3.6
3	800	750	770	1.2	0.37	81.9	49.3	23.1	20.2	4.8	4.2
4	850	800	840	1.1	0.38	83.8	46.9	23.7	22.9	5.2	4.6

Note: The carbon to gas percent (C.G.) and the yields are on a weight basis and defined as in Chapter 3 except that the C.G. includes ethylene as well as ethane and ethyne.

During 70:30 experiments using the larger reactor, the CO yield was relatively constant at ~47-49%. This yield was lower than that observed during 50:50 bio-oil methanol experiments under the same conditions where the CO yield was 56-57%. The observed CO yield during 70:30 experiments using the smaller reactor at this λ decreased from as high as 83% to 43% with increasing temperature (see Figure 5.3).

The CO_2 yields increased from 17.2 to 22.9% as the temperature was increased during 70:30 experiments using the larger reactor. The CO_2 yield from the 50:50 mixture was ~18%. These yields were similar to those observed in the smaller reactor at λ= ~0.4 using the 70:30 mixture, where the variation was between 14 and 22% and also increased with temperature (see Figure 5.5).

The H_2 yield increased from ~21 to ~24% as temperature was increased during experiments using the 70:30 mixture and the larger reactor. These yields were slightly lower than those observed from the 50:50 mixture (24 to 28%. This observation was consistent with the experiments performed using the smaller reactor where 20-30% H_2 yield was observed during 50:50 mixture experiments, but only 15-20% H_2 yield was observed during 70:30 mixture experiments (see Figure 5.2).

6.3 90:10 Bio-oil:Methanol

Table 6.3 shows the results of the larger reactor experiments using the 90:10 (wt. %) bio-oil:methanol mixture (1 g/min). The temperature of the upper heater was varied between 700 and 850ºC, while the temperature of the lower heater was varied between 650 and 800ºC. The gas temperature ranged from 575 to 850ºC. The higher temperature than the furnace set point in the case of Run 6 was likely due to the thermocouple being in a hot pocket stemming from increased oxidation. The combined flow rate of N_2 and O_2 was 4.3 for Runs 1, 2, and 3 while the combined flow was 6.4 SLPM for all others. The higher flow rates served to dilute the feed sufficiently to avoid the flames that were observed during Runs 1, 2, and 3. The estimated R.T. for the first three runs was between 1.2 and 1.4 seconds. The increased flow rates led to residence times of 0.9 to 1 seconds for the rest of the runs. The range of λ was 0.27 to 0.44 for the first three runs and 0.36 to 0.54 for the last three runs. Experiments were not performed using a 90:10 mixture with the smaller system due to inconsistencies in the feeding at such low flow rates during initial attempts.

The C.G. from the Runs 1, 2, and 3 were similar to the C.G. from the rest

Table 6.3. Results of 90:10 bio-oil:methanol mixture experiments using the larger reactor system at NREL.

Run	Temperature (℃)			Est. R.T. (s)	λ	C.G. (%)	Yields (%)				
	Upper heater	Lower heater	Gas				CO	H_2	CO_2	CH_4	C_2H_4
1	700	650	700	1.3	0.27	63	37.7	14.7	14.5	3.5	3.7
2	750	700	670	1.4	0.44	79.3	45.4	15.1	25.1	3.2	3.7
3	800	750	850	1.2	0.44	67.4	30.5	19.7	32.5	1.4	0.7
4	750	700	575	1.0	0.44	67.6	38.7	6.1	19.3	2.8	3.7
5	750	700	700	0.9	0.54	77.2	44.0	7.7	24.3	2.6	3.6
6	800	750	630	1.0	0.44	71.8	43.8	8.8	16.9	3.5	4.5
7	850	800	635	1.0	0.36	67.6	42.3	10.6	11.9	4.1	4.9
8	850	800	660	1.0	0.44	77.7	47.6	11.3	16.2	4.0	4.9
9	850	800	680	0.9	0.54	84.1	50.1	11.8	23.0	3.5	4.3

Note: The carbon to gas percent (C.G.) and the yields are on a weight basis and defined as in Chapter 3 except that the C.G. includes ethylene as well as ethane and ethyne.

of the runs. The C.G. for all 90:10 experiments varied from 63 to 84% and increased with both increasing λ and increasing temperature. However, the C.G. during Run 7 (67.6%), which had conditions closest to the 70:30 experiments, was much lower than the 83-84% observed during 50:50 and 70:30 experiments at the same temperature and λ (Run 7 in Table 6.1 and Run 4 in Table 6.2). This result suggested that the radical pool was enhanced by the presence of methanol and that there may be reason to add more than 10% methanol to the bio-oil. However, the lower C.G. could also have been due to imperfect mixing. Good mixing is likely more important in the case of bio-oil due to the non-volatile components.

The CO yield during 90:10 experiments varied between 30 and 50% and increased with increasing λ and increasing temperature. However, higher λ as well as higher temperatures were required to get CO yields similar to those observed during 50:50 and 70:30 experiments. Again this could reflect imperfect mixing or the need for higher levels of methanol.

The CO_2 yield during Runs 1, 2, and 3 were much higher (as high as 32.5%) than during the rest of the runs (12 to 24%). This was a result of the increase in combustion that was observed visually as flames during the first three runs. An increased CO_2 yield with increasing λ was observed. From the data, no clear temperature effect was observed. The CO_2 yield during 90:10 was typically higher than what was typical for the 50:50 experiments, but comparable to the 70:30 CO_2 yield.

The CH_4 yield varied from 1.4 to 4.1% while the C_2H_4 yield varied from 0.7 to 4.9%. These yields were comparable to those observed from the other two mixtures. It should also be noted that benzene was observed (1-1.5% yield) during a few of the last six experiments.

An increase in H_2 yield with increasing temperature and λ was observed. Even the first three runs, which had the highest H_2 yield, had a lower H_2 yield than was observed during 50:50 or 70:30 experiments. This result was further evidence that much of the H_2 comes from the methanol.

6.4 Summary

In general, similar trends to those observed with the smaller reactor during bio-oil:methanol mixture experiments were observed during experiments using the larger reactor. These included a persistence of the relatively high CO yield. However, the CO yield was not as high as during the experiments performed using the smaller reactor. Consequently, the ratio of CO to CO_2 was not as favorable. The observed discrepancies could be due in part to imperfect mixing. Additionally, heat transfer was more of an issue with the larger reactor due to its larger diameter. The observed temperature at the center of the reactor was lower than that observed near the walls. Such phenomena could lead to both hot and cold zones within the reactor, which would affect the results. It was not clear whether the ethylene observed during these experiments was due to these same phenomena or due to imperfect mixing resulting in excessive combustion of some parts of the system while other parts were more pyrolytic in nature. The formation of ethylene during the NPOX step is of concern since it could lead to carbon deposits.

The results of the 90:10 experiments performed on the larger reactor showed a decrease in H_2 yield beyond what had been observed previously. However, the considerable yield of CO can be reacted with water over a water gas shift catalyst to generate more H_2. Furthermore, unconverted species as well as methane should be reformed over a catalyst to generate additional H_2. These results suggest that a higher methanol content than 10% may be beneficial. However, until the mixing issues are sorted out it will be difficult to draw a definitive conclusion.

CHAPTER 7
CATALYTIC BIO-OIL REFORMING

Although the focus of the present work was on the non-catalytic partial oxidation (NPOX) step described in the previous chapters, limited catalytic experiments were performed primarily to determine the importance of the NPOX step. A catalyst survey was performed in order to identify a suitable catalyst. Once a suitable catalyst had been identified, the NPOX residence time was varied such that its effects on the post catalyst product distribution could be assessed.

7.1 Catalyst Survey

A survey of precious metal catalysts (Englehard) was performed using the 120 kHz nozzle and the 50:50 bio-oil:methanol mixture with a NPOX residence time of ~0.3 s. The catalysts used for these experiments consisted of 0.5 wt% rhodium, ruthenium, platinum, or palladium, all supported by alumina. Experiments were performed using pure alumina as well. While all the catalysts were impregnated on the same size alumina spheres, only cylindrical alumina pellets (of similar size) were available for the blank runs. This difference did not appear to affect the results as experiments showed the alumina to be inactive. Two grams of each catalyst were used in each case, resulting in a fixed bed height of approximately 2 cm. It should be noted that for this survey, no water was added to the system to generate additional steam. However, both the water in the initial bio-oil and any steam generated from the NPOX reaction were available to participate in the catalytic chemistry.

By using a catalyst after the NPOX chemistry, one hopes to drive the system to equilibrium. Calculations were performed using Chemkin 4.1 to determine the predicted equilibrium composition under the conditions used in experiments. These calculations were possible because Chemkin needs only the C/H/O composition to minimize the Gibbs free energy (provided that the

temperature is held constant) rather than requiring the relative amounts of each species in bio-oil. In these calculations, graphitic carbon was used to represent residual carbon. Table 7.1 shows the results of the catalytic experiments as well as the gas phase experimental results and equilibrium calculations for O:C of 1.3. Because H_2O is not inert over the catalyst, the actual O:C is used in this chapter. From Table 7.1, it is clear that the rhodium data came closest to the equilibrium predictions. Table 7.2 compares equilibrium predictions at the best gas phase

Table 7.1. Equilibrium predictions and NPOX results compared to the results obtained in catalytic experiments (O:C = 1.3; λ = 0.24). (oxygen flow of 23 sccm, helium flow of 380 sccm, and bio-oil:methanol flow of 0.12 g/min) CH_3OH is reported as conversion (wt. %). All carbon containing products are reported as a yield (wt. %) based on the carbon entering the system. H_2 and H_2O yields are based on the total hydrogen entering the system.

Species	Equilibrium	NPOX	Alumina	Pd	Pt	Rh	Ru
CH_3OH	100.00	49.13	38.75	82.09	88.20	99.64	75.39
CO	68.70	38.56	36.00	50.87	45.46	61.15	48.35
CO_2	23.77	7.20	7.46	9.56	11.55	23.25	9.28
H_2	80.30	13.12	9.19	34.14	31.18	83.69	27.56
H_2O	13.49	38.46	37.98	40.57	45.31	17.83	40.69
CH_4	3.89	5.19	5.33	7.71	8.19	5.90	9.47
Residual Carbon	3.64	0.99	1.55	7.66	10.37	4.38	6.87
Benzene	0.00	1.33	0.95	4.37	2.32	1.43	2.04

Table 7.2. Equilibrium predictions compared to results of the gas phase and catalytic experiments (O:C = 1.7; λ = 0.39). (oxygen flow of 42 sccm, helium flow of 361 sccm, and bio-oil:methanol flow of 0.12 g/min) CH_3OH is given as a conversion (wt. %) based on the carbon entering the system. H_2 and H_2O are yields based on the total hydrogen entering the system.

Species	Equilibrium	Gas Phase	Rh
CH_3OH	100.00	87.47	99.98
CO	56.98	60.34	52.91
CO_2	41.82	11.31	37.60
H_2	72.32	27.71	74.07
H_2O	25.76	54.30	31.68
CH_4	1.20	6.51	4.99
Residual Carbon	0.00	0.93	1.44
Benzene	0.00	2.67	0.45

conditions (O:C = 1.7) to experiments under the same conditions both in the gas phase and with a rhodium catalyst. Again, rhodium comes close to the equilibrium values. Of particular interest is the achievement of equilibrium yields of H_2 and near equilibrium yields of CO with rhodium under both conditions. Also note that the gas-phase production of CO for the O:C=1.7 case is slightly above equilibrium

7.2 Importance of NPOX Residence Time

Based on the catalytic survey described above, a rhodium catalyst was obtained from Professor Lanny Schmidt's group at the University of Minnesota. This catalyst consisted of 1.3 mm diameter spheres of catalyst (1% rhodium, 1 % ceria on alumina support). The catalyst was similar to that used in several of their studies[33,44] except that spheres were used rather than foam monoliths. Catalytic experiments were performed at 650 ºC using a 1 gram (0.8 cm) bed of catalyst. A reduced amount of catalyst (as compared to experiments described above) was used due to the higher loading (1% vs. 0.5%). These experiments were performed using the same 120 kHz nozzle used for the earlier catalysis experiments. The purpose of these experiments was to determine the effect of the various levels of conversion in the gas-phase reactions on the subsequent catalytic reactions. This was accomplished by changing the reactor length such that the NPOX residence times were ~0.2 s for the short reactor and ~0.3 s for the long reactor. The reason for reducing the length of the reactor rather than simply adjusting the flow rates was to ensure that the observed differences were due to kinetics rather than changes in transport. It should be noted that the only steam present was from the water present in the original bio-oil as well as water derived from the NPOX reactions. Based on the NPOX results discussed in Chapter 3, the steam to carbon ratio (molar) at the beginning of the catalytic bed was ~0.7. Also, all of the oxygen introduced at the top of the reactor (with the bio-oil) was consumed prior to reaching the catalyst. Although in practice additional steam would be added, for ease of comparison, no steam was added to these experiments. The overall O:C ratio (including oxygen in water) was 1.7. This

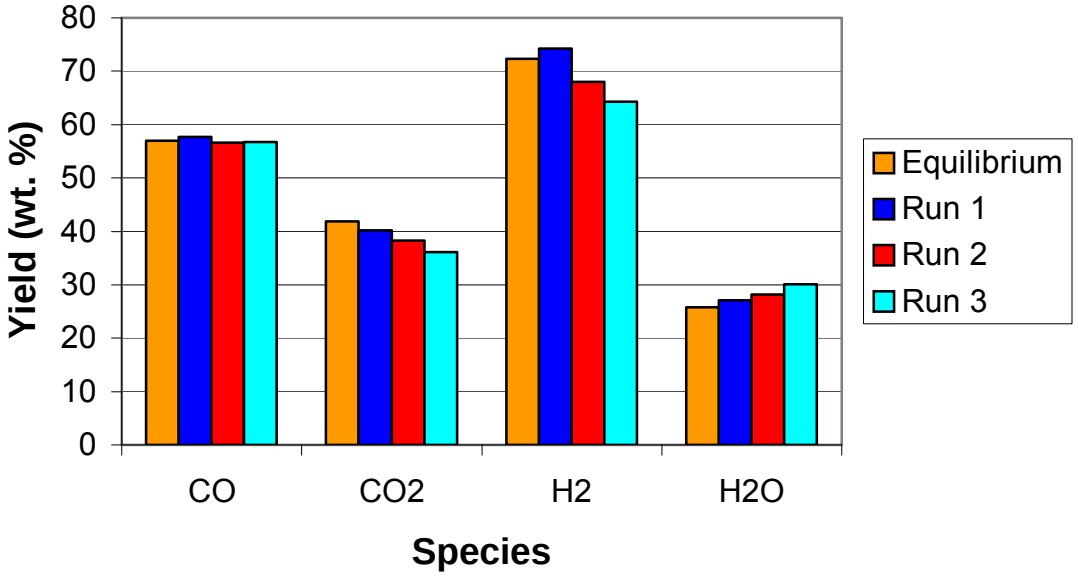

Figure 7.1. Comparison of major product yields (wt. %) with equilibrium calculations (performed using Chemkin 4.1) for three runs using the longer reactor (T = 650ºC; O:C = 1.7; S:C = ~ 0.7; NPOX R.T = ~0.3 s) with a bed of University of Minnesota catalyst (1 % Rhodium, 1 % Ceria on alumina support).

overall O:C ratio corresponds to an effective O:C of ~1.5 in the gas phase experiments described above.

Using both the long and short reactor, three consecutive runs were performed with each run followed by burn off of carbon deposition on the catalyst. The major product yields (defined in the same manner as described earlier) for the short and long reactors for each run are presented in Figures 7.1 and 7.2, respectively. The equilibrium yields were also calculated using Chemkin 4.1. The yields of all species for both residence times were close to equilibrium during all runs. However, the yields for these species were slightly lower with the short reactor (i.e. shorter gas phase residence time). Additionally, in the case of the long reactor a decrease in both the H_2 and CO_2 yield was observed from one run to the next. There was also a corresponding increase in the H_2O yield. These changes were attributed to catalyst deactivation.

The deactivation began during the first run and was especially evident in the case of benzene. As shown in Figure 7.3, benzene was nearly completely converted over the catalyst during the early stages of the run, but began to grow

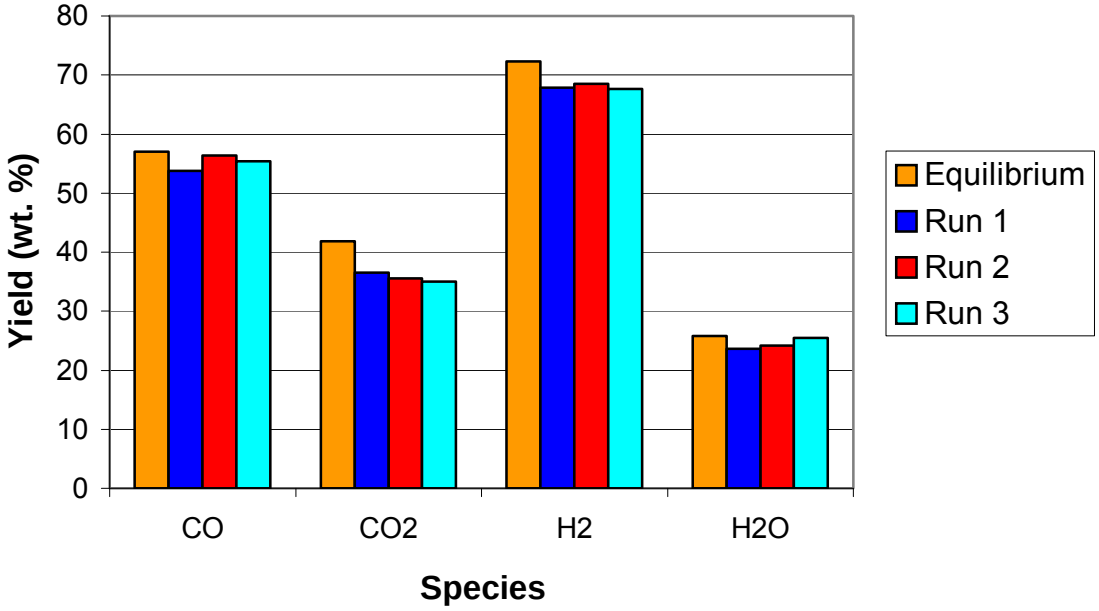

Figure 7.2. Comparison of major product yields (wt. %) with equilibrium calculations (performed using Chemkin 4.1) for three runs using the shorter reactor (T = 650 ºC; O:C = 1.7; S:C = ~ 0.7; NPOX R.T. = ~0.2 s) with a bed of University of Minnesota catalyst (1 % Rhodium, 1 % Ceria on alumina support).

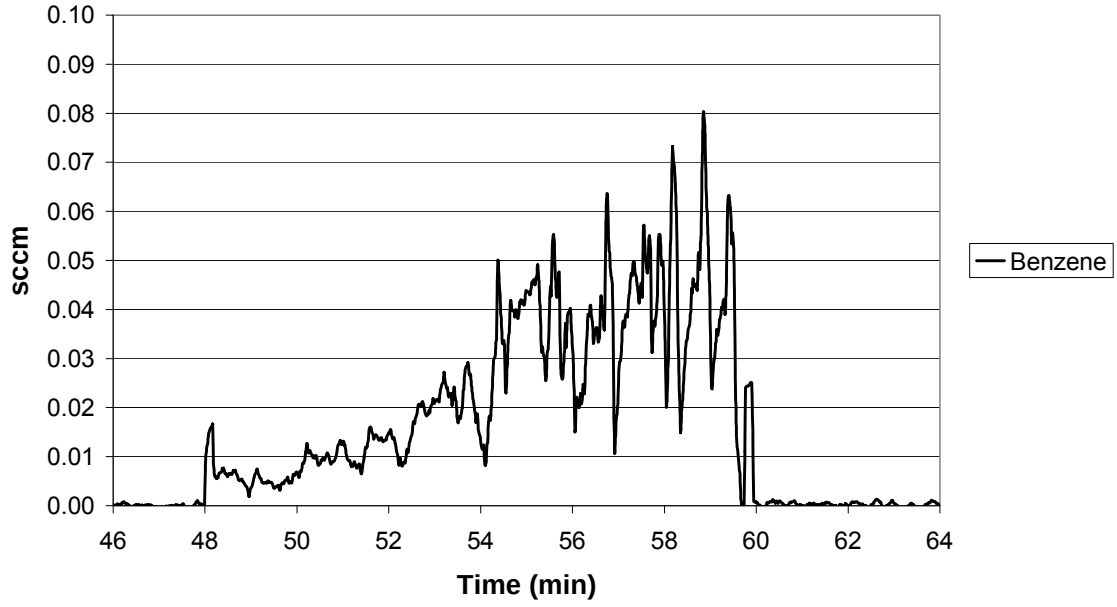

Figure 7.3. Benzene profile for Run 1 (long reactor).

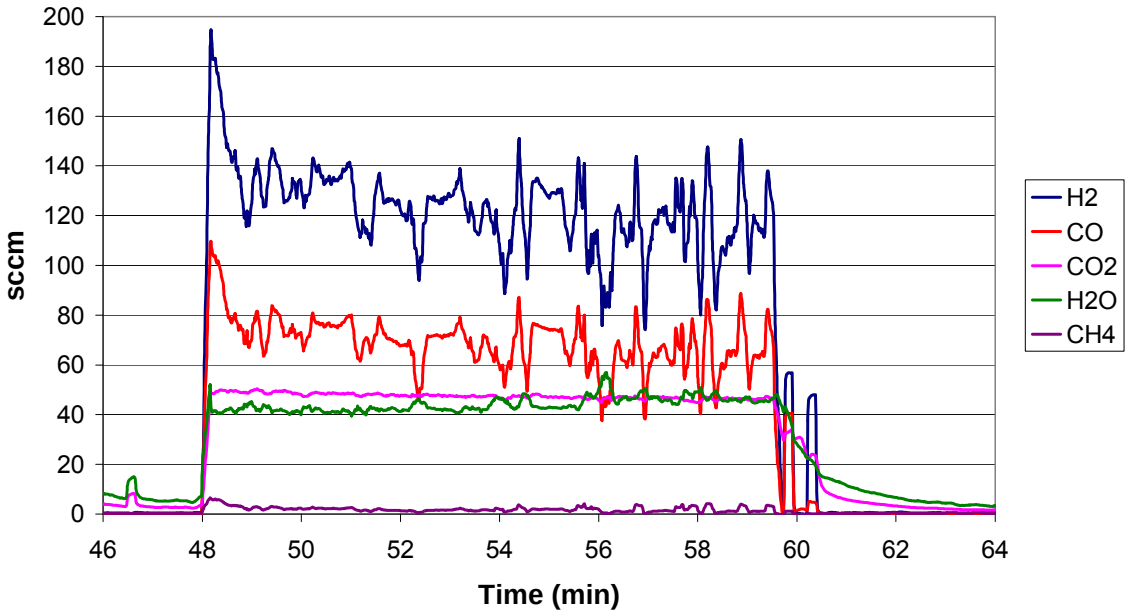

Figure 7.4. Profile of all other species for Run 1 (long reactor).

in after just a few minutes. The deactivation was more subtle in the case of major products, but Figure 7.4 shows a slight decrease in H_2 with a corresponding increase in H_2O. One would expect a corresponding increase in CO and decrease in CO_2, but such changes were not apparent in the data. Burnoff between runs did not lead to a recuperation of the original activity. The degree of deactivation appeared to be slightly less with the short reactor as these species did not seem to change as much.

Figures 7.5 and 7.6 compare the minor product yields (wt. %) with equilibrium calculations for the three catalytic runs using the long and short reactor (described above), respectively. All species were above the equilibrium yield for all runs during experiments using the long reactor. This was also true for the shorter reactor except in the case of the methane yield, which was below the equilibrium value for all runs. Catalyst deactivation was observed with respect to benzene conversion (it was formed in the gas-phase and was destroyed on the catalyst) for both reactors; it was higher with each successive run. However, the amount of benzene present was higher in all cases for the long reactor. The

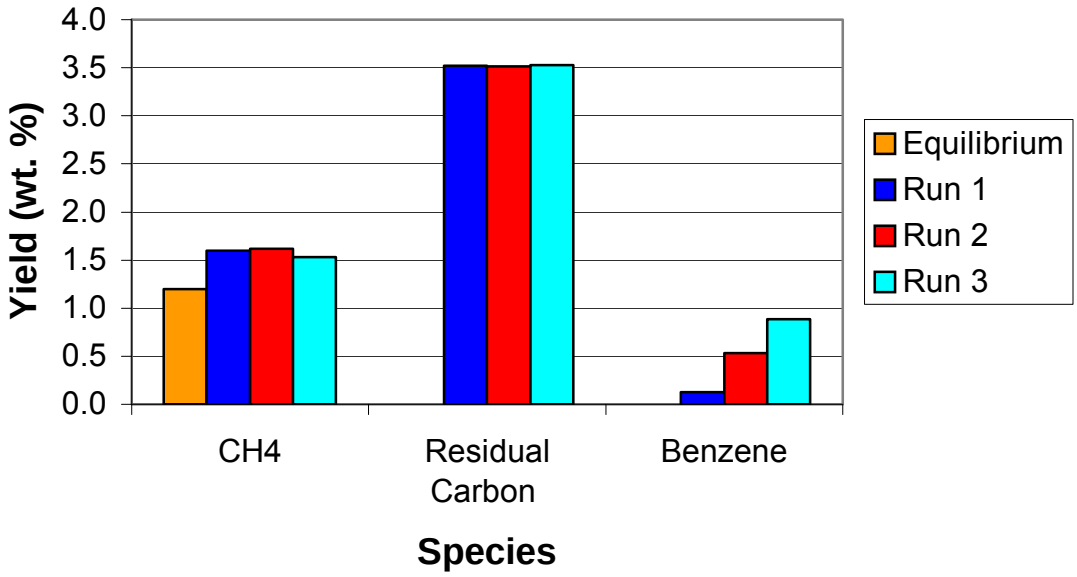

Figure 7.5. Comparison of minor product yields (wt. %) with equilibrium calculations (performed using Chemkin 4.1) for three runs using the longer reactor (T = 650 ºC; O:C = 1.7; S:C= ~ 0.7: NPOX R.T = ~0.3 s) with a bed of University of Minnesota catalyst (1 % Rhodium, 1 % Ceria on alumina support).

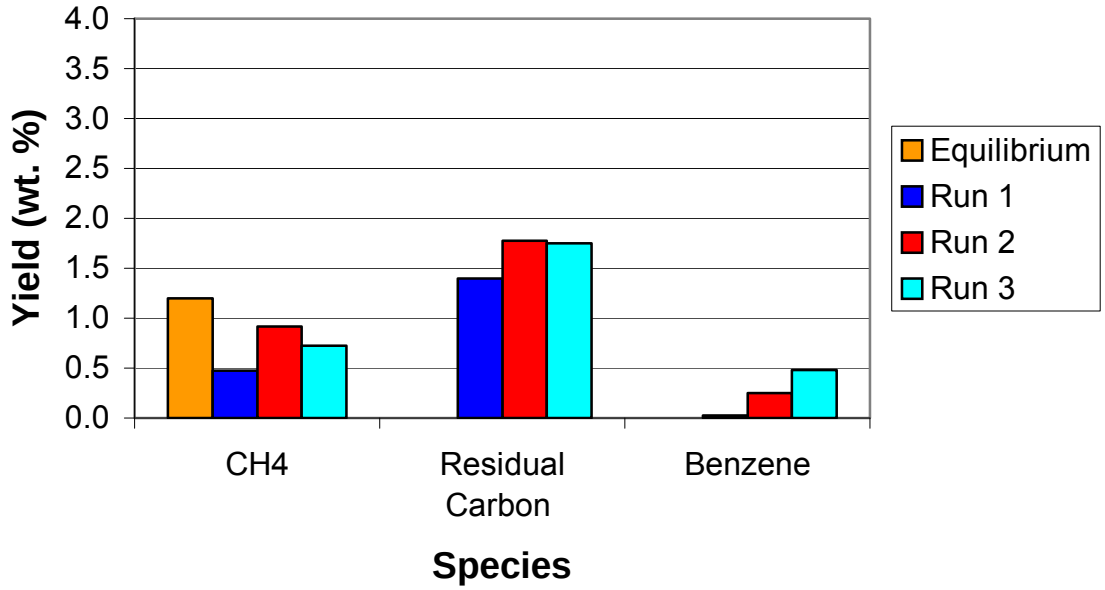

Figure 7.6. Comparison of minor product yields (wt. %) with equilibrium calculations (performed using Chemkin 4.1) for three runs using the shorter reactor (T = 650 ºC; O:C = 1.7; S:C = ~ 0.7; NPOX R.T = ~0.2 s) with a bed of University of Minnesota catalyst (1 % Rhodium, 1 % Ceria on alumina support).

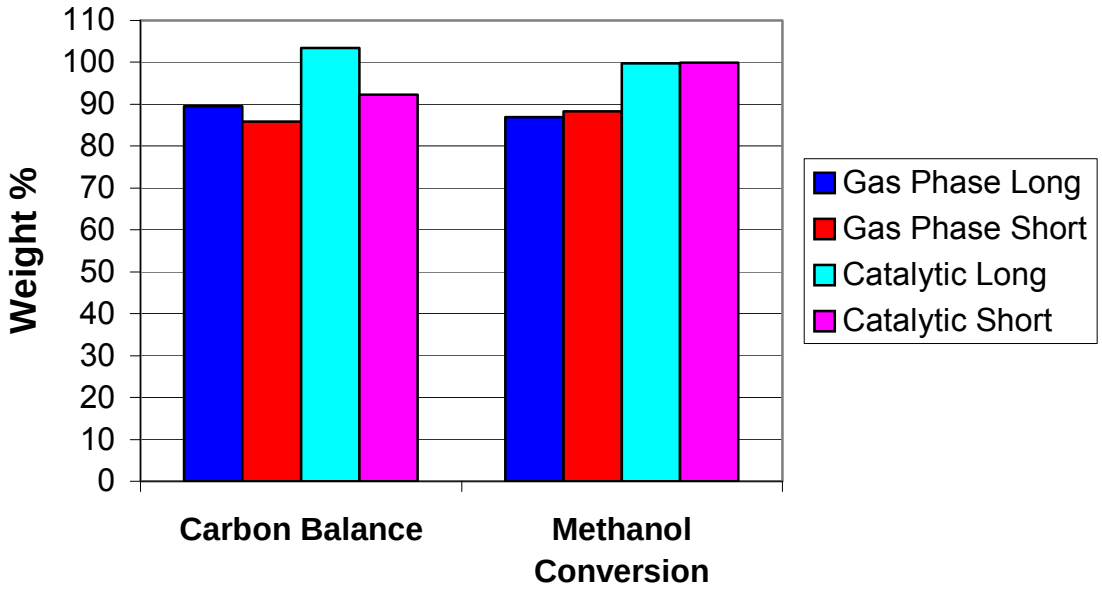

Figure 7.7. Carbon balances and methanol conversion (wt. %) for gas phase and the first run of catalytic (University of Minnesota catalyst) experiments (T = 650 ºC; O:C = 1.7; S:C = ~ 0.7).

residual carbon yield was also lower for the short reactor than it was with the longer reactor.

Because the degree of deactivation was different for the two reactors, Figures 7.7 through 7.9 compare the gas phase results to just the first run of the catalytic results (where the catalyst was freshest) for both reactors. Figure 7.7 shows carbon balances as well as methanol conversion (wt. %) for gas phase and the first run of catalytic experiments (described above). For both gas phase and catalytic experiments, the longer residence lead to a carbon balance closer to 100 % indicating that a longer gas phase residence time lead to higher bio-oil conversion (even with a catalyst present). The methanol conversion was nearly identical for both reactors whether looking just at NPOX (~87%) or after the catalyst (where it reached the equilibrium value of 100% conversion).

The major product yields (wt. %) for gas phase as well as catalytic experiments using both the longer and shorter reactor are shown in Figure 7.8. The higher conversion in the case of the longer reactor leads to product yields which are closer to equilibrium in all cases. The shift from higher CO and H_2O

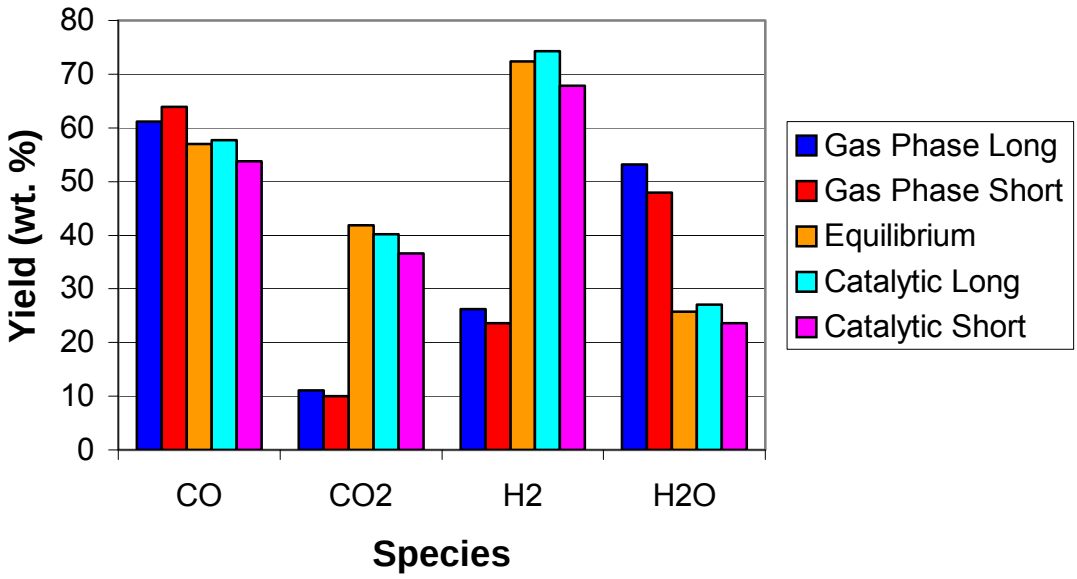

Figure 7.8. Major product yields (wt. %) for gas phase as well as catalytic experiments (University of Minnesota catalyst) using both the longer and shorter reactor (T = 650 ºC; O:C = 1.7; S:C = ~ 0.7).

yields in the gas phase (compared to their post catalyst yields) to higher H_2 and CO_2 yields (compared to their gas phase yields) after the catalyst was consistent with the expected promotion of the water gas shift reaction by the catalyst.

The minor product yields (both gas phase and catalytic for long and short reactors) are shown in Figure 7.9. As with the major products, the higher conversion in the gas phase at the longer residence time leads to higher yields of all of the minor products. In the case of residual carbon and benzene, the longer residence time would seem less desirable. However, when the increase in the overall conversion and major product yields is considered, the longer residence time would be more desirable.

7.3 Staged Oxygen Addition

As discussed in Chapter 3, staged O_2 addition did not appear to be advantageous during the NPOX step. However, equilibrium calculations suggested that adding O_2 would shift the overall concentration out of the region

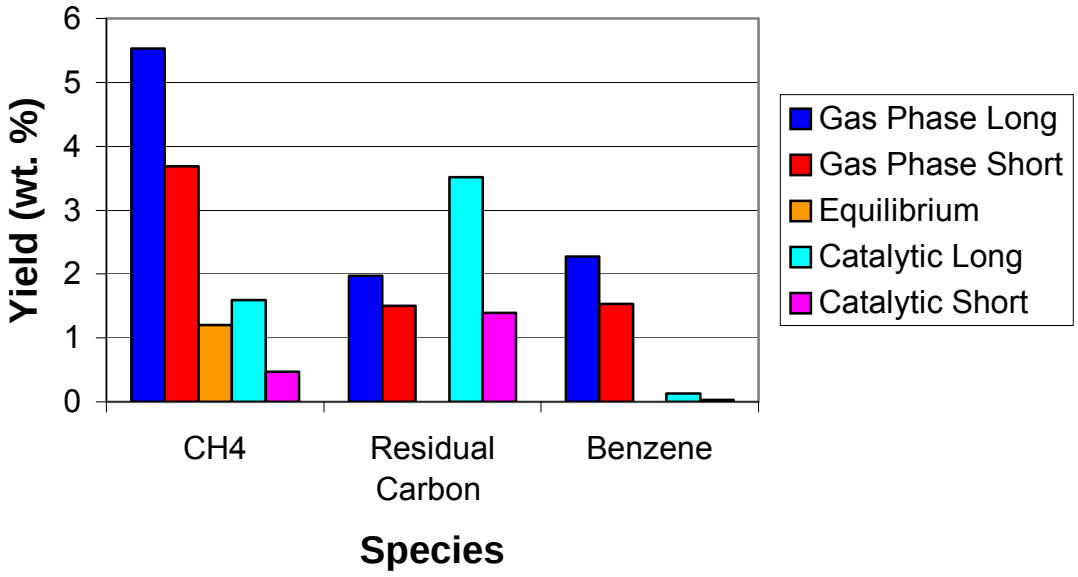

Figure 7.9. Minor product yields (wt. %) for gas phase as well as catalytic experiments (University of Minnesota catalyst) using both the longer and shorter reactor (T = 650 ºC; O:C = 1.7; S:C = ~ 0.7).

where deposits are predicted to occur (see Figure 3.4). Accordingly, experiments were performed using the same reactor configuration as in Section 3.6.

Table 7.3 shows the result of staged O_2 addition experiments performed at 650ºC using the 50:50 bio-oil methanol mixture (0.16 g/min) with a gas phase residence time of ~0.3 s (long reactor) using 1 g of the University of Minnesota catalyst. The overall O:C ratio was 1.77. Although the steam to carbon ratio after the NPOX step (i.e., what the catalyst sees) is not known for certain, it was likely between 0.7 and 1.0 based on other experimental observations.

While the O:C was slightly higher during these experiments than that in Section 7.2, they are close enough for good comparison. The observed methanol conversion and carbon balance was similar in both cases. While the H_2 yield was lower during the staged oxygen addition (48-52%) than during experiments without the staged O_2 addition (60-70%), it was more stable. The CO yield was also lower during staged O_2 addition (37-40% vs. 57-58%), while the CO_2 yield was higher during the staged O_2 addition experiments (52-54% vs. 36-40%). CH_4, residual carbon, and benzene yields were lower during staged oxygen

addition. The deactivation with respect to benzene did occur, but to a lesser extent. The positive effects on these minor products were overshadowed by the negative effects on the H_2 and CO.

Table 7.3. Results of catalytic staged oxygen addition experiments at 650ºC. The University of Minnesota catalyst (1 g) was used.

Run	1	2	3	4
Upper O_2 flow (sccm)	48.5	48.5	48.5	48.5
Lower O_2 flow (sccm)	20	20	20	20
effective O:C	1.64	1.64	1.64	1.64
overall O:C	1.77	1.77	1.77	1.77
Methanol Conversion (%)	99.99	99.99	99.98	99.98
$Y_{H2,Overall}$ (wt. %)	50.7	52.0	49.0	47.8
$Y_{H2O,Overall}$ (wt. %)	36.2	35.9	36.1	36.9
$Y_{CO,Overall}$ (wt. %)	37.0	39.6	39.3	40.1
$Y_{CO2,Overall}$ (wt. %)	54.2	54.0	53.3	52.3
$Y_{CH4,Overall}$ (wt. %)	0.5	0.6	0.8	1.2
$Y_{Benzene,Overall}$ (wt. %)	0.001	0.028	0.163	0.291
$Y_{Residual\ carbon,Overall}$ (wt. %)	1.1	1.6	1.5	2.6
$C.G._{.Overall}$ (wt. %)	91.7	94.1	93.4	93.6
$C.A._{.Overall}$ (wt. %)	92.9	95.8	95.2	96.6

7.4 Summary

Although the reactions are relatively fast and the change in gas phase residence time (from 0.2 to 0.3 s) does not have a large impact on the major product yields (in particular the CO yield was high in both cases), the gas phase residence time does impact the overall conversion as well as the minor product yields. Hence the rates of the gas phase reactions are important to the overall process and should be an important consideration as the process is further developed. As expected the role of the catalyst was to complete the conversion as well as catalyze the water gas shift reaction. One could increase the amount

of catalyst (in the case of the shorter residence) to improve the overall conversion. However, the goal of this work is to minimize the amount of catalyst required. As was the case with the NPOX staged oxygen addition, staged oxygen addition did not appear to be advantageous with the catalyst step either.

CHAPTER 8
PROCESS SIMULATION AND ECONOMIC ANALYSIS

Aspen modeling was used to simulate the process of reforming bio-oil to hydrogen in order to gain a better understanding of the thermal efficiencies involved and to use as the basis for an economic analysis. However, in order to get a better understanding of the process as a whole, further information of the pyrolysis process is required. As was discussed in Chapter 1, fast pyrolysis of biomass is a process that has been studied since the 1980s. Figure 8.1 shows a schematic of a typical fast pyrolysis process. Biomass is fed into a fluid bed reactor where it is rapidly heated (~1000ºC/s) to temperatures typically between 450 and 550ºC. Daugaard and Brown determined the heat required for the pyrolysis of several biomass feedstocks[51]. The average value was 1.5 MJ/kg. Although bio-oil yields are highly dependent on the original feedstock[52], typical bio-oil yields are ~75% with the remaining 25% split between char (12%) and permanent gases (13%)[53]. There is more than enough heating value in the char and permanent gas stream to provide the energy for the process including the

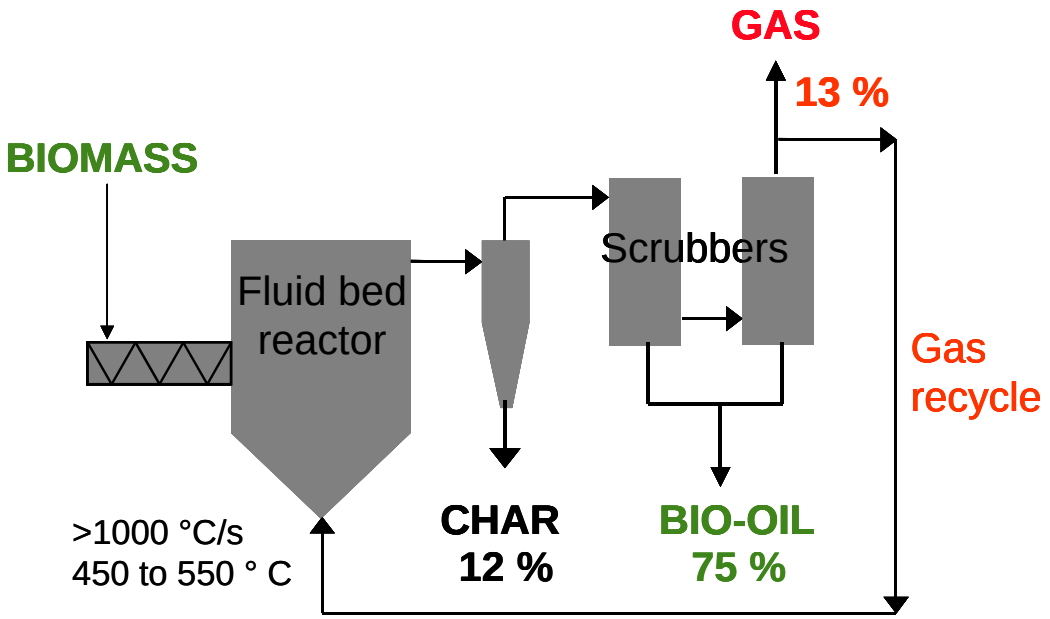

Figure 8.1. Schematic of typical biomass pyrolysis process.

drying of the biomass. Hence the thermal efficiency is only dependent on how much of the heating value of the original biomass ends up in the bio-oil. The thermal efficiency of the pyrolysis process is typically 65-75% based on the usual compositions of biomass and bio-oil and their resulting lower heating values (LHVs). This efficiency for bio-oil production will be combined with the results of the Aspen model to obtain an overall thermal efficiency.

Because one cannot simply select bio-oil as a component in Aspen, it was necessary to develop a surrogate bio-oil based on the typical components found in bio-oil as well as their compositions. By applying certain assumptions, experimental data were used to develop a process simulation to compute material and energy balances as well as the thermal efficiency. Based on the first simulation study as well as additional data, a second generation simulation was developed. The results of the second generation simulation were used to perform an economic hydrogen analysis (H2A).

As part of the transition to a hydrogen economy, the US Department of Energy tasked a group of analysts to create a standardized analysis procedure (H2A) for comparing different routes to producing H_2[54]. As part of this analysis, both centralized and distributed routes are considered. Nineteen case studies are currently available to the public[55]. Of these, six are termed “Forecourt” or “Distributed” routes. The only case for lignocellulosic biomass is a centralized gasification process. The H2A is particularly useful for comparing the hydrogen production cost and process energy efficiency. It should be noted that the H2A utilizes the 2005 value of a dollar as a basis for economic analysis. A discussion of the available cases as well as the H2A performed on the current process will follow the discussion of the Aspen simulations discussed above.

8.1 Surrogate Development

The surrogate was developed based on the typical composition of bio-oil as presented in “Fast Pyrolysis of Biomass: A Handbook” edited by Bridgewater et al.[45] (see Table 8.1). The primary considerations in developing this surrogate were to match the elemental carbon, hydrogen, and oxygen composition of the

bio-oil used during experiments and also match the heating value. It is also important to match the heat capacity of bio-oil since the amount of energy required to heat the oil to the desired reaction temperature was a critical component of the energy balance as well as the overall efficiency of the system.

Table 8.1 Typical composition of biomass.

Species	Typical percentage
organic acids	5 to 10
aldehydes	5 to 20
ketones	0 to 10
phenolics	20 to 30
Furans	0 to 8.6
water	15 to 30

The species used to develop the surrogate mixture need to be representative of the species in bio-oil but that are also contained in Aspen. However, it should be noted that the oligomeric components of the pyrolytic lignin fraction, which typically have molecular weights in the range of 400-2000, were difficult to represent accurately. The most suitable species available in Aspen to represent the functional groups in pyrolytic lignin were anisole and phenol. The other species chosen along with their compositions in the surrogate are given in Table 8.2. Upon comparing Tables 8.1 and 8.2, one will notice that some of the components in the surrogate have a higher concentration than is typically found in bio-oil (e.g. glyoxal and hydroxyacetaldehyde, which are both aldehydes, have a combined composition of 24% whereas the typical composition of aldehydes in bio-oil is only 20%). As stated above, one of the most important considerations was to get the elemental composition of the surrogate to match the bio-oil used in experiments. In order to accomplish this while still having a relatively simple surrogate, it was necessary to go outside the bounds in the case of some components. Additionally, phenol and anisole (phenolics) are not typically found in bio-oil. However, they were selected due to their inclusion in Aspen as well as the fact that components such as guaiacol and syringol are present

Table 8.2 Composition of surrogate.

Species	Surrogate Composition (%)
acetic acid	11
glyoxal	14
hydroxyacetaldehyde	10
acetone	11
phenol	23
anisole	5
furfural	8
ethanol	1
water	17

in bio-oil and have the hydroxy and methoxy groups present in phenol and anisole, respectively. Although ethanol is not shown in Table 8.1, ethanol can be a component in bio-oil in compositions up to 1.4%[45].

The surrogate has an elemental composition nearly identical to that of the bio-oil used in the experiments. The carbon content of the surrogate is 48.0 wt. % as compared to 48.2 wt. % (wet basis) in the case of the actual bio-oil. The hydrogen (7.3 wt. %) and oxygen contents (44.7 wt. %) were both 0.1 wt % higher than the actual oil on a wet basis. The LHV of the surrogate is 19 MJ/kg, which is within the range (15-19 MJ/kg) that is typical for bio-oil. The heat capacity of the surrogate (2.2 J/g-K at 25ºC) is similar to that found experimentally (2.6 J/g-K)[56]. Based on the above comparison of the surrogate to the experimental bio-oil as well as typical bio-oils, the surrogate adequately represents the bio-oil speciation given the limitation of using the species available in Aspen. Hence, results obtained from Aspen modeling using the surrogate should provide a good representation of the actual process.

8.2 Assumptions for First Generation Process Simulation

In addition to the assumption that the surrogate would provide a good representation of bio-oil, other assumptions were made:

- The laboratory scale experimental partial oxidation results from the preliminary data described in Chapter 3 were assumed to scale up without major changes. The yields of major species were specified (based on experimental yields) using the RYIELD unit operation in ASPEN. Because carbon balances were typically around 90% during the preliminary experiments used as a guideline for these simulations, small amounts of naphthalene and anthracene (both observed experimentally) were added as products of the RYIELD reactor in order to get reasonable mass closure (within 3% for carbon, hydrogen, and oxygen).

- Equilibrium was assumed to be achievable in both the steam reforming and water gas shift reactions. Additionally, the water gas shift reaction was assumed to be nearly inactive in catalyzing the methanation reaction, which was accomplished by specifying that methane was 99% inert. The RGIBBS unit operation was used to calculate equilibrium at the temperature of these reactors.

- Pressure of 1 atm in reactors.

- Heat losses were neglected (i.e. perfect heat exchangers).
- 85 % of the hydrogen was assumed to be recoverable via pressure swing adsorption (PSA).
- A steam to carbon ratio of 3 was used including steam generated in the NPOX step.
- Air was used as the oxygen source for partial oxidation.

8.3 First Generation Process Simulation

The focus of the first generation process simulations was on material and energy balances. The effects of both the temperature of the catalytic step and preheating of the air and bio-oil fed to the burner on the amount of bio-oil required for process heat (and consequently the efficiency) were explored. Figure 8.2 shows a basic schematic of the Aspen model, which also included heat exchangers, pumps, compressors, etc. Details of the feed conditioning step are shown in Figure 8.3. In this step bio-oil and methanol were mixed, preheated,

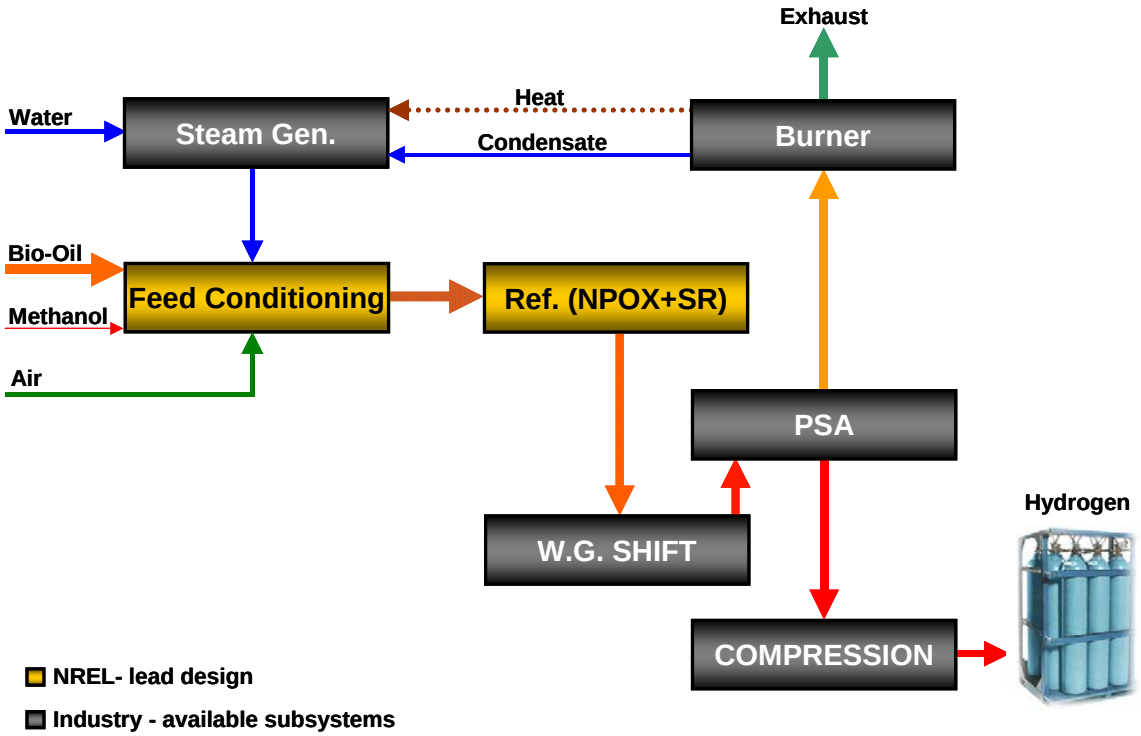

Figure 8.2. Process outline used for ASPEN model.

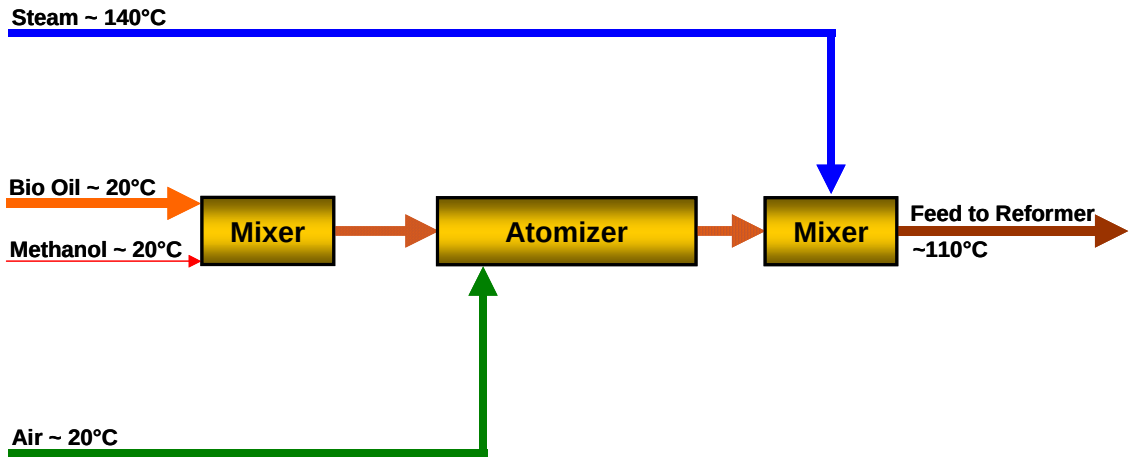

Figure 8.3. Details of feed conditioning.

and fed to the reactor using an atomizer after mixing with steam. (The ultrasonic nozzle may prove too costly and a different means of atomizing may be necessary; see H2A in Section 8.6.) The reforming step included both the NPOX and catalytic (SR) steps described previously. Some of the bio-oil/methanol mixture along with any unrecovered/unconverted combustibles were burned to provide process heat for running the endothermic catalytic steam reformer as well as generating steam. Before the water gas shift reaction, the effluent from the steam reformer must be cooled. This heat is sufficient to preheat the feed (see Figure 8.4).

As discussed in Section 8.2, the preliminary experimental results were used as a guideline for specifying the RYIELD reactor, which was used to model the NPOX step in Aspen. Because those experiments produced 90% carbon accounting rather than 100%, it was assumed that the remainder was higher molecular weight species. Anthracene and naphthalene (both observed experimentally) were chosen to represent the missing carbon, which led to elemental mass closures that were within 3.3% (see Table 8.3).

Both the steam reforming (SR) and water gas shift (WGS) steps were modeled using an RGIBBS reactor, which calculates equilibrium compositions by minimizing the Gibbs free energy. The steam to carbon ratio entering the SR reactor was ~3. This ratio included the steam generated from the NPOX step as

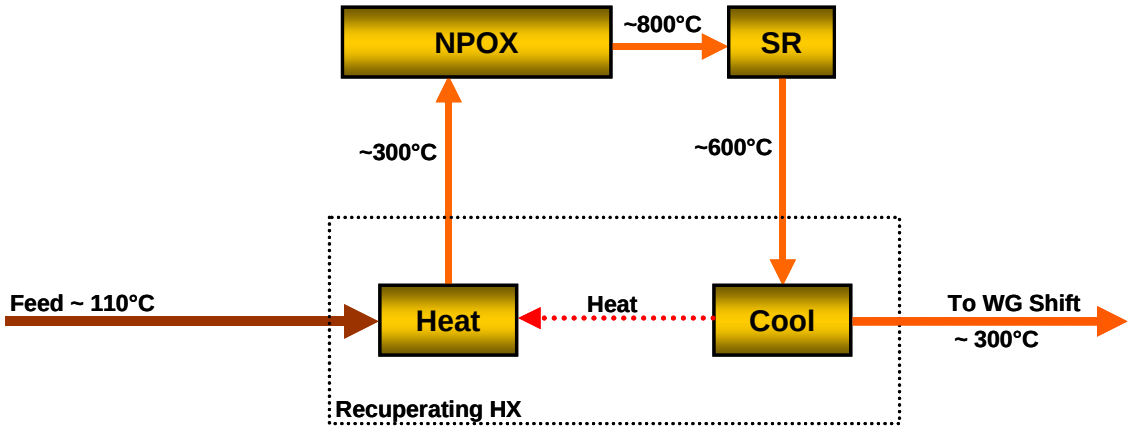

Figure 8.4. Details of reforming and heat recuperation.

well as that generated from vaporizing the bio-oil and added water. The water in the effluent of the WGS reactor was condensed out (modeled using a heat exchanger and specifying the temperature such that the water was condensed) prior to compressing the now dry syngas in preparation to be fed into a separator to model the PSA unit. In this step, 85% of the H_2 was assumed to be recovered. The remainder of the reactor effluent was fed to a combustor along with additional bio-oil/methanol required to provide heat for the SR reactor and for steam generation.

Table 8.3 Elemental mass closures (from Aspen simulations) across RYIELD reactor.

	Mass Flow Into NPOX Reactor (kg/day)	Mass Flow Out of NPOX Reactor (kg/day)	Percent Different
Total	68481	68481	
C	7518	7332	2.46
H	4357	4500	-3.30
O	38839	38510	0.85
Napthalene	0	348	
Anthracene	0	348	
C (solid)	0	383	

The effects of preheating the feeds to the combustor as well as the effects of the SR temperature on the thermal efficiency were explored. In cases where the feeds to the combustor were preheated, the air was preheated to 400ºC while the leftover reactor effluent was preheated to 300ºC. The bio-oil was not preheated. The SR temperatures used were 650ºC, 750ºC, and 850ºC.

Two cases for each temperature were performed: one with preheat of combustor feeds and one without the preheat. The results of these cases are shown in Table 8.4. In this table, η_{th} is thermal efficiency. In the first three cases, the feed to the combustor was not preheated, while in the last three cases it was. Each case was based on producing 1500 kg of H_2 per day, which is the standard set forth by the US Department of Energy for distributed H_2 production.

The thermal efficiency was defined as the LHV of H_2 produced divided by the LHV of the bio-oil required (total). The thermal efficiency was increased by decreasing T_{SR} since less bio-oil was burned for process heat. Additionally, preheating the feed to the combustor led to higher efficiencies. The heat used to preheat the combustor feed came from the exhaust. The remaining exhaust heat was used to produce steam. The highest efficiency (57%) was for Case 6, which had the lowest T_{SR} (650ºC) and had the combustor feed preheat. In this case, just 3% of the bio-oil had to be burned to provide process heat. Minimizing the amount of bio-oil that must be burned was highly desirable since it led to a higher number of kg H_2 produced per kg bio-oil used (0.102 vs. 0.082 for the worst case). The H2A (see below for more info on H2A) for biomass gasification utilizes the assumption that 0.078 kg H_2 can be produced per kg of biomass[51]. Based on a yield of 75% bio-oil from the original biomass, Case 6 would give 0.0765 kg H_2 per kg biomass. Hence, the present process simulation suggests that the process proposed in this study has the potential to give the nearly the same H_2

Table 8.4. Results of 6 cases of first generation aspen modeling.

Case	Preheat	T_{SR} (^oC)	Bio-oil for H_2 (kg/day)	Bio-oil for process heat (kg/day)	Methanol in feed (kg/day)	Fraction of bio-oil burned	kg H_2 per kg bio-oil	T_{exh} (^oC)	η_{th}
1	N	850	14265	3928	1585	0.22	0.082	705	46 %
2	N	750	14265	2962	1585	0.17	0.087	592	49 %
3	N	650	14265	1945	1585	0.12	0.092	447	52 %
4	Y	850	14265	1606	1585	0.10	0.095	387	53 %
5	Y	750	14265	839	1585	0.06	0.099	224	56 %
6	Y	650	14265	479	1585	0.03	0.102	140	57 %

yields as biomass gasification. However, it should be noted that some of that H_2 comes from the methanol.

8.4 Additional Assumptions for Second Generation Process Simulation

In general, the assumptions used for the second generation simulation were the same as those used for the first generation. However, the following changes were made:

- The improved experimental results from Chapter 4 were used rather than those from Chapter 3.
- In preparation for the PSA step, all reactors were run at 21.4 atm. It required less energy to pressurize the bio-oil as a liquid than to compress the product gases. The resulting pressure increase was assumed to have no effect on the NPOX reactor yields (i.e., they were still based on experimental data under atmospheric conditions). Obviously the gas phase reactions have pressure dependence.
- A series of 5 RGIBBS reactors with heat exchangers between them was used for the SR reactor in place of the single RGIBBS. By using this scheme, one can better emulate a catalyst-coated heat exchanger.

8.5 Second Generation Process Simulation

Other than the changes to the assumptions described above, the only other significant changes were adjustments such that utilities (e.g., electricity, cooling water, etc.) could be better estimated for use in the H2A analysis to determine the estimated bio-oil production cost. These changes included better heat integration such that no bio-oil was required for process heat.

Because of the change to the 5 reactor/heat exchanger scheme for the SR, the reactor temperature varied between ~750 and ~830ºC. There was sufficient heat in the reactor effluent after the recovery of 85% of the hydrogen to provide the heat for the SR as well as to preheat the feed to the combustor and to generate steam (the final exhaust temperature was 115ºC). Although the change in pressure was assumed to have no effect on the NPOX yield, the equilibrium calculations performed by the RGIBBS reactors did account for the

increased pressure, which led to an increase in the bio-oil/methanol required to produce the H_2. As a result, the amount of bio-oil required to produce 1500 kg/day of H_2 was 14,762 kg/day (mixed with 1641 kg/day of methanol). The best case of the first generation simulation (Case 6) required a total of 14,744 kg/day (mixed with 1638 kg/day of methanol) of bio-oil to produce the same amount of H_2. (Note: the bio-oil that was burned also included 10% methanol).

The thermal efficiency of the second generation model was the same as Case 6 of the first generation model (57%). While this result was a bit surprising since the heat integration was improved, it suggested that the improved heat integration was offset by the change in thermodynamics at the higher pressure. Taking into account the efficiency of the biomass to pyrolysis efficiency, this gives an overall process efficiency of between 37% and 43%. Perhaps just as important as the efficiency of the process is the final cost of the hydrogen, which will be discussed as part of the H2A analysis in Section 8.6.

8.6 H2A Results

An H2A has been performed for the process described above. Before presenting the results of this analysis, the results of the other available cases will be discussed. As a reference, one kg of H_2 has nearly the same energy content as 1 gallon of gasoline. The DOE goal is to provide \$2.00 to \$3.00/kg H_2 (delivered, untaxed) irrespective of the means of production[39].

8.6.1 Centralized Cases

With the exception of the nuclear case (which only has a future case), the centralized cases that are available have both a current and future case. These cases include:

- Biomass gasification
- Grid electrolysis
- Coal gasification (with and without CO_2 sequestration)
- Natural gas reforming (with and without CO_2 sequestration)
- Nuclear energy via high temperature electrolysis

Table 8.5. H2A results for centralized cases.

	Production Cost		Process Efficiency	
	Current	Future	Current	Future
Biomass gasification	$1.61	$1.47	46.1%	48.3%
Grid electrolysis	$4.50	$3.24	62.5%	74.7%
Coal gasification (without CO_2 sequestration)	$1.41	$1.45	55.9%	64.2%
Coal gasification (with CO_2 sequestration)	$2.05	$2.00	53.8%	62.1%
Natural gas reforming (without CO_2 sequestration)	$1.32	$1.40	72.0%	72.0%
Natural gas reforming (with CO_2 sequestration)	$1.64	$1.65	70.9%	71.1%
Nuclear energy via high temperature electrolysis		$2.93		83.4%

Table 8.5 gives both the current and future case hydrogen production costs as well as process efficiencies. The production costs are on a \$/kg H_2 basis and do not include costs for delivery or dispensing. The efficiencies are defined as the LHV of H_2 divided by the LHV of the feed. Based on the current results, natural gas reforming without CO_2 sequestration (\$1.32/kg H_2) is the most cost effective method for producing H_2 followed closely by coal gasification (\$1.41/kg H_2). Natural gas reforming is the most energy efficient process. Although less efficient than either natural gas reforming or coal gasification, biomass gasification is economically third at \$1.61/kg H_2. However, biomass gasification becomes the most economical method when CO_2 sequestration is factored into coal gasification and natural gas reforming. In the future cases, biomass gasification is projected to be competitive even without taking into account CO_2 sequestration. Biomass gasification has the advantage of being a CO_2 neutral

process since the CO_2 liberated upon reforming is used during the next cycle to assist in plant/tree growth.

8.6.2 Distributed Cases

Each of the distributed cases has both a current and future case, which include:

- Grid electrolysis
- Natural gas
- Ethanol

The results of the distributed cases are given in Table 8.6. These cases include additional expenses due to compression, storage, and dispensing (CSD) costs. Because distributed H_2 production is intended for H_2 fueled vehicles, the CSD costs must be included. However, it should be noted that CSD costs could arise in the case of centralized H_2 production depending on the use of the H_2. Again, natural gas reforming is the most economical with a total current cost of \$3.49/kg H_2 and has the highest efficiency at 68.5%. The future case has slightly lower cost and higher efficiency. Ethanol, which could come from biomass, is a distant second with a total current cost of \$5.06/kg H_2 and an efficiency of 64.9%. These numbers improve slightly in the future case, but not sufficiently to meet the DOE goal of \$2.00 to \$3.00/kg H_2 (delivered, untaxed)[39].

Table 8.6. H2A results for distributed cases.

	Production Cost		CSD Cost		Process Efficiency	
	Current	Future	Current	Future	Current	Future
Grid electrolysis	\$4.23	\$3.10	\$1.82	\$1.82	60.5%	60.5%
Natural gas reforming	\$1.61	\$1.59	\$1.88	\$1.88	68.5%	71.1%
Ethanol	\$3.18	\$2.91	\$1.88	\$1.88	64.9%	69.5%

8.6.3 Results of H2A for Present Study

Based on the second generation process simulation, an H2A (current case) was performed for the bio-oil to hydrogen process. From an efficiency standpoint, processes based on biomass are less efficient than any of the other cases. The current case is no exception with a process efficiency of 45% from the H2A analysis. This efficiency is different than that from the process simulations since it includes the energy costs for utilities used during the process as well as CSD. The H2A also uses different assumptions than were used in the process simulation.

Perhaps more important than the efficiencies are the economics of the process. The CSD costs were the same as the natural gas and ethanol distributed cases ($1.88). The production cost of H_2 was $2.35/kg. This cost could be reduced by finding a means other than ultrasonic atomization (such as a diesel fuel injector) for feeding the bio-oil and a less expensive catalyst. These costs currently contribute nearly $0.20/kg to the overall cost. The current production cost puts the present process behind natural gas but ahead of ethanol in terms of the distributed cases. This method of producing H_2 also appears to be less economical than biomass gasification ($1.61/kg) as well as the all other centralized cases except for grid electrolysis. However, it should be noted that the present process is more versatile since it does not require the transport of H_2. In addition to the CSD costs, biomass gasification and the other centralized cases would have higher transport costs. Additionally, biomass gasification does not scale down well[57].

8.7 Summary

A surrogate has been developed to use during process simulations in Aspen. Both first and second generation process simulations have been performed using the surrogate in order to gain a better idea of the process efficiency. The best efficiency for bio-oil to H_2 was 57% based on these simulations. The resulting overall process efficiency (including production of bio-oil) was 37% to 43%.

Taking into account the utility and compression costs, the H2A gives a process efficiency of 45% for the bio-oil to H_2 process. The H2A shows a total cost of $4.23/kg, which is higher than the $2.00 to $3.00/kg required by the DOE. However, further advances in the present technology as well as separation technology could allow the present process to be more competitive with distributed natural gas. Additionally, the present process has the advantage of being based off of a renewable resource. Biomass gasification is also based off a renewable resource and can produce hydrogen at $1.61/kg, but this is based off a centralized plant. The resulting H_2 would either need to be used close to the plant or transported (incurring additional costs).

CHAPTER 9
METHANOL EXPERIMENTS AND MODELING

Detailed kinetic models include a description of the overall chemical process in terms of individual elementary chemical reactions. Such models, when properly constructed and validated, provide important insights into the chemical mechanism and can often be used to identify more favorable operating conditions. There are several mechanisms in the literature that have been developed specifically for methanol pyrolysis and/or oxidation. A group headed by Dr. Joseph W. Bozzelli at the New Jersey Institute of Technology looked at both pyrolysis (1-10 atm; 800ºC) and oxidation (1-5 atm; 600 to 800ºC)[58]. This model will be designated the NJIT model. A group headed by Dr. Fredrick L. Dryer at Princeton University has focused recently on methanol oxidation over a much wider temperature and pressure range[59,60]. Their original model will be designated the Princeton model, whereas their update will be designated updated Princeton.

At CSM, Dr. Dean's group has been working on a mechanism for the pyrolysis and oxidation of hydrocarbons. Although not specifically developed for methanol or other oxygenated species, the chemistry for many oxygenates (including methanol) is included in the mechanism. This kinetic mechanism consists of 3546 reactions and 354 species. It is the combination of a nC_6 pyrolysis model and an ethane oxidation model and will be designated the CSM model. The nC_6 model has been described by Randolph and Dean[61]. The oxidation component of the model was developed by Naik and Dean[62] to describe ethane oxidation and pyrolysis over a very wide range of conditions. Obviously such a large model is not necessary to describe the methanol system, but it was available and was used to assure completeness. Since the previous focus for validation of this mechanism has been on hydrocarbons, it is necessary to begin the expansion of the mechanism to oxygenates with methanol (one of the simplest oxygenates). Modifications have been made to this model and will

be discussed. The updated model will be designated the CSM model +2 since two reactions were updated.

In addition to model validation, the objective of the methanol experiments was to verify the repeatability of experiments using the NREL system. The results of these experiments were compared to the kinetic mechanisms described above to assess whether these experimental results were consistent with gas phase chemistry. However, because the system at NREL was not specifically designed for kinetic experiments, there is a lack of a detailed knowledge of the precise temperature–time history within the reactor, which makes a quantitative comparison problematic. Further experiments were performed using the CFCC system. These experiments were also used for model validation. The chapter concludes with a discussion of methanol experiments performed using the larger reactor at NREL.

9.1 Modeling of NREL Experimental Data

Using the NREL system, experiments were performed at 650ºC using the 120 kHz ultrasonic nozzle to feed methanol (0.066 g/min). The helium and oxygen flows were varied between 357 to 403 sccm and 0 to 46 sccm (corresponds to oxygen to carbon – O:C – ratios ranging from 1 to 2.5), respectively. With the 10 sccm of argon, the total inlet flow of gases was maintained at 413 sccm. The initial methanol mole faction was always 0.10. The resulting residence time was ~0.45 s within 15ºC of 650ºC. The final methanol mole fraction as well as that of the observed products (CO, CO_2, H_2, H_2O, and CH_2O) will be discussed and compared to the kinetic mechanisms. Although CH_4 was predicted by both mechanisms in very small amounts, it was not observed experimentally.

In order to perform the model calculations, the reactor dimensions, flow rates/compositions, pressure, and the temperature profiles were input to Chemkin Pro. Temperature profiles were obtained under reactive conditions by using a reactor with a thermocouple well down the center and with measurements taken every 1 cm. Figure 9.1 shows the complete temperature

profile, while figure 9.2 shows just the zone where the temperatures start to deviate from each other.

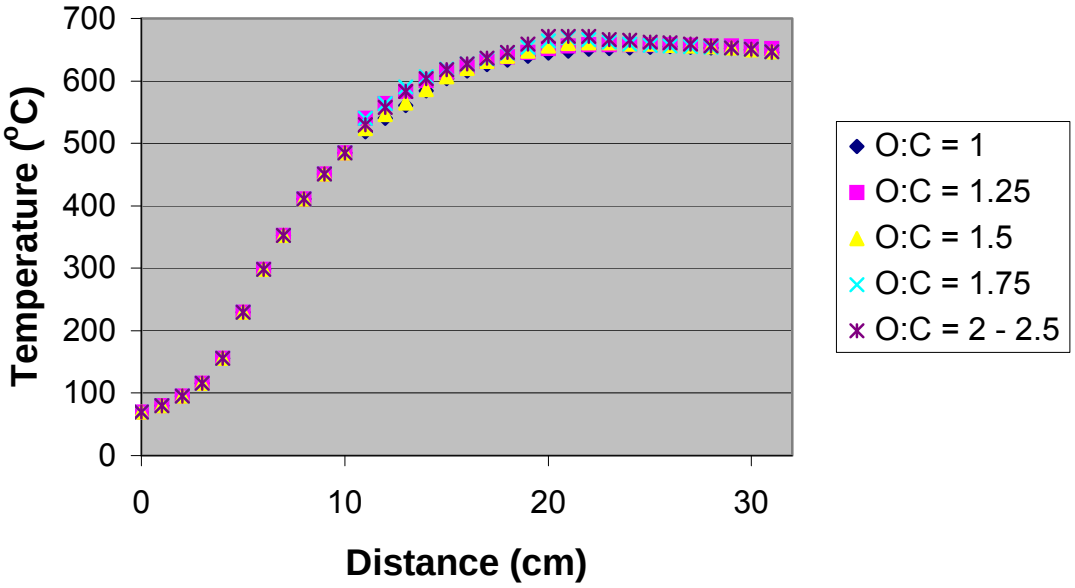

Figure 9.1. Temperature profiles under reactive conditions at varied molar O:C ratios for NREL methanol experiments (650ºC; ~0.45 s).

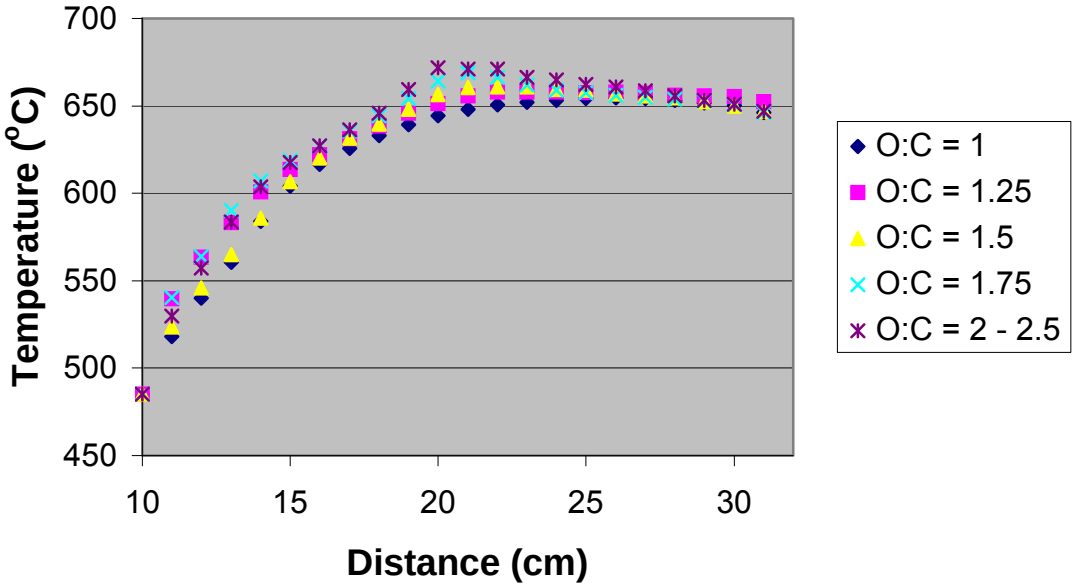

Figure 9.2. Temperature profiles in the zone where they deviate from each other under reactive conditions at varied molar O:C ratios for NREL methanol experiments (650ºC; ~0.45 s).

9.1.1 Methanol

The experimental data as a function of molar O:C ratio were compared to predictions from the three literature models as well as the two CSM models (see Figure 9.3). Here, the O:C ratio included the oxygen in the methanol (i.e., O:C = 1 was pyrolysis). The predictions by all three literature models did a good job of predicting the methanol conversion at high O:C ratios. However all three models over-predicted the conversion at low O:C ratios. The NJIT model came closest to the methanol conversion over all O:C ratios. Both CSM models predicted the same methanol conversion and do a better job than any model at lower O:C ratios, but not as good at higher O:C (2 to 2.5).

Methanol exhibited almost no reactivity under pyrolysis conditions, but significant reactivity once oxygen was added. This reflects the lower activation energy that is typical for partial oxidative reactions. The experimental results showed good reproducibility.

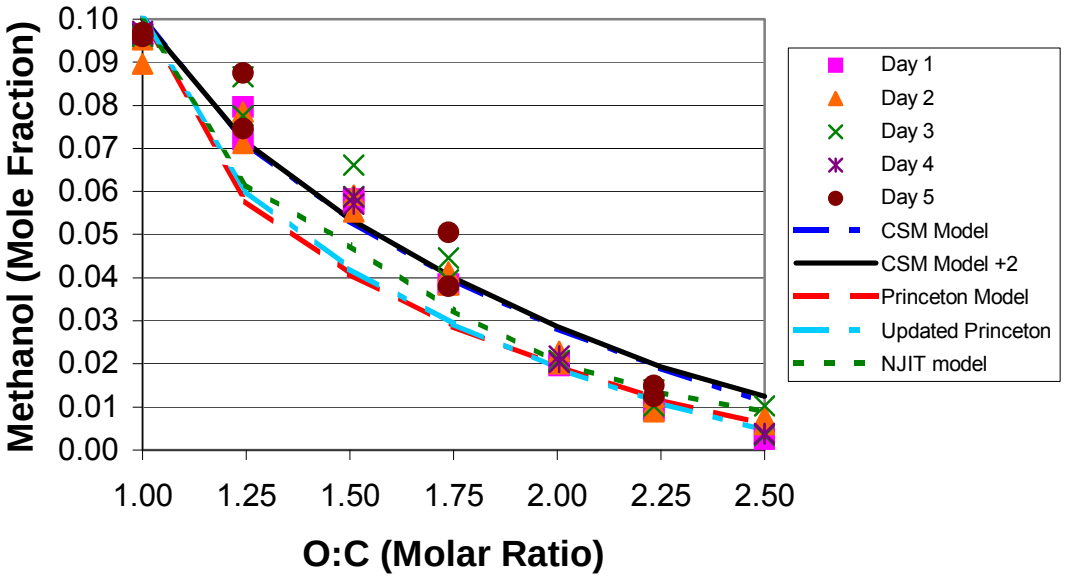

Figure 9.3. Methanol mole fraction compared to three kinetic mechanisms available in the literature as well as the CSM models as a function of O:C ratio at 650ºC and a residence time of ~0.45 s.

9.1.2 Formaldehyde

As is discussed by Held and Dryer[59], formaldehyde is a very important intermediate in oxidation chemistry. Hence, accuracy in its prediction is of utmost importance. Figure 9.4 compares the experimental data to the three literature models as well as the original CSM model. The CSM model over-predicted the selectivity to formaldehyde. All the other models did a much better job of predicting the formaldehyde selectivity with the original Princeton model doing the best job at lower O:C and the updated Princeton model doing slightly better at higher O:C.

Based on these results, both a sensitivity and rate of production analysis was performed to determine which reactions were most important with respect to formaldehyde production. Over the course of this analysis, two key reactions were identified:

$$CH_2O+HO_2 \leftrightarrow HCO+H_2O_2 \quad (9.1)$$

$$C.H_2OH+CH_2O \leftrightarrow CH_3OH+HCO \quad (9.2)$$

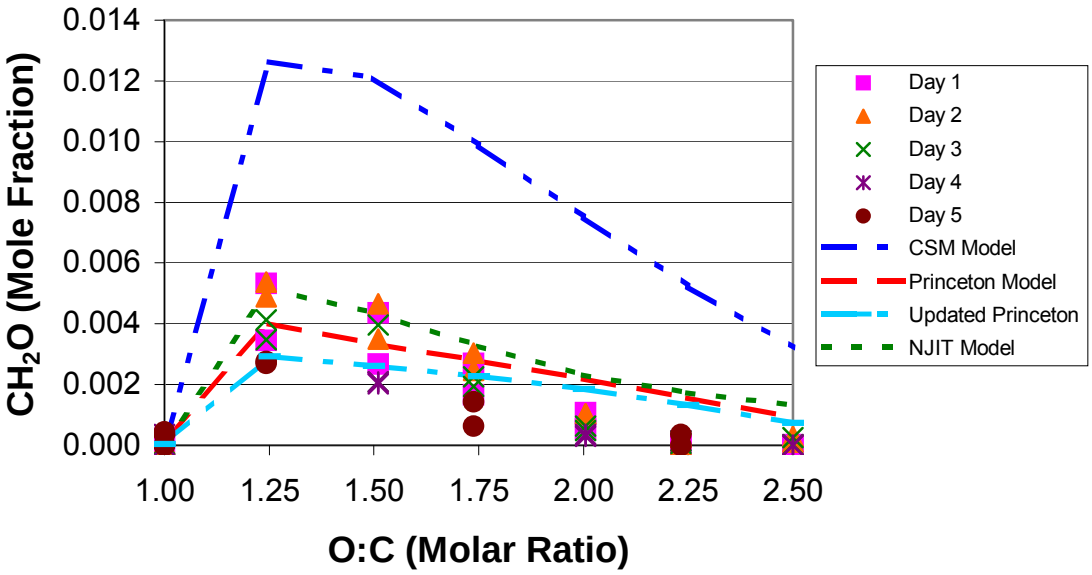

Figure 9.4. CH_2O mole fraction compared to kinetic mechanisms as a function of O:C ratio at 650ºC and a residence time of ~0.45 s.

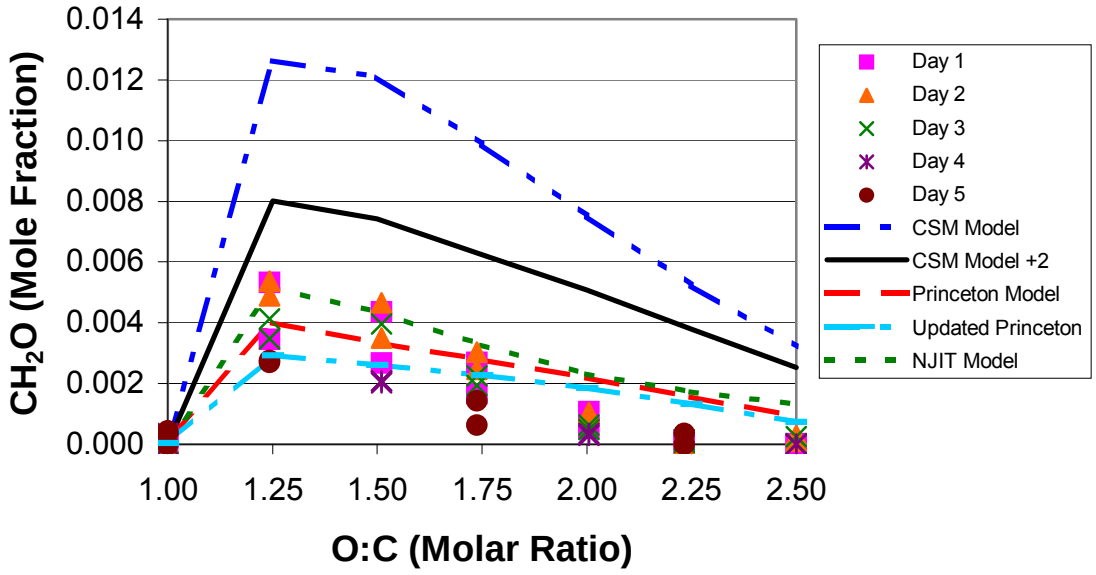

Figure 9.5. CH_2O mole fraction compared to kinetic mechanisms with as a function of O:C ratio at 650ºC and a residence time of ~0.45 s. (CSM model +2 added.)

The kinetic parameters of Reaction 9.1 were modified in the CSM model to reflect the original Princeton model since those parameters were based on experimental data whereas the initial parameters in the CSM model were estimated. This change had little effect. Because Reaction 9.2 was not present in the CSM model, it was added. The resulting CSM mechanism is designated CSM model +2. The second modification led to a significant improvement in the CSM model. However, there is still room for further improvement.

9.1.3 Carbon Monoxide

The decrease in selectivity to CH_2O that came about as a result of modifying the kinetic parameters of Equations 9.1 and 9.2 was expected to slightly increase the selectivity to CO. Since the concentration of CH_2O was quite low, a large change was not expected. Figure 9.6 shows a slight increase in CO using the CSM model +2. Both CSM models did a better job of predicting CO production at lower O:C ratios, but the other three models did a better job of

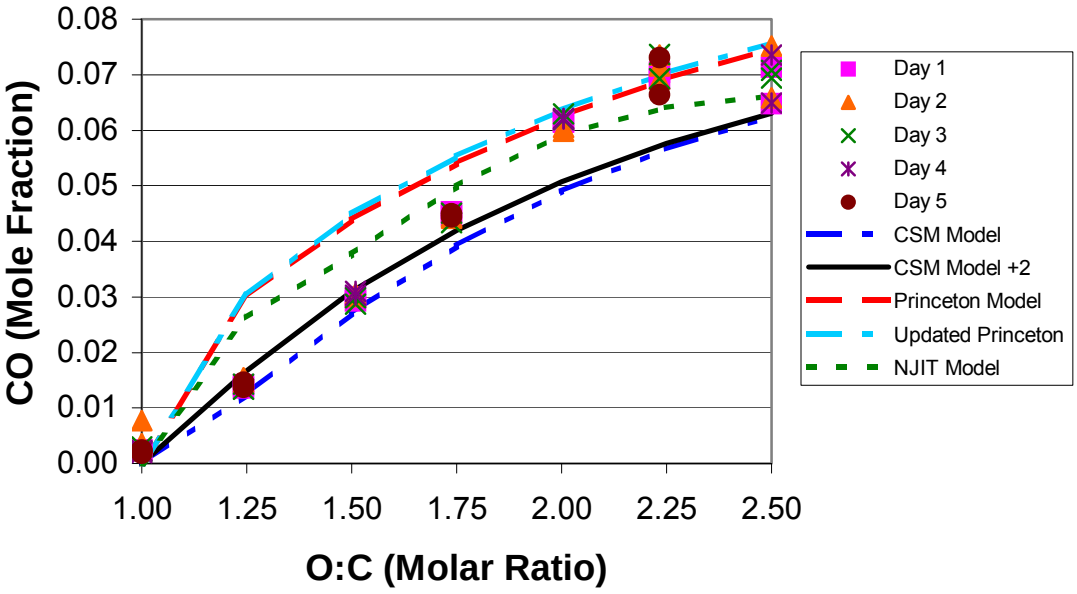

Figure 9.6. CO mole fraction compared to kinetic mechanisms as a function of O:C ratio at 650ºC and a residence time of ~0.45 s.

predicting the CO at higher O:C ratios. However, the CSM model +2 was slightly closer to the CO concentrations at higher O:C ratios than was the original CSM model. The underprediction of the CO by the CSM models was due at least in part to the underprediction of methanol conversion. The updated Princeton model prediction of CO was slightly worse than the original.

The production of CO increased significantly as the O:C ratio was increased and reached a maximum at an O:C 2.25 to 2.5. However, it may have been starting to decline at O:C = 2.5, suggesting that CO was being oxidized to CO_2. Again the data showed good reproducibility.

9.1.4 Carbon dioxide

Unlike the CO selectivity, the selectivity to CO_2 was the same for both CSM models. Figure 9.7 shows the experimental CO_2 mole fraction compared to the kinetic models. All models did a reasonably good job of predicting CO_2, but the NJIT model did the best job followed closely by the CSM models. Although the updated Princeton model does a better job than the original, it still under-predicts the CO_2 production.

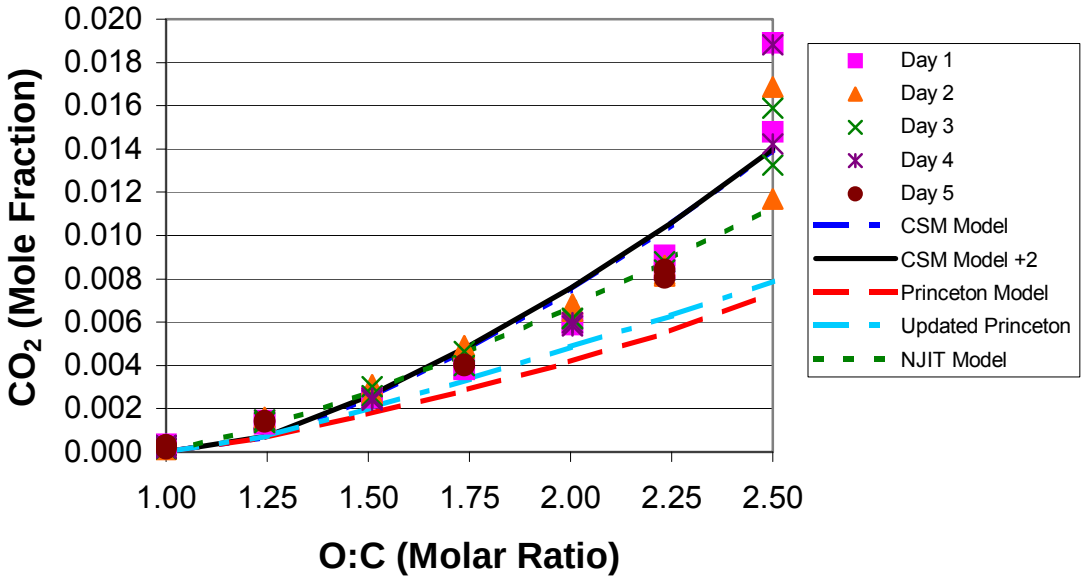

Figure 9.7. CO_2 mole fraction compared to kinetic mechanisms as a function of O:C ratio at 650ºC and a residence time of ~0.45 s.

The CO_2 production increased with increasing O:C ratio, but the increase was not as significant as was the case with CO. Similar trends were observed for the bio-oil:methanol mixture experiments (see Chapter 3). The CO_2 data was reproducible up to O:C of 2.25. The higher degree of scatter at an O:C of 2.5 may be reflective of entrance into a region of higher combustion conditions.

9.1.5 Hydrogen

At low O:C ratios (below 2), both CSM models and the updated Princeton model did a good job of predicting the H_2 mole fraction with the CSM model doing a better job (see Figure 9.8). The NJIT model was slightly worse. The original Princeton model over-predicted the H_2 yields under these conditions. However, as the O:C ratio is increased, all models predicted the H_2 production to taper off and even go down slightly. The experimental data did not reflect this. While the reproducibility in the H_2 data was good up to O:C of 1.75, above 1.75 there was significantly more scatter in the data. It was not clear what caused the increase in scatter.

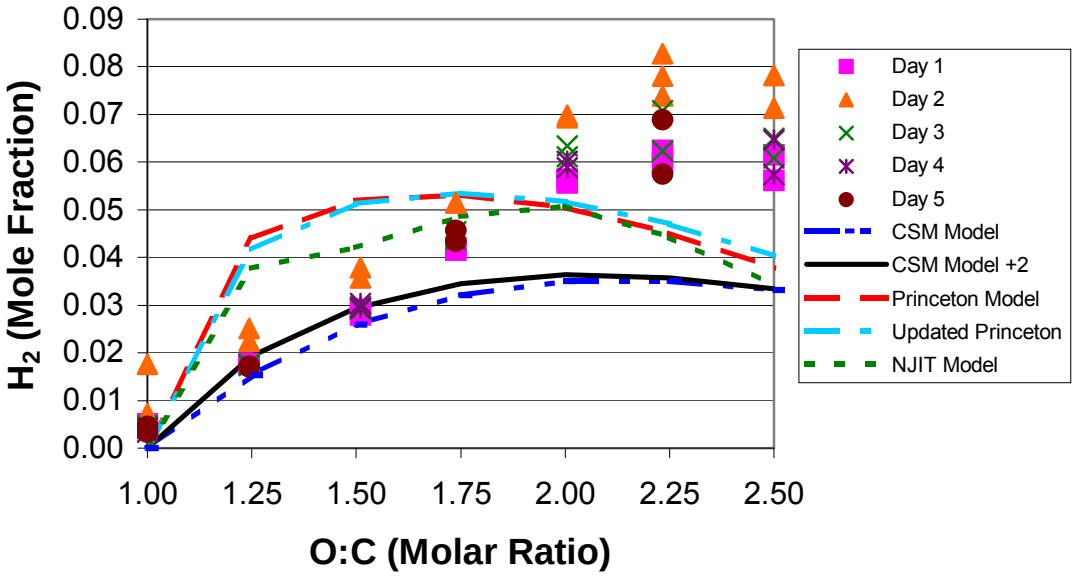

Figure 9.8. H_2 mole fraction compared to kinetic mechanisms as a function of O:C ratio at 650ºC and a residence time of ~0.45 s.

9.1.6 Water

As seen in Figure 9.9, all models do an excellent job of predicting the H_2O production with only a slight deviation at the highest O:C ratio in the case of the Princeton models. H_2O data showed good reproducibility under all conditions.

9.1.7 Carbon, hydrogen, and oxygen balances

The carbon, hydrogen, and oxygen balances from the experimental data are shown in Figures 9.10, 9.11, and 9.12 respectively. Carbon balances were typically within 5% of 100%. Hydrogen balances exhibited the highest deviations from 100% at up to 20 to 25%. This deviation could stem in part from measured values of H_2 being too high. Experimental error from other species must have contributed as well since the H_2 yields were never higher than 40%. However, if it were assumed that half of the deviation were due to methanol that would lead to a reduction of ~25% in the value of the H_2 mole fraction. Oxygen balances were typically within 10% of 100% and often within 5%. Because of the relatively small amounts of each species, small errors in their values can lead to much larger errors in the mass closures.

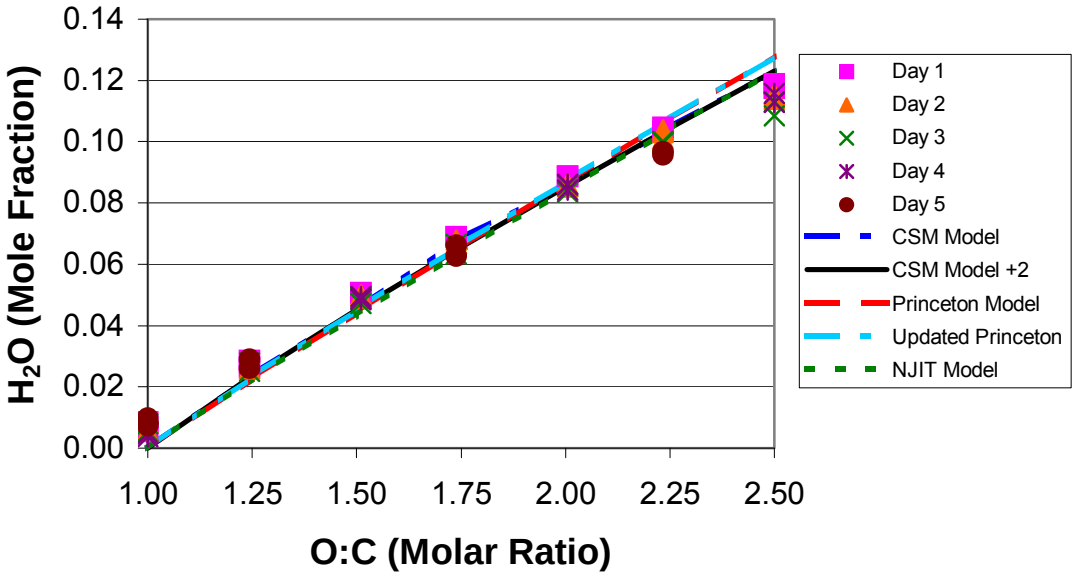

Figure 9.9. H_2O mole fraction compared to kinetic mechanisms as a function of O:C ratio at 650ºC and a residence time of ~0.45 s.

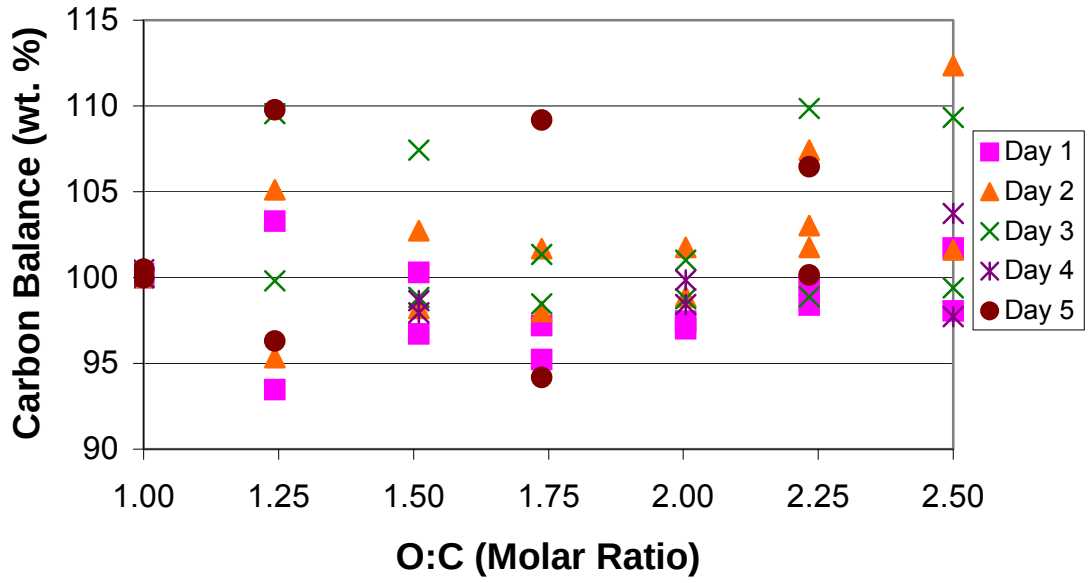

Figure 9.10. Carbon balances for methanol experiments using NREL system at 650ºC and a residence time of ~0.45 s.

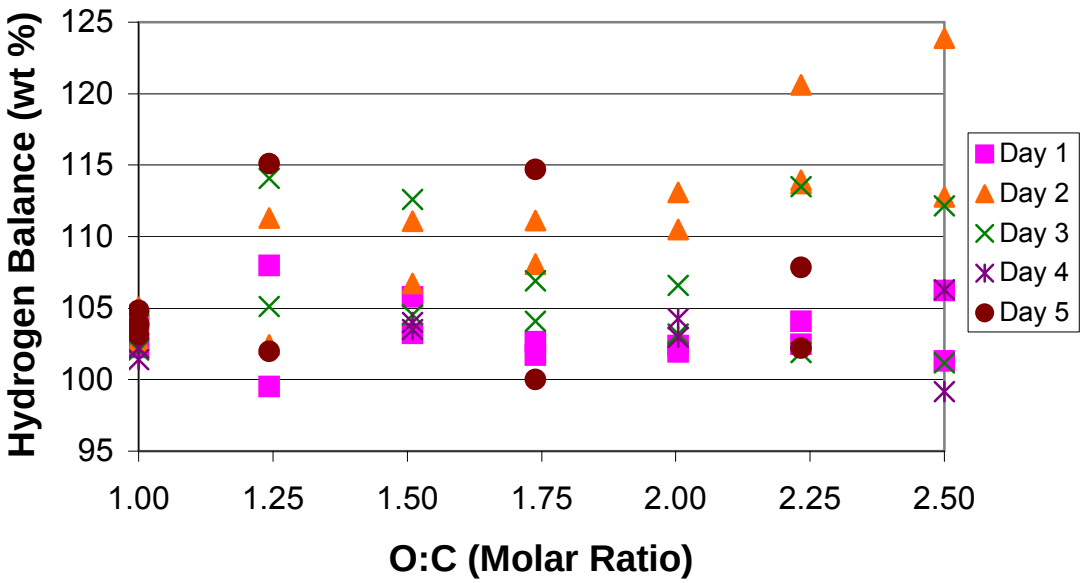

Figure 9.11 Hydrogen balances for methanol experiments using NREL system at 650ºC and a residence time of ~0.45 s.

9.1.8 Summary

With the exception of H_2 and CO_2 (at O:C 2.5), the experimental data was quite reproducible. The various kinetic models did a reasonable job of predicting the results in most cases. The biggest exception was the H_2 data. The CSM model did a slightly better job than the other models at predicting the data with the exception of the formaldehyde data. The general agreement with the models suggested that the experimental results were consistent with that expected from exclusively gas phase chemistry.

9.2 Modeling of CFCC Experimental Data

Although the NREL data suggested that the observed results were consistent with gas phase chemistry, it was desired to further explore the methanol chemistry in a reactor system specifically designed for kinetic measurements. The CFCC apparatus was designed for such experiments. However, this system has been used exclusively for experiments with hydrocarbons. The major issue is that the GC columns designed for analysis of

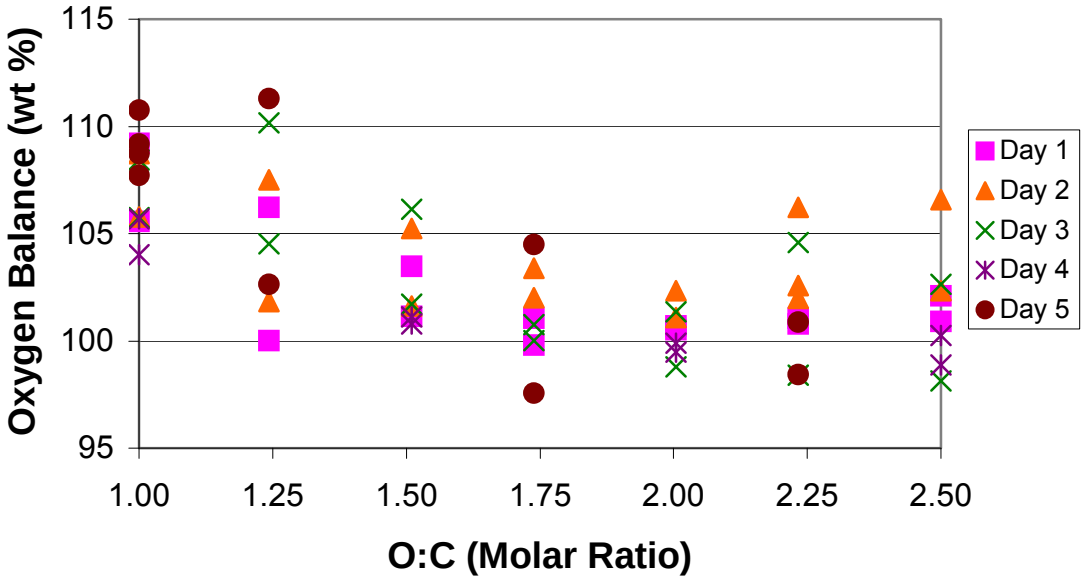

Figure 9.12. Oxygen balances for methanol experiments using NREL system at 650ºC and a residence time of ~0.45 s.

hydrocarbons are not suitable for polar oxygenates. In particular, it was not possible to detect CH_2O or H_2O with the columns used. There were difficulties in getting consistent carbon mass closures as well as problems with data reproducibility, making model validations difficult.

Table 9.1 shows both a pyrolysis and a partial oxidation experiment (three injections each for each experiment), neither of which had acceptable carbon mass balances. In both experiments, the measured mole fractions of the reactor effluent were within experimental error from one injection to the next. The sum of the mole fractions also seemed reasonable as it was within 5% of 1.0 in both cases. However, the carbon mass balance calculated from these data was not within the acceptable 5% limit. As noted above, this may have been due to missing CH_2O. Closer analysis showed that in order to get 100% carbon balance for the pyrolysis data shown in Table 9.1 the CH_2O mole fraction would need to be ~0.04. The same analysis for the partial oxidation data gave a mole fraction of ~0.013. This seemed plausible since the sum of the mole fractions would be within experimental error, but one must be careful when forcing mass balances in this manner as one cannot be sure whether just the right combination of errors

Table 9.1. Methanol experimental results using the CFCC system that illustrate the difficulty of obtaining mass closure.

	Pyrolysis			Partial Oxidation		
Injection	1	2	3	1	2	3
Initial Conditions						
Temperature (^{o}C)	800	800	800	650	650	650
O_2 Flow (sccm)	0	0	0	5.8	5.8	5.8
N_2 flow (sccm)	56.8	56.8	56.8	154.2	154.2	154.2
CH_3OH flow (μl/s)	0.71	0.71	0.71	0.601	0.601	0.601
He flow (sccm)	20.6	20.6	20.6	45.5	45.5	45.5
O:C ratio	1.00	1.00	1.00	1.53	1.53	1.53
λ	0	0	0	0.18	0.18	0.18
Est. R.T. (s)	1.0	1.0	1.0	0.5	0.5	0.5
Effluent mole fractions						
N_2	0.510	0.509	0.505	0.661	0.659	0.661
He	0.180	0.182	0.180	0.194	0.201	0.195
CH_3OH	0.147	0.145	0.147	0.046	0.045	0.045
H_2	0.108	0.107	0.108	0.026	0.026	0.026
CO	0.044	0.043	0.039	0.034	0.029	0.030
CH_4 (FID)	7.1E-04	6.7E-04	6.9E-04	1.7E-04	1.9E-04	4.0E-04
CO_2	0	0	0	0	0	0
CH_2O	0*	0*	0*	0*	0*	0*
Total	0.990	0.987	0.980	0.960	0.960	0.957
Methanol Conversion (%)	35.6	36.8	35.2	48.3	49.5	49.2
Carbon Mass Balance (%)	83.9	82.1	82.3	90.6	82.4	84.6

* Not measured

led to this result. It was also possible that the observed mole fraction of the other species was low.

Table 9.2 shows two partial oxidation experiments under the same conditions (again with replicate measurements). By comparing the methanol mole fractions for the three runs as well as the resulting carbon balance one gets a clearer perspective on how even a small error in the data can lead to large errors in the mole fraction. While the scatter of the data in each run were consistent with the expected experimental error, comparison of the replicates for Experiment 2 illustrates how a small difference in the CO mole fraction can lead to large differences in the carbon balance. The same was true of other species. This result was due to the low concentrations in the reactor effluent, which led to low signals.

Although the difficulties described above precluded a comprehensive comparison of the data to the kinetic model predictions, selected comparisons were performed to connect these data to the NREL experiments. One pyrolysis experiment as well as one partial oxidation experiment was selected for comparison to the models. As with the NREL experiments, temperature profiles were obtained for use in the modeling of the CFCC data. These profiles were taken under N_2 flow at a residence time in the reactor of ~1 s (see Figure 9.13).

9.2.1 Modeling of Pyrolysis Data

The pyrolysis experiment was selected since it yielded nearly complete methanol conversion as well as an average carbon balance of 98.7%. The average hydrogen and oxygen balances were 97.6 and 96.9%, respectively. The nominal temperature for this experiment was 900ºC. The residence time in the 21 cm hot zone (within 15ºC of set point) was ~0.5 s, which was based on the original Princeton model calculation since that model did the best job of predicting the data of this experiments. This estimate is model dependent, since the flow velocity is dependent not only upon the temperature profile, but also on the calculated extent of conversion (which determines the change in mole fraction). The initial mole fraction of methanol was 0.250.

Table 9.2. Methanol experimental results using CFCC system illustrating the difficulty associated with reproducibility.

	Experiment 1			Experiment 2		
Injection	1	2	3	1	2	3
Initial Conditions						
Temperature (^{o}C)	650	650	650	650	650	650
O_2 Flow (sccm)	2.9	2.9	2.9	2.9	2.9	2.9
N_2 flow (sccm)	202.6	202.6	202.6	157.1	157.1	157.1
He flow (sccm)	0	0	0	45.5	45.5	45.5
CH_3OH flow (μl/s)	0.601	0.601	0.601	0.601	0.601	0.601
O:C ratio	1.27	1.27	1.27	1.27	1.27	1.27
λ	0.09	0.09	0.09	0.09	0.09	0.09
Est. R.T. (s)	0.5	0.5	0.5	0.5	0.5	0.5
Effluent mole fractions						
N_2	0.875	0.875	0.880	0.682	0.682	0.686
He	0	0	0	0.195	0.196	0.197
CH_3OH	0.060	0.056	0.057	0.060	0.063	0.062
H_2	0.023	0.022	0.022	0.024	0.023	0.022
CO	0.018	0.019	0.017	0.015	0.019	0.017
CH_4 (FID)	5.9E-05	5.8E-05	6.7E-05	6.2E-05	7.5E-05	8.0E-05
CO_2	0	0	0	0	0	0
CH_2O	0*	0*	0*	0*	0*	0*
Total	0.975	0.973	0.976	0.976	0.983	0.985
Methanol Conversion (%)	36.6	40.5	40.0	34.2	31.3	32.2
Carbon Mass Balance (%)	82.3	80.2	78.2	81.8	89.2	86.1

* Not measured

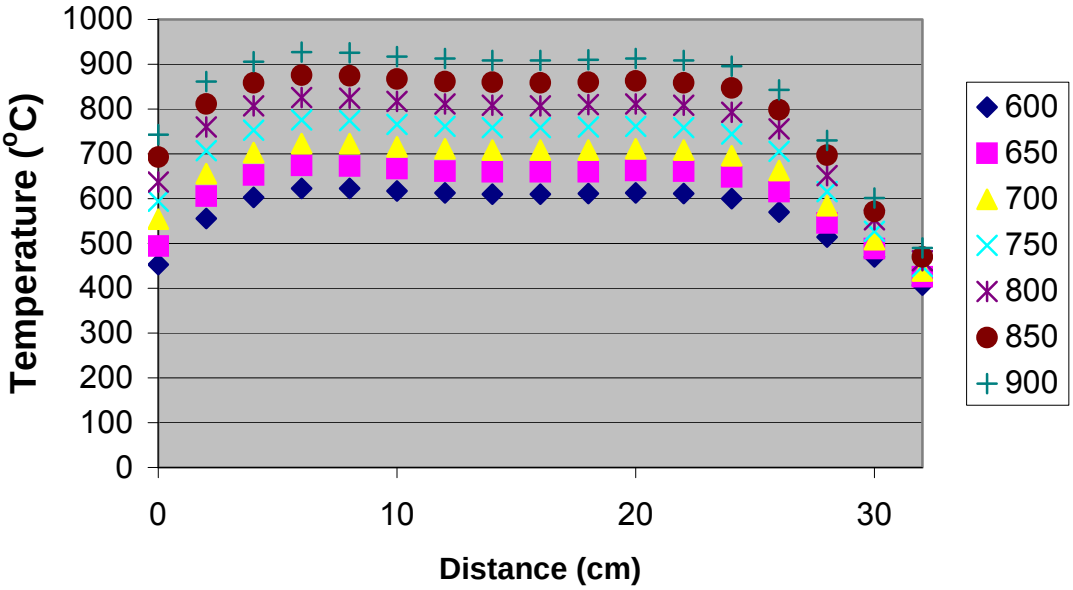

Figure 9.13. Temperature profiles for CFCC methanol experiments. These profiles were taken under N_2 flow such that the residence time was ~1 s.

Figure 9.14 shows the results of the pyrolysis experiment compared to the five kinetic models. In order to show the CH_4 and CO_2 mole fractions on the figure, they were multiplied by 10. While the NJIT model did a good job of predicting the results of this experiment, the original Princeton model was better. The other three models all underpredicted the methanol conversion and consequently the CO and H_2 yields. It was especially surprising that the updated Princeton model did not do a better job. The motivation behind the update was to improve the combustion (oxidative) chemistry[60]. It would appear that any such improvements may have been at the cost of the pyrolysis chemistry.

The results presented here were typical of what was observed when comparing the models to pyrolysis data. As was the case during the NREL modeling, the CSM models predicted a substantially higher yield of CH_2O than did the other models even though they predicted lower methanol conversion (see Figure 9.15). The Princeton model, which was shown to predict CH_2O more accurately, predicted a much lower CH_2O yield. The low CH_2O yield may have led to the good carbon mass closure in this case.

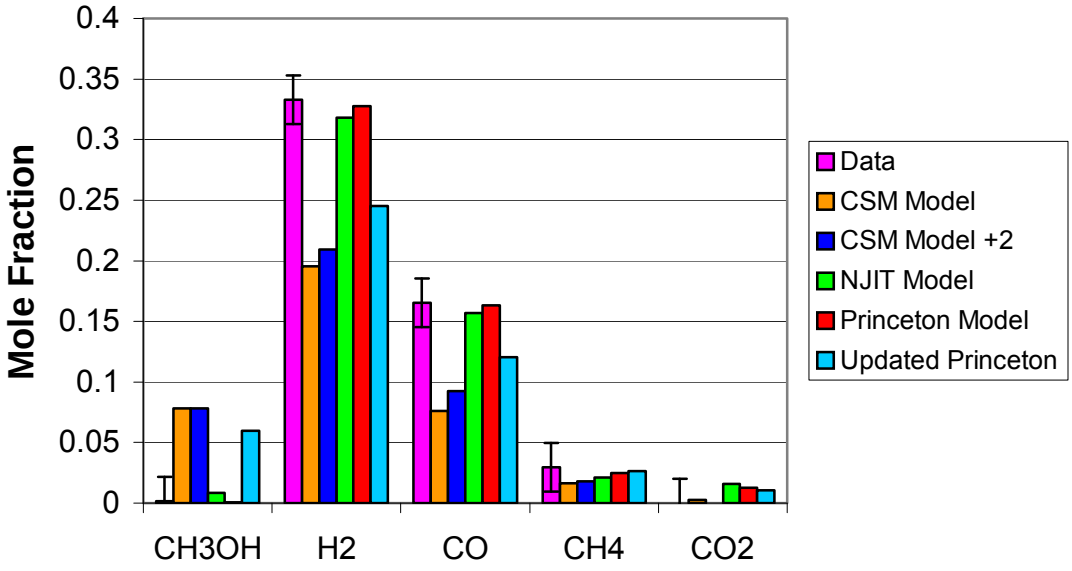

Figure 9.14. Mole fractions of CH_3OH, H_2, CO, CH_4 (x10) and CO_2 (x10) for pyrolysis experiments at the CFCC (900ºC; ~0.5 s) compared to kinetic models.

9.2.2 Modeling of Partial Oxidation Data

The partial oxidation experiment was selected since it was performed under conditions similar to those in the NREL experiments and had reasonable mass balances (C = 98.0%; H = 94.9%; O = 87.0%). Although the O balance was low, assuming that the missing H_2 was either H_2O or CH_2O led to an O mass balance of 97.2% and only required that the combined H_2O and CH_2O mole fraction be 0.01. The resulting sum of mole fractions (1.01) was still within the experimental error. If all of it were assumed to be CH_2O, the resulting carbon mass balance would be 109%, suggesting that much of the missing oxygen was due to water. This experiments was performed at 650ºC with a residence time of ~0.4 s and O:C of 1.13 (λ = 0.04). The initial methanol mole fraction was 0.096.

Figure 9.16 compares the modeling predictions to the experimental results for this partial oxidation experiment. It should be noted that the temperature profiles used for the model calculations were the same as those used for the pyrolysis experiments. Some change in the temperature profiles might have occurred, which might lead to the some underprediction of conversion with the models. In this case, the CSM models and the NJIT model did a better job of

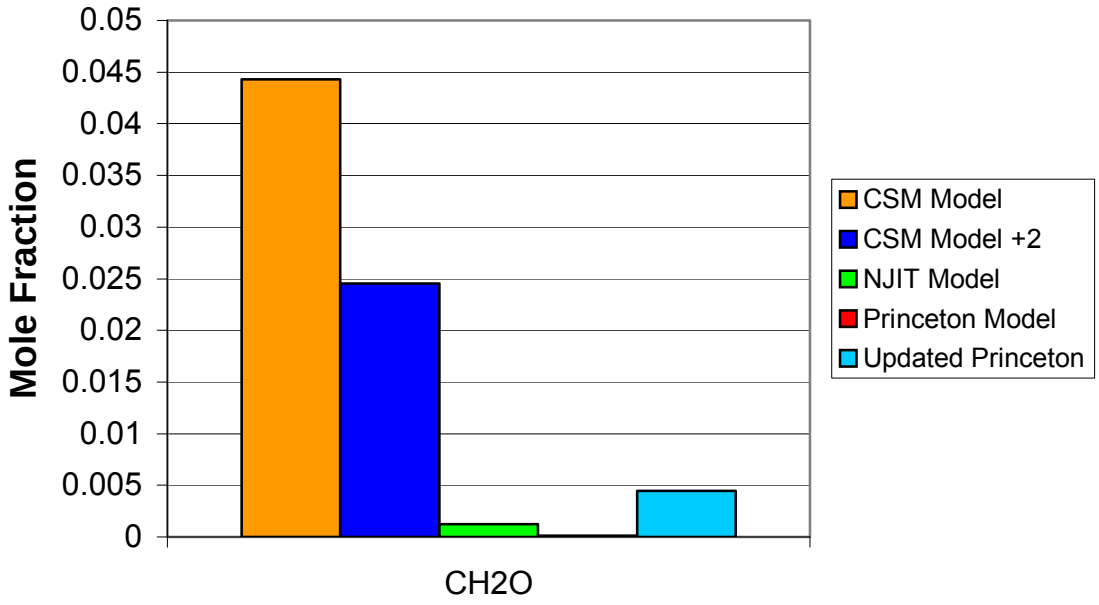

Figure 9.15. Model predictions of CH_2O yield for pyrolysis experiment at the CFCC (900ºC; ~0.5 s).

predicting the experimental CH_3OH conversion than did the Princeton models. The NJIT and CSM models underpredicted the H_2 and CO yield, while the Princeton models overpredicted them. The updated Princeton model did a slightly better job than did the original Princeton model. The Princeton models slightly overpredicted the CH_4 yield, but did a much better job than the other three models. It should be noted that in Figure 9.16, the CH_4 mole fractions are multiplied by 100. The CSM models predicted more CH_2O than did the other models (see Figure 9.17). Again, the Princeton models predicted a low CH_2O yield, which could be why the carbon closure was acceptable in this case. These results were consistent with the results of partial oxidative experiments and modeling performed at NREL under similar conditions.

9.2.3 Summary

Although both the mass balances and reproducibility issues generated substantial uncertainty regarding the CFCC methanol experiments, one pyrolysis and one partial oxidation model was compared to the kinetic models. Due to the

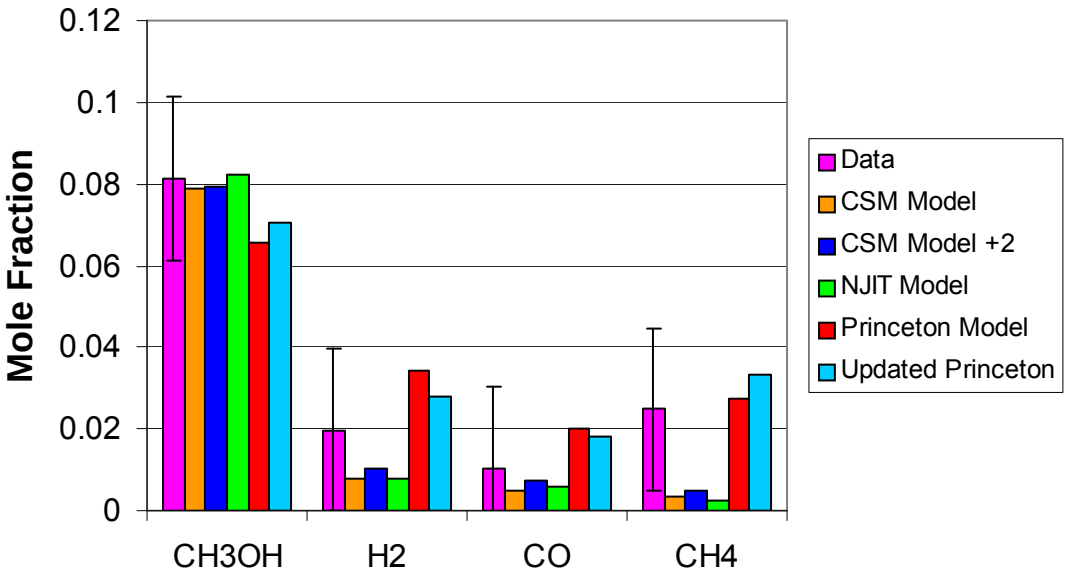

Figure 9.16. Mole fractions of CH_3OH, H_2, CO, and CH_4 (x100) for partial oxidation experiment at the CFCC (650ºC; ~0.4 s; λ = 0.04) compared to kinetic models.

uncertainty in the data, no definitive conclusions about the models could be drawn. However, the CSM models and the updated Princeton model seemed to be too slow under pyrolysis conditions. A second area of improvement for the CSM model, which was originally identified during NREL methanol experiments, was the chemistry related to formaldehyde production and destruction.

9.3 Large NREL Reactor Methanol Experiments

Methanol experiments were performed on the large reactor at NREL. The upper heater was varied from 700 to 800ºC, while the lower heater was varied from 590 to 760ºC. The resulting gas temperature was between 560 and 760ºC. The inconsistent gas temperature reflects the imperfect mixing as well as the heat transfer difficulties of this system. The estimated residence time (Est. R.T.) was varied from 0.9 to 1.4 while the equivalence ratio (λ) was varied between 0.16 and 0.33 (O:C = 1.5 to 2.0).

Table 9.3 shows the results of large reactor experiments. Of the runs shown, Run 2 is most like the earlier experiments performed at NREL. The

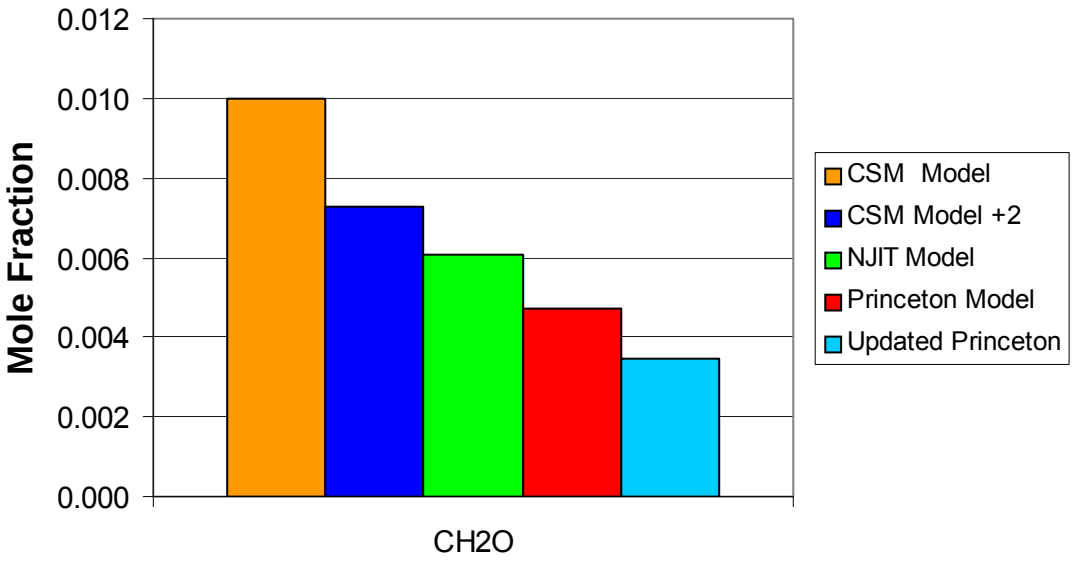

Figure 9.17. Model predictions of CH_2O yield for pyrolysis experiment at the CFCC (650ºC; ~0.4 s; λ = 0.04).

largest difference is the residence time, which should not matter since it has been observed that virtually no reaction occurs at 650ºC without oxygen present. Although methanol conversion was not measured directly due to it being condensed prior to the analytical equipment, the C.G. should be equivalent to methanol conversion since methanol was the only source of carbon during these experiments. The results of Run 2 were consistent with the earlier data. The C.G. was 37.4% while the methanol conversion under similar conditions using the smaller reactor system was ~40%. The CO and H_2 yield for the larger reactor were 31.7 and 21.6%, respectively. The smaller reactor gave a CO yield of ~32% and an H_2 yield of ~15-19%. The CO_2 yield was slightly higher for the larger reactor than the smaller reactor (5.5 vs. 3.2%). Using either system the CH_4 and C_2H_4 yields were negligible.

Further analysis of Table 9.3 showed that methanol conversion (C.G.) generally increased with increasing temperature as well as increasing λ, which led to increases in CO and H_2 yield. As has been seen previously, the CO_2 increase with increasing λ was not as dramatic as the CO increase. The methane yield was minimal under all conditions, but was highest at the highest λ. The

Table 9.3. Methanol experiments performed using large NREL reactor.

Run	Temperature (°C)			Est. R.T. (s)	λ	C.G. (%)	Yields (%)				
	Upper heater	Lower heater	Gas				CO	H_2	CO_2	CH_4	C_2H_4
1	700	650	590	1.0	0.19	14	11.8	7.6	2.2	0.0	0.0
2	700	650	630	1.4	0.20	37.4	31.7	21.6	5.5	0.0	0.1
3	750	700	550	1.4	0.26	54.8	42.2	30.5	10.1	2.4	0.1
4	750	700	580	1.3	0.18	39.0	30.5	24.9	7.2	1.5	0.2
5	750	700	620	1.3	0.18	45.4	33.6	28.3	7.7	0.8	0.1
6	750	700	680	1.2	0.33	66.3	50.3	33.5	13.7	2.1	0.1
7	750	700	685	1.2	0.16	41.0	33.9	27.8	6.3	0.6	0.1
8	800	750	640	1.3	0.17	56.5	47.1	41.2	7.7	1.4	0.4
9	800	750	730	0.9	0.20	48.2	39.5	31.6	8.5	0.0	0.2
10	800	750	760	1.3	0.20	57.6	47.9	38.1	8.8	0.7	0.3

Note: The carbon to gas percent (C.G.) and the yields are on a weight basis and defined as in Chapter 3 except that the C.G. includes ethylene as well as ethane and ethyne. Because methanol was the only source of carbon, the C.G. is also a measure of the carbon conversion.

ethylene yield was even less than the methane yield.

9.4 Summary

The reasonably good agreement between the model predictions and the NREL data using the smaller reactor suggested that the data were consistent with exclusively gas phase chemistry. In addition, this agreement suggests that the use of the model to obtain the temperature dependence of the CO and CO_2 yields in the procedure to extract the bio-mass contributions is appropriate. Unfortunately, the CFCC data set proved inadequate for systematic comparisons of model predictions. Nevertheless, selected comparisons suggested not only wide variations between the model predictions but some substantial discrepancies in methanol conversion. These discrepancies were particularly large for conditions with little or no added oxygen. It is possible that some of these apparent mechanistic deficiencies might be related to the inability to

measure CH_2O in the CFCC experiments. However, the low selectivity to formaldehyde predicted by most of the models suggest that this might not be a major factor. The calculations reinforced the conclusion (originally drawn from the NREL comparisons) that the formaldehyde component of the CSM mechanism needs improvement.

CHAPTER 10
MODEL COMPOUNDS

In an attempt to understand the reasons for the surprisingly high yields of CO from bio-oil, a series of experiments were performed using model compounds that contained the functionalities found in bio-oil. The choice of these compounds was driven primarily by the earlier identification of a suitable surrogate mixture for bio-oil (Chapter 8). The primary objective of performing experiments on other model compounds was to determine the source of the trend of dramatic increases in CO yield with increasing added O_2 without observing a large increase in CO_2.

In this chapter, experiments performed using both pure components as well as mixtures of model compounds will be discussed. These experiments were only semi-quantitative in that the flows of CO and CO_2 were determined, but no effort was made to attain carbon closure. Especially in the case of the larger lignin derived molecules where a significant product distribution was possible, calibrating for carbon closure would have been both difficult and time consuming without much value added.

Rather than presenting the data as yields as a function of O:C ratio (or λ), the data in this chapter will be presented as flow rates of CO and CO_2 as a function of the O_2 flow. The reason for doing this is so that the pure compound experiments can be more easily compared to the mixture experiments where the flow rate of one of the compounds was held constant and the same flows of O_2 were added regardless of how much of the second compound was added. The addition of this second compound, which replaced some of the helium, led to a dramatic increase in the carbon content. Hence trying to relate the O:C ratio from the mixture to the pure compounds would have been somewhat confusing. The increase in carbon content without significant increases in O_2 also led to overall yields during the mixture experiments which were much lower than during pure component experiments even when the CO and CO_2 flow was increased. The O_2

was not increased for safety reasons as well as so that any observed increases in product yields would be due to the synergies in the mixture.

10.1 Pure Components

In addition to the compounds that comprised the surrogate developed for Aspen modeling (see Table 10.1), other species found in bio-oil as well as species with the same functional group as those found in components of bio-oil were selected. This was possible since model compounds were no longer restricted to those found in Aspen. The additional compounds included formaldehyde, acetaldehyde, glyoxal, methanol, guaiacol, eugenol, and dimethoxybenzene. Although dimothoxybenzene is not a component of bio-oil, many components of benzene have the methoxy group including syringol, which has two. Syringol was not available for these experiments.

Table 10.1 Composition of surrogate developed in Chapter 8.

Species	Surrogate Composition (%)
acetic acid	11
glyoxal	14
hydroxyacetaldehyde	10
acetone	11
phenol	23
anisole	5
furfural	8
ethanol	1
water	17

All model compound experiments were performed at 650ºC under flow conditions similar to the bio-oil experiments. The oxygen level was varied from 0 to as high as high as 91.6 sccm. For reference purposes, all figures will also show a trendline of the estimated bio-oil (Method 2) product flow rates of CO and CO_2 from the 50:50 bio-oil methanol experiments (Chapter 4).

Figure 10.1 shows the results of these experiments for both acetic acid and acetaldehyde. The CO flow in the case of acetaldehyde (up to 8.5wt.% in bio-oil) paralleled the significant increase with increasing O_2 added observed during the bio-oil experiments. Because acetaldehyde has the same molecular weight as CO_2, the flow rates of CO_2 from acetaldehyde could not be determined. The CO_2 yield from acetic acid increased from 8.8 to 51 sccm as the oxygen was increased. The carbon atoms not involved in the acidic group led to CO yields

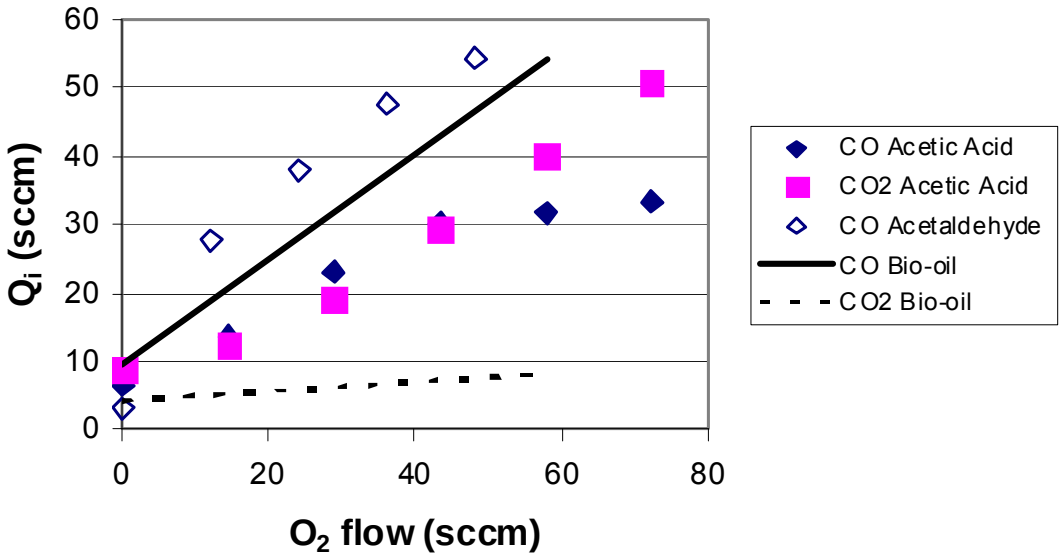

Figure 10.1. Outlet flow of CO and CO_2 during acetic acid and acetaldehyde experiments at 650ºC. The solid line is the estimated CO (Method 2) produced from the 50:50 bio-oil:methanol experiments while the dotted line is the CO_2 produced from those experiments.

from 6.5 to 31.9. Clearly the ratio of CO to CO_2 was not the same as that observed during the bio-oil experiments, but it was significant that acetic acid could be a source of CO since its typical concentration in bio-oil can be up to 12 wt.%.

The acetaldehyde belongs to a class of species that were expected to have the best possibility for producing CO. These species are compounds that have functional groups with a carbon atom bonded to a single oxygen atom such as ketones, alcohols, aldehydes, etc. Compounds expected to have higher CO_2 yields are those where a carbon atom is already bonded to two oxygen atoms such as acids and esters. While it is possible for acids and esters to lead to CO production provided they have more carbon atoms than the one in the acidic group, the yield of CO is expected to be lower just as is seen in the case of acetic acid. Likewise, in the case of compounds with groups that have higher potential for CO yields as described above, it is possible to get CO_2 through oxidation of CO. However, the results of bio-oil experiments suggested that the CO_2 formed was coming primarily from bio-oil rather than oxidation of CO. The added O_2

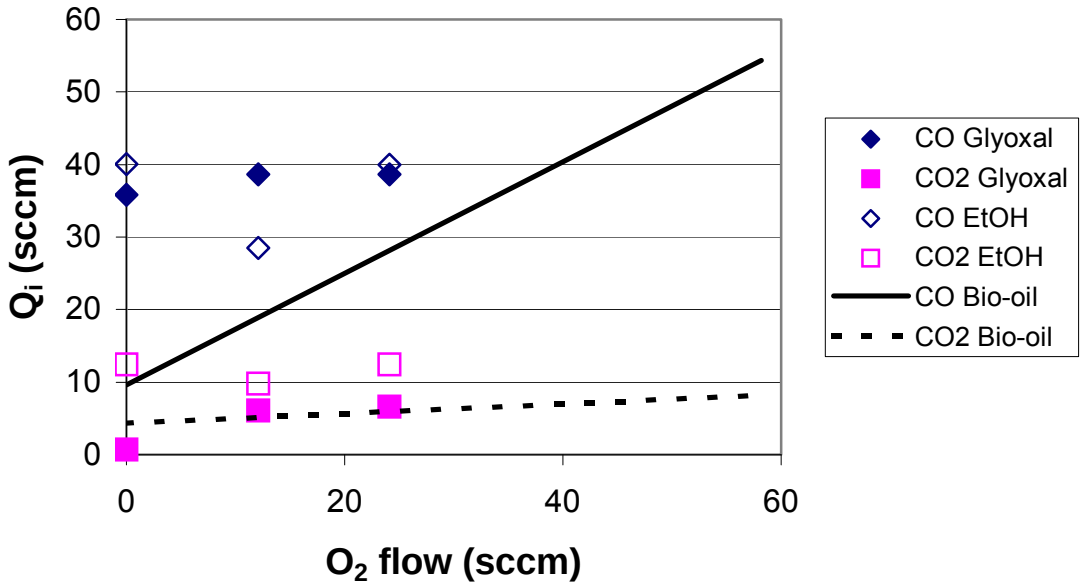

Figure 10.2. Outlet flow of CO and CO_2 from glyoxal and ethanol experiments at 650ºC. The solid line is the estimated CO (Method 2) produced from the 50:50 bio-oil:methanol experiments while the dotted line is the CO_2 produced from those experiments.

appeared to be liberating the CO rather than oxidizing it to a great extent since the CO_2 yields were relatively low and only increased slightly when O_2 was added.

The results of experiments performed with ethanol and glyoxal (40wt.% in H_2O) are shown in Figure 10.2. Although neither of these compounds demonstrated increased CO with increased O_2 under the conditions of these experiments, the CO to CO_2 ratio was favorable and did not change much with increased O_2 flow. This was particularly noteworthy in the case of glyoxal since its concentration in bio-oil can be as high as 4.6 wt.%. Ethanol can be a component of bio-oil, but typically not more than 1.4 wt.%.

Hydroxyacetaldeyde (up to 13% in bio-oil) and formaldehyde (up to 3.3% in bio-oil) both showed initial increases in the flow of the product CO with increasing O_2, but the CO flow started to decrease as the O_2 flow was further increased. These results are shown in Figure 10.3. Not surprisingly, as the CO flow decreased, the CO_2 flow increased. The hydroxyacetaldyde (HAA) was

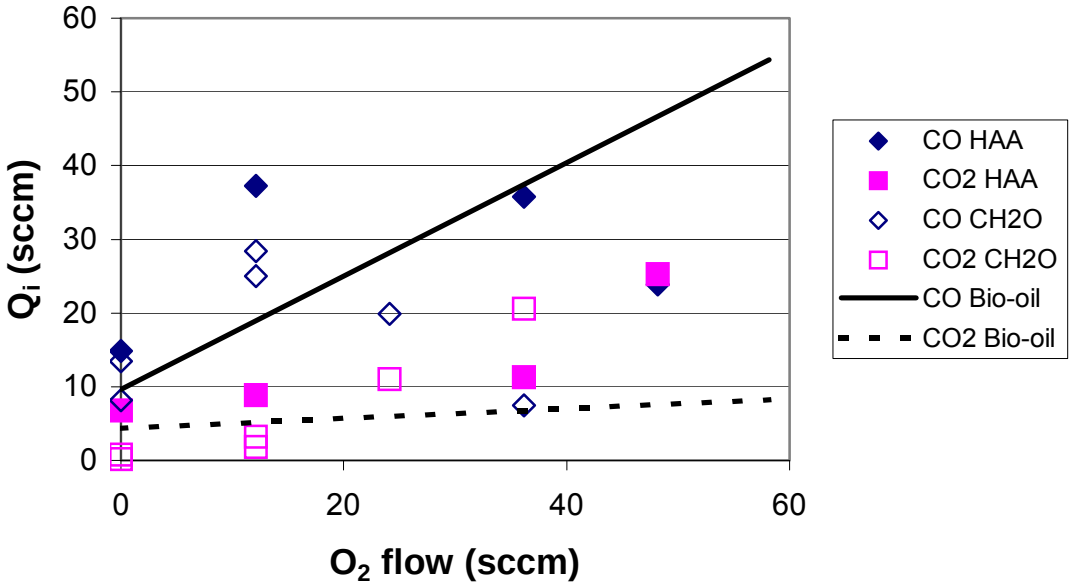

Figure 10.3. Outlet flow of CO and CO_2 from hydroxyacetaldehyde (HAA) and formaldehyde (CH_2O) experiments at 650ºC. The solid line is the estimated CO (Method 2) produced from the 50:50 bio-oil:methanol experiments while the dotted line is the CO_2 produced from those experiments.

introduced in a 10wt.% aqueous solution whereas the aqueous solution was 37wt.% in the case of formaldehyde

Figure 10.4 shows the CO and CO_2 flow from experiments performed using methanol (up to 2.4% in bio-oil) and acetone (up to 2.8% in bio-oil). Methanol showed a high propensity for CO formation without significant CO_2 formation until the O_2 flow rate was above 30 sccm. Acetone had an initial increase in CO followed by a decrease as the O_2 was increased. So far, the compounds used have been derived from the aqueous fraction of bio-oil (i.e., all compounds are water soluble). Components in this fraction are typically derived from cellulose and hemicellulose. The rest of the compounds are found primarily in the pyrolytic lignin fraction (i.e., water insoluble fraction; derived primarily from lignin).

The results from the first pair (anisole and phenol as a 5wt.% aqueous mixture) are shown in Figure 10.5. As noted in Chapter 8, anisole is not present

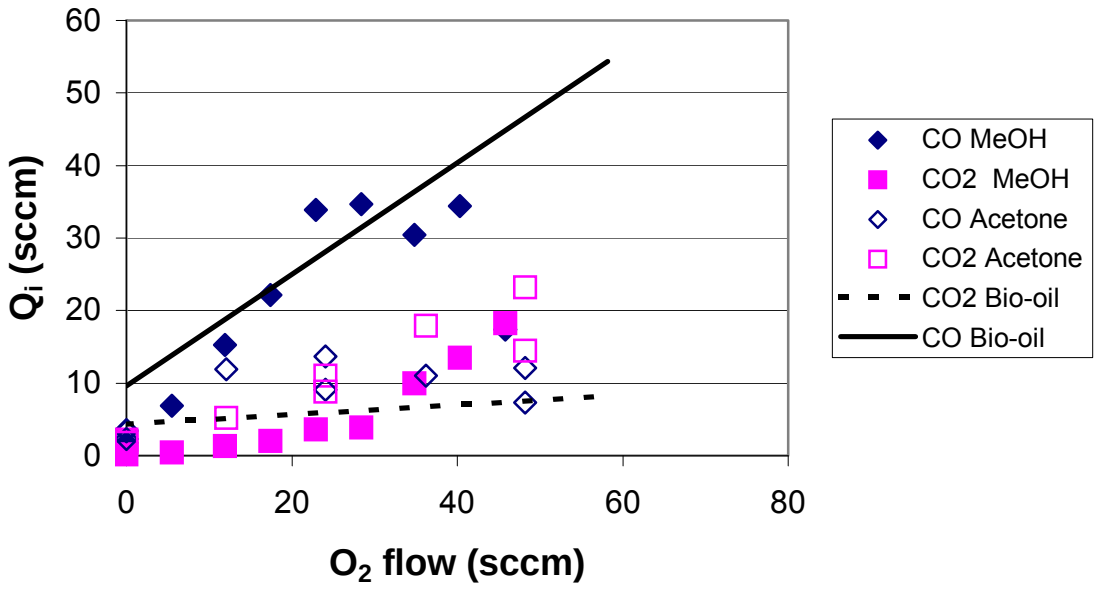

Figure 10.4. Outlet flow of CO and CO_2 from methanol (MeOH) and acetone experiments at 650ºC. The solid line is the estimated CO (Method 2) produced from the 50:50 bio-oil:methanol experiments while the dotted line is the CO_2 produced from those experiments.

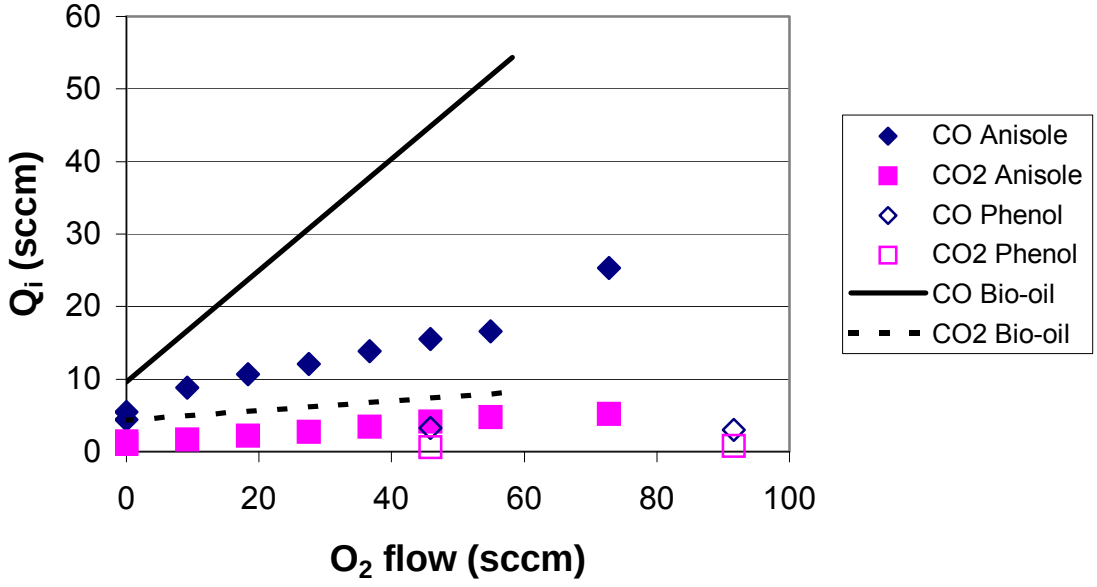

Figure 10.5. Outlet flow of CO and CO_2 from anisole and phenol experiments at 650ºC. The solid line is the estimated CO (Method 2) produced from the 50:50 bio-oil:methanol experiments while the dotted line is the CO_2 produced from those experiments.

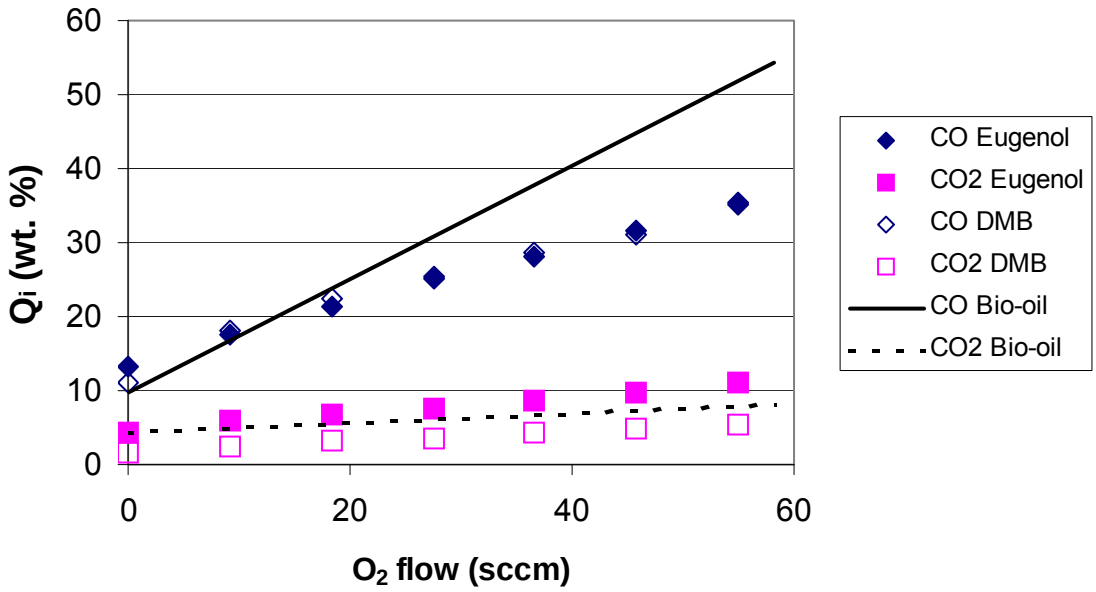

Figure 10.6. Outlet flow of CO and CO_2 from eugenol and dimethoxybenzene (DMB) experiments at 650ºC. The solid line is the estimated CO (Method 2) produced from the 50:50 bio-oil:methanol experiments while the dotted line is the CO_2 produced from those experiments.

in bio-oil, but the methoxy functional group attached to a benzene ring is common to many of the components of bio-oil. Anisole showed a steady CO to CO_2 ratio with increasing O_2 flow, but not the dramatic increase in CO observed during bio-oil experiments. Phenol (up to 3.8% in bio-oil) was unreactive under these conditions. The hydroxy group is also commonly found on benzene rings in bio-oil.

Eugenol (up to 2.3%) contains both a hydroxy and methoxy group. The results of its experiments as well as those for dimethoxybenzene are shown in Figure 10.6. Both these compounds showed a favorable and nearly identical CO to CO_2 ratio, which increased with increasing O_2. However, the ratio did not increase as dramatically as it did for bio-oil.

Guaiacol (up to 1.1%) is another compound that contains both the hydroxy group and the methoxy group. Its experimental results as well as those for furfural (up to 1.1%) are shown in Figure 10.7. Both these compounds showed the dramatic increase in CO yield with minimal increase in CO_2 yield that was

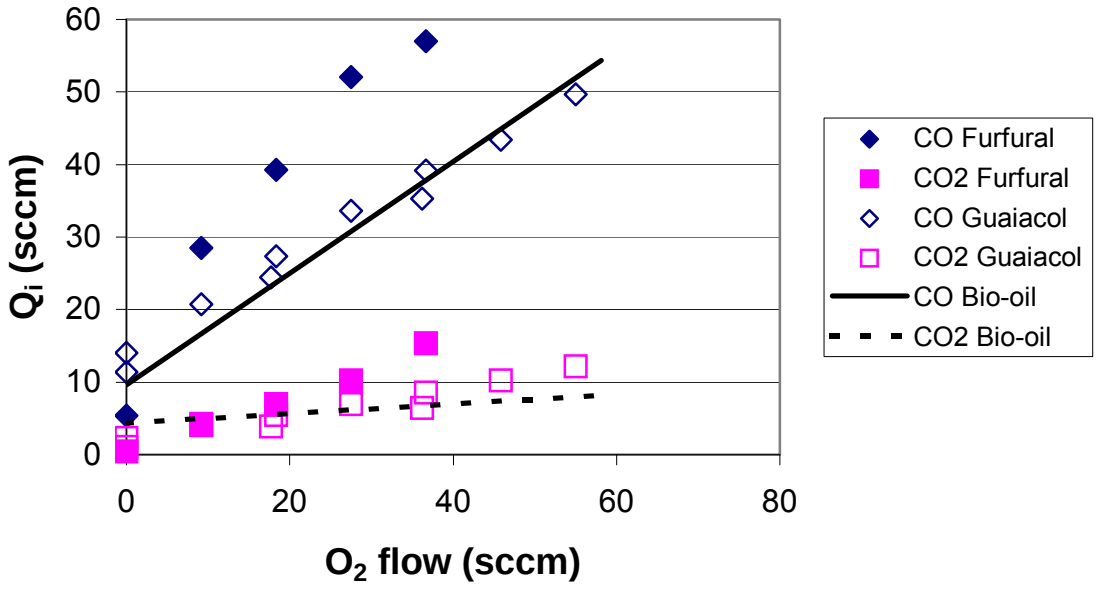

Figure 10.7. Outlet flow of CO and CO_2 from furfural and guaiacol experiments at 650ºC. The solid line is the estimated CO (Method 2) produced from the 50:50 bio-oil:methanol experiments while the dotted line is the CO_2 produced from those experiments.

observed during the bio-oil experiments. The increase was most dramatic with furfural.

10.2 Model Compound Mixtures

In order to explore potential synergies between cellulose/hemicellulose derived components and lignin derived components, experiments were performed using one component from each mixture. Methanol and HAA (10% aqueous mixture) were selected from the cellulose/hemicellulose compounds, while phenol, anisole, eugenol, guaiacol, and furfural (lignin fraction) were all used. It should be noted that while furfural is actually derived from cellulose/hemicellulose, it typically ends up with the lignin fraction when bio-oil is fractionated. Experiments were performed with all the possible combinations that had one compound from each fraction at 650ºC and flow rates identical to those used in the pure component experiments in the case of the lignin fractions. The

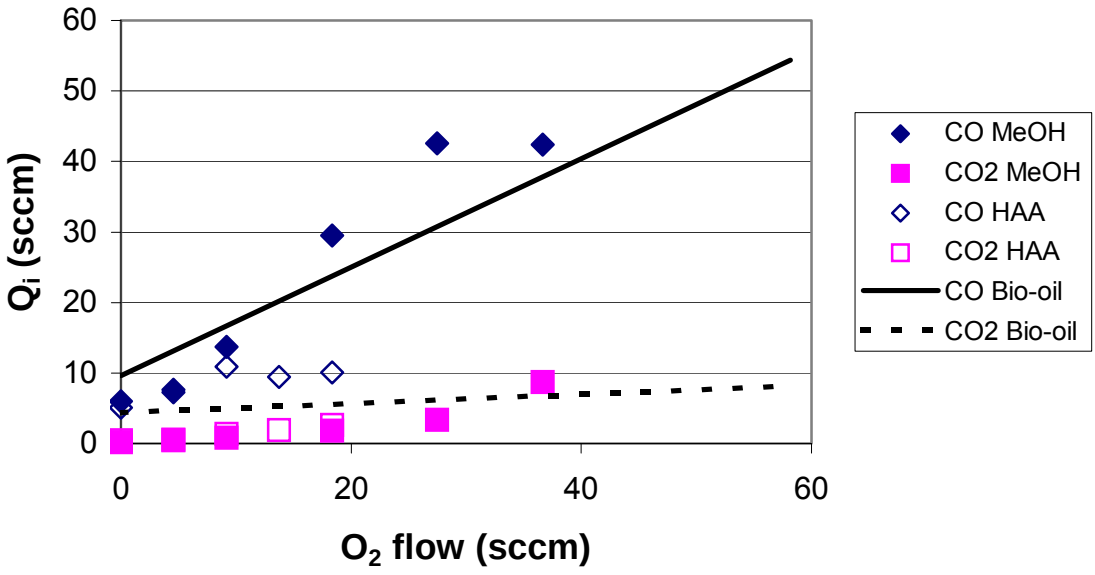

Figure 10.8. Outlet flow of CO and CO_2 from experiments using mixtures of phenol with either methanol or HAA at 650ºC. The solid line is the estimated CO (Method 2) produced from the 50:50 bio-oil:methanol experiments while the dotted line is the CO_2 produced from those experiments.

methanol and HAA replaced some of the helium such that the overall flow rate remained unchanged from the pure components experiments.

Figure 10.8 shows the results of experiments where phenol (5wt.% aqueous solution) was mixed with either methanol or the HAA solution. Both mixtures showed an increase in the CO yield without significant increase in the CO_2 yield. In the case of the methanol mixture, the increase in CO was much more dramatic. However, this increase can by explained at least in part by higher methanol flows than HAA flows, which was introduced as an aqueous mixture. Upon first glance one might assume that the products were from either the methanol or the HAA since the phenol was unreactive during pure component experiments. However, looking at the phenol signal as a percentage of the total signal reveals a dramatic decrease in the phenol concentration (see Figure 10.9). The radicals introduced into the system by either HAA or methanol were able to generate apparently equal reaction in the case of the phenol, which was especially remarkable in the case of HAA considering less of it was introduced.

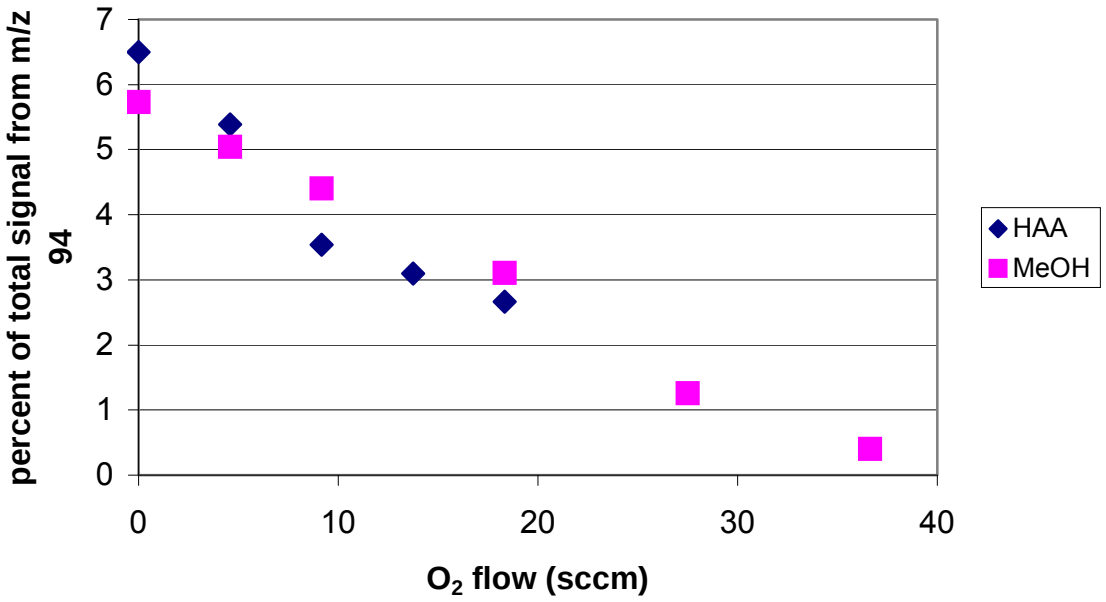

Figure 10.9. Conversion of phenol during experiments where it was mixed with HAA or methanol at 650ºC.

This finding illustrates the importance of performing the mixture experiments.

The experimental results of a mixture of anisole with either methanol or HAA are shown in Figure 10.10. While the methanol mixture appeared to have a more significant increase in the CO product flow, the result was a bit misleading since the amount of HAA that could be introduced was limited by the requirement that it be introduced in an aqueous solution. In spite of this limitation, the HAA mixture had a favorable increase in CO flow as O_2 flow increased without a significant increase in the CO_2 flow. It was notable that any interactions between the two components in either mixture did not lead to a reduction of the CO to CO_2 ratio observed in pure component experiments.

Mixing guaiacol with either HAA or methanol led to flow rates of CO that were higher than during pure guaiacol experiments (see Figure 10.11). While this might seem like an obvious result given the increased carbon in the system, the oxygen in the system was not increased. Although the O:C ratio was not significantly different from pure guaiacol experiments during the HAA mixture experiments due to the relatively small amount of HAA added, the ratio was

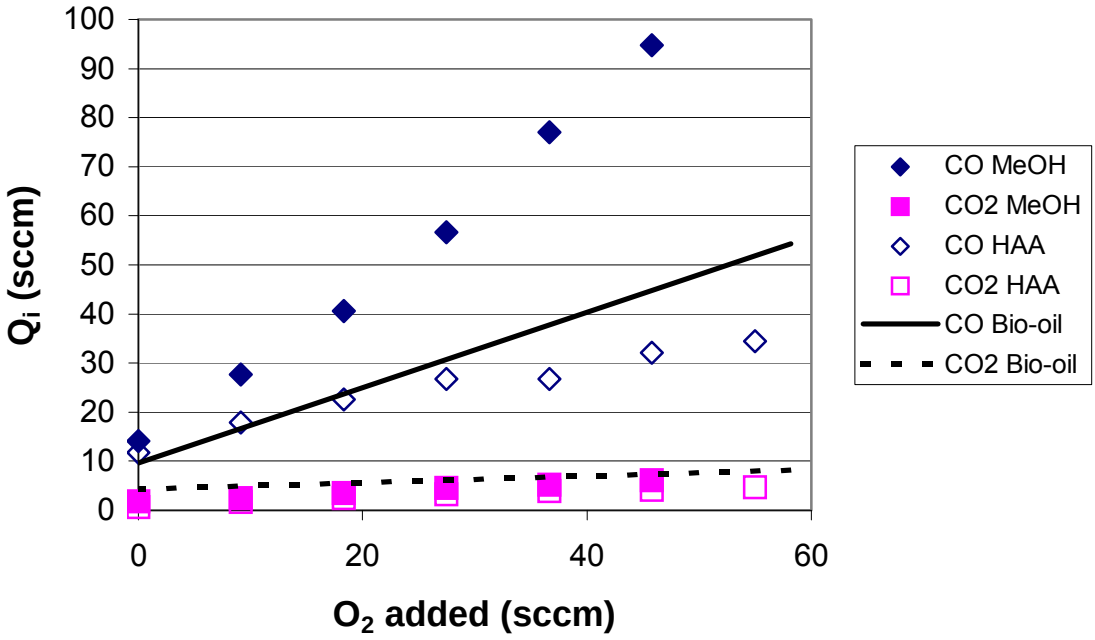

Figure 10.10. Outlet flow of CO and CO_2 from experiments using mixtures of anisole with either methanol or HAA at 650ºC. The solid line is the estimated CO (Method 2) produced from the 50:50 bio-oil:methanol experiments while the dotted line is the CO_2 produced from those experiments.

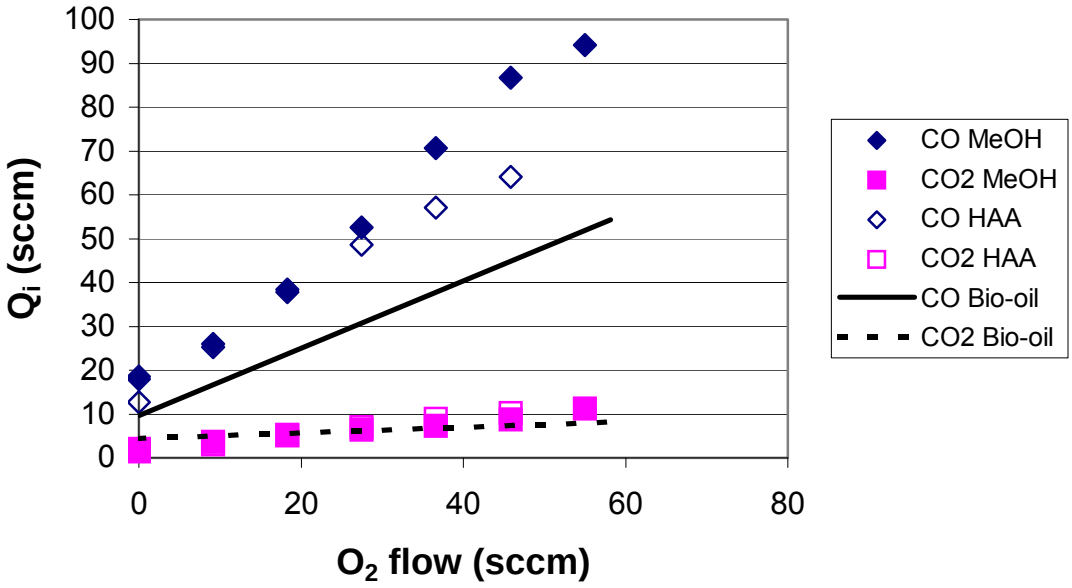

Figure 10.11. Outlet flow of CO and CO_2 from experiments using mixtures of guaiacol with either methanol or HAA at 650ºC. The solid line is the estimated CO (Method 2) produced from the 50:50 bio-oil:methanol experiments while the dotted line is the CO_2 produced from those experiments.

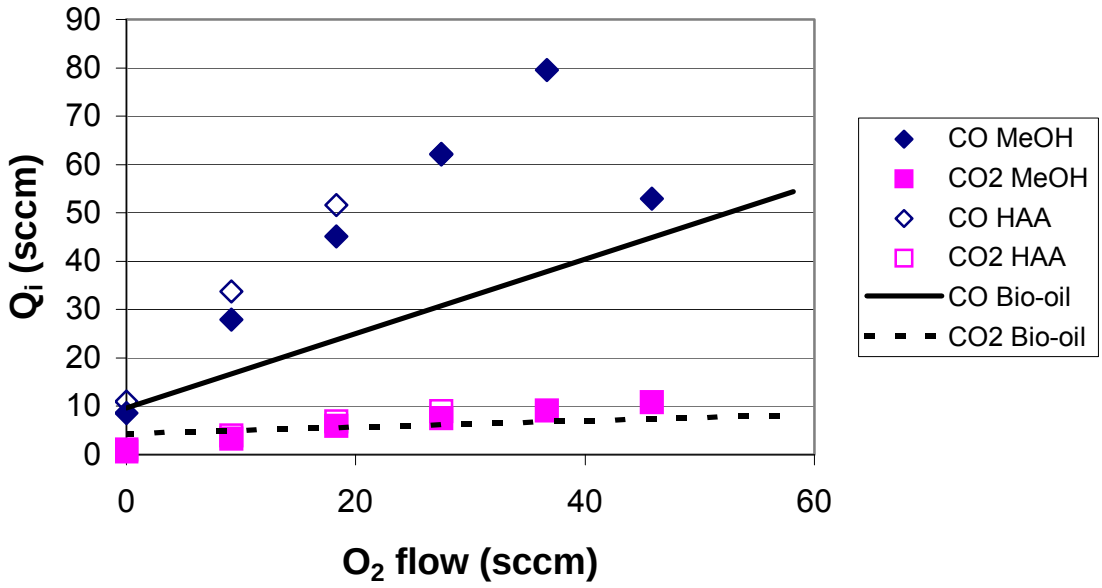

Figure 10.12. Outlet flow of CO and CO_2 from experiments using mixtures of furfural with either methanol or HAA at 650ºC. The solid line is the estimated CO (Method 2) produced from the 50:50 bio-oil:methanol experiments while the dotted line is the CO_2 produced from those experiments.

significantly lower during methanol mixture experiment due to a much higher carbon flow. The difference actually increased when O_2 was added since the O:C ratio in the pure component mixture experiments increased more rapidly than did the ratio during methanol mixture experiments. It was also notable that the two mixtures resulted in nearly identical CO flows at low O_2 flows, but the mixture with HAA tailed off at higher O_2 flows.

The results of mixture experiments using furfural with either methanol or HAA gave results similar to pure furfural experiments (see Figure 10.12). However, as with the guaiacol experiments the CO flow rate was higher during the mixture experiments than during the pure furfural experiments. The same arguments about the O:C ratio apply to this mixture. It is not clear what may have caused the decrease in the CO flow at an O_2 flow of 45 sccm. If it had been due to combusion or oxidation of CO, one would have expected a corresponding increase in the CO_2 flow.

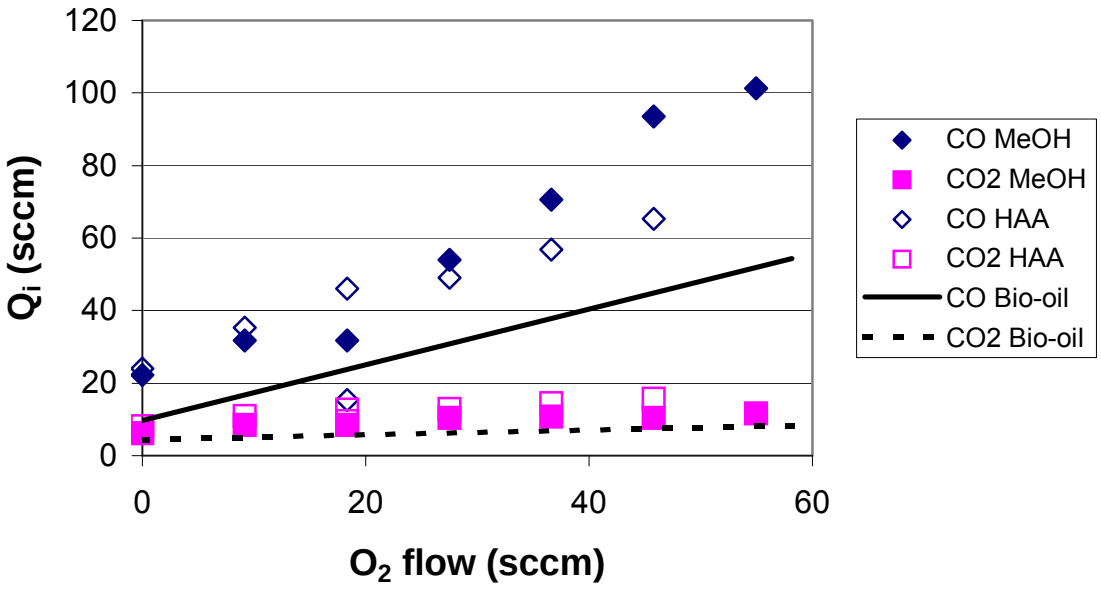

Figure 10.13. Outlet flow of CO and CO_2 from experiments using mixtures of eugenol with either methanol or HAA at 650ºC. The solid line is the estimated CO (Method 2) produced from the 50:50 bio-oil:methanol experiments while the dotted line is the CO_2 produced from those experiments.

Figure 10.13 shows the results of mixtures of eugenol with either HAA or methanol. The same observations as were seen in the case of furfural and guaiacol mixtures were true for the eugenol mixtures.

10.3 Summary

Many of the model compounds that are present in bio-oil give rise to trends similar to those observed during bio-oil:methanol mixture experiments. Namely, there was a significant increase in CO yield with increasing O_2 added to the system without observing much increase in the CO_2 yield. The lignin components showed an especially high tendency toward a CO to CO_2 ratio similar to that observed during bio-oil:methanol experiments. This observation seemed to be enhanced by the presence of methanol or HAA during mixture experiments. While the overall O_2 available was lower compared to the amount of O_2 in the system, the observed flows of CO were actually higher. In the case of phenol, the presence of methanol or HAA made reaction possible, which had not

been observed during pure phenol experiments in the presence of O_2. This observation illustrates the importance of model compound experiments.

CHAPTER 11
CONCLUSIONS AND FUTURE WORK

The focus of the present research was to demonstrate that synthesis gas could be produced from bio-oil without the use of a catalyst. The concept behind this was that biomass could be pyrolyzed near the source to produce bio-oil and bio-oil then transported to service stations where it would be converted to H_2. This chapter will discuss the conclusions as well as the recommendations for future work.

11.1 Conclusions

It was remarkable that such high yields of CO could be achieved through non-catalytic partial oxidative chemistry (NPOX) chemistry. Up to 80% yields from bio-oil have been observed on a bench scale system. This yield occurred without significant yields of CO_2. This was accomplished by first mixing the bio-oil with methanol to reduce its viscosity. This mixture was then volatilized using an ultrasonic nozzle and mixed with controlled amounts of oxygen at high temperatures (625-850ºC) for short residence times (~0.3 s). The oxygen concentration was varied to give equivalence ratio (λ) of up to 0.42 with the optimum range for synthesis gas production being between 0.31 and 0.35. Under these conditions, the H_2 yields were as high as 30% while the CO_2 yields were only ~10%. Most experiments were performed with a 50:50 bio-oil methanol mixture. Comparison of these results with those from a 70:30 mixture did not lead to any significant differences in CO and CO_2 yields, suggesting that the impact of methanol on these species was minimal. However, a decrease in the overall H_2 yield was observed suggesting that much of the H_2 yield was due to the methanol.

Catalytic experiments showed that the non-catalytic step had the potential to decrease the required catalyst loading, which would be especially important if a less expensive alternative to the rhodium based catalyst identified in the

present work cannot be found. The rhodium based catalyst was shown to give significant H_2 yields (~80%) that were consistent with equilibrium.

To further characterize this system, experiments were performed using several different reactor configurations with the bio-oil:methanol mixture. Similar results were obtained. Experiments using model compounds containing the oxygen functionalities found in bio-oil confirmed that the high CO yields observed with bio-oil could be understood in terms of the structure of the bio-oil components. Detailed kinetic modeling of methanol pyrolysis and partial oxidation experiments confirmed that the observed conversion and product distribution were consistent with a free radical gas-phase reaction mechanism.

Aspen modeling was used to evaluate the process as a whole. The thermal efficiency estimated from this model was 57%. An H2A analysis based on this process showed that H_2 could be produced for \$4.23/kg H_2. Although this was higher than the cost associated with centralized fossil fuels and biomass gasification, the distributed H_2 generation approach presented here is sufficiently promising to warrant continued investigation.

11.2 Future Work

Although the results of the present work show that the process has great promise, additional research is required. The following are recommendations for this work:

1. Explore the effect of residence time to further assess the importance of the NPOX step.
2. Perform further experiments using the larger reactor at NREL. It is especially important to ensure efficient mixing and improve heat transfer. Additional experiments with the 90:10 mixture under varied conditions are advisable to see whether similar results to those obtained in the present work can be attained with lower methanol dilution. Catalytic experiments could provide further insight as to the importance of the NPOX step.
3. Install a heater in the center of the reactor could help provide more uniform temperature.

4. Identify a suitable, more economic catalyst to replace rhodium since its use could prove too costly.

5. Determine the droplet size distributions of the two nozzles used in the present research under flow conditions using the various bio-oil mixtures. This determination could help with the understanding of how the atomization affects the bio-oil conversion.

6. Explore other means of feeding the bio-oil into the system, such as a diesel injector, since the ultrasonic nozzle technology may prove too costly for a commercial process. Additionally, the ultrasonic nozzles are only available for small scale applications.

7. Continue to pursue a suitable data set for methanol model validation using the CFCC system. In particular, the capability to measure formaldehyde would help towards this.

8. Explore further the observed deficiencies in the CSM kinetic model. Namely, the chemistry with respect to formaldehyde production/destruction seemed to need improvement as did the pyrolysis chemistry.

9. Explore additional model compounds as well as look at those presented in this work at different temperatures to gain further insight into the chemistry involved. This could assist in optimizing the process.

10. Perform experiments using a bio-oil:methanol mixture with the carbon in methanol having isotopic labels could help quantify the origin of the CO and CO_2 during those experiments.

REFERENCES CITED

1. Perlack R, Wright L, Turhollow A, Graham R, Stokes B, Erbach D. Biomass as Feedstock for a Bioenergy and BioproductsIndustry: the Technical Feasibility of a Billion-Ton Annual Supply: A joint U.S. Department of Energy and U.S. Department of Agriculture report DOE-GO-102995-2135 and ORNL/TM 2005-66, April 2005, http://www1.eereenergy/gov/biomass/pdfs/final_billionton_vision_report2.pdf.

2. US Department of Energy. Hydrogen, Fuel Cells and Infrastructure Technologies Program: Multi-Year Research, Development and Demonstration Plan. Washington, DC: 2006.

3. Czernik S, Elam C, Evans R, Milne T. Thermal and Chemical Biomass Conversion. In: Bridgwater AV, D.G.B. B (eds): CPL Press: Newbury, UK, 2006.

4. Czernik S, Evans R, French R. Hydrogen from biomass-production by steam reforming of biomass pyrolysis oil. Catalysis Today. 2007;129:265-8.

5. Bridgewater AV, Peacocke GVC. Fast pyrolysis processes for biomass. Volume 4 (1): Elsevier; 2000. 1-73 p.

6. Czernik S, Bridgwater AV. Overview of applications of biomass fast pyrolysis oil. Energy & Fuels. 2004;18(2):590-8.

7. Oasmaa A, Czernik S. Fuel oil quality of biomass pyrolysis oils - State of the art for the end user. Energy & Fuels. 1999;13(4):914-21.

8. Wang D, Czernik S, Montane D, Mann M, Chornet E. Biomass to hydrogen via fast pyrolysis and catalytic steam reforming of the pyrolysis oil or its fractions. Industrial & Engineering Chemistry Research. 1997;36(5):1507-18.

9. Wang D, Czernik S, Chornet E. Production of hydrogen from biomass by catalytic steam reforming of fast pyrolysis oils. Energy & Fuels. 1998;12(1):19-24.

10. Marquevich M, Czernik S, Chornet E, Montane D. Hydrogen from biomass: Steam reforming of model compounds of fast-pyrolysis oil. Energy & Fuels. 1999;13(6):1160-6.

11. Garcia L, French R, Czernik S, Chornet E. Catalytic steam reforming of bio-oils for the production of hydrogen: effects of catalyst composition. Applied Catalysis A-General. 2000;201(2):225-39.

12. Czernik S, French R, Feik C, Chornet E. Hydrogen by catalytic steam reforming of liquid byproducts from biomass thermoconversion processes. Industrial & Engineering Chemistry Research. 2002;41(17):4209-15.

13. Panigrahi S, Dalai AK, Chaudhari ST, Bakhshi NN. Synthesis gas production from steam gasification of biomass-derived oil. Energy & Fuels. 2003;17(3):637-42.

14. Takanabe K, Aika K, Seshan K, Lefferts L. Sustainable hydrogen from bio-oil - Steam reforming of acetic acid as a model oxygenate. Journal of Catalysis. 2004;227(1):101-8.

15. Galdamez JR, Garcia L, Bilbao R. Hydrogen production by steam reforming of bio-oil using coprecipitated Ni-Al catalysts. Acetic acid as a model compound. Energy & Fuels. 2005;19(3):1133-42.

16. Rioche C, Kulkarni S, Meunier FC, Breen JP, Burch R. Steam reforming of model compounds and fast pyrolysis bio-oil on supported noble metal catalysts. Applied Catalysis B-Environmental. 2005;61(1-2):130-9.

17. Kechagiopoulos PN, Voutetakis SS, Lemonidou AA, Vasalos IA. Hydrogen production via steam reforming of the aqueous phase of bio-oil in a fixed bed reactor. Energy & Fuels. 2006;20(5):2155-63.

18. Takanabe K, Aika K, Inazu K, Baba T, Seshan K, Lefferts L. Steam reforming of acetic acid as a biomass derived oxygenate: Bifunctional pathway for hydrogen formation over Pt/ZrO2 catalysts. Journal of Catalysis. 2006;243(2):263-9.

19. Basagiannis AC, Verykios XE. Catalytic steam reforming of acetic acid for hydrogen production. International Journal of Hydrogen Energy. 2007;32(15):3343-55.

20. Basagiannis AC, Verykios XE. Steam reforming of the aqueous fraction of bio-oil over structured Ru/MgO/Al2O3 catalysts. Catalysis Today. 2007;127(1-4):256-64.

21. Bimbela F, Oliva M, Ruiz J, Garcia L, Arauzo J. Hydrogen production by catalytic steam reforming of acetic acid, a model compound of biomass pyrolysis liquids. J Anal Appl Pyrolysis. 2007(79):112-20.

22. Ramos MC, Navascues AI, Garcia L, Bilbao R. Hydrogen production by catalytic steam reforming of acetol, a model compound of bio-oil. Industrial & Engineering Chemistry Research. 2007;46(8):2399-406.

23. Wang ZX, Dong T, Yuan LX, et al. Characteristics of bio-oil-syngas and its utilization in fischer-tropsch synthesis. Energy & Fuels. 2007;21(4):2421-32.

24. Wang ZX, Pan Y, Dong T, et al. Production of hydrogen from catalytic steam reforming of bio-oil using C12A7-O--based catalysts. Applied Catalysis a-General. 2007;320:24-34.

25. Domine ME, Iojoiu EE, Davidian T, Guilhaume N, Mirodatos C. Hydrogen production from biomass-derived oil over monolithic Pt- and Rh-based catalysts using steam reforming and sequential cracking processes. Catalysis Today. 2008(133-135):565-73.

26. Panigrahi S, Chaudhari ST, Bakhshi NN, Dalai AK. Production of synthesis gas/high-Btu gaseous fuel from pyrolysis of biomass-derived oil. Energy & Fuels. 2002;16(6):1392-7.

27. Davidian T, Guilhaume N, Iojoiu E, Provendier H, Mirodatos C. Hydrogen production from crude pyrolysis oil by a sequential catalytic process. Applied Catalysis B-Environmental. 2007;73(1-2):116-27.

28. Iojoiu EE, Domine ME, Davidian T, Guilhaume N, Mirodatos C. Hydrogen production by sequential cracking of biomass-derived pyrolysis oil over noble metal catalysts supported on ceria-zirconia. Applied Catalysis A-General. 2007;323:147-61.

29. Davidian T, Guilhaume N, Daniel C, Mirodatos C. Continuous hydrogen production by sequential catalytic cracking of acetic acid - Part I. Investigation of reaction conditions and application to two parallel reactors operated cyclically. Applied Catalysis a-General. 2008;335(1):64-73.

30. Davidian T, Guilhaume N, Provendier H, Mirodatos C. Continuous hydrogen production by sequential catalytic cracking of acetic acid. Part II. Mechanistic features and characterisation of catalysts under redox cycling. Applied Catalysis A-General. 2008;337(2):111-20.

31. van Rossum G, Kersten SRA, van Swaaij WPM. Catalytic and noncatalytic gasification of pyrolysis oil. Industrial & Engineering Chemistry Research. 2007;46(12):3959-67.

32. Heinrich E, Raffelt K, Stahl R, Weirich F (eds). Clean syngas from bio-oil/char slurries. Newbury Berks: CPL Press; 2006. 1565-79 p.

33. Rennard DC, Dauenhauer PJ, Tupy SA, Schmidt LD. Autothermal catalytic partial oxidation of bio-oil functional groups: Esters and acids. Energy & Fuels. 2008;22(2):1318-27.

34. Shin EJ, Nimlos MR, Evans RJ. The formation of aromatics from the gas-phase pyrolysis of stigmasterol: kinetics. Fuel. 2001;80:1681-7.

35. Shin E-J, Nimlos MR, Evans RJ. A study of the mechanisms of vanillin pyrolysis by mass spectrometry and multivariate analysis. Fuel. 2001;80:1689-96.

36. Shin E-J, Evans RJ, Nimlos M. Aromatic Compounds formation during biomass gasification/pyrolysis. ACS 233rd Annual Meeting. Chicago, IL, 2007.

37. Britt PF, Buchanan ACI, Kidder MM, et al. Mechanistic investigation into the formation of polycyclic aromatic hydrocarbons from the pyrolysis of plant steroids. Fuel. 2001;80:1727-46.

38. McGrath T, Sharma R, Hajaligol M. An experimental investigation into the formation of polycyclic-aromatic hydrocarbons (PAH) from pyrolysis of biomass materials. 2001:1787-97.

39. U.S. Department of Energy and Department of Transportation. Hydrogen Posture Plan: An integrated, research, Development and Demonstration plan. Washington, DC:2006.

40. Evans RJ, Czernik S, French R, Marda J. Distributed Bio-Oil Reforming, DOE Hydrogen Program FY2006 Annual Progress Report, 2006.

41. Al Shoaibi AS. Experimental and Modeling Analysis of Hydrocarbon Pyrolysis. PhD Disertation. Coloado School of Mines, 2007.

42. Scahill JW, Diebold JP, Feik CJ. Removal of Residual Char Fines from Pyrolysis Vapors by Hot-Gas Filtration. In: Bridgwater AV, Boocock DGB (eds). Developments in Thermochemical Biomass Conversion. London: Blackie Academic & Professional, 1997:253-66.

43. Evans RJ, Milne TA. Molecular Characterization of the Pyrolysis of Biomass. 1. Fundamentals. Energy and Fuels. 1987;1:123-37.

44. Degenstein NJ, Subramanian R, Schmidt LD. Partial oxidation of n-hexadecane at short contact times: Catalyst and washcoat loading and catalyst morphology. Applied Catalysis A: General. 2006; 305:146–159.

45. Bridgewater A, Czernik S, Diebold J, Meier D, Oasmaa A, Peacocke C, Piskorz J, Radlein D. Fast Pyrolysis of Biomass: A Handbook. CPL Press. Newbury, UK. 1999.

46. Sasaki K, Teraoka Y. Equilibria in fuel cell gases - II. The C-H-O ternary diagrams, Journal of the Electrochemical Society. 2003;150:A885-A888.

47. Yi YF, Rao AD, Brouwer J, Samuelsen GS, Fuel flexibility study of an integrated 25 kW SOFC reformer system, Journal of Power Sources 144 (1), 67-76, 2005.

48. Strohm JJ, Zheng J, Song CS. Low-temperature steam reforming of jet fuel in the absence and presence of sulfur over Rh and Rh-Ni catalysts for fuel cells. Journal of Catalysis 2006;238:309-320.

49. Gupta, GK, Marda, JR, Dean, AM, Colclasure, AM, Zhu, H, Kee, RJ. Performance predictions of a tubular SOFC operating on a partially reformed JP-8 surrogate. Journal of Power Sources. 2006;162:553-562.

50. Hrdlicka J, Feik C, Carpenter D, Pomeroy M. Parametric gasification of oak and pine feedstocks using the TCPDU and slipstream water-gas shift catalysis. Technical Report. http://wwwnrelgov/docs/fy09osti/44557pdf: NREL/TP-510-44557, 2008.

51. Daugaard DE, Brown RC. Enthalpy for Pyrolysis for Several Types of Biomass Energy & Fuels. 2003;17:934-939.

52. Mohan D, Pittman CU Jr, Steele PH. Pyrolysis of Wood/Biomass for Bio-oil: A Critical Review. Energy & Fuels. 2006, *20,* 848-889.

53. Bridgwater AV, Ed. Progress in Thermochemical Biomass Conversion, Volume 2; Blackwell Science: London, 2001.

54. U.S. Department of Energy: Hydrogen Program, DOE H2A Analysis, 2003. http://www.hydrogen.energy.gov/h2a_analysis.html.

55. U.S. Department of Energy: Hydrogen Program, DOE H2A Production Case Studies, 2003. http://www.hydrogen.energy.gov/h2a_prod_studies.html.

56. Peacocke GVC, Russell PA, Jenkins JD, Bridgewater AV, Physical properties of flash pyrolysis liquids. Biomass and Bioenergy. 1994;7:169-177.

57. Czernik, S. Personal communication, 2005.

58. Ing W-C, Sheng CY, Bozzelli JW. Development of a detailed high-pressure reaction model for methane/methanol mixtures under pyrolytic and oxidative conditions and comparison with experimental data. Fuel Processing Technology. 2003;83:11-145.

59 Held, TJ, Dryer, FL. A comprehensive mechanism for methanol oxidation. International Journal of Chemical Kinetics. 1998;30:805-830.

60. Li, J, Zhao, Z, Kazakov, A, Chaos, M, Dryer, FL, Scire, JJ, jr. A comprehensive kinetic mechanism for CO, CH_2O, and CH_3OH combustion. International Journal of Chemical Kinetics. 2007;39:109-136.

61. Randolph KL, Dean AM. Hydrocarbon fuel effects in solid-oxide fuel cell operation: an experimental and modeling study of n-hexane pyrolysis. Phys Chem Chem Phys. 2007;9:4245-58.

62. Naik CV, Dean AM. Detailed kinetic modeling of ethane oxidation. Comb Flame. 2006;145:16-37.

APPENDIX A
METHODS FOR ESTIMATING SOURCE OF CO AND CO_2

In order to estimate how much CO and CO_2 were coming from methanol so that the contributions form bio-oil could be determined, pyrolysis and oxidation experiments with neat methanol were performed at 650˚C at a residence time similar to that used in the bio-oil-methanol mixture experiments. It was assumed that there are no interactions between methanol and bio-oil during the mixture experiments, which implied that the measured selectivity to CO and CO_2 as a function of conversion during the neat methanol experiments could be applied to the mixture experiments to estimate the respective amounts of each species formed from methanol and from bio-oil. The process for making this estimate is described below.

The major products of the neat methanol experiments were CO, CO_2, H_2O and H_2. Though trace amounts of formaldehyde and methane were observed, they were sufficiently small to be neglected. Hence, CO and CO_2 accounted for nearly all of the carbon from conversion of methanol during these experiments.

Data collected from the neat methanol experiments were used to create a correlation between the conversion of methanol and the ratio of CO to CO_2 (R_{CO-CO2}) formed (see Figure A.1). This correlation was then used to determine R_{CO-CO2}, and consequently the amounts of CO and CO_2 assumed to form from methanol in bio-oil:methanol mixtures for the observed methanol conversions. Finally, the amounts of carbon oxides obtained from partial oxidation of bio-oil were calculated as a difference of the total CO and CO_2 measured and those coming from methanol. A complication in this analysis is that, for high levels of methanol conversion (corresponding to high values of O:C), there were significant differences in the measured R_{CO-CO2}. Under these conditions, this ratio is very sensitive to methanol conversion; small errors in measurement of conversion are the likely source of this scatter. This led to a correlation in which there were two R_{CO-CO2} values possible for a given methanol conversion at high

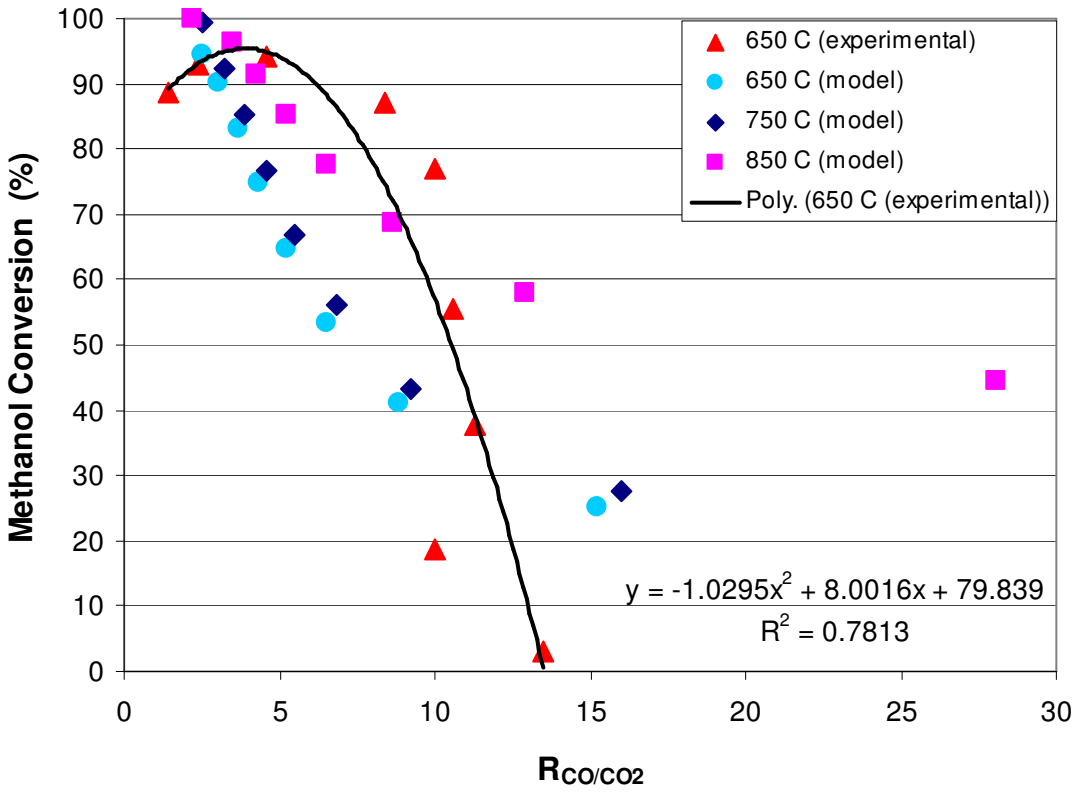

Figure A.1. Comparison of measured CO/CO_2 selectivity vs. methanol conversion at 650ºC to that predicted by a detailed kinetic model at 650, 750, and 850ºC. Experimental data were used to create a correlation for the calculation of CO and CO_2 from methanol (and bio-oil by difference).

conversion levels. For these cases the higher value for the ratio was used. Use of the lower value led to the result that all of the CO_2 in the mixture experiments was coming from methanol. That conclusion is inconsistent with the observations at lower levels of conversion. In addition, the O:C ratio in the mixture experiments corresponded to the O:C values in the neat methanol experiments that yielded for higher values for $R_{CO\text{-}CO2}$. The ambiguity in assignment of the ratio at high levels of conversion is accounted for in the error bars assigned to the estimated CO and CO_2 yields from bio-oil.

A detailed kinetic model was used to perform calculations at 650, 750, 850ºC to verify that the correlation (described above) obtained from the 650ºC experiments could be applied at all temperatures. The kinetic mechanism used

consists of 3546 reactions and 354 species. It is the combination of a nC_6 pyrolysis model and an ethane oxidation model. The nC_6 model has been described by Randolph and Dean[61]. The oxidation component of the model was developed by Naik and Dean[62] to describe ethane oxidation and pyrolysis over a very wide range of conditions. (Obviously such a large model is not necessary to describe the methanol system, but it was available and was used to assure completeness.) Lack of a detailed knowledge of the precise temperature –time history within the reactor makes a quantitative comparison problematic. However, the trends should be reliable. In general, one sees from Fig. A1 that a temperatures changes from 650 to 750ºC there is little effect on the predicted ratio of CO to CO_2 production for a given methanol conversion. The 850ºC predictions illustrate significant effects of temperature at lower levels of conversion. However, the predictions for all temperatures cluster close together and agree quite well with the data at high methanol conversions, and this is the region of greatest interest for the present analysis. These predictions suggest that the measurements obtained at 650ºC can be applied with reasonable confidence to estimate CO and CO_2 production from methanol for all of the mixture experiments.

APPENDIX B
CONTENTS OF DVD

The enclosed DVD includes data and files used to make figures and tables in the thesis. The file formats are .doc (created using MS Word 2000),.xls (created using MS Excel 2000), and .pdf (created using Adobe Acrobat Professional). In addition to a .pdf copy of the thesis, folders containing data from the following Chapters are included:

1. Chapter 3
2. Chapter 4
3. Chapter 5
4. Chapter 7
5. Chapter 9
6. Chapter 10

In addition to data actually used in Chapter 9, the folder labeled Chapter 9 includes data collected at CFCC that was not used in the thesis due to the reasons discussed in Chapter 9.